Tests of Fluid-to-Fluid Scaling Laws for Supercritical Heat Transfer

by

Abderrazzak Mouslim

Thesis submitted to the Faculty of Engineering
in partial fulfillment of the requirements for the degree of
MASTER OF APPLIED SCIENCE
in Mechanical Engineering

Ottawa-Carleton Institute for Mechanical and Aerospace Engineering
University of Ottawa
Ottawa, Canada

Abstract

A comparison of available fluid-to-fluid scaling laws for scaling convective heat transfer at supercritical pressures showed that the ones suggested by Zahlan, Groeneveld and Tavoularis (ZGT) have some advantages. The applicability of the ZGT laws was tested for pairs of fluids including carbon dioxide, water or Refrigerant R134a. The conditions of previous measurements taken in the Supercritical University of Ottawa Loop with CO_2 flowing vertically upwards in an electrically heated tube with 8 mm ID were scaled to equivalent conditions in R134a and new measurements of the heat transfer coefficient (HTC) were taken in the same tube using the latter fluid. The inlet pressure was 1.13 times the critical pressure (4.06 MPa), the mass flux was in the range from 212 kg/m^2s to 1609 kg/m^2s, the heat flux was in the range from 2 kW/m^2 to 137 kW/m^2, and the inlet temperature was in the range from 62 °C to 105 °C. The HTC at equivalent conditions in water was also determined with the use of transcritical look-up tables. Average and linearly varying corrections to the ZGT scaling laws were derived by statistical analysis for each pair of fluids under NHT or DHT conditions. Such corrections reduced the standard deviation of the scaling error but did not eliminate the presence of large errors under many sets of conditions. As expected, scaling errors were in general larger for DHT than NHT conditions. The present results did not reveal any systematic and correctable dependence of the scaling error upon the mass flux or heat flux but showed that scaling errors became particularly large as the bulk temperature T_b approached the pseudocritical temperature T_{pc}. In conclusion, the ZGT scaling laws appear to be fairly accurate for the three pairs of fluids considered in the liquid–like region with $T_b/T_{pc} \leq 0.94$ and possibly in the gas–like region with $T_b/T_{pc} \geq 1.02$, whereas outside this range scaling errors could be significant. It was also found that the ZGT scaling laws do not scale accurately the onset of DHT in different fluids.

Acknowledgements

I cannot express enough gratefulness to my supervisor, Professor Stavros Tavoularis, for his continued support, vast academic and industrial knowledge, encouragement, and motivation during my graduate studies. I offer my sincere appreciation for the learning opportunities provided by my Professor. I could not have hoped for a better supervisor.

I would also like to thank my thesis examiners, Professors D. Groeneveld and M. Yaras, for their useful criticisms.

This project is part of the Canadian Gen-IV National Program. I thankfully acknowledge the financial support of the Natural Resources Canada for this program through the Office of Energy Research and Development, Atomic Energy of Canada Limited, and Natural Sciences and Engineering Research Council of Canada.

Last but not least, I would like to thank all my family and friends who supported me in contributing to this project.

Contents

List of Tables

List of Figures

Nomenclature

Roman symbols

A	Area, m^2; average
a, b	Coefficients
c_p	Specific heat at a constant pressure, $\mathrm{J\,kg^{-1}\,K^{-1}}$
d	Test section inner diameter, mm
E	Internal energy, W
e	Relative error
$e^{'}$	Standard deviation
G	Mass flux, $\mathrm{kg\,m^{-2}\,s^{-1}}$
g	Gravitational acceleration, $\mathrm{m\,s^{-2}}$
Gr	Grashof number $= g\beta(T_w - T_b)d^3/\nu^2$
H	Specific enthalpy, $\mathrm{kJ\,kg^{-1}}$
h	Convective heat transfer coefficient, $\mathrm{W\,m^{-2}\,K^{-1}}$
I	Current, A
k	Thermal conductivity, $\mathrm{W\,m^{-1}\,K^{-1}}$
L	Length, m

M	Molecular weight, $\mathrm{g\,mol^{-1}}$
$\dot{m}$	Mass flow rate, $\mathrm{kg\,s^{-1}}$
N	Number of samples
Nu	Nusselt number $= hd/k$
P	Pressure, kPa, MPa
Pr	Prandtl number $= c_p\mu/k$
Q	Heating power, W
q	Heat flux, $\mathrm{kW\,m^{-2}}$
ΔQ	Power imbalance, kW
Q_e	Percent power imbalance error, %
R	Electric resistance, Ω
r	Radius, m
Re	Reynolds number $= Gd/\mu$
Ri	Richardson number $= Gr/Re^2$
T	Temperature, °C, K
t	Time, s
V	Voltage, V
v	Velocity, $\mathrm{m\,s^{-1}}$; specific volume, $\mathrm{m^3\,kg^{-1}}$
x	Variable
z	Compressibility factor
z_h	Axial location, m

Greek letters

β	Volumetric thermal expansion coefficient, K^{-1}
Δ	Difference
γ	Constant
μ	Dynamic viscosity, $\mathrm{kg\,m^{-1}\,s^{-1}}$; arithmetic mean
ν	Kinematic viscosity, $\mathrm{m^2\,s^{-1}}$
ρ	Density, $\mathrm{kg\,m^{-3}}$
ρ_e	Electrical resistivity, $\Omega \cdot \mathrm{m}$

Subscripts

av	Average correction
ave	Time averaged
b	Bulk
C	CO_2
c	Critical
$corr$	Correlated
e	Error
exp	Experimental
h	Heated
hy	Hydraulic
i	Inner; index
in	Inlet

lf Linear-least-squares fit correction

max Maximum value

min Minimum value

o Outer

out Outlet

pc Pseudocritical

R R134a

ref Reference

sca Scaled

W H_2O

w wall

1 Fluid one

2 Fluid two

RMS/rms Root mean square

Overbar

– Averaged over a temperature range

Abbreviations

CNL Canadian Nuclear Laboratories

CO_2 Carbon dioxide

DAS Data acquisition system

DHT Deteriorated heat transfer

EG Ethylene glycol

EHT Enhanced heat transfer

Gen-IV Generation IV

GIF Generation IV International Forum

GWP Global warming potential

H_2O Chemical formula of water

HE Heat exchanger

HTC Heat transfer coefficient

HTD Heat transfer deterioration

I.D./ID Inner diameter

NHT Normal heat transfer

NIST Thermophysical properties software of different fluids (Lemmon et al., 2002)

ODP Ozone-depleting potential

OPPSEC Ozone Protection Programs Section Environment Canada

PR Pressure ratio

PT Pressure transducer

R134a HFC refrigerants R134a (Freon)

RTD Resistance temperature detector

SC Supercritical

SCUOL Supercritical University of Ottawa Loop

SCWR Supercritical Water-Cooled Reactor

STD Standard deviation

TC Thermocouple

TC-LUT Trans-critical look-up tables

TS Test section

Vt Vent

Chapter 1

Introduction

1.1 Motivation

The current membership of Generation IV (Gen-IV) International Forum (GIF) consists of 14 countries, which are Argentina, Australia, Brazil, Canada, People's Republic of China, Euratom, France, Japan, Republic of Korea, Russia Federation, Republic of South Africa, Switzerland, United Kingdom, and United States (GIF, 2017). GIF members were committed to developing the next nuclear energy systems, Gen-IV reactors, that would be characterised by improved efficiency, safety and proliferation resistance, minimised waste and natural resource utilisation, and lower cost to build and operate. GIF considered six reactor concepts for further research and development: Gas-cooled Fast Reactor (GFR), Lead-cooled Fast Reactor (LFR), Molten Salt Reactor (MSR), Supercritical Water-cooled Reactor (SCWR), Sodium-cooled Fast Reactor (SFR) and Very High Temperature Reactor (VHTR). These concepts are illustrated in Figure 1.1.

Canada selected to pursue the development of the SCWR concept, expected to be commercialised after 2030. This task was undertaken by the Canadian Nuclear Laboratories (CNL), because of its extensive experience in the design of pressure-tube nuclear reactors. Figure 1.2 shows the suggested Canadian SCWR core design and the layout of a SCWR nuclear power plant (Yetisir et al., 2016).

The benefits of using supercritical water as a working fluid in the SCWR system are as follows (Yetisir et al., 2016; GIF, 2017).

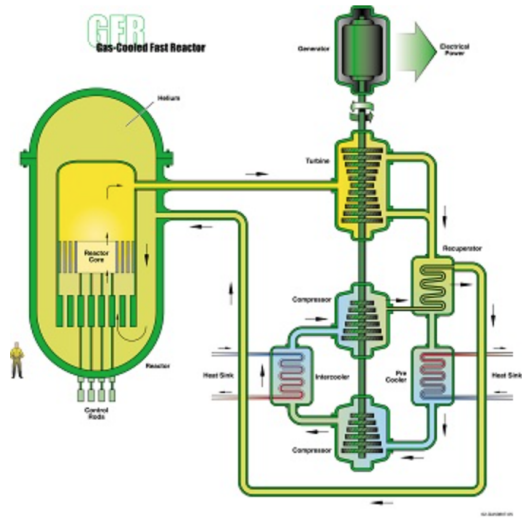

(a) Gas – cooled Fast Reactor (GFR)

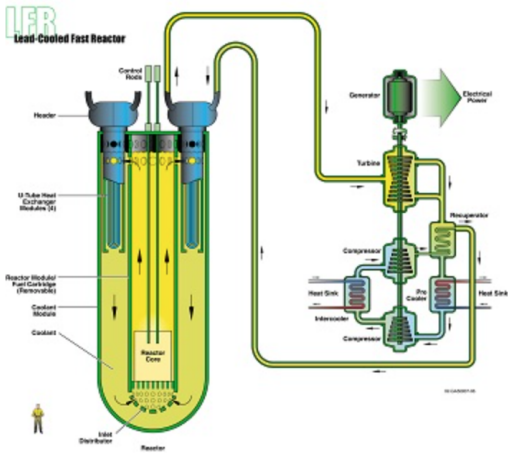

(b) Lead – cooled Reactor (LFR)

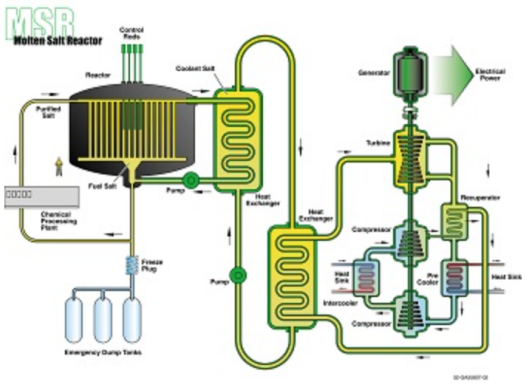

(c) Molten Salt Reactor (MSR)

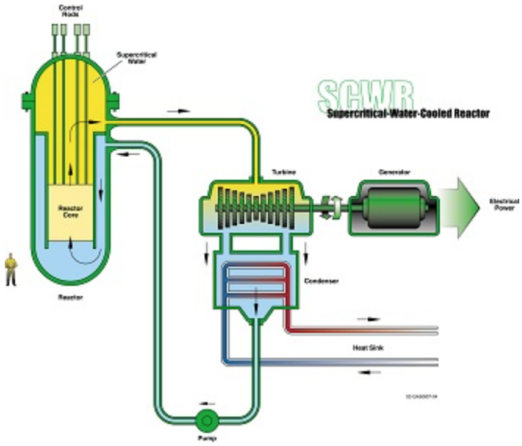

(d) Supercritical Water – cooled Reactor (SCWR)

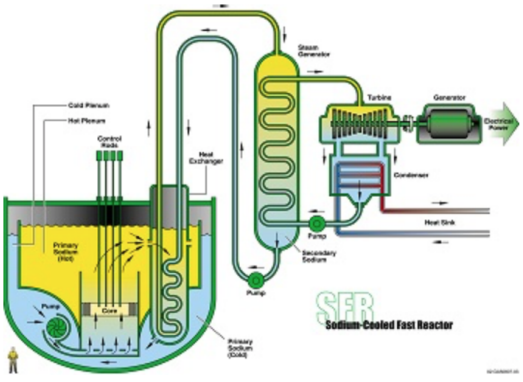

(e) Sodium – cooled Fast Reactor (SFR)

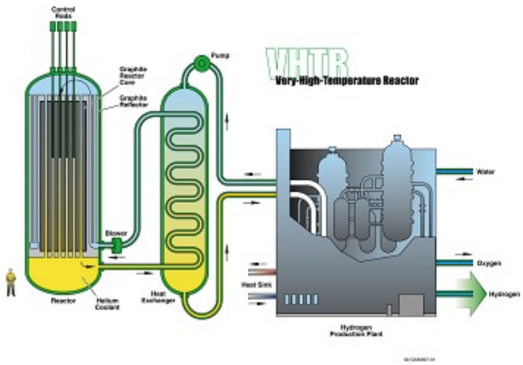

(f) Very High Temperature Reactor(VHTR)

Figure 1.1: The six nuclear reactor concepts that were selected by GIF members (GIF, 2017).

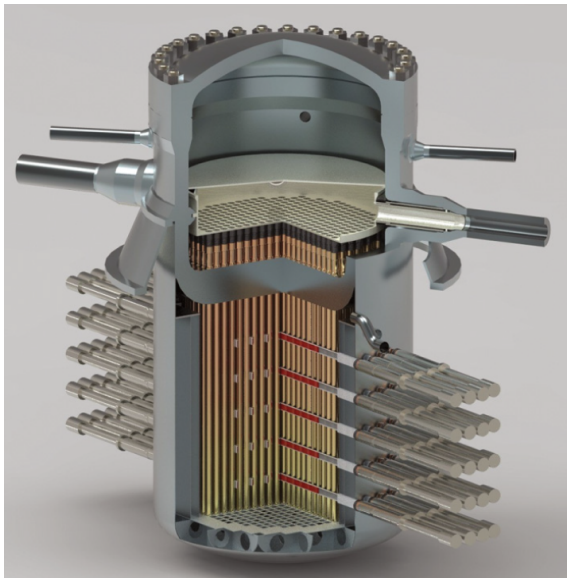

(a) 3D view of SCWR core (Yetisir et al., 2016)

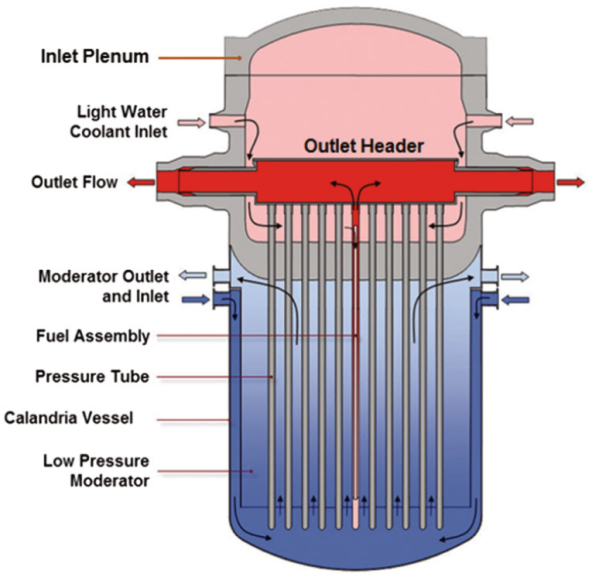

(b) 2D view of SCWR core (Yetisir et al., 2016)

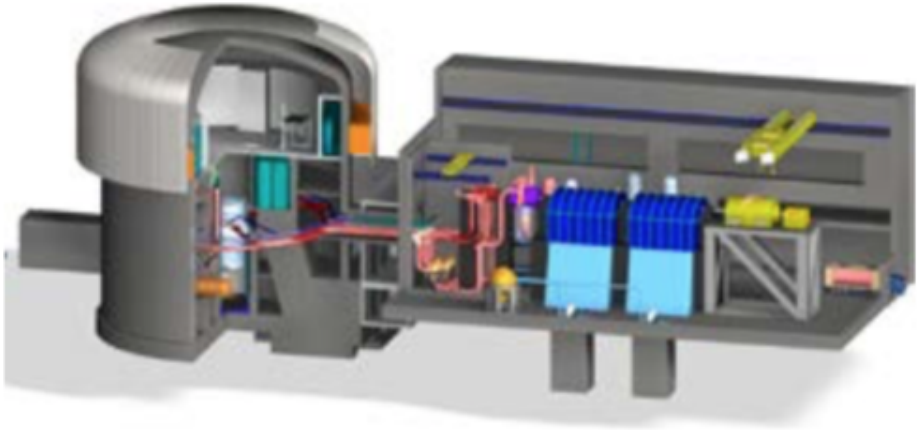

(c) Layout of SCWR plant (GIF, 2016)

Figure 1.2: The Canadian SCWR design concept.

- The nuclear plant-cycle efficiency would increase to more than 50%, which is significantly higher than the 35% efficiency of the existing CANDU reactors. This increase in efficiency is to a large extent due to the higher temperatures in the SCWR.
- The plant would be more compact as the result of the elimination of heat exchangers, steam generators, steam dryers and other components that are used in current CANDU technology. The high enthalpy of SCWR coolant would also allow a decrease in size of the SCWR core and turbine systems.
- SCWR would be safer because, as long as the pressure is maintained at supercritical levels, they would not be subjected to the limitation of critical heat flux and the resulting dryout and possible meltdown of the reactor core.
- Nuclear waste would be reduced by the use of Thorium as fuel in SCWR. Thorium is a slightly radioactive element that transforms into fissionable Uranium-233 when hit by high-energy neutrons produced by an igniter like Plutonium, but, after usage, Uranium-233 produces less long-lived contaminated waste products than the common Uranium-235 used in current nuclear power plants.
- The risk of nuclear weapon proliferation would be reduced by the easy detection and remote handling of Uranium-232 in spent fuel.
- SCWR can be designed for a wide range of electric powers. The current concept is designed to produce 1 GW to 1.5 GW of electric power. A different design being considered is meant to generate 10 MW to 300 MW of electric power so that it could power small communities.

In support of developing and implementing the SCWR system design, a reliable database in supercritical water must be produced. However, experimenting with supercritical water is subjected to great technical and economic challenges due to the high pressures and temperatures required by GIF. A convenient alternative is the use of surrogate fluids, which have thermodynamic properties that behave similarly to the corresponding properties of water, but whose critical pressure and temperature are substantially lower than those of water. Two such fluids are CO_2 and Refrigerant R134a (R134a or Freon). Data collected using

surrogate fluids must then be converted accurately to water at equivalent conditions via suitable fluid-to-fluid scaling laws.

An important limitation of SCWR operation is the possible occurrence of deteriorated heat transfer (DHT), which may lead to wall material overheating and possible meltdown. Conditions for the onset of DHT in SCWR must be investigated carefully.

1.2 Objectives

The main objectives of this thesis are the following ones.

- To verify the fluid-to-fluid scaling laws for normal supercritical heat transfer that were suggested by Zahlan et al. (2014) for the pair CO_2-H_2O and to test the accuracy of the same scaling laws for the pair H_2O-CO_2, if necessary proposing a correction.
- To collect measurements in an electrically heated 8 mm tube cooled by R134a at conditions that were scaled from equivalent conditions in CO_2 with the use of Zahlan et al. (2014) scaling laws; these experiments were meant to include conditions with normal and mildly or strongly deteriorated heat transfer in CO_2.
- To test the performance of the Zahlan et al. (2014) scaling laws for the pairs CO_2-R134a and R134a$-CO_2$ and to determine corrections and their uncertainties for normal supercritical heat transfer in both fluids; to repeat this analysis for the cases with deteriorated heat transfer in CO_2.
- To test the performance of the Zahlan et al. (2014) scaling laws for the pairs R134a$-H_2O$ and H_2O-R134a and to determine corrections and their uncertainties.

1.3 Plan

This thesis is composed of five chapters. Chapter 1 explains the Canadian SCWR concept and outlines some fundamental information concerning heat transfer in supercritical fluids as a motivation for the thesis; it also summarises the objectives of the present work and presents a plan for the thesis. Chapter 2 describes the different modes of supercritical heat transfer,

a comparison of the thermophysical properties of the fluids CO_2, R134a and H_2O, as well as a literature review on fluid-to-fluid modelling for supercritical heat transfer. Chapter 3 describes the experimental facility, instrumentation and measurement procedures that were used for this work. Chapter 4 presents the experimental results and discusses the tests of fluid-to-fluid scaling laws for the three fluids, whereas Chapter 5 summarises the main conclusions of the thesis and presents some recommendations for future work.

Chapter 2

Background

2.1 Supercritical fluids

The critical point of a fluid is a point on a temperature-pressure phase diagram at which its liquid and vapour phases cannot be distinguished. A supercritical fluid is a fluid at a pressure and a temperature that exceed those at its critical point. At each supercritical pressure, the specific heat of the fluid has a maximum value at a specific temperature, called the pseudocritical temperature. The pseudocritical line is the locus of pseudocritical points on a phase diagram. The phase diagram and the specific heat of water are shown in Figure 2.1 (Pioro et al., 2011). Figure 2.2 shows that, in the vicinity of the pseudocritical temperature, the thermophysical properties of a fluid change drastically.

Figure 2.3 shows normalised temperature differences for the fluids H_2O, CO_2 and R134a *vs.* the pressure ratio P/P_c, where P_c is the critical pressure (Zahlan et al., 2014). This figure shows a strong thermodynamic similarity among these three fluids at both subcritical and supercritical pressure regions. Table 2.1 lists the values of the main pseudocritical properties of these three fluids at a pressure equal to 1.13 times P_c, which is the designed pressure for the Canadian SCWR system. The same table shows that the pressure and temperature of CO_2 and R134a are much lower than those of H_2O.

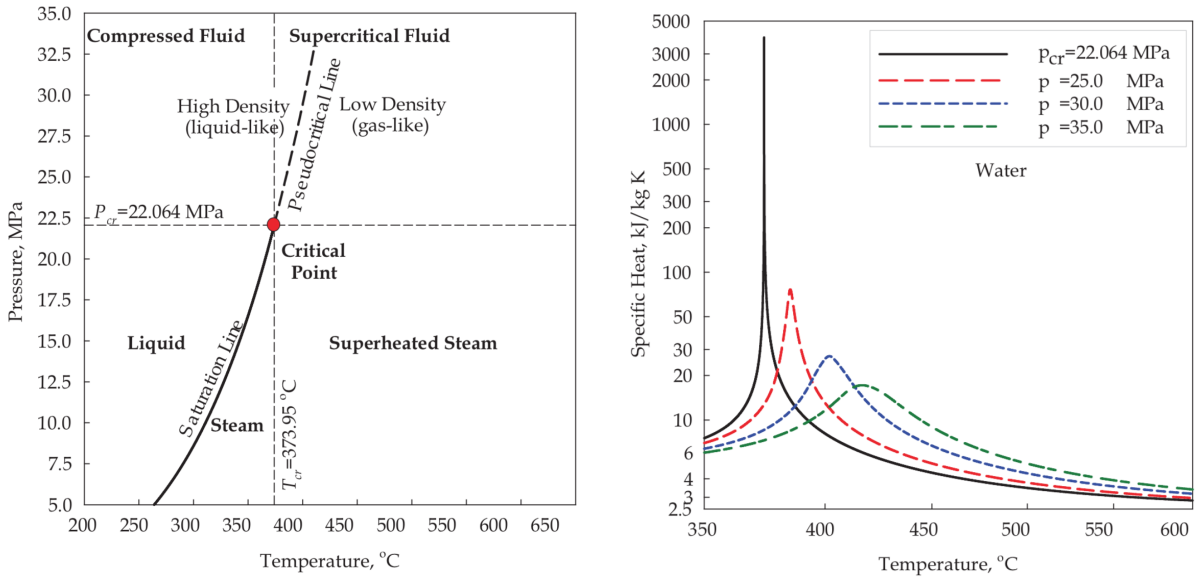

Figure 2.1: Pressure-temperature phase diagram of water (left) and water specific heat dependence on pressure and temperature (right)(Pioro et al., 2011).

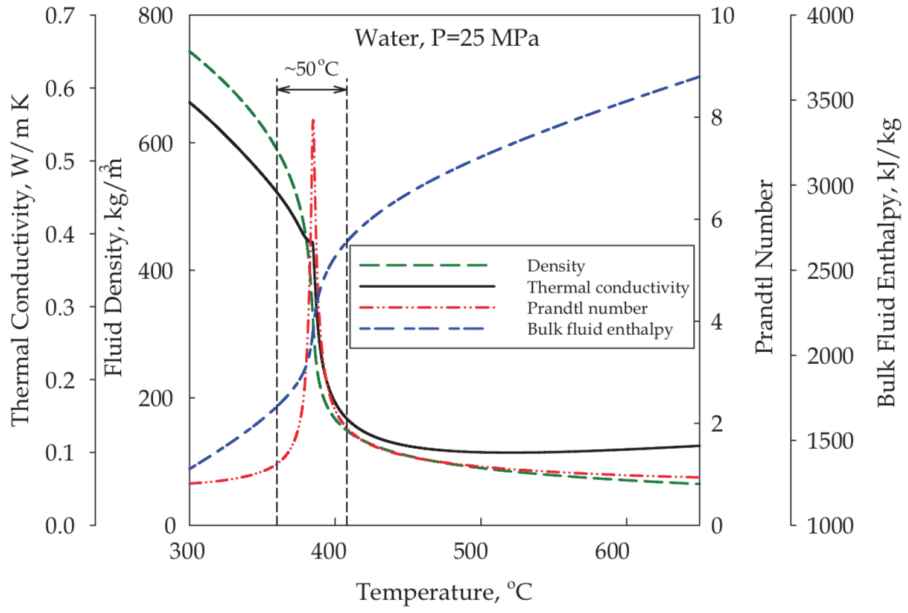

Figure 2.2: Thermophysical changes of some selected thermodynamic properties of water at 25 MPa (Pioro et al., 2011).

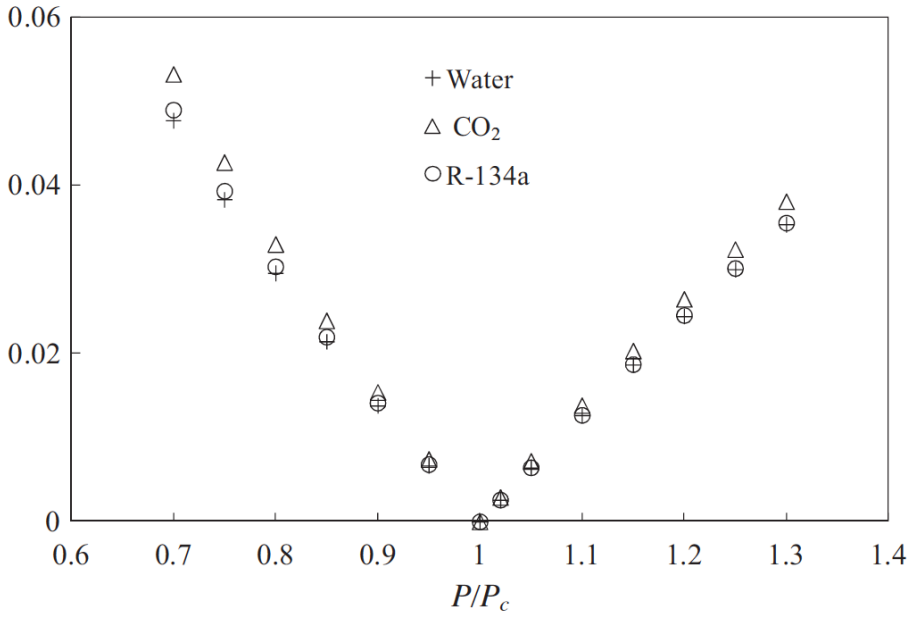

Figure 2.3: Comparison of normalised saturation T_{sat} and pseudocritical T_{pc} temperature differences at different normalised pressures for water, CO_2 and R134a; the symbols show the corresponding values of $(T_c - T_{sat})/T_{sat}$ for the subcritical range $(P/P_c < 1)$ or $(T_{pc} - T_c)/T_{pc}$ for the supercritical range $(P/P_c > 1)$ (Zahlan et al., 2014).

Table 2.1: Values of pseudocritical properties of H_2O, CO_2 and R134a at $P = 1.13P_c$ (Lemmon et al., 2002)

Property	H_2O	CO_2	R134a
Critical pressure, P_c [MPa]	22.1	7.38	4.06
Pressure, P [MPa]	24.93	8.34	4.59
Pseudocritical temperature, T_{pc} [°C]	384.6	36.5	107.3
Pseudocritical density, ρ_{pc} [$\mathrm{kg\,m^{-3}}$]	319	473	514
Pseudocritical thermal conductivity, k_{pc} [$\mathrm{W\,m^{-1}\,K^{-1}}$]	0.3842	0.0792	0.0516
Pseudocritical thermal expansion, β_{pc} [$\mathrm{K^{-1}}$]	0.1321	0.1806	0.1563
Pseudocritical enthalpy, H_{pc} [$\mathrm{kJ\,kg^{-1}}$]	21.52×10^2	3.41×10^2	3.98×10^2
Pseudocritical dynamic viscosity, μ_{pc} [Pa s]	3.97×10^{-5}	3.67×10^{-5}	3.51×10^{-5}
Pseudocritical Prandtl number, Pr_{pc} [-]	8.10	9.36	7.51

2.2 Heat transfer modes in supercritical fluids

Compared with heat transfer in flows with constant values of their thermophysical properties, heat transfer in supercritical fluids may take place in three different modes:

- normal heat transfer (NHT),
- deteriorated heat transfer (DHT) and
- enhanced heat transfer (EHT).

An illustration of the three modes occurring along a heated vertical tube is shown in Figure 2.4. Heat transfer deterioration (HTD) limits the operation of SCWR, as it may lead to excessive wall temperatures in the core and eventual meltdown. This phenomenon has been attributed to buoyancy forces and/or acceleration of the flow (Fewster and Jackson, 2004). The bulk heat transfer coefficient (HTC), or equivalently the bulk Nusselt number Nu_b, for NHT can be predicted reasonably accurately with the use of available correlations, but the prediction of the onset of DHT and the value of the HTC under DHT conditions remain a challenge (Kline et al., 2018). EHT is usually characterised by a relatively high value of HTC, which may be observed in some part of a heated test section right after a spike in wall temperature.

2.3 Thermophysical property variations of the three fluids

Values of the thermophysical properties of many fluids, including water, carbon dioxide and different refrigerants, at different pressures and temperatures spanning the subcritical, critical and supercritical regimes can be found using the NIST REFPROP software (Lemmon et al., 2002).

This section presents plots of the main normalised thermophysical properties of the fluids H_2O, CO_2 and R134a for $P = 1.13P_c$ versus a normalised temperature. Two sets of plots are presented: one set uses T_b/T_{pc} as the independent variable, whereas the other set uses

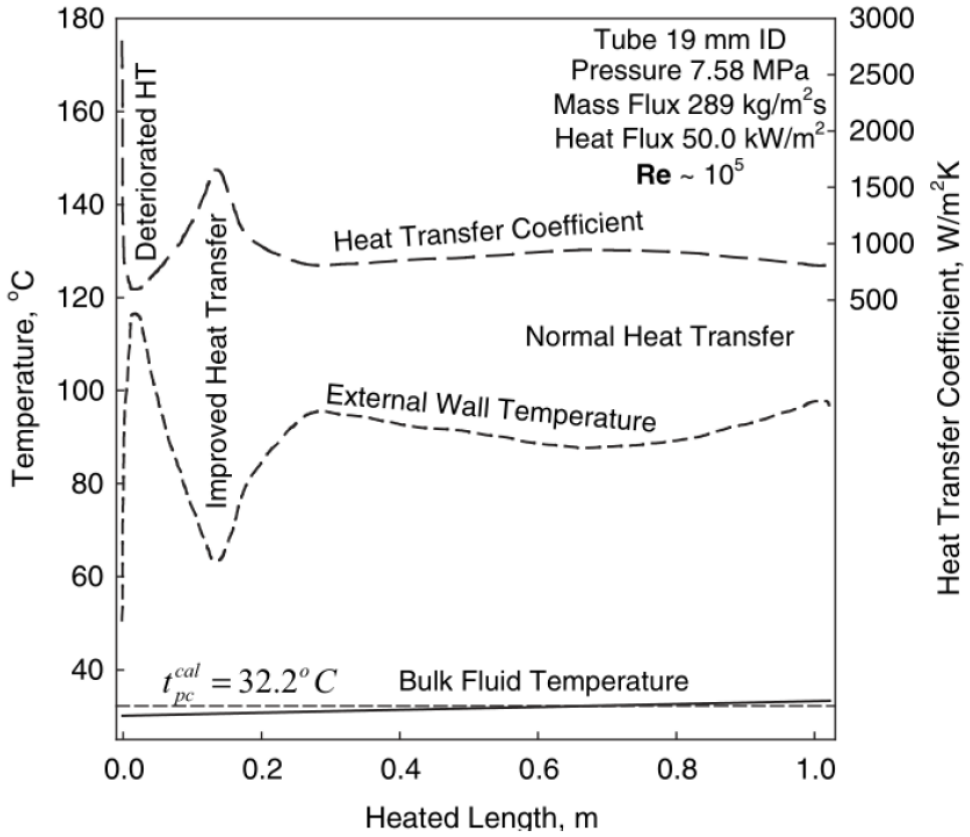

Figure 2.4: Wall temperature and heat transfer coefficient profiles along a vertical heated tube cooled by an upward flow of supercritical CO_2 showing the three heat transfer modes (Fewster, 1976).

the variable

$$T^* = \frac{T_b - T_{pc}}{T_{pc} - T_c} \tag{2.1}$$

(Ambrosini, 2011; Pucciarelli and Ambrosini, 2016). Plots of the same thermophysical properties *vs.* a normalised specific enthalpy H are also presented in this section. Two independent variables were also used: H_b/H_{pc} and

$$H^* = \frac{(H_b - H_{pc})}{c_{p,pc}}\beta_{pc}. \tag{2.2}$$

Additional plots of thermophysical properties of the three fluids showing a detail in the pseudocritical region have been included in Appendix A.

Figure 2.5 shows the relationships between the normalised enthalpies H/H_{pc} and H^* and the normalised temperatures T/T_{pc} and T^* for the three fluids. In all cases, there is a monotonic increase for either enthalpy with an increase of either temperature, but the rate of increase is much higher near the pseudocritical values than elsewhere, as a consequence of the large specific heat values in that region.

Figures 2.6, 2.7 , 2.8, 2.9 and 2.10 show, respectively, the variations of the normalised density, thermal conductivity, dynamic viscosity, Prandtl number and specific heat *vs.* normalised bulk temperatures (T_b/T_{pc} and T^*) and enthalpies (H_b/H_{pc} and H^*) for the three fluids H_2O, CO_2 and R134a. A perfect thermodynamic similarity of the three fluids would only be achieved if all three curves in each plot collapsed, but this is clearly not the case. For example, when plotted *vs.* a normalised temperature, the normalised densities for CO_2 and R134a are relatively close to each other, but significantly different from that for H_2O; when plotted *vs.* a normalised enthalpy, all three curves are distinct. Because of these differences, fluid-to-fluid scaling can only be approximate, if at all possible. A careful inspection of all plots did not reveal any significant advantage of using T^*, H_b/H_{pc} or H^* rather than the simpler variable T_b/T_{pc} in terms of collapsing the corresponding curves for the three fluids, or even a pair of fluids.

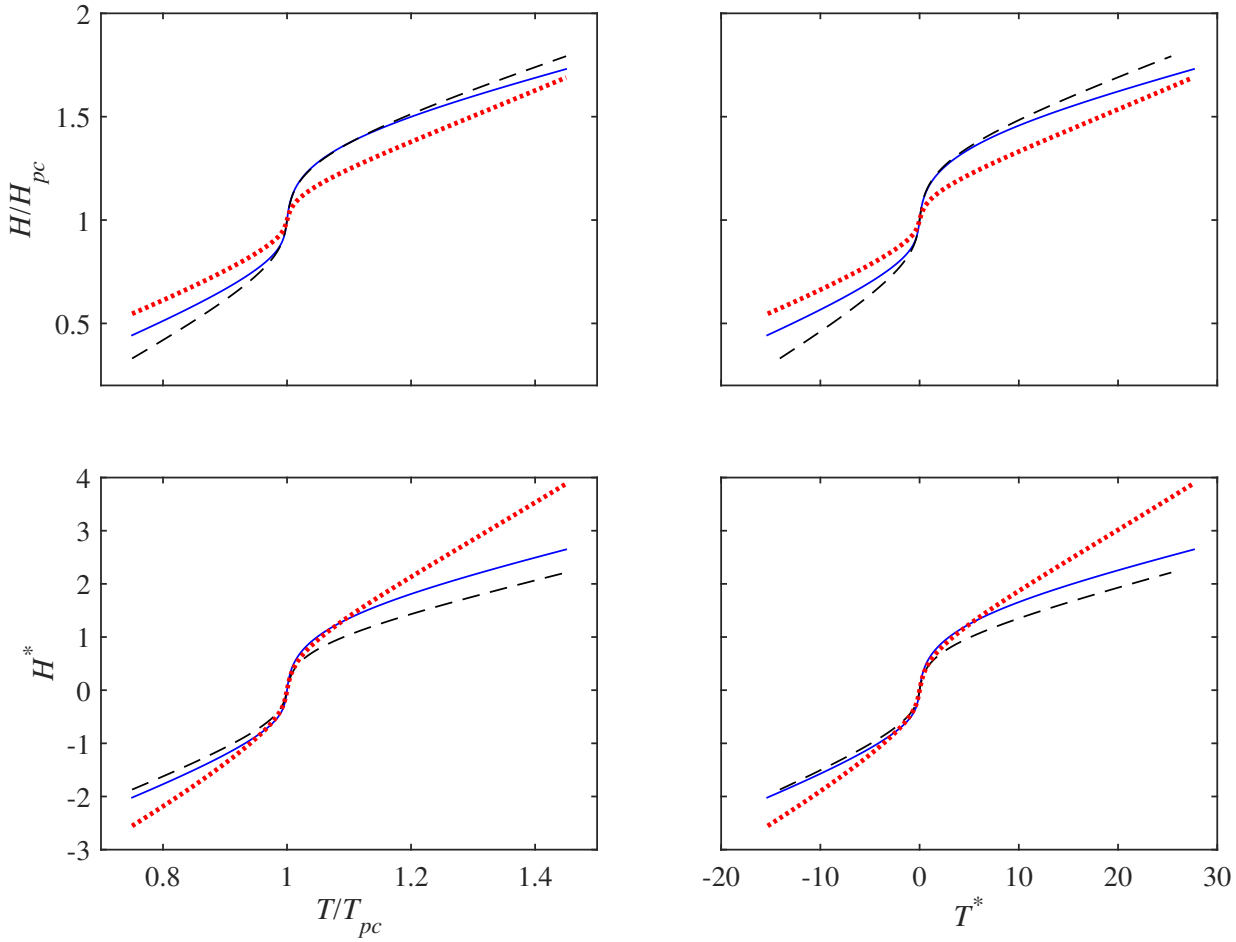

Figure 2.5: Normalised bulk enthalpies versus temperatures; blue solid, black dashed, and red dotted lines correspond, respectively, to H_2O, CO_2, and R134a (Lemmon et al., 2002).

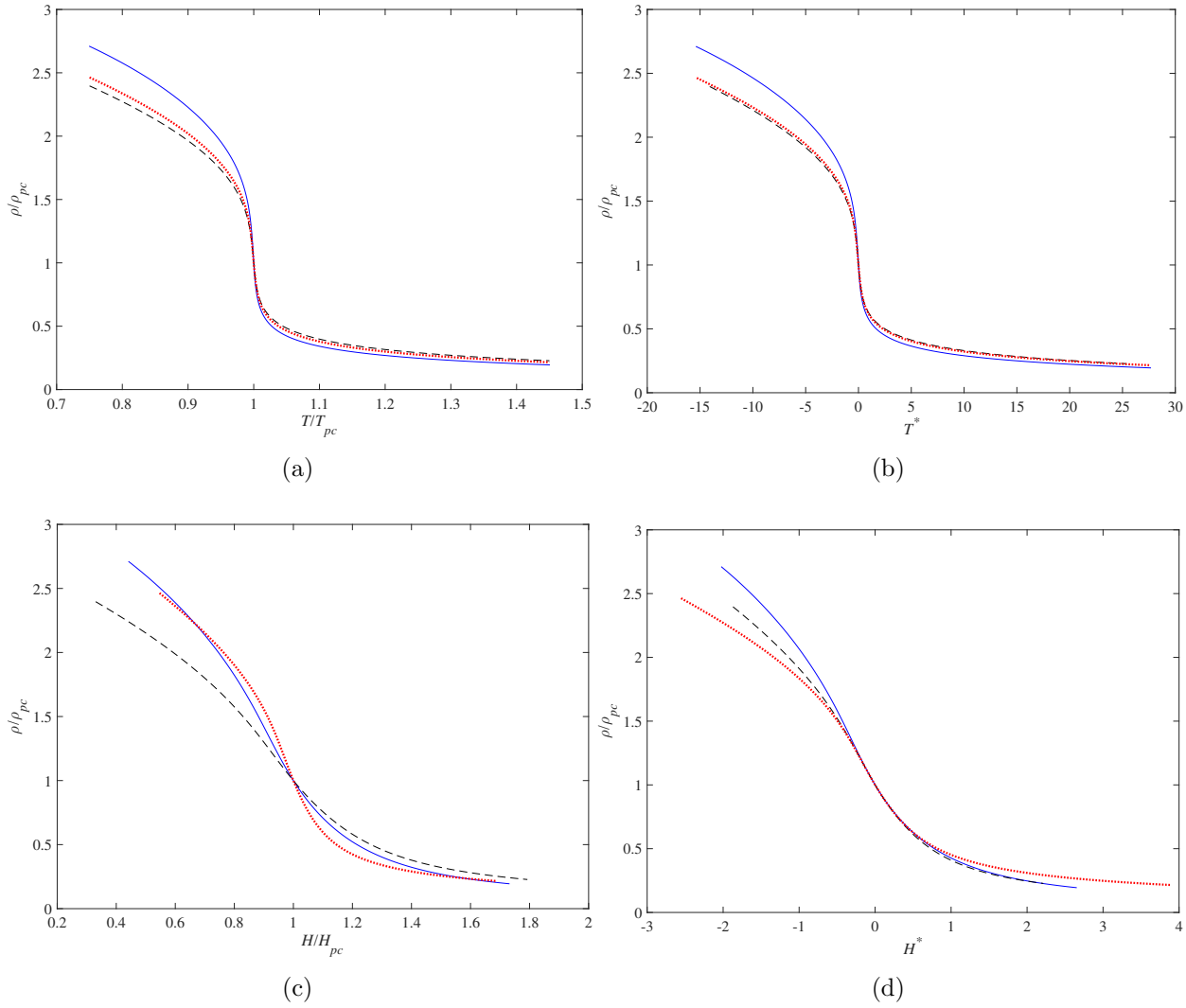

Figure 2.6: Thermophysical property variation of normalised density of the three fluids H_2O, CO_2 and R134a *vs.* normalised bulk temperatures (upper plots) and enthalpies (lower plots); blue solid, black dashed, and red dotted lines correspond, respectively, to H_2O, CO_2, and R134a (Lemmon et al., 2002).

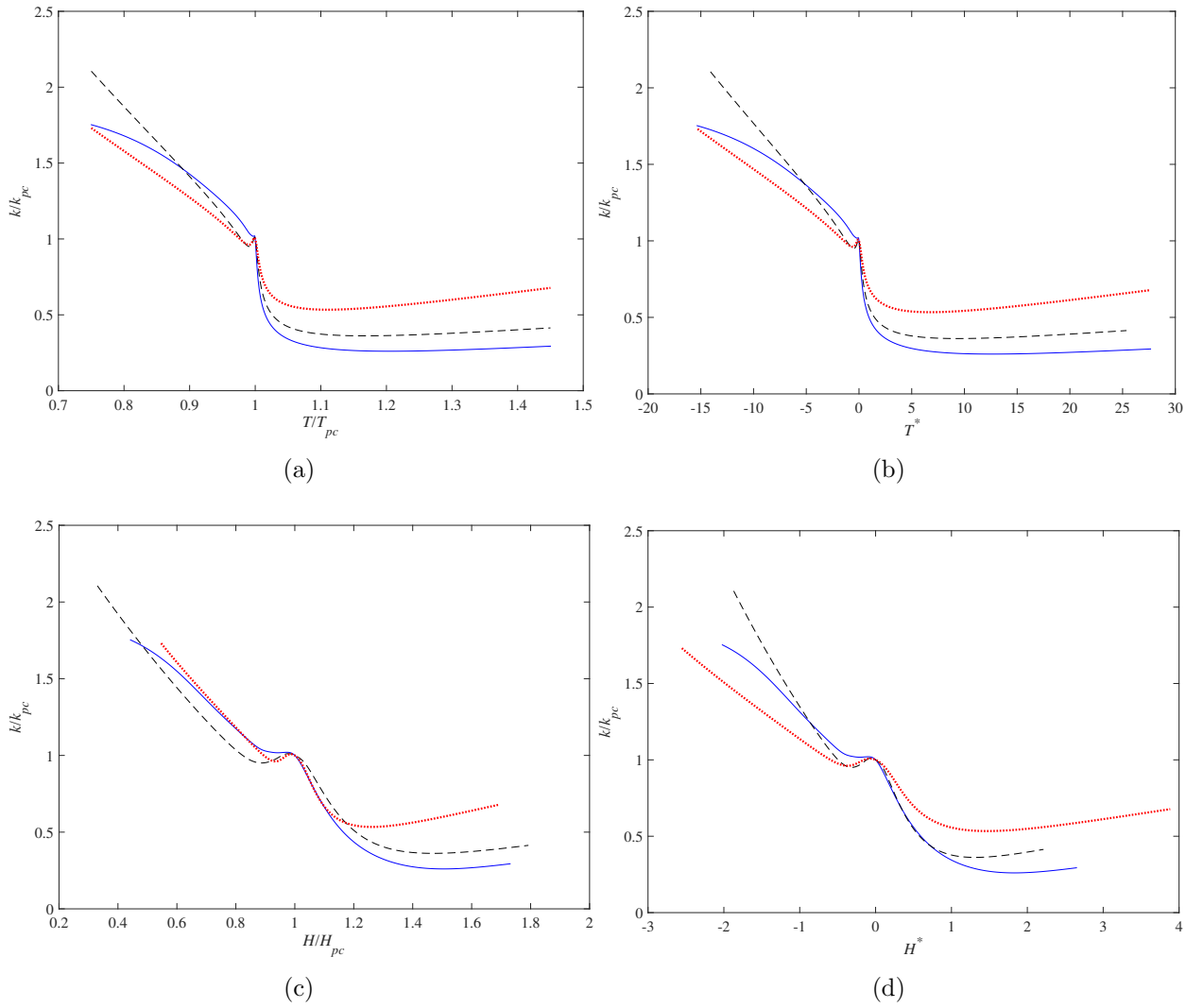

Figure 2.7: Thermophysical property of normalised thermal conductivity of the three fluids H_2O, CO_2 and R134a versus normalised bulk temperatures (upper plots) and enthalpies (lower plots); blue solid, black dashed, and red dotted lines correspond, respectively, to H_2O, CO_2, and R134a (Lemmon et al., 2002).

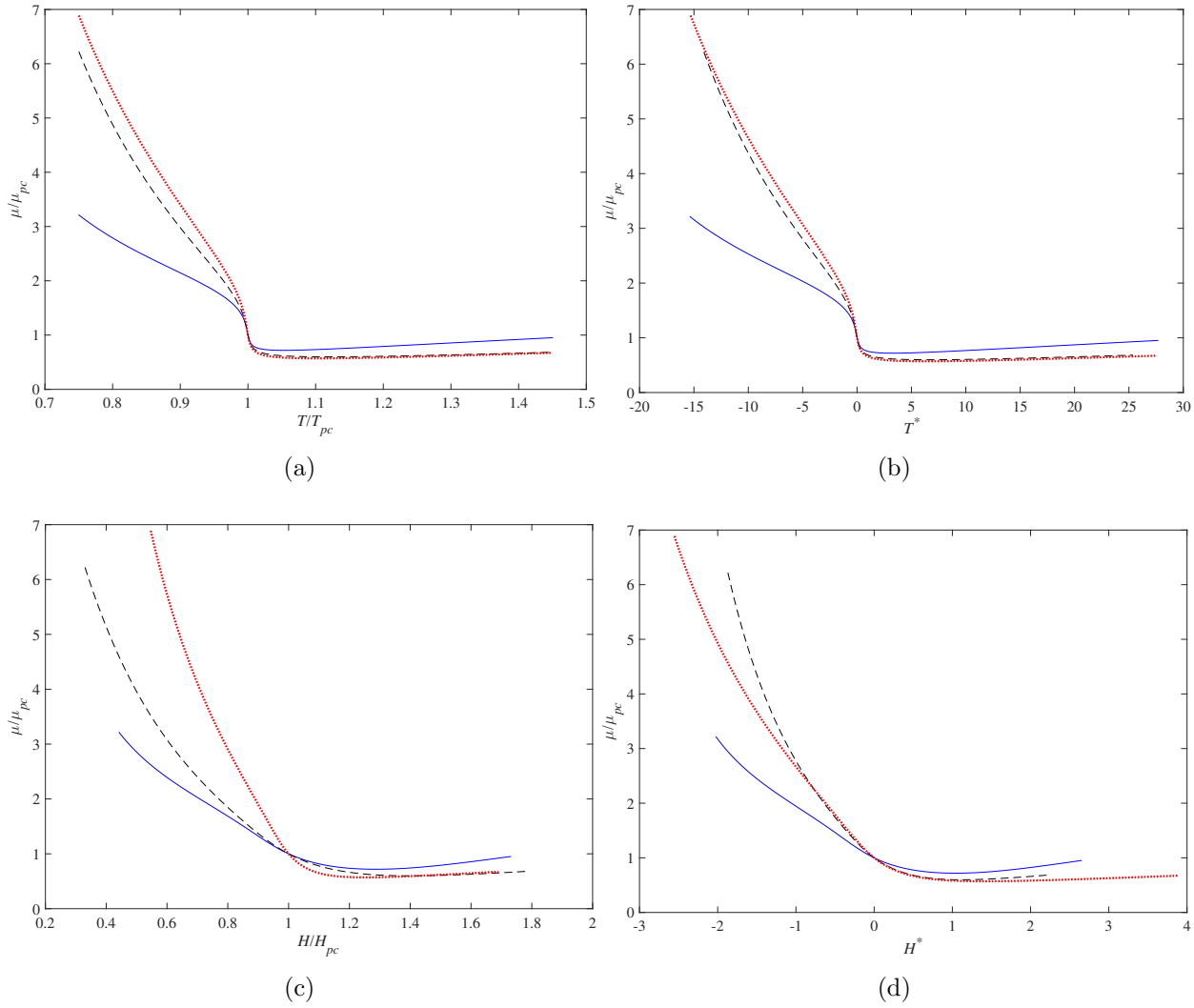

Figure 2.8: Thermophysical property of normalised dynamic viscosity of the three fluids H_2O, CO_2 and R134a *vs.* normalised bulk temperatures (upper plots) and enthalpies (lower plots); blue solid, black dashed, and red dotted lines correspond, respectively, to H_2O, CO_2, and R134a (Lemmon et al., 2002).

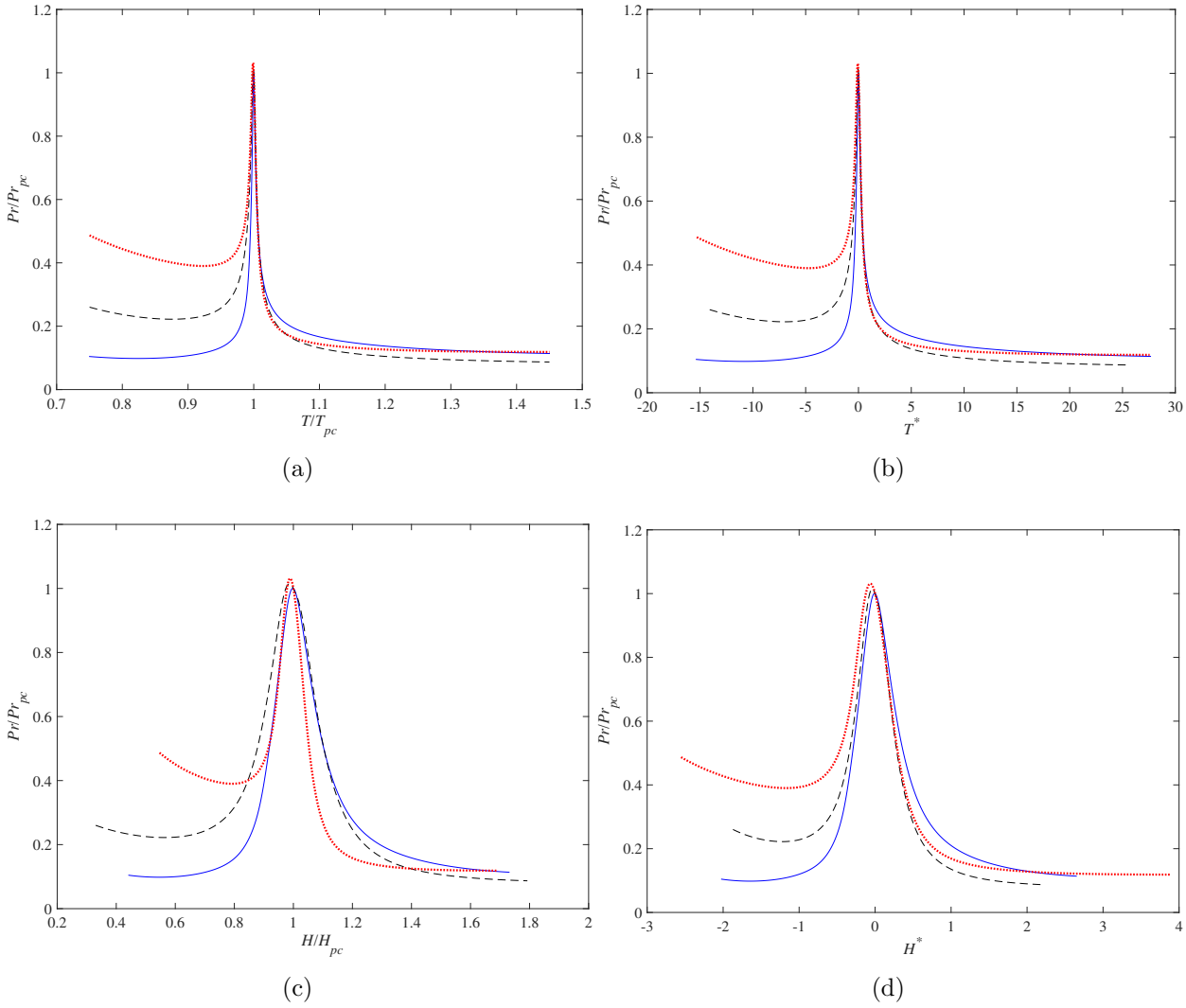

Figure 2.9: Thermophysical property of normalised Prandtl number of the three fluids H_2O, CO_2 and R134a versus normalised bulk temperatures (upper plots) and enthalpies (lower plots); blue solid, black dashed, and red dotted lines correspond, respectively, to H_2O, CO_2, and R134a (Lemmon et al., 2002).

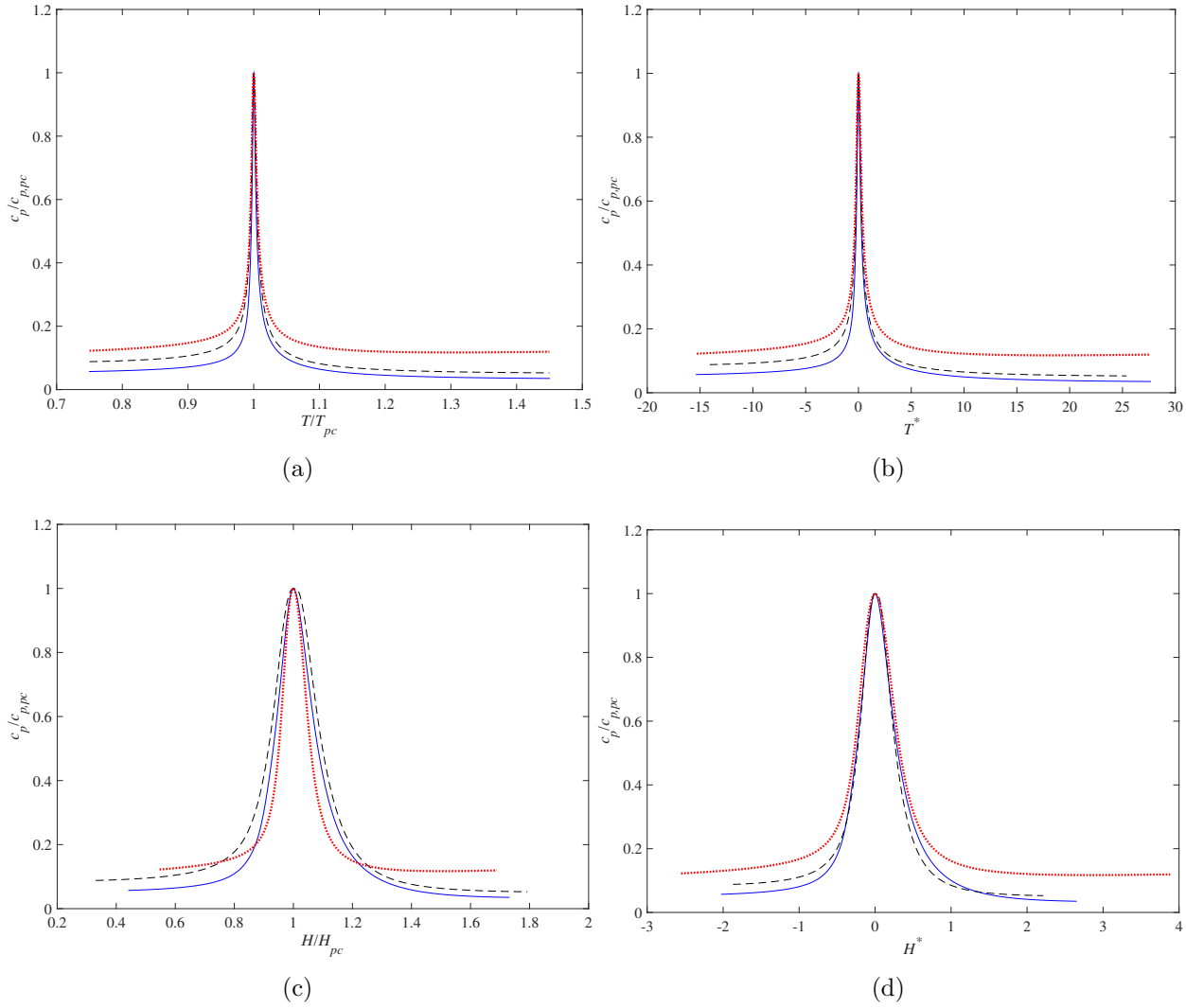

Figure 2.10: Thermophysical property of normalised specific heat of the three fluids H_2O, CO_2 and R134a versus normalised bulk temperatures (upper plots) and enthalpies (lower plots); blue solid, black dashed, and red dotted lines correspond, respectively, to H_2O, CO_2, and R134a (Lemmon et al., 2002).

2.4 Fluid-to-fluid scaling laws for supercritical fluids

A set of dimensionless flow equations for vertical upward forced convection in a tube with a heated wall were presented and analysed by Jackson and Hall (1979) with the objective of determining similarity conditions between two flows of the same fluid in different channels. This analysis was extended by Jackson (2007, 2008) but without explicitly presenting a complete set of scaling laws for two different fluids. All scaling of properties in this work was done for conditions at the inlet of the heated test section. A set of scaling laws for scaling heat transfer in supercritical H_2O to CO_2 at equivalent conditions was presented by Zwolinski et al. (2011). Like Jackson (2007, 2008), these authors also scaled the properties at inlet conditions, but, unlike the earlier work, they used the pseudocritical temperature, rather than the critical one, as a temperature scale. The scaling laws of Zwolinski et al. (2011) for two fluids 1 and 2 are as follows:

$$\left(\frac{z_h}{d}\right)_1 = \left(\frac{z_h}{d}\right)_2, \tag{2.3}$$

$$\left(\frac{P_{in}}{P_c}\right)_1 = \left(\frac{P_{in}}{P_c}\right)_2, \tag{2.4}$$

$$\left(\frac{T_{in}}{T_{pc}}\right)_1 = \left(\frac{T_{in}}{T_{pc}}\right)_2, \tag{2.5}$$

$$\left(\frac{Gd}{\mu_{in}}\right)_1 = \left(\frac{Gd}{\mu_{in}}\right)_2, \tag{2.6}$$

$$\left(\frac{qd}{k_{in}T_{in}}\right)_1 = \left(\frac{qd}{k_{in}T_{in}}\right)_2, \text{ and} \tag{2.7}$$

$$(Nu_{in})_1 = (Nu_{in})_2 \text{ or } \left(\frac{hd}{k_{in}}\right)_1 = \left(\frac{hd}{k_{in}}\right)_2. \tag{2.8}$$

In these relationships, scaling at a distance z_h from the inlet of the heated channel is based on the inlet conditions, rather than the local ones. This introduces significant uncertainty, because the thermophysical properties of supercritical fluids are very sensitive to the temperature, especially in the vicinity of the pseudocritical value. Another source of uncertainty is the fact that these laws do not account for Prandtl number differences between the two fluids, which could have a significant effect on heat transfer. Indeed, Zahlan et al. (2014) demonstrated that this approach resulted in excessive errors while scaling data in water to those in CO_2. Consequently, we will not consider these fluid-to-fluid scaling laws.

A set of supercritical fluid-to-fluid scaling laws that were based on the local bulk conditions was presented by Cheng et al. (2011). These laws were derived by an analysis of the continuity, momentum, energy and surface heat transfer equations. To eliminate the effect of channel geometry, these authors assumed that both fluids flowed vertically upward in long cylindrical tubes with the same inner diameter d. The difference between the local bulk temperature T_b and the pseudocritical temperature was scaled by the difference $T_{pc} - T_c$. This scale, however, vanishes at the critical point, near which scaling would be subjected to large uncertainty. The scaling of the wall heat flux q was based on an attempt to match the dimensionless temperature boundary conditions at the heated wall. To do so, the wall temperature would be required, but this would be generally unknown. To resolve this problem, Cheng et al. (2011) scaled the temperature difference $T_w - T_b$ by the scale $T_{pc} - T_c$. The mass flux G was scaled not by matching the local Reynolds numbers, but by matching the Nusselt numbers determined from the Dittus-Boelter correlation for convective heat transfer at low subcritical pressures. This correlation includes an empirical correction for the Prandtl number effect, which, however, is known to be inaccurate at supercritical pressures, especially near the pseudocritical temperature. The scaling laws of Cheng et al. (2011) are as follows:

$$d_1 = d_2, \tag{2.9}$$

$$\left(\frac{P}{P_c}\right)_1 = \left(\frac{P}{P_c}\right)_2, \tag{2.10}$$

$$\left(\frac{T_b - T_{pc}}{T_{pc} - T_c}\right)_1 = \left(\frac{T_b - T_{pc}}{T_{pc} - T_c}\right)_2, \tag{2.11}$$

$$\left(\frac{GdPr_b^{\frac{5}{12}}}{\mu_b}\right)_1 = \left(\frac{GdPr_b^{\frac{5}{12}}}{\mu_b}\right)_2, \tag{2.12}$$

$$\left(\frac{qd}{k_b(T_{pc} - T_c)}\right)_1 = \left(\frac{qd}{k_b(T_{pc} - T_c)}\right)_2, \text{ and} \tag{2.13}$$

$$(Nu_b)_1 = (Nu_b)_2 \text{ or } \left(\frac{hd}{k_b}\right)_1 = \left(\frac{hd}{k_b}\right)_2. \tag{2.14}$$

Ambrosini (2011) also suggested scaling laws for supercritical water, CO_2 and refrigerant R23. He scaled the streamwise location of the point of interest and the flow velocity at the inlet by introducing a parameter m, raised to the power $-3/2$, the value of which was set

to 2.0 for the CO_2-H_2O pair and to 2.5 for the $R23-H_2O$ pair. The local enthalpy was scaled by the pseudocritical volumetric expansion coefficient β_{pc} and the pseudocritical heat capacity $c_{p,pc}$. The heat flux was scaled by β_{pc}, $c_{p,pc}$, the area of the tube test section A and the mass flux G, which was calculated from the inlet velocity. The pressure was not scaled by the critical pressure, but by a pressure at which the maximum pseudocritical Prandtl number would match the value for water at the reference pressure of 25 MPa. The scaling expressions of Ambrosini (2011) are as follows:

$$z_{h,1} = m^{-3/2} z_{h,2}, \tag{2.15}$$

$$v_{in,1} = m^{-3/2} v_{in,2}, \tag{2.16}$$

$$\left(\frac{(H_b - H_{pc})\beta_{pc}}{c_{p,pc}}\right)_1 = \left(\frac{(H_b - H_{pc})\beta_{pc}}{c_{p,pc}}\right)_2, \text{ and} \tag{2.17}$$

$$\left(\frac{q\beta_{pc}}{AGc_{p,pc}}\right)_1 = \left(\frac{q\beta_{pc}}{AGc_{p,pc}}\right)_2. \tag{2.18}$$

These scaling laws will not be considered further, as they were based on inlet conditions and are incomplete for the present purposes.

Zahlan et al. (2014) suggested modified forms of the scaling laws of Cheng et al. (2011). Noting that the corresponding values of the ratio $(T_{pc} - T_c)/T_{pc}$ within a significant range of the ratio P/P_c are not very different for the three fluids CO_2, H_2O and R134a, they used T_{pc}, rather than $T_{pc} - T_c$, as a temperature scale, thus avoiding the singularity at the critical pressure. Moreover, instead of the original Dittus-Boelter correlation, they used a modified form that allows an empirical adjustment of the exponents in the Reynolds and Prandtl numbers, thus making it more accurate for supercritical fluids. These expressions allow for an empirical correction of mass flux scaling that accounts for Prandtl number effects. The exponent of this correction was computed by minimizing the error in the scaled heat transfer coefficient in CO_2 at conditions equivalent to those in water. The scaling expressions of

Zahlan et al. (2014) are as follows:

$$d_1 = d_2, \tag{2.19}$$

$$\left(\frac{P}{P_c}\right)_1 = \left(\frac{P}{P_c}\right)_2, \tag{2.20}$$

$$\left(\frac{T_b}{T_{pc}}\right)_1 = \left(\frac{T_b}{T_{pc}}\right)_2, \tag{2.21}$$

$$\left(\frac{GdPr_b^{0.66}}{\mu_b}\right)_1 = \left(\frac{GdPr_b^{0.66}}{\mu_b}\right)_2, \tag{2.22}$$

$$\left(\frac{qd}{k_b T_{pc}}\right)_1 = \left(\frac{qd}{k_b T_{pc}}\right)_2, \text{ and} \tag{2.23}$$

$$(Nu_b)_1 = (Nu_b)_2 \text{ or } \left(\frac{hd}{k_b}\right)_1 = \left(\frac{hd}{k_b}\right)_2. \tag{2.24}$$

Pucciarelli and Ambrosini (2016), among others, have attempted to use the results of numerical simulations instead of experimental results for testing fluid-to-fluid scaling laws, but found that their analyses were not sufficiently accurate for this purpose.

Feuerstein et al. (2017) developed scaling laws for normal and deteriorated supercritical heat transfer in water and R134a based on numerical and thermal resistance analyses. The predictions of HTC were assessed indirectly with the use of heat transfer correlations. As in previous scaling laws, the pressure was scaled by P_c. However, instead of scaling T_b, they scaled the difference of the local bulk enthalpy and pseudocritical enthalpy by the pseudocritical volumetric expansivity β_{pc} and the pseudocritical specific heat capacity $c_{p,pc}$. The heat flux was scaled in the same way as suggested by Cheng et al. (2011). The mass flux was scaled by introducing a new dimensionless group, which includes the Reynolds number raised to the power -0.9, the volumetric expansivity β, the heat flux q and the specific heat

c_p. The scaling expressions of Feuerstein et al. (2017) are as follows:

$$\left(\frac{P}{P_c}\right)_1 = \left(\frac{P}{P_c}\right)_2, \tag{2.25}$$

$$\left(\frac{(H_b - H_{pc})\beta_{pc}}{c_{p,pc}}\right)_1 = \left(\frac{(H_b - H_{pc})\beta_{pc}}{c_{p,pc}}\right)_2, \tag{2.26}$$

$$\left(\frac{qd}{k_b(T_{pc} - T_c)}\right)_1 = \left(\frac{qd}{k_b(T_{pc} - T_c)}\right)_2, \tag{2.27}$$

$$\left(\frac{q\beta Re^{-0.9}}{Gc_p}\right)_1 = \left(\frac{q\beta Re^{-0.9}}{Gc_p}\right)_2, \text{ and} \tag{2.28}$$

$$(Nu_b)_1 = (Nu_b)_2 \text{ or } \left(\frac{hd}{k_b}\right)_1 = \left(\frac{hd}{k_b}\right)_2. \tag{2.29}$$

As demonstrated in Section 2.3, the normalised thermophysical properties of the three fluids maintained significant differences when plotted against the normalised local bulk enthalpy H^* (Equation (2.2)) and so we do not see any advantage in using H^*, rather than the simpler normalised local bulk temperature T_b/T_{pc}, as an independent variable.

Azih and Yaras (2017) proposed scaling laws for deteriorated, normal and enhanced supercritical heat transfer in water, CO_2, He and R134a in tubes. They scaled the pressure and mass flux at the inlet conditions like Jackson (2007, 2008), and the reduced enthalpy at the inlet conditions like Ambrosini (2011). The same authors scaled the wall heat flux by $\beta_{pc}, c_{p,pc}$ and G. The scaling expressions of Azih and Yaras (2017) are as follows:

$$\left(\frac{P_{in}}{P_c}\right)_1 = \left(\frac{P_{in}}{P_c}\right)_2, \tag{2.30}$$

$$\left(\frac{(H_{in} - H_{pc})\beta_{pc}}{c_{p,pc}}\right)_1 = \left(\frac{(H_{in} - H_{pc})\beta_{pc}}{c_{p,pc}}\right)_2, \tag{2.31}$$

$$\left(\frac{Gd}{\mu_{in}}\right)_1 = \left(\frac{Gd}{\mu_{in}}\right)_2, \tag{2.32}$$

$$\left(\frac{q\beta_{pc}}{Gc_{p,pc}}\right)_1 = \left(\frac{q\beta_{pc}}{Gc_{p,pc}}\right)_2, \text{ and} \tag{2.33}$$

$$\left(\frac{g\beta_{in}q(\rho_{in}d)^2}{k_{in}G^2}\right)_1 = \left(\frac{g\beta_{in}q(\rho_{in}d)^2}{k_{in}G^2}\right)_2. \tag{2.34}$$

The first four of these expressions are sufficient to provide the scaled $P, T_{b,in}, G$ and q. The authors suggested using the last expression, which represents the equality of Richardson

numbers, as a check for the validity of scaling. The expectation of these laws is that scaling the inlet conditions would ensure similarity of the entire flow in the tube under, irrespectively of heat transfer mode. Azih and Yaras (2017) proposed a criterion for separating NHT and DHT cases, that was based on the values of Equations (2.30) and (2.33). A scrutiny of the assumptions made in the derivation of these laws is left for future work.

Most recently, Yu et al. (2018) introduced a scaling method in which they replaced the thermophysical properties by properties multiplied by the compressibility factor

$$z = \frac{P/\rho}{nRT} \tag{2.35}$$

or its inverse. In this expression, n, R and T are, respectively, the number of moles of the material, the gas constant and the absolute temperature. There is no scientific evidence that any of the thermophysical properties of different materials are related to their compressibility factors (Poling et al., 2001) and the plots presented by Yu et al. (2018) show little, if any, improvement in the tendency of the modified normalised properties for the three fluids to collapse on the same function of the normalised temperature by comparison to the correct thermophysical properties. The collapse of the ratios ρ^*/ρ^*_{pc} (and, equivalently, of the corresponding specific volume ratios) for the three fluids is a direct consequence of the definition of the modified density as the density of a perfect gas, namely, as $\rho^* = P/(nRT)$, which obviously does not apply to supercritical fluids. Yu et al. (2018) further stated that the modification factor (namely z) at pseudocritical conditions becomes equal to 1, a value that is far from the true one; for example, at $P/P_c = 1.13$ and $T_b = T_{pc}$, $z = 0.290, 0.300$ and 0.259, respectively, for R134a, CO_2, and H_2O. The scaling expressions of Yu et al. (2018)

are as follows:

$$\left(\frac{P}{P_c}\right)_1 = \left(\frac{P}{P_c}\right)_2, \tag{2.36}$$

$$\left(\frac{T_b}{T_{pc}}\right)_1 = \left(\frac{T_b}{T_{pc}}\right)_2, \tag{2.37}$$

$$\left(\frac{Gd}{\mu_b^*}\right)_1 = \left(\frac{Gd}{\mu_b^*}\right)_2, \tag{2.38}$$

$$\left(\frac{q}{Gd(H_{pc}-H_c)}\right)_1 = \left(\frac{q}{Gd(H_{pc}-H_c)}\right)_2, \tag{2.39}$$

$$\left(\frac{hd}{k_b^*}\right)_1 = \left(\frac{hd}{k_b^*}\right)_2, \tag{2.40}$$

where

$$\mu_b^* = \mu_b/z, \text{ and} \tag{2.41}$$

$$k_b^* = \begin{cases} k_b z & \text{for} \quad T_b < T_{pc} \\ k_b/z & \text{for} \quad T_b > T_{pc} \ . \end{cases} \tag{2.42}$$

In this scaling, the pressure and temperature have been scaled as in the scaling laws by Zahlan et al. (2014). Curiously, however, Yu et al. (2018) provide an example of scaling conditions in R134a to equivalent conditions in water, in which T_c, rather than T_{pc}, seems to have been used as a scale. As a result, the value of T_b reported by Yu et al. (2018) was 1.22% higher than the value corresponding to T_{pc}. Similarly, Yu et al. (2018) calculated values of G and q that correspond to T_c and were, respectively, 90% larger and 50% smaller than values corresponding to T_{pc}. The mass flux was scaled by matching the modified Reylolds numbers, thus not accounting for the Prandtl number effect. The heat flux was scaled by matching the enthalpy rise along a fixed length of the channel, normalised by the difference between the pseudocritical and critical enthalpies; this condition is different from the conditions proposed by Cheng et al. (2011) and Zahlan et al. (2014). The expressions proposed by Yu et al. (2018) are meant to scale fluids in tubes with different diameters, thus allowing additional uncertainty, which is not present in the previous two sets of scaling laws.

A summary of the previously discussed fluid-to-fluid scaling laws for normal supercritical convective heat transfer is given in Appendix F.

2.5 Calculation of equivalent conditions

Given a set of experimental conditions P, T_b, G and q in fluid 1, one can use available scaling laws to calculate the equivalent conditions in fluid 2. The direct method of testing the accuracy of these scaling laws is to perform experiments in fluid 2 at the equivalent conditions, measure the heat transfer coefficient $h_{exp,2}$ and compare it to the value $h_{sca,2}$, which is calculated from the experimental value h_1 with the use of the corresponding scaling law. Instead of this direct approach, previous authors have employed an indirect one, thus avoiding the need to perform new experiments in fluid 2. In the indirect approach, a value h_2 was calculated first and then it was used to compute a corresponding wall temperature T_w from the expression

$$q = h(T_w - T_b) \ . \tag{2.43}$$

T_w was used by Zahlan et al. (2014) to determine $h_{corr,2}$, as an estimate of $h_{exp,2}$ in water at conditions equivalent to those in CO_2, from the transcritical look-up tables (TC-LUT) of Zahlan et al. (2015b). A similar approach was presumably employed by Yu et al. (2018) to determine $h_{corr,2}$ in water at conditions equivalent to those in R134a from an empirical heat transfer correlation. The indirect approach has the obvious disadvantage of embedding the uncertainty of the TC-LUT or the heat transfer correlation into the scaling law uncertainty. Even if the TC-LUT or correlation were perfectly accurate, the value of $h_{corr,2}$ would not necessarily be the same as $h_{exp,2}$, because the value of T_w would not be the actual one but one determined under the assumption that the scaling laws apply perfectly to the case. An iterative procedure may turn out to give more accurate tests of scaling laws, but this has not yet been attempted.

Before proceeding to test the accuracy of the available fluid-to-fluid scaling laws, it seems worthwhile to compare the values of the corresponding equivalent conditions that are provided by different sets of scaling laws. To do so, we selected 10 representative sets of conditions corresponding to normal heat transfer in CO_2 flowing upwards in a tube with 8 mm ID (Kline et al., 2018) and then we used the different scaling laws to determine the equivalent conditions in R134a flowing in the same tube. Detail information regarding these 10 data points can be found in Appendix B. Based on a comparison of the scientific soundness and convincing demonstration of the predictive capability of each set of available laws, we chose

the ones by Zahlan et al. (2014) as a reference case and calculated the percent differences in equivalent condition values calculated from these and other scaling laws. Among the latter, we considered the scaling laws proposed by Cheng et al. (2011), Feuerstein et al. (2017) and Yu et al. (2018), as well as a set of the laws proposed by Yu et al. (2018), but with the actual thermophysical properties and not those modified by the compressibility factor; the main reason for the latter test is to evaluate the sensitivity of equivalent conditions to the scaling of wall heat flux. The results for each of the 10 selected points are listed in Tables 2.3 to 2.6, whereas Table 2.7 lists the averages and standard deviations of the percent differences between values in R134a predicted by different scaling laws and the scaling laws of Zahlan et al. (2014) over the set of 10 points.

A careful inspection of these tables, leads to the following observations.

- All four sets of scaling laws were applied at the same reduced pressure and so the corresponding means and standard deviations of pressure differences vanished.

- The standard deviations of the test conditions for all scaling laws were relatively small and so the means can be taken as representative of the corresponding percent differences at all 10 points. It is noted, however, that the mean and STD of the modified thermophysical properties by Yu et al. (2018) were very large, which is additional evidence of the inappropriateness of these parameters.

- An overall comparison of the mean differences between various properties scaled by the scaling laws of Cheng et al. (2011) and Feuerstein et al. (2017) from those of Zahlan et al. (2014) shows that they are all smaller than 10% and, with one exception (the heat flux predicted by the laws of Cheng et al. (2011) was about 9% smaller than the Zahlan et al. (2014) value, as a consequence of its insufficient correction for the Prandtl number effect), smaller than 4%. Consequently, we can confidently assess that tests of the Zahlan et al. (2014) laws may also serve as tests of these two other sets of fluid-to-fluid scaling laws.

- The laws proposed by Yu et al. (2018) resulted in very large differences in mass and heat fluxes. The differences between the modified values of viscosity and Prandtl number were 4.6 times larger than the corresponding actual values and their STD attained the

maximum possible value for positive random variables. In view of these irregularities and the previously observed theoretical and numerical inconsistencies of this work, these laws will not be considered any further.

- The scaling laws of Yu et al. (2018) with actual thermophysical properties, also resulted in large differences in the scaled mass and heat fluxes. The difference in G is attributed to the lack of correction for Prandtl number effects. The difference in q has in a small part the same source, but is mainly due to the scaling by the enthalpy difference. As will be shown in Chapter 4, HTD cases in CO_2 ended up to have NHT in R134a, when scaled by the Zahlan et al. (2014) laws. Reducing the heat flux by 65% will aggravate this discrepancy. Considering this and other limitations, we will also disregard the laws of Yu et al. (2018) with actual thermophysical properties.

The accuracy of the Azih and Yaras (2017) criterion for separating NHT and DHT cases was tested by three examples using measurements in CO_2 and R134a at equivalent conditions in the $d = 8$ mm tube at SCUOL.

- The first example is test #30 in Appendix B, for which NHT occurred in both fluids. The conditions in CO_2 were: $d = 8$ mm, $P = 8.34$ MPa, $T_{in} = 281$ K, $q = 125$ kW m^{-2}, $G = 1520$ kg m^{-2} s^{-1}, $H_{in} = 214$ kJ kg^{-1}, $\mu_{in} = 9.75 \times 10^{-5}$ Pa s, $k_{in} = 0.0065$ W m^{-1} K^{-1}, $\beta_{in} = 0.0065$ K^{-1}, $\rho_{in} = 922$ kg m^{-3}, $c_{p,pc} = 22.01$ kJ kg^{-1} K^{-1}, $q^* = 0.68 \times 10^{-3}$ (Equation (2.33), as defined by Azih and Yaras (2017)) and $Ri = 0.0017$. The corresponding equivalent test conditions in R134a were: $d = 8$ mm, $P = 4.59$ MPa, $T_{in} = 356$ K, $q = 72$ kW m^{-2}, $G = 1511$ kg m^{-2} s^{-1}, $H_{in} = 324$ kJ kg^{-1}, $\mu_{in} = 9.69 \times 10^{-5}$ Pa s, $k_{in} = 0.0595$ W m^{-1} K^{-1}, $\beta_{in} = 0.0073$ K^{-1}, $\rho_{in} = 959$ kg m^{-3}, $c_{p,pc} = 11.03$ kJ kg^{-1} K^{-1}, $q^* = 0.68 \times 10^{-3}$ and $Ri = 0.0022$. The values of q^* in both fluids were lower than the threshold value 10^{-3} by Azih and Yaras (2017) for NHT at $P/P_c = 1.13$, which means that the present results are compatible with the suggestion of these authors. It is noted that the modified Richardson number in R134a was 29% higher than that in CO_2. This is a measurable, albeit not excessive difference. The equivalent conditions in R134a, according to the Zahlan et al. (2014) laws (Appendix B), were $q = 96$ kW m^{-2} and $G = 1561$ kg m^{-2} s^{-1}. The scaled G by the two methods were nearly the same, while q was lower when scaled by the Azih and Yaras (2017)

method. This implies that, if tests were performed in R134a at conditions scaled by the latter method, they would be in NHT.

- The second example is test #8 in Appendix C, for which DHT occurred in CO_2 and NHT occurred in R134a. The conditions in CO_2 were: $d = 8$ mm, $P = 8.34$ MPa, $T_{in} = 283$ K, $q = 105$ kW m^{-2}, $G = 700$ kg m^{-2} s^{-1}, $H_{in} = 220$ kJ kg^{-1}, μ_{in} =9.33×10^{-5} Pa s, $k_{in} = 0.1065$ W m^{-1} K^{-1}, $\beta_{in} = 0.0070$ K^{-1}, $\rho_{in} = 906$ kg m^{-3}, $c_{p,pc} = 22.01$ kJ kg^{-1} K^{-1}, $q^* = 1.23 \times 10^{-3}$ and $Ri = 0.0073$. The corresponding equivalent test conditions in R134a were: $d = 8$ mm, $P = 4.59$ MPa, $T_{in} = 358$ K, $q = 61$ kW m^{-2}, $G = 703$ kg m^{-2} s^{-1}, $H_{in} = 328$ kJ kg^{-1}, μ_{in} =9.37×10^{-5} Pa s, $k_{in} = 0.0586$ W m^{-1} K^{-1}, $\beta_{in} = 0.0078$ K^{-1}, $\rho_{in} = 946$ kg m^{-3}, $c_{p,pc} = 11.03$ kJ kg^{-1} K^{-1}, $q^* = 0.71 \times 10^{-3}$ and $Ri = 0.0092$. The values of q^* in both fluids were compatible with the Azih and Yaras (2017) threshold. It is noted that the modified Richardson number in R134a was 26% higher than in CO_2, which once more demonstrates a measurable difference. The equivalent conditions in R134a, according to the Zahlan et al. (2014) laws (Appendix C), were $q = 80$ kW m^{-2} and $G = 720$ kg m^{-2} s^{-1}. The scaled G by the two methods were nearly the same, while q was lower when scaled by the Azih and Yaras (2017) method. This implies that, if tests were performed in R134a at conditions scaled by the latter method, they would be in NHT and so neither scaling procedure would result in DHT in both fluids.

- The third example is test #20 in Appendix C, for which DHT occurred in both fluids. The conditions in CO_2 were: $d = 8$ mm, $P = 8.34$ MPa, $T_{in} = 285$ K, $q = 115$ kW m^{-2}, $G = 701$ kg m^{-2} s^{-1}, $H_{in} = 225$ kJ kg^{-1}, μ_{in} =8.98×10^{-5} Pa s, $k_{in} = 0.1039$ W m^{-1} K^{-1}, $\beta_{in} = 0.0075$ K^{-1}, $\rho_{in} = 893$ kg m^{-3}, $c_{p,pc} = 22.01$ kJ kg^{-1} K^{-1}, $q^* = 1.35 \times 10^{-3}$ and $Ri = 0.0085$. The corresponding equivalent test conditions in R134a were: $d = 8$ mm, $P = 4.59$ MPa, $T_{in} = 360$ K, $q = 68$ kW m^{-2}, $G = 710$ kg m^{-2} s^{-1}, $H_{in} = 331$ kJ kg^{-1}, μ_{in} =9.10×10^{-5} Pa s, $k_{in} = 0.0578$ W m^{-1} K^{-1}, $\beta_{in} = 0.0083$ K^{-1}, $\rho_{in} = 933$ kg m^{-3}, $c_{p,pc} = 11.03$ kJ kg^{-1} K^{-1}, $q^* = 0.78 \times 10^{-3}$ and Ri= 0.0105. The value of q^* in CO_2 is higher than the Azih and Yaras (2017) threshold, but the one for R134a is significantly lower than this threshold, thus violating the expression suggested by these authors. It is noted that the modified Richardson number in R134a was 24%

higher than in CO_2, once more a measurable difference. The equivalent conditions in R134a, according to the Zahlan et al. (2014) laws (Appendix C), were $q = 87\ \mathrm{kW\,m^{-2}}$ and $G = 708\ \mathrm{kg\,m^{-2}\,s^{-1}}$. The scaled G by the two methods were nearly the same, while q was higher when scaled by the Azih and Yaras (2017) method. This implies that, if tests were performed in R134a at conditions scaled by the latter method, they would be in DHT.

Table 2.2 summarises the values of q^* and the experimentally observed heat transfer modes for the three previous examples. As mentioned previously, five of these cases were compatible with the Azih and Yaras (2017) threshold for DHT, however, the last case contradicted this criterion by a significant amount. This raises serious reservations concerning the use of this and possibly similar general criteria for separating cases with DHT from NHT in different fluids. The phenomenon of DHT is too complex to be described by simple semi-empirical relationships.

Table 2.2: Modified heat flux values and heat transfer modes for six present experiments in CO_2 and R134a for comparison with the Azih and Yaras (2017)DHT threshold $q^* \approx 10^{-3}$

Example #	Fluid	Heat transfer mode	q^*
1	CO_2	NHT	0.68×10^{-3}
	R134a	NHT	0.68×10^{-3}
2	CO_2	DHT	1.23×10^{-3}
	R134a	NHT	0.71×10^{-3}
3	CO_2	DHT	1.35×10^{-3}
	R134a	DHT	0.78×10^{-3}

Table 2.3: Ten test conditions in CO_2, at PR= 1.13, scaled to equivalent R134a by three distinct scaling laws

#	Property	CO_2 data (Kline et al., 2018)	Equivalent values for R134a				
			Zahlan et al. (2014)	Cheng et al. (2011)	Feuerstein et al. (2017)	Yu et al. (2018)	Yu et al. (2018) (actual properties)
1	P [MPa] (ΔP [%])	8.34	4.59	4.59 (0)	4.59 (0)	4.59 (0)	4.59 (0)
	T_b [K] (ΔT_b [%])	305	374	375 (0)	376 (0)	374 (0)	374 (0)
	G [$\mathrm{kg\,m^{-2}\,s^{-1}}$] ($\Delta G$ [%])	600	685	662 (-3)	701 (+2)	732 (+7)	682 (0)
	q [$\mathrm{kW\,m^{-2}}$] (Δq [%])	80	64	59 (-8)	63 (-1)	23 (-64)	22 (-66)
	h [$\mathrm{kW\,m^{-2}\,K^{-1}}$] ($\Delta h$ [%])	3.05	1.99	1.98 (0)	1.97 (-1)	1.85 (-7)	1.99 (0)
	k_b [$\mathrm{W\,m^{-1}\,K^{-1}}$] ($\Delta k_b$ [%])	0.0772	0.0503	0.0501 (0)	0.0498 (-1)	0.0098 (-81)	0.0503 (0)
	μ_b [Pa s] ($\Delta \mu_b$ [%])	5.5×10^{-5}	6.2×10^{-5}	6.1×10^{-5}(-2)	5.9×10^{-5}(-5)	3.2×10^{-4}(+413)	6.2×10^{-5}(0)
	Pr_b [-] (ΔPr_b [%])	3.76	3.74	3.84 (+3)	4.02 (+)8	19.17 (+413)	3.74 (0)
2	P [MPa] (ΔP [%])	8.34	4.59	4.59 (0)	4.59 (0)	4.59 (0)	4.59 (0)
	T_b [K] (ΔT_b [%])	304	373	374 (0)	375 (0)	373 (0)	373 (0)
	G [$\mathrm{kg\,m^{-2}\,s^{-1}}$] ($\Delta G$ [%])	700	786	766 (-3)	807 (+3)	858 (+9)	799 (+2)
	q [$\mathrm{kW\,m^{-2}}$] (Δq [%])	90	72	66 (-9)	71 (-1)	26 (-64)	24 (-66)
	h [$\mathrm{kW\,m^{-2}\,K^{-1}}$] ($\Delta h$ [%])	3.08	2.00	1.99 (-1)	1.97 (-1)	1.86 (-7)	2.00 (0)
	k_b [$\mathrm{W\,m^{-1}\,K^{-1}}$] ($\Delta k_b$ [%])	0.0784	0.0508	0.0506 (-1)	0.0501 (-1)	0.0097 (-81)	0.0508 (0)
	μ_b [Pa s] ($\Delta \mu_b$ [%])	5.7×10^{-5}	6.5×10^{-5}	6.4×10^{-5} (-2)	6.1×10^{-5} (-6)	3.4×10^{-4} (+425)	6.5×10^{-5} (0)
	Pr_b [-] (ΔPr_b [%])	3.47	3.55	3.64 (+2)	3.81 (+7)	18.65 (+425)	3.55 (0)
3	P [MPa] (ΔP [%])	8.34	4.59	4.59 (0)	4.59 (0)	4.59 (0)	4.59 (0)
	T_b [K] (ΔT_b [%])	304	373	374 (0)	375 (0)	373 (0)	373 (0)
	G [$\mathrm{kg\,m^{-2}\,s^{-1}}$] ($\Delta G$ [%])	700	786	766 (-3)	807 (+3)	859 (+9)	800 (+2)
	q [$\mathrm{kW\,m^{-2}}$] (Δq [%])	95	76	69 (-9)	75 (-1)	28 (-64)	26 (-66)
	h [$\mathrm{kW\,m^{-2}\,K^{-1}}$] ($\Delta h$ [%])	4.92	3.19	3.17 (-1)	3.14 (-1)	2.97 (-7)	3.19 (0)
	k_b [$\mathrm{W\,m^{-1}\,K^{-1}}$] ($\Delta k_b$ [%])	0.0785	0.0508	0.0506 (-1)	0.0501 (-1)	0.0097 (-81)	0.0508 (0)
	μ_b [Pa s] ($\Delta \mu_b$ [%])	5.7×10^{-5}	6.5×10^{-5}	6.4×10^{-5} (-2)	6.1×10^{-5} (-6)	3.4×10^{-4} (+425)	6.5×10^{-5} (0)
	Pr_b [-] (ΔPr_b [%])	3.46	3.55	3.63 (+2)	3.81 (+7)	18.64 (+425)	3.55 (0)

Table 2.4: Ten test conditions in CO_2, at PR= 1.13, scaled to equivalent R134a by three distinct scaling laws-Cont.

#	Property	CO_2 data (Kline et al., 2018)	Equivalent values for R134a				
			Zahlan et al. (2014)	Cheng et al. (2011)	Feuerstein et al. (2017)	Yu et al. (2018)	Yu et al. (2018) (actual properties)
4	P [MPa] (ΔP [%])	8.34	4.59	4.59 (0)	4.59 (0)	4.59 (0)	4.59 (0)
	T_b [K] (ΔT_b [%])	302	371	372 (0)	373 (+1)	371 (0)	371 (0)
	G [$\mathrm{kg\,m^{-2}\,s^{-1}}$] ($\Delta G$ [%])	1009	1107	1091 (-1)	1143 (+3)	1246 (+12)	1160 (+5)
	q [$\mathrm{kW\,m^{-2}}$] (Δq [%])	125	99	90 (-9)	97 (-2)	37 (-63)	34 (-66)
	h [$\mathrm{kW\,m^{-2}\,K^{-1}}$] ($\Delta h$ [%])	4.36	2.80	2.78 (-1)	2.74 (-2)	2.61 (-7)	2.80 (0)
	k_b [$\mathrm{W\,m^{-1}\,K^{-1}}$] ($\Delta k_b$ [%])	0.0807	0.0518	0.0514 (-1)	0.0507 (-2)	0.0096 (-82)	0.0518 (0)
	μ_b [Pa s] ($\Delta \mu_b$ [%])	6.1×10^{-5}	7.0×10^{-5}	6.8×10^{-5} (-2)	6.5×10^{-5} (-7)	3.8×10^{-4} (+441)	7.0×10^{-5} (0)
	Pr_b [-] (ΔPr_b [%])	3.13	3.36	3.42 (+2)	3.58 (+7)	18.14 (+441)	3.36 (0)
5	P [MPa] (ΔP [%])	8.34	4.59	4.59 (0)	4.59 (0)	4.59 (0)	4.59 (0)
	T_b [K] (ΔT_b [%])	293	360	362 (0)	366 (+2)	360 (0)	360 (0)
	G [$\mathrm{kg\,m^{-2}\,s^{-1}}$] ($\Delta G$ [%])	1502	1519	1551 (+2)	1583 (+4)	1897 (+25)	1765 (+16)
	q [$\mathrm{kW\,m^{-2}}$] (Δq [%])	100	76	69 (-9)	72 (-5)	30 (-60)	28 (63)
	h [$\mathrm{kW\,m^{-2}\,K^{-1}}$] ($\Delta h$ [%])	6.46	3.98	3.92 (-1)	3.77 (-5)	3.70 (-7)	3.98 (0)
	k_b [$\mathrm{W\,m^{-1}\,K^{-1}}$] ($\Delta k_b$ [%])	0.0935	0.0575	0.0567 (-1)	0.0546 (-5)	0.0097 (-83)	0.0575 (0)
	μ_b [Pa s] ($\Delta \mu_b$ [%])	7.7×10^{-5}	9.0×10^{-5}	8.7×10^{-5} (-3)	8.0×10^{-5} (-11)	5.4×10^{-4} (+495)	9.0×10^{-5} (0)
	Pr_b [-] (ΔPr_b [%])	2.38	2.98	3.01 (+1)	3.09 (+4)	17.75 (+495)	2.98 (0)
6	P [MPa] (ΔP [%])	8.34	4.59	4.59 (0)	4.59 (0)	4.59 (0)	4.59 (0)
	T_b [K] (ΔT_b [%])	300	369	370 (0)	372 (+1)	369 (0)	369 (0)
	G [$\mathrm{kg\,m^{-2}\,s^{-1}}$] ($\Delta G$ [%])	1500	1609	1602 (0)	1667 (+4)	1864 (+16)	1735 (+8)
	q [$\mathrm{kW\,m^{-2}}$] (Δq [%])	175	137	124 (-9)	133 (-3)	51 (-62)	48 (-65)
	h [$\mathrm{kW\,m^{-2}\,K^{-1}}$] ($\Delta h$ [%])	8.34	5.30	5.25 (-1)	5.15 (-3)	4.93 (-7)	5.30 (0)
	k_b [$\mathrm{W\,m^{-1}\,K^{-1}}$] ($\Delta k_b$ [%])	0.0835	0.0531	0.0526 (-1)	0.0516 (-3)	0.0095 (-82)	0.0531 (0)
	μ_b [Pa s] ($\Delta \mu_b$ [%])	6.4×10^{-5}	7.4×10^{-5}	7.3×10^{-5} (-3)	6.9×10^{-5} (-8)	4.1×10^{-4} (+456)	7.4×10^{-5} (0)
	Pr_b [-] (ΔPr_b [%])	2.86	3.21	3.26 (+2)	3.40 (+6)	17.83 (+456)	3.21 (0)

Table 2.5: Ten test conditions in CO_2, at PR= 1.13, scaled to equivalent R134a by three distinct scaling laws-Cont.

#	Property	CO_2 data (Kline et al., 2018)	Equivalent values for R134a				
			Zahlan et al. (2014)	Cheng et al. (2011)	Feuerstein et al. (2017)	Yu et al. (2018)	Yu et al. (2018) (actual properties)
7	P [MPa] (ΔP [%])	8.34	4.59	4.59 (0)	4.59 (0)	4.59 (0)	4.59 (0)
	T_b [K] (ΔT_b [%])	298	366	367 (0)	370 (+1)	366 (0)	366 (0)
	G [kg m^{-2} s^{-1}] (ΔG [%])	1499	1574	1582 (+1)	1634 (+4)	1875 (+19)	1744 (+11)
	q [kW m^{-2}] (Δq [%])	150	116	106 (-9)	112 (-4)	45 (-62)	41 (-65)
	h [kW m^{-2} K^{-1}] (Δh [%])	8.22	5.16	5.10 (-1)	4.98 (-4)	4.80 (-7)	5.16 (0)
	k_b [W m^{-1} K^{-1}] (Δk_b [%])	0.0868	0.0545	0.0539 (-1)	0.05 (-4)	0.0096 (-82)	0.0545 (0)
	μ_b [Pa s] ($\Delta \mu_b$ [%])	6.8×10^{-5}	8.0×10^{-5}	7.7×10^{-5} (-3)	7.2×10^{-5} (-9)	4.5×10^{-4} (+471)	8.0×10^{-5} (0)
	Pr_b [-] (ΔPr_b [%])	2.65	3.10	3.14 (+1)	3.26 (+5)	17.69 (+471)	3.10 (0)
8	P [MPa] (ΔP [%])	8.34	4.59	4.59 (0)	4.59 (0)	4.59 (0)	4.59 (0)
	T_b [K] (ΔT_b [%])	290	356	358 (+1)	363 (+2)	356 (0)	356 (0)
	G [kg m^{-2} s^{-1}] (ΔG [%])	1520	1507	1550 (+3)	1569 (+4)	1931 (+28)	1796 (+19)
	q [kW m^{-2}] (Δq [%])	125	94	85 (-9)	88 (-6)	38 (-60)	35 (-63)
	h [kW m^{-2} K^{-1}] (Δh [%])	6.38	3.87	3.81 (-2)	3.64 (-6)	3.60 (-7)	3.87 (0)
	k_b [W m^{-1} K^{-1}] (Δk_b [%])	0.0983	0.0596	0.0587 (-2)	0.0561 (-6)	0.0098 (-84)	0.0596 (0)
	μ_b [Pa s] ($\Delta \mu_b$ [%])	8.2×10^{-5}	9.7×10^{-5}	9.4×10^{-5} (-3)	8.5×10^{-5} (-13)	5.9×10^{-4} (+508)	9.7×10^{-5} (0)
	Pr_b [-] (ΔPr_b [%])	2.26	2.95	2.96 (0)	3.03 (+3)	17.94 (+508)	2.95 (0)

Table 2.6: Ten test conditions in CO_2, at PR= 1.13, scaled to equivalent R134a by three distinct scaling laws-Cont.

#	Property	CO_2 data (Kline et al., 2018)	Equivalent values for R134a				
			Zahlan et al. (2014)	Cheng et al. (2011)	Feuerstein et al. (2017)	Yu et al. (2018)	Yu et al. (2018) (actual properties)
9	P [MPa] (ΔP [%])	8.34	4.59	4.59 (0)	4.59 (0)	4.59 (0)	4.59 (0)
	T_b [K] (ΔT_b [%])	293	360	361 (0)	366 (+2)	360 (0)	360 (0)
	G [kg m^{-2} s^{-1}] (ΔG [%])	1520	1532	1566 (+2)	1597 (+4)	1922 (+25)	1788 (+17)
	q [kW m^{-2}] (Δq [%])	125	95	86 (-9)	90 (-5)	38 (-60)	35 (-63)
	h [kW m^{-2} K^{-1}] (Δh [%])	7.11	4.36	4.30 (-1)	4.13 (-5)	4.06 (-7)	4.36 (0)
	k_b [W m^{-1} K^{-1}] (Δk_b [%])	0.0943	0.0579	0.0571 (-1)	0.0549 (-5)	0.0097 (-83)	0.0579 (0)
	μ_b [Pa s] ($\Delta \mu_b$ [%])	7.8×10^{-5}	9.1×10^{-5}	8.8×10^{-5} (-3)	8.1×10^{-5} (-11)	5.4×10^{-4} (+497)	9.1×10^{-5} (0)
	Pr_b [-] (ΔPr_b [%])	2.36	2.98	3.00 (+1)	3.08 (+3)	17.77 (+497)	2.98 (0)
10	P [MPa] (ΔP [%])	8.34	4.59	4.59 (0)	4.59 (0)	4.59 (0)	4.59 (0)
	T_b [K] (ΔT_b [%])	295	363	364 (0)	368 (+1)	363 (0)	363 (0)
	G [kg m^{-2} s^{-1}] (ΔG [%])	1520	1561	1584 (+1)	1626 (+4)	1912 (+22)	1779 (+14)
	q [kW m^{-2}] (Δq [%])	125	96	87 (-9)	91 (-4)	37 (-61)	35 (-64)
	h [kW m^{-2} K^{-1}] (Δh [%])	7.90	4.91	4.84 (-1)	4.69 (-4)	4.57 (-7)	4.91 (0)
	k_b [W m^{-1} K^{-1}] (Δk_b [%])	0.0905	0.0562	0.0555 (-1)	0.0537 (-4)	0.0096 (-83)	0.0562 (0)
	μ_b [Pa s] ($\Delta \mu_b$ [%])	7.3×10^{-5}	8.5×10^{-5}	8.3×10^{-5} (-3)	7.7×10^{-5} (-10)	5.0×10^{-4} (+485)	8.5×10^{-5} (0)
	Pr_b [-] (ΔPr_b [%])	2.48	3.02	3.05 (+1)	3.15 (+4)	17.68 (+485)	3.02 (0)

Table 2.7: Means and standard deviations of percent differences of R134a properties, scaled from CO_2 properties, from corresponding values by Zahlan et al. (2014)

Property	Cheng et al. (2011)		Feuerstein et al. (2017)		Yu et al. (2018)		Yu et al. (2018) (actual properties)	
	Mean [%]	STD [%]	Mean [%]	STD [%]	Mean [%]	STD [%]	Mean [%]	STD [%]
Pressure, P	0	0	0	0	0	0	0	0
Temperature, T_b	+0.3	0	+1.0	1	0	0	0	0
Mass flux, G	-0.1	2	+3.5	1	+17.4	8	+9.2	7
Heat flux, q	-8.9	0	-3.3	2	-61.9	2	-64.6	1
HTC, h	-1.0	0	-3.3	2	-6.9	0	0	0
Thermal conductivity, k_b	-1.0	1	-3.3	2	-82.1	1	0	0
Dynamic viscosity, μ_b	-2.7	0	-8.7	3	+461.5	34	0	0
Prandtl number, Pr_b	+1.5	1	+5.4	2	461.5	34	+10.3	0

Chapter 3

Experimental facility and procedures

3.1 Experimental facility

The flow loop: A schematic diagram of the Supercritical University of Ottawa Loop (SCUOL), configured for operation with R134a, is shown in Figure 3.1. The same loop, although configured for operation with CO_2, has been described in detail by Jiang (2015) and Kline (2017). The characteristics of the main components of the loop are summarised in the following paragraphs.

R134a supply: The loop was filled from a low pressure (483 kPa) cylinder containing R134a (1,1,1,2 Tetrafluoroethane), supplied by Linde Canada Limited, Mississauga, Ontario, Canada. The cylinder was connected to the loop through a pressure regulator (Yellow Jacket® Brass Manifold Gauge "Serie 41"). The fluid in the cylinder is in a liquid state and has neither colour nor odour. The melting and boiling temperatures of R134a are, respectively, -101 °C and -36 °C. According to the supplier, when R134a is used and handled according to specification, it is not hazardous. Its ozone-depleting potential (ODP) is zero, whereas its global warming potential (GWP) is 1320 (DuPont™Suva®, 2005). According to Canadian law (Canada Gazette Part II, Vol. 137, No. 18, 2003) it is prohibited to release from a loop system any refrigerants CFH/HCFC/HFC/PFC into the atmosphere and a leak test must be done at least once per year (Government of Canada, 2017). If a leak is found, the leak must be repaired, or the refrigerant is to be recovered to prevent any loss of the

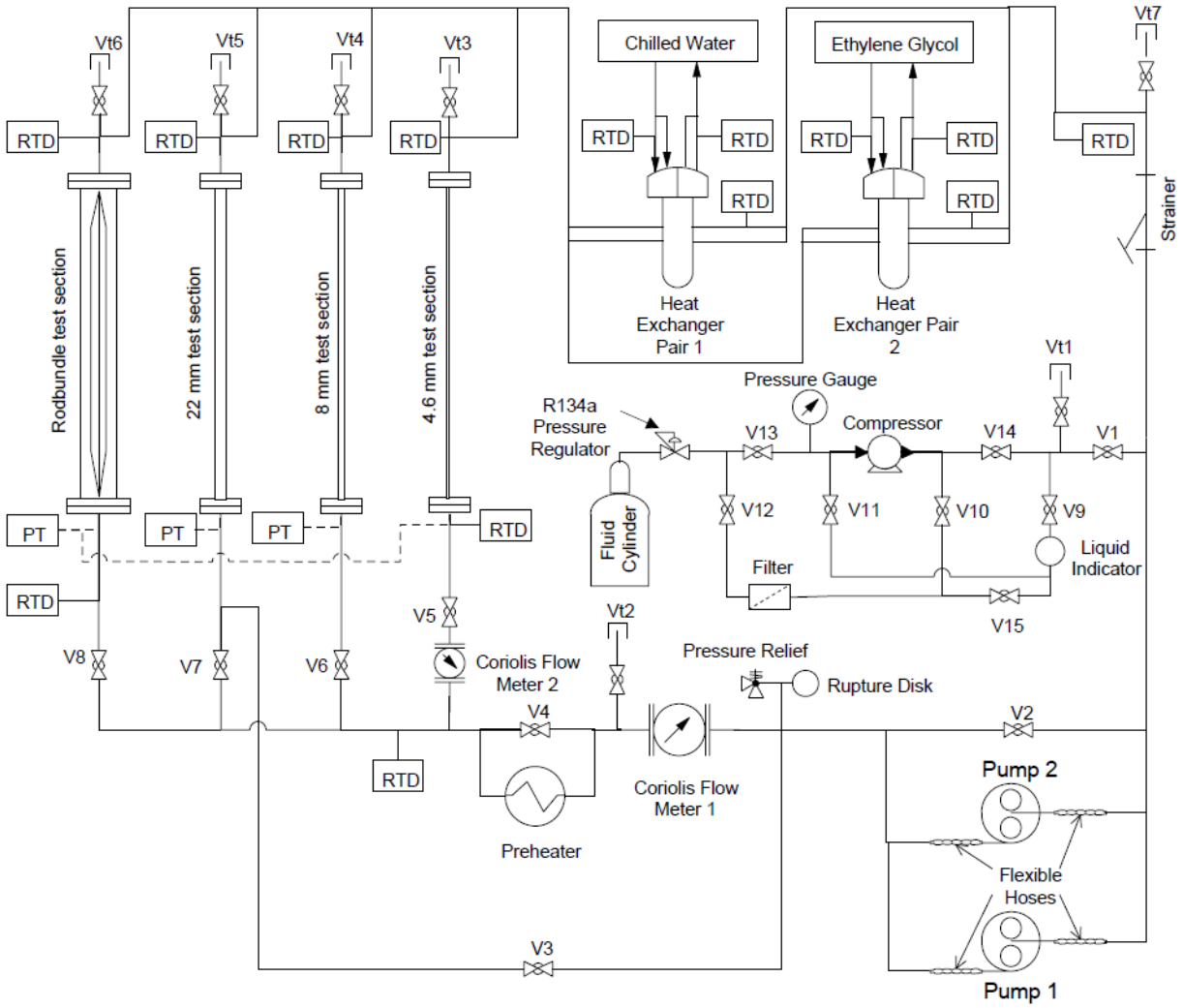

Figure 3.1: Schematic diagram of the multi-fluid loop; RTD marks the position of a resistance temperature detector; PT marks the position of a pressure transducer; Vx marks the position of valve x; Vtx marks the position of vent x.

fluid to the environment. A release report must be submitted to Ozone Protection Programs Section Environment Canada (OPPSEC) every six months if 10 to 100 kg of a refrigerant were lost. If the lost quantity of refrigerant exceeds 100 kg, OPPSEC must be informed within 24 h (Government of Canada, 2017).

Compressor and refrigerant recovery machine: This device (Yellow Jacket® - 95760 - Recover XL Unit 115/60) was installed in the loop and served the following purposes: i) it pumped the fluid from the low pressure cylinder into the loop; ii) it raised the pressure of the fluid in the loop from approximately 483 kPa to 1400 kPa; iii) it reduced the pressure of the fluid in the loop during testing, when it exceeded the desired value; and iv) it recovered the fluid after usage from the loop back to the cylinder. A liquid indicator (SA-12FM 1/4 in Female x Male Flare;) and a liquid filter (Emerson - 047602 - EK 052S) were connected to the loop with hoses (Yellow Jacket® 29986-1/4 in PLUS II) to ensure that the fluid was stored in a liquid state, it was not decomposed and had no impurities.

Pumps: Depending on the desired flow rate, one or two gear pumps (Micro Pump Model GL-H23.JFS.E-M2N1CH15) connected in parallel were used to circulate the working fluid through the loop. To ensure that sufficient fluid was always flowing through the pump(s), and thus to prevent possible pump overpressuring and/or overheating which could lead to failure, even if all test section isolation valves (V3 and V5 - V8 in Figure 3.1) were closed, some flow was always maintained in the bypass loop by keeping the bypass valve V2 partially open.

Preheater: The desired working fluid temperature T_{in} at the inlet of the test section was adjusted with the use of a 21.3 kW electrical preheater (CAST-X 3000 circulation heater, Part Number BX17E6G300U-WTT, Cast Aluminum Solutions, Batavia, Illinois, USA), designed to operate at a maximum pressure of 17.2 MPa.

Cooling systems: The working fluid was cooled by passing through two pairs of heat exchangers (Model FXF-6223U, Sentry Equipment Corp, Oconomowoc, Wisconsin, USA) in a configuration shown in Figure 3.2. The units in each pair were connected in parallel and the two pairs were also connected in parallel. The secondary fluids of the two pairs

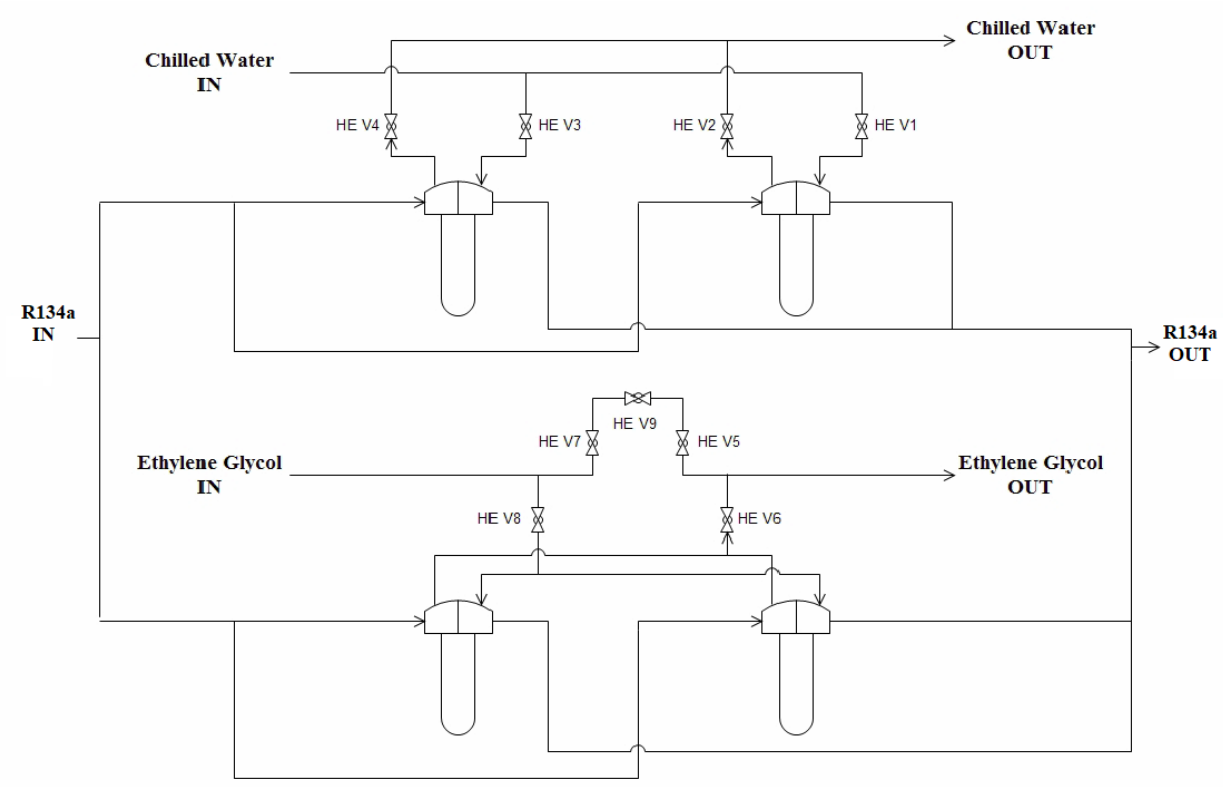

Figure 3.2: Schematic diagram of the heat exchanger flow configuration (adapted from Kline (2017)).

were, respectively, centrally supplied chilled water and ethylene glycol. Chilled water was supplied at approximately 9 °C during summer and 14 °C during winter. The flow rate of the chilled water was adjusted using valves HE V1 and HE V3. Ethylene glycol was supplied at a temperature ranging from 5 °C to 20 °C, depending on the desired inlet temperature of the working fluid in the test section, by a dedicated loop consisting of a reservoir, a radiator, two pumps (Dynapump® Model JSB-2HP-1S, Chempump, a division of Teikoku USA Inc., Houston, Texas, USA), and tubes connected to the pair of ethylene glycol heat exchangers. The reservoir and the radiator were installed in an adjacent walk-in freezer room. One pump circulated ethylene glycol from the reservoir through the heat exchangers, whereas a second pump circulated ethylene glycol from the reservoir through the radiator. Flow rate of ethylene glycol through the heat exchangers was regulated using valve HE V8.

Loop pressure regulation: In previous experiments, SCUOL was connected to bellows-type accumulators, which helped maintain an approximately constant pressure following changes in other operating parameters. These accumulators were disconnected from the loop, as it was found that they developed a leak, which contaminated the working fluid with Nitrogen that was contained in the secondary side of the accumulators. Loop pressure variations when operating the 4.6 mm, 8 mm or rod bundle test sections could be dampened by operating valve V3 in a secondary bypass branch connected to the 22 mm test section. When the 8 mm test section was used (valve V6 is open), the pressure variation of the loop was dampened by opening partially or fully valve V3 while valves V5, V7, and V8 were closed.

Test section: The test section (TS) used in the present study was a vertical tube with an inner diameter of 8 mm, a thickness of 1 mm and a heated length of 1940 mm, as seen in Figure 3.3. This tube was made of Inconel® 600 (Special Metals Corporation of Huntington, West Virginia, USA), having a density of 8470 $\mathrm{kg\,m^{-3}}$, a thermal conductivity of 14.9 $\mathrm{W\,m^{-1}\,°C}$ at 20 °C and an electrical resistivity of 1.03 $\mu\Omega\,\mathrm{m}$ at 20 °C.

The test section was thermally insulated with three layers of insulating materials as follows: i) a tape (Fibreglass-Reinforced Foil Tape, McMaster Carr, Ohio, USA), characterised by a maximum temperature of 315 °C, was wrapped around each thermocouple, ensuring that the self-adhesive silicone pad containing the wire of the thermocouple was in direct contact with the outer surface of the test section; ii) a fibreglass cloth ribbon was wrapped around the entire TS, providing some thermal insulation itself and protecting the thermocouples from the outer insulation; iii) the TS was wrapped by fibreglass pipe insulation (Rigid High-Temperature Fibreglass Pipe Insulation, McMaster Carr, Ohio, USA), characterised by a maximum temperature of 450 °C and 40 mm in thickness.

Power supply: The test section wall was heated directly by an electric current that was supplied by an electrical power supply, which is characterised by a maximum current of 3000 A and a nominal voltage of 60 V. The electrical power was drawn from the University's 380 V, 60 Hz, 3-phase AC power grid and the AC current was rectified so that the power provided to the TS was a non-negative voltage, fluctuating at a frequency of 360 Hz. Because

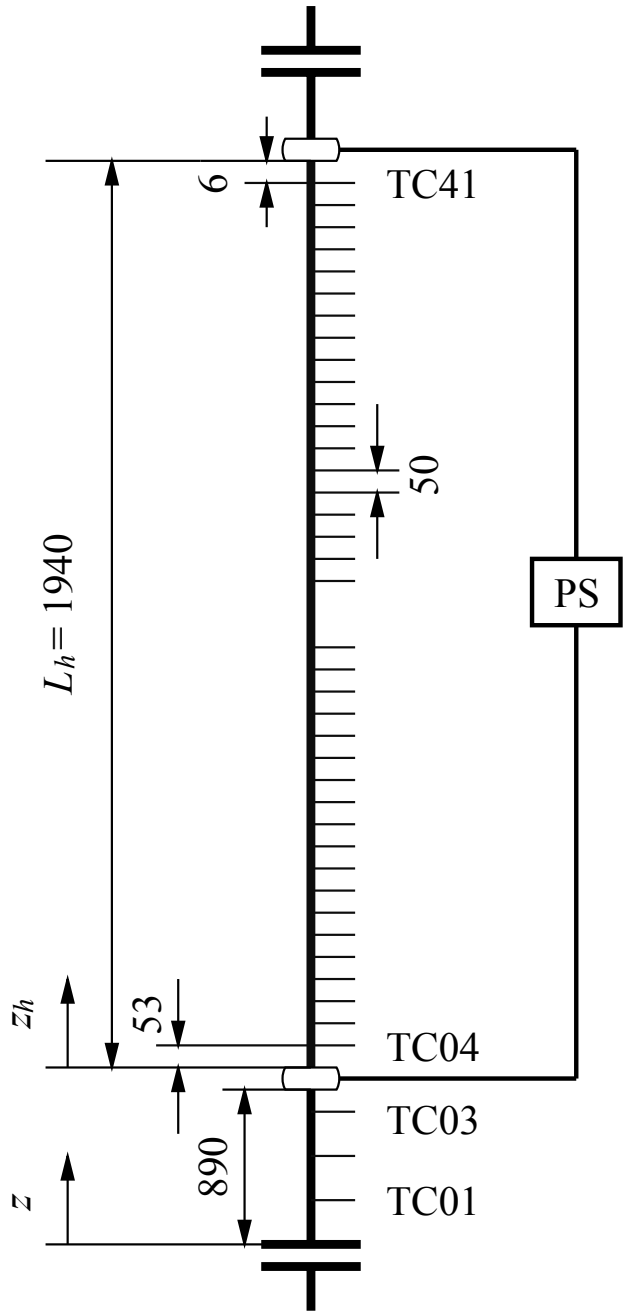

Figure 3.3: Schematic diagram of the SCUOL's 8 mm test section, showing the locations of the thermocouples; PS represents power supply; TC represents thermocouples; L_h represents test section's length; dimensions are in mm(Kline, 2017).

of the thermal inertia of the wall material, the wall temperature was maintained constant in time. Heavy electrical cables, rated at 500 A each, connected the power supply to machined copper blocks clamped at the two ends of the heated test section.

Safety devices: All tests were conducted while a high-volume room ventilation system and an oxygen depletion sensor (Oxyguard®, OxyGuard International A/S, Farum, Denmark) were in operation. To avoid excessive pressure build-up in the loop caused by unforeseen accidents, a high-pressure relief valve (Swagelok® SS-R4S8, Swagelok Central Ontario, Ontario, Canada) was installed and set to a maximum pressure of 9.65 MPa (1400 psia). A secondary safety device against over-pressurization of the loop was a rupture disc (25.4 mm PolySD Bolted Type Series, Fike Canada Inc., Burlington, Ontario, Canada), set to a maximum pressure of 10.3 MPa (1500 psia).

3.2 Measurement procedures

Details of the instrumentation and measurement procedures have been reported by Jiang (2015) and Kline (2017). Control of the facility operations and recording of measurements were performed with the use of a dedicated computerized data acquisition system (DAS - National Instruments, Austin, Texas, USA). The different modules of the DAS system are mentioned in the following paragraphs.

Test section voltage measurement: A 24-bit, high frequency, digital voltage measurement module (National Instrument NI 9225) was used to measure the time series of the voltage difference across the power clamps that provided power to the heated test section. The module had a range of ± 300 V and an uncertainty of 0.034 V. A function in the Labview data acquisition program was used to calculate the RMS voltage.

Mass flow rate measurement: The mass flow rate of R134a in the test section was measured by a Coriolis flow meter (Micro Motion ELITE CFM050M320N0A2E2ZZ) with an uncertainty of 0.05%.

Pressure measurement: The absolute pressure at the inlet of the test section was measured with a pressure transducer (Omega PX01C1-3KA5T) with an uncertainty of 214 kPa. This was used as the nominal pressure for the entire test section.

Inlet and outlet fluid temperature measurement: The fluid temperatures at the inlet and outlet of the test section were measured with ultra-precise immersion RTD sensors (Omega P-M-1/10-1/8-5-1/2-G-15) having a range from 0 °C to 100 °C and an uncertainty of 0.35 K.

Test section wall temperature measurement: The test section wall temperature was measured using 44 T-type thermocouples (Omega SA1XL-T-SRTC) attached to the TS outside wall. These had an uncertainty of 0.50 K and a time constant that was at most 0.15 s.

Heating power calculation: The electrical resistance of the heated test section was determined as

$$R = \frac{\rho_e L_h}{A}, \tag{3.1}$$

where ρ_e is the electrical resistivity of Inconel® provided by Special Metals and Sancro® supplied by Sandvik, L_h is the heated length and A is the cross-sectional area of the TS wall. The values of these parameters (Jiang, 2015) are listed in Table 3.1. The measured

Table 3.1: Electrical properties of the test section

Test Section (Material)	ρ_e ($\mu\Omega \cdot$ m)	L_h (m)	A_{cs} (m^2)	R (Ω)
8 mm tube (Inconel® 600)	1.03	1.94	2.827×10^{-5}	0.0707

RMS voltage V_{rms} and the TS electrical resistance were used to calculate the electrical power as

$$Q = \frac{V_{rms}^2}{R}. \tag{3.2}$$

Wall heat flux calculation: Under the assumption that there were no heat losses to

the surroundings or axial heat conduction to the unheated test section, the wall heat flux was calculated as

$$q = \frac{Q}{\pi d L_h}. \tag{3.3}$$

Inner wall temperature calculation: The inner wall temperature T_w of the heated test section was estimated from the axisymmetric heat diffusion equation with uniform internal energy generation as

$$T_w = T_{w,o} + \frac{2q_{loss}r_o - q_v {r_o}^2}{2k} ln\left(\frac{r_o}{r_i}\right) + \left({r_o}^2 - {r_i}^2\right)\frac{q_v}{4k}, \tag{3.4}$$

where $T_{w,o}$ is the measured local outer wall temperature, q_{loss} is the heat loss to the environment (neglected in this analysis), r_o is the tube outer radius, r_i is the tube inner radius, k is the local thermal conductivity of the TS material, and q_v is the volumetric heat generation that was calculated as

$$q_v = \frac{Q}{\pi\left({r_o}^2 - {r_i}^2\right) L_h}. \tag{3.5}$$

The local thermal conductivity k of Inconel® 600 was estimated from the local outer wall temperature using the following linear fit (Jiang, 2015) to data in the range from 20 °C to 300 °C provided by the manufacturer

$$k = 0.0146 T_{w,o} + 14.509. \tag{3.6}$$

Bulk fluid enthalpy calculation: The bulk fluid specific enthalpy along the heated test section was calculated from the simplified energy equation as

$$H_b = H_{b,in} + \frac{Q}{\dot{m}}\frac{z_h}{L_h}, \tag{3.7}$$

where $H_{b,in}$ is the inlet bulk enthalpy, $\dot{m}$ is the mass flow rate, and z_h is the vertical distance along the heated TS. The corresponding local bulk fluid temperature T_b and the thermophysical properties of R134a were calculated from the NIST database (Lemmon et al., 2002).

Heat transfer coefficient calculation: The local convective heat transfer coefficient was calculated as

$$h = \frac{q}{T_w - T_b}. \tag{3.8}$$

3.3 Power imbalance estimation

Application of the steady first law of thermodynamics to a control volume that surrounds the heated test section provides the imbalance between the heating power Q and the power Q_{fluid} given to the working fluid as

$$\Delta Q = Q - Q_{fluid} = Q - \dot{m}\left[\left(H_{b,out} + \frac{v_{out}^2}{2} + gz_{h,out}\right) - \left(H_{b,in} + \frac{v_{in}^2}{2} + gz_{h,in}\right)\right]. \quad (3.9)$$

In this expression, $H_{b,in}$ and $H_{b,out}$ are the bulk specific enthalpies of the fluid evaluated at the inlet and outlet temperatures measured by the corresponding RTDs; v_{in} and v_{out} are the corresponding bulk fluid velocities, calculated from the measured mass flux $\dot{m}$ and density values evaluated at the inlet and outlet temperatures; and $z_{h,in}$ and $z_{h,out}$ are the elevations of the inlet and outlet positions. The percent power imbalance, which represents an overall relative measurement error, was calculated as

$$Q_e = \left(1 - \frac{Q_{fluid}}{Q}\right) \times 100. \quad (3.10)$$

Figure 3.4 shows that the percent power imbalance was lower than 5% for 65% of the examined cases and that this imbalance exceeded 10% only for three cases at very low heating powers. This error may be attributed in part to instrumentation uncertainty and in part to the uncertainty of thermophysical property values.

3.4 Loop operation procedures

Determination of operating conditions: First, a number of points in the CO_2 databases for the 8 mm test section compiled by Zahlan et al. (2015a) and Kline et al. (2018) were selected. It was ensured that the measurements at all these points were collected at locations that were away from the heated section ends. The values of pressure, local bulk temperature, mass flux, wall heat flux and local heat transfer coefficient were recorded for each point in the CO_2. These values were converted to equivalent values in R134a using the fluid-to-fluid scaling laws of Zahlan et al. (2014). For each set of these values, the loop operation was adjusted so that measurements in R134a at the equivalent pressure, mass flux, wall heat flux and local bulk temperature could be collected at a specific location of the test section.

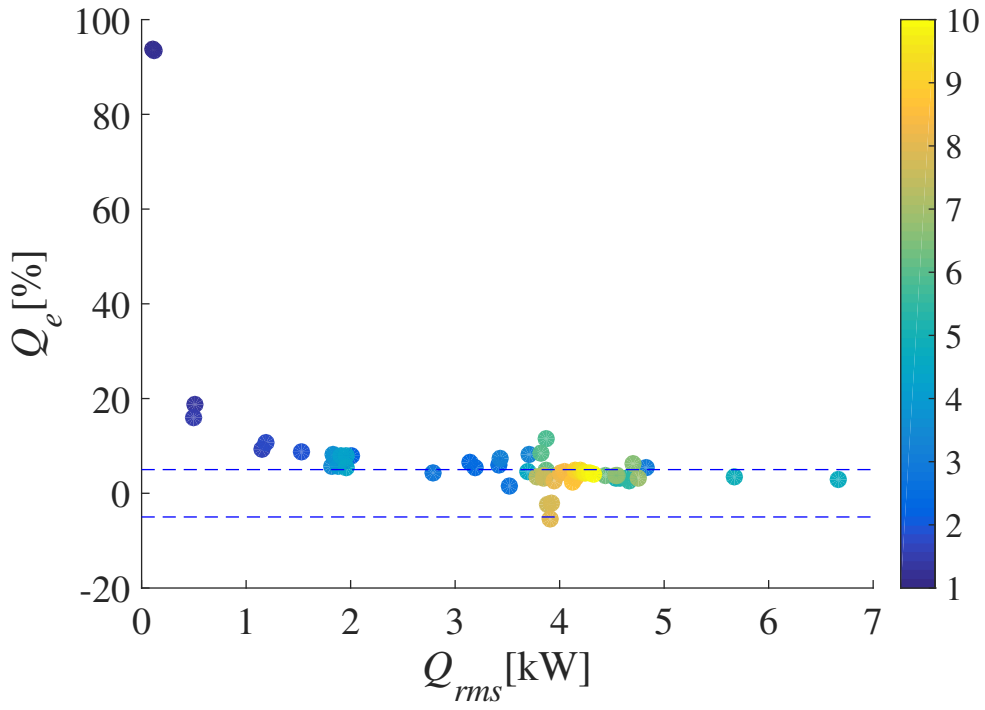

Figure 3.4: Percent power imbalance error versus heating power; blue dashed lines represent ±5% error.

The following paragraphs explain the procedures that were used for adjusting the values of various parameters.

Pressure and mass flux adjustment: A typical set of measurements that were collected during a day corresponded to fixed pressure and mass flux and specified ranges of heat flux and inlet temperature. The loop was filled with liquid R134a from the Freon cylinder using the compressor machine (Figure 3.1) until the pressure of the test section (TS) became approximately 1.40 MPa. To extract the necessary quantity for the day from the cylinder, the freezer room and the ethylene glycol temperatures, respectively, were set to $-30\,^{\circ}\mathrm{C}$ and $20\,^{\circ}\mathrm{C}$ and the flow rate of the chilled water supplied to the pair of the chilled water heat exchangers was adjusted with the use of valves HE V1 and HE V2 (Figure 3.2). To control the pressure and mass flux in the TS, bypass valves V2 and V3 (Figure 3.1) were set to fifty percent open, while valves V5, V7 and V8 were closed. As needed, one or two pumps were used and set gradually from 0 to 90% of the motor capacity to get a steady flow in the loop. Then, the power to the test section and the preheater were turned on and gradually increased to the lowest targeted settings for the planned test matrix of the day. As the temperature of the fluid in the loop increased by either increasing the power to the TS and/or the inlet temperature by increasing the preheater temperature, the pressure would increase. When the pressure of the loop exceeded the desired value, valve V1 (Figure 3.2) was operated to bleed the necessary amount of R134a from the loop to the cylinder so that the loop pressure was reduced to the desired level. It is noted that the loop pressure also changed following changes in the ethylene glycol temperature or the mass flow rate of the chilled water, which could be controlled using valves HE V1 and HE V2 (Figure 3.2). More details about mass flux adjustments were reported by Kline (2017).

Heat flux and inlet temperature adjustment: After all conditions for a particular test were achieved, measurements were recorded during approximately 1 min, which is equivalent approximately to 350 KiB of data in a text file. It is noted that steady state was achieved within 1 min to 5 min after the heat flux was adjusted and within 10 min to 30 min after the inlet temperature was adjusted. At the end of the day, the loop was shut down by following the shutdown guidelines.

Chapter 4

Results and discussion

4.1 Selection of data in carbon dioxide tests

All present tests of fluid-to-fluid scaling laws were performed in three fluids, CO_2, R134a and H_2O, at conditions that were equivalent to those in selected CO_2 data measured in SCUOL at specified locations in a tube with 8 mm ID, as reported by Zahlan et al. (2015a) and Kline et al. (2018). To avoid strong effects of thermal boundary layer development, all data were taken at locations that were significantly downstream of the heated section entrance. All data were taken at a pressure $P = 1.13P_c$, which is the design pressure of the Canadian SCWR. The range of T_b was chosen wide enough to include T_{pc} and the range of G was as wide as possible so that the chosen data points were representative of the entire set of data available from SCUOL. The range of q was also fairly wide, so that both NHT (39 points) and DHT (23 points) data were included in the tests. The experimental conditions corresponding to all CO_2 tests considered are listed in Appendix B for NHT and in Appendix C for DHT.

4.2 Calculation of equivalent conditions

For each set of conditions P, T_b, G and q in CO_2 (both NHT and DHT), equivalent conditions in R134a and H_2O were computed with the use of the scaling laws of Zahlan et al. (2014). The values of h predicted by these scaling laws for R134a and H_2O, based on measurements

of h in CO_2, were also calculated. The corresponding experimental values h_{exp} in R134a were found directly by performing new measurements at the equivalent conditions. To keep the uncertainty as low as possible, we applied the equivalent conditions in R134a at the same location of the test section as in the CO_2 tests, so that measurements of wall temperature in both fluids were taken with the same thermocouple. This was achieved by calculating the appropriate inlet temperature T_{in} in the R134a tests from the energy equation along the test section (Equation (3.7)). The experimental HTC in H_2O was approximated by the corresponding value of h_{corr} given by the TC-LUT of Zahlan et al. (2015b), which applies to both NHT and mild DHT. The values of all required properties were determined from the NIST tables. Table 4.1 lists a summary of the ranges of conditions for the three fluids of interest.

An example of the calculation of conditions in R134a and water that are equivalent to conditions measured in CO_2 in the $d = 8$ mm test section at $z_h = 0.953$ m by TC number 19 (Figure 3.3) is given in the following. The conditions in CO_2 were: $P = 8.34$ MPa, $T_b = 296.75$ K, $G = 699\ \mathrm{kg\,m^{-2}\,s^{-1}}$, $q = 50\ \mathrm{kW\,m^{-2}}$ and $T_{in} = 11.3$ °C. The corresponding equivalent test conditions in R134a were: $d = 8$ mm (Equation (2.19)), $z_h = 0.953$ m (Equation (2.3)), $P = 4.59$ MPa (Equation (2.20)), $T_b = 380.45$ K (Equation (2.21)), $G = 725\ \mathrm{kg\,m^{-2}\,s^{-1}}$ (Equation (2.23)), $q = 38\ \mathrm{kW\,m^{-2}}$ (Equation (2.22)) and $T_{in} = 78$ °C. The corresponding equivalent test conditions in H_2O were: $d = 8$ mm, $z_h = 0.953$ m, $P = 24.93$ MPa, $T_b = 630.31$ K, $G = 1161\ \mathrm{kg\,m^{-2}\,s^{-1}}$, $q = 555\ \mathrm{kW\,m^{-2}}$ and $T_{in} = 331$ °C.

Table 4.1: Ranges of test flow conditions, at PR = 1.13, of the fluids R134a, CO_2, and H_2O

Fluids	P/P_c [-]	T_b/T_{pc} [-]	G [$\mathrm{kg\,m^{-2}\,s^{-1}}$]	q [$\mathrm{kW\,m^{-2}}$]	T_{in} [°C]
R134a	1.13	0.92-1.01	212-1609	2-137	62-105
CO_2	1.13	0.92-1.01	200-1520	3-175	5-35
H_2O	1.13	0.92-1.01	337-12101	34-1975	370-511

4.3 Calculation of scaling errors

The HTC scaling errors for each pair of fluids at equivalent conditions were found as follows.

- A number of experimental points with conditions P, T_b, G, q were selected from the CO_2 tests of Zahlan et al. (2015a) and Kline et al. (2018); the measured HTC for each case were recorded.
- Equivalent conditions P, T_b, G, q for R134a and H_2O were calculated for each experimental point in CO_2 using the fluid-to-fluid scaling laws of Zahlan et al. (2014).
- Experiments in R134a were conducted at the previously specified conditions; the HTC was measured directly and recorded for each point.
- The TC-LUT was used to determine the HTC at the previously specified conditions in water, as an approximation of the corresponding experimental value. In the following, we will also refer to this HTC as experimental.
- The experimental values of the HTC in the three fluids were used to compute the corresponding Nusselt numbers Nu_b; if the scaling laws were perfectly accurate, these three values should have been the same; this not being the case, however, the differences between the Nusselt numbers of two fluids represent estimates of the total errors, which include errors of the scaling laws and errors in any other step of the entire process.
- Statistical analysis of the errors for all experimental points considered provided estimates of the uncertainty of the fluid-to-fluid scaling laws; this was done separately for each pair of fluids and separately for points with NHT or DHT in CO_2.
- The subscripts 1 and 2 in the scaling laws will be replaced by the subscripts C, R and W, respectively, for CO_2, R134a and water.

Different estimates of scaling law uncertainty were determined as follows.

- We plotted the values of the ratio $Nu_{b,2}/Nu_{b,1}$ *vs.* $Nu_{b,1}$ for all points considered.
- We calculated the error of each point as

$$e_{2,1} = \frac{Nu_{b,2}}{Nu_{b,1}} - 1 \ . \tag{4.1}$$

- We calculated the average $A_{2,1}$ of $e_{2,1}$ for all points considered.
- Next, we calculated the error with respect to the fitted average as

$$e_{2,1,av} = \frac{Nu_{b,2}}{Nu_{b,1}} - A_{2,1} \ . \tag{4.2}$$

- Using linear least squares fit, we fitted a straight line $a_{2,1}Nu_{b,1} + b_{2,1}$ to the data for all points considered.
- Finally, we calculated the error with respect to the fitted line as

$$e_{2,1,lf} = \frac{Nu_{b,2}}{Nu_{b,1}} - (a_{2,1}Nu_{b,1} + b_{2,1}) \ . \tag{4.3}$$

To characterise statistically the different types of error, we will present their standard deviations (to be denoted by a prime, as for example $e'_{2,1}$), as well as their probability density functions (PDF). A near-normal PDF would point towards a prevalence of precision (namely random) uncertainty of the scaling laws, whereas deviations from normality may reveal the existence of biases (Tavoularis, 2009).

Tables 4.2 and 4.3 list the various types of fits and errors for the six pairs of fluids separately for NHT and DHT.

Table 4.2: Fitted expressions and standard deviations to Nu_b ratios for NHT

Fluids 2,1	$A_{2,1}$	$a_{2,1}$	$b_{2,1}$	$e'_{2,1}$	$e'_{2,1,av}$	$e'_{2,1,lf}$
$CO_2 - H_2O$ (CW)	1.17	1.13×10^{-3}	0.76	0.33	0.28	0.25
$H_2O - CO_2$ (WC)	0.91	-9.60×10^{-4}	1.34	0.28	0.26	0.17
R134a $- CO_2$ (RC)	1.27	-3.03×10^{-4}	1.40	0.38	0.27	0.26
$CO_2 -$ R134a (CR)	0.82	-1.65×10^{-4}	0.91	0.25	0.18	0.18
R134a $- H_2O$ (RW)	1.48	9.02×10^{-4}	1.15	0.65	0.44	0.42
$H_2O -$ R134a (WR)	0.74	-7.09×10^{-4}	1.13	0.35	0.23	0.15

Table 4.3: Fitted expressions and standard deviations to Nu_b ratios for DHT

Fluids 2,1	$A_{2,1}$	$a_{2,1}$	$b_{2,1}$	$e'_{2,1}$	$e'_{2,1,av}$	$e'_{2,1,lf}$
$CO_2 - H_2O$ (CW)	1.06	1.59×10^{-3}	0.75	0.12	0.10	0.06
$H_2O - CO_2$ (WC)	0.95	-1.02×10^{-3}	1.17	0.10	0.09	0.03
R134a $- CO_2$ (RC)	1.72	5.37×10^{-3}	0.59	0.97	0.63	0.48
$CO_2 -$ R134a (CR)	0.67	-8.53×10^{-4}	1.01	0.44	0.28	0.18
R134a $- H_2O$ (RW)	1.86	1.14×10^{-2}	-0.36	1.19	0.80	0.51
$H_2O -$ R134a (WR)	0.65	-9.91×10^{-4}	1.04	0.48	0.32	0.20

4.4 Validation of scaling laws for the CO_2-H_2O pair

Zahlan et al. (2014) scaled their CO_2 conditions into equivalent conditions in H_2O but plotted the ratio of experimental HTC values in these fluids *vs.* the water value. Consequently, in these tests, H_2O served as Fluid 1 and CO_2 served as Fluid 2. We will first repeat such tests for the presently chosen points to ensure that they conform with the Zahlan et al. (2014) scaling laws. We will also test scaling in the reverse direction, namely with CO_2 as Fluid 1 and H_2O as Fluid 2 to determine any difference in the scaling law uncertainty when fluids are interchanged.

Figure 4.1 shows the ratio of experimental Nu_b for NHT in CO_2 (fluid 2) and H_2O (fluid 1), plotted against $Nu_{b,W}$. Lines showing the unit value, averages and linear fits through the data are shown in this figure as well in similar figures for different pairs of fluids, to be shown below. The average value is measurably different from unit, but the two STD (*i.e.* with respect to unit and the average) are only slightly different, which demonstrates that the bias of this sample of measurements is very small compared to the precision uncertainty and so may be disregarded. The results also show a weak but measurable upward trend, which is comparable to the one reported by Zahlan et al. (2014). The difference between the corresponding STD is also small and so there would be only a slight improvement, on the average, if the linear fit were used to correct the Zahlan et al. (2014) expression. All things considered, the latter expression seems to be validated, within its own uncertainty, by the present results. Figure 4.2 shows the probability density function versus error (namely

difference from the fitted value or line) for NHT in CO_2 and H_2O. The three PDF have nearly Gauusian central sections, but are visibly skewed and contain values that are far from the peak. The PDF that corresponds to the linear fit appears to be quasi-Gaussian on the low side but maintains strong skewness on the right side. In summary, the use of a linear fit does not normalise the error and so it preserves some bias.

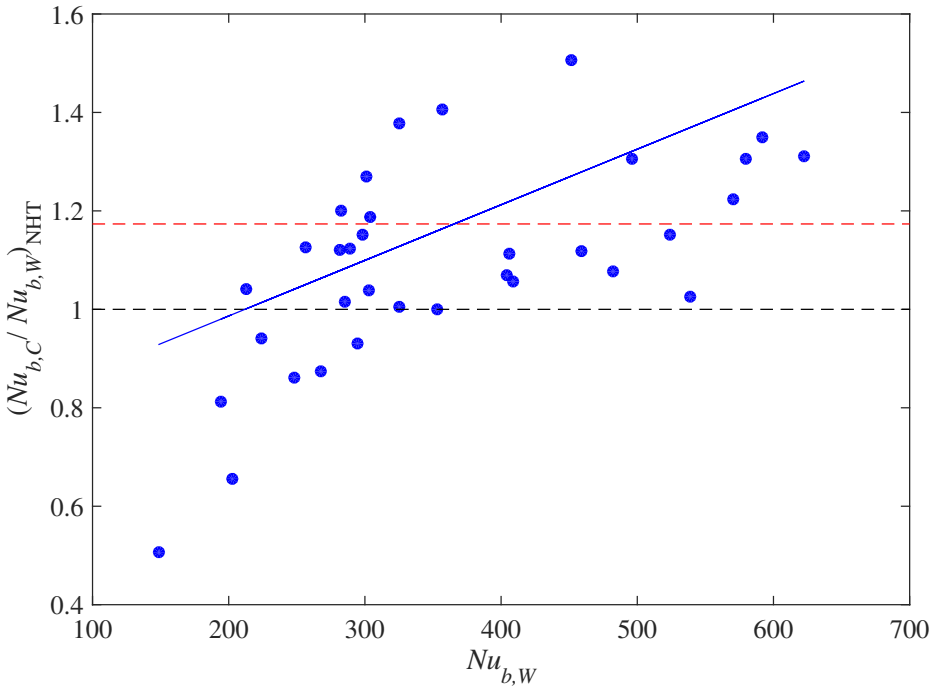

Figure 4.1: Ratios of experimental Nu_b in CO_2 and H_2O *vs.* $Nu_{b,W}$ for NHT; black dashed line indicates unit, red dashed line indicates average and solid blue line indicates linear-least-squares fit.

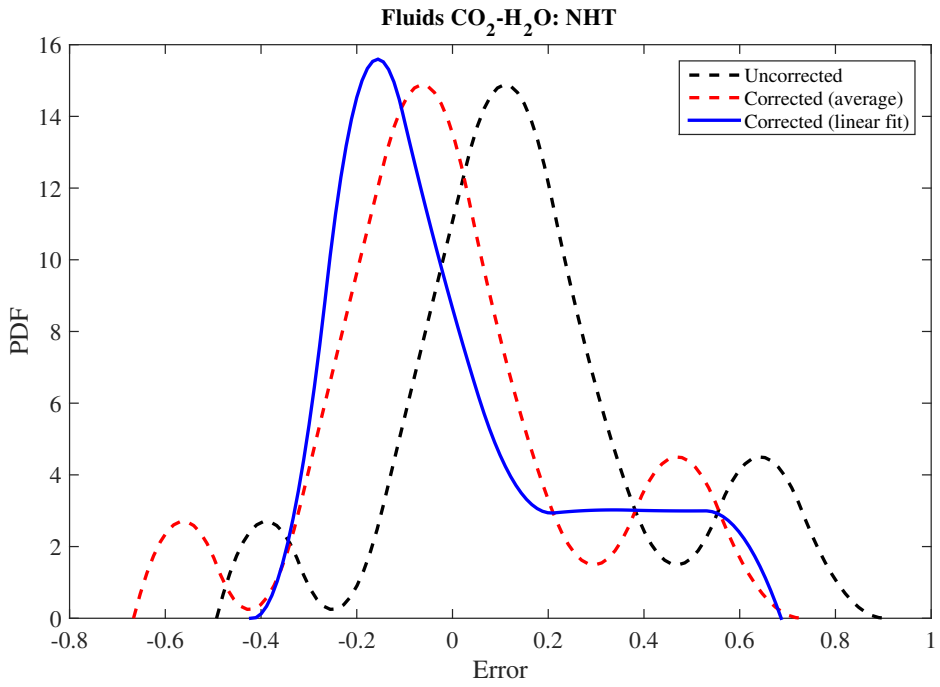

Figure 4.2: Probability density function of the fluids CO_2 and H_2O *vs.* error for NHT.

Figures 4.3 and 4.4 show, respectively, the ratio of experimental Nu_b for NHT in H_2O (fluid 2) and CO_2 (fluid 1) and the corresponding PDF of errors. As the direction of scaling is the reverse of the previous case, the trend of the linear fit is opposite to the previous one. In any case, the bias may also be considered as quite small, compared to the precision uncertainty. The use of the linear fit reduces the uncertainty by a relatively small amount. Again, the Zahlan et al. (2014) laws appear to cover this case as well.

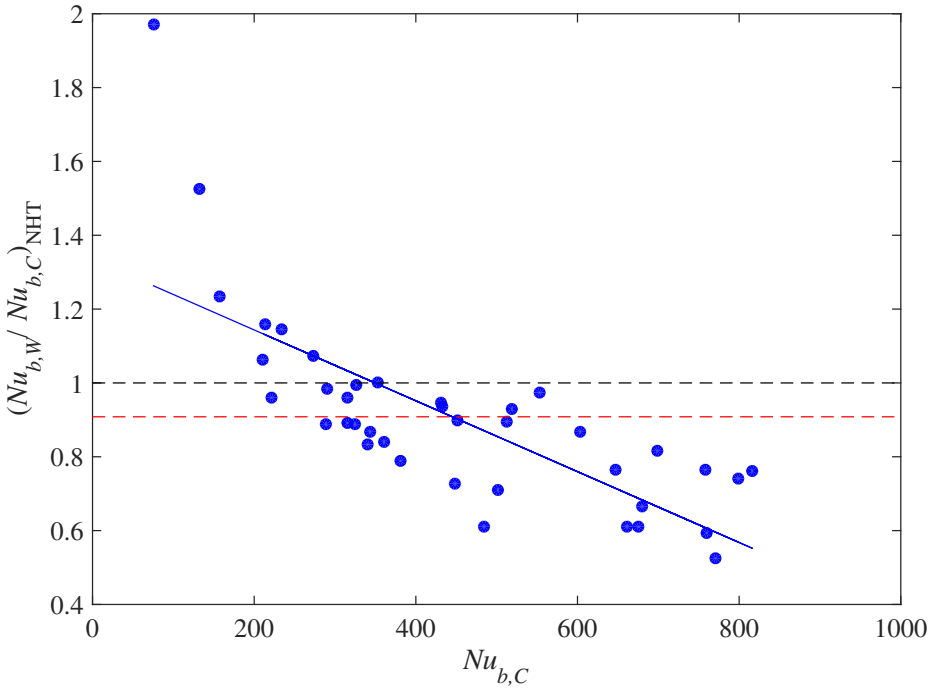

Figure 4.3: Ratios of experimental Nu_b in H_2O and CO_2 *vs.* $Nu_{b,C}$ for NHT; black dashed line indicates unit, red dashed line indicates average and solid blue line indicates linear-least-squares fit.

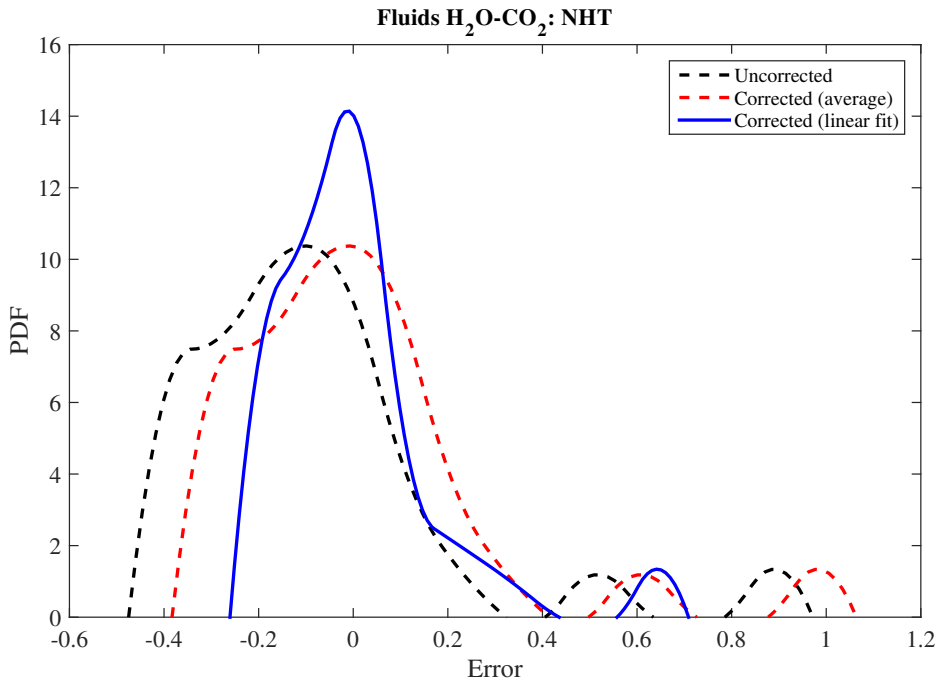

Figure 4.4: Probability density function of the fluids H_2O and CO_2 *vs.* error for NHT.

We now proceed to test the fluid-to-fluid scaling laws for cases with mild DHT in CO_2. Although these scaling laws were not meant to apply to DHT, it is reminded that the TC-LUT included cases with mild DHT in water and so the experimental HTC values in both fluids would be fairly accurate. Figures 4.5 to 4.8 show ratios of experimental bulk Nusselt numbers and corresponding PDF for DHT in H_2O and CO_2 in both scaling directions. Each plot resembled the corresponding plot in NHT and in fact the scaling laws under test appeared to fit better the DHT data than the NHT data. There is no obvious explanation for this observation, but it is noted that the main discrepancies from the scaling laws for the NHT cases occur for very low Nu_b. This issue deserves closer attention.

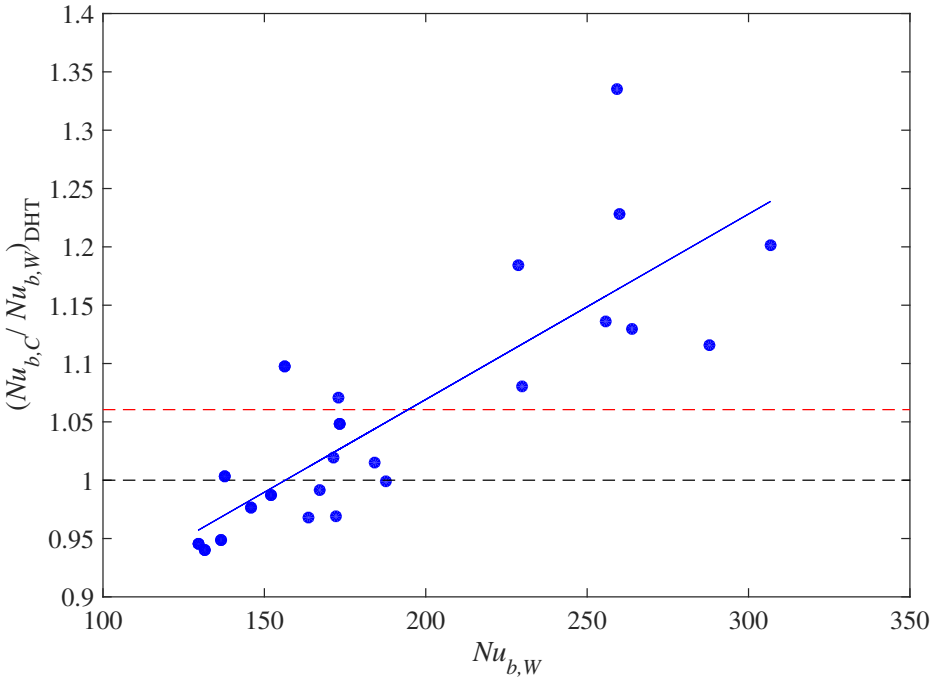

Figure 4.5: Ratios of experimental Nu_b in CO_2 and H_2O *vs.* $Nu_{b,W}$ for DHT; black dashed line indicates unit, red dashed line indicates average and solid blue line indicates linear-least-squares fit.

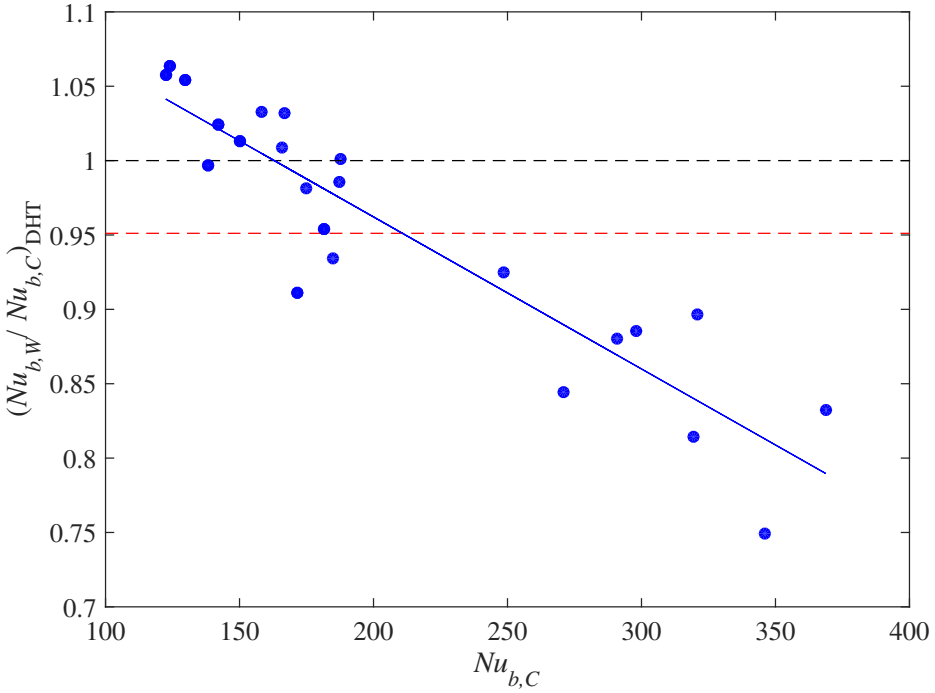

Figure 4.6: Ratios of experimental Nu_b in H_2O and CO_2 *vs.* $Nu_{b,C}$ for DHT; black dashed line indicates unit, red dashed line indicates average and solid blue line indicates linear-least-squares fit.

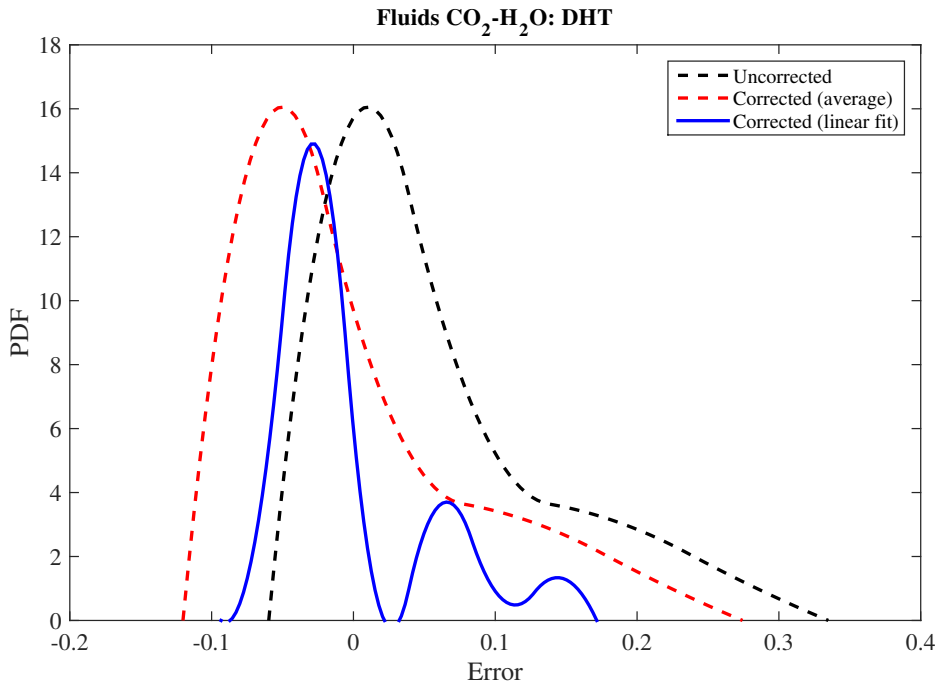

Figure 4.7: Probability density function of the fluids CO_2 and H_2O *vs.* error for DHT.

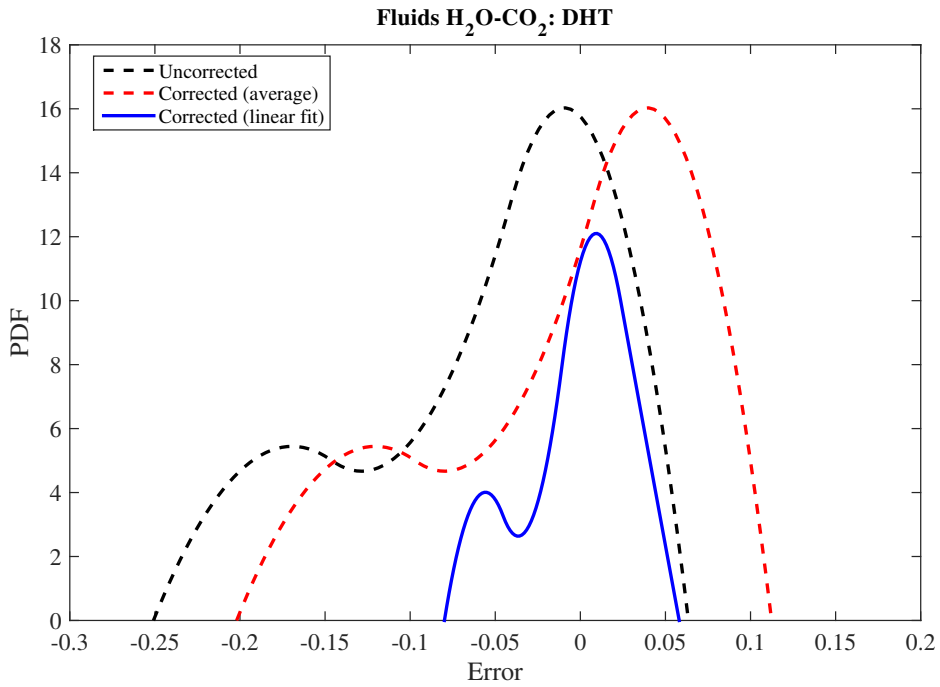

Figure 4.8: Probability density function of the fluids H_2O and CO_2 *vs.* error for DHT.

4.5 Direct tests of scaling laws for the CO_2−R134a pair

This section describes the main tests of the fluid-to-fluid scaling laws and the only ones in the literature that are direct, as they do not use a heat transfer correlation or LUT to estimate the HTC in fluid 2 but values of HTC measured in both fluids under equivalent conditions.

4.5.1 Normal heat transfer

Figure 4.9 shows typical measurements of wall temperature and bulk Nusselt number profiles, plotted against bulk enthalpy in the two fluids R134a − CO_2 at equivalent conditions for NHT in both fluids. The conditions of the four experimental points that are enclosed by red circles in the CO_2 profiles were scaled to equivalent conditions in R134a and full profiles at these conditions were measured in new experiments in R134a. The scaled T_w and Nu_b at the same locations in the R134a tests as in the CO_2 tests, as well as corrected values of these parameters based on the means and linear fits, have also been marked by coloured symbols in the R134a plots. A full set of T_w and Nu_b profiles in the two fluids at equivalent conditions with NHT in both fluids have been shown in Appendix D. It is interesting to notice that the profiles for all four cases in R134a essentially collapsed.

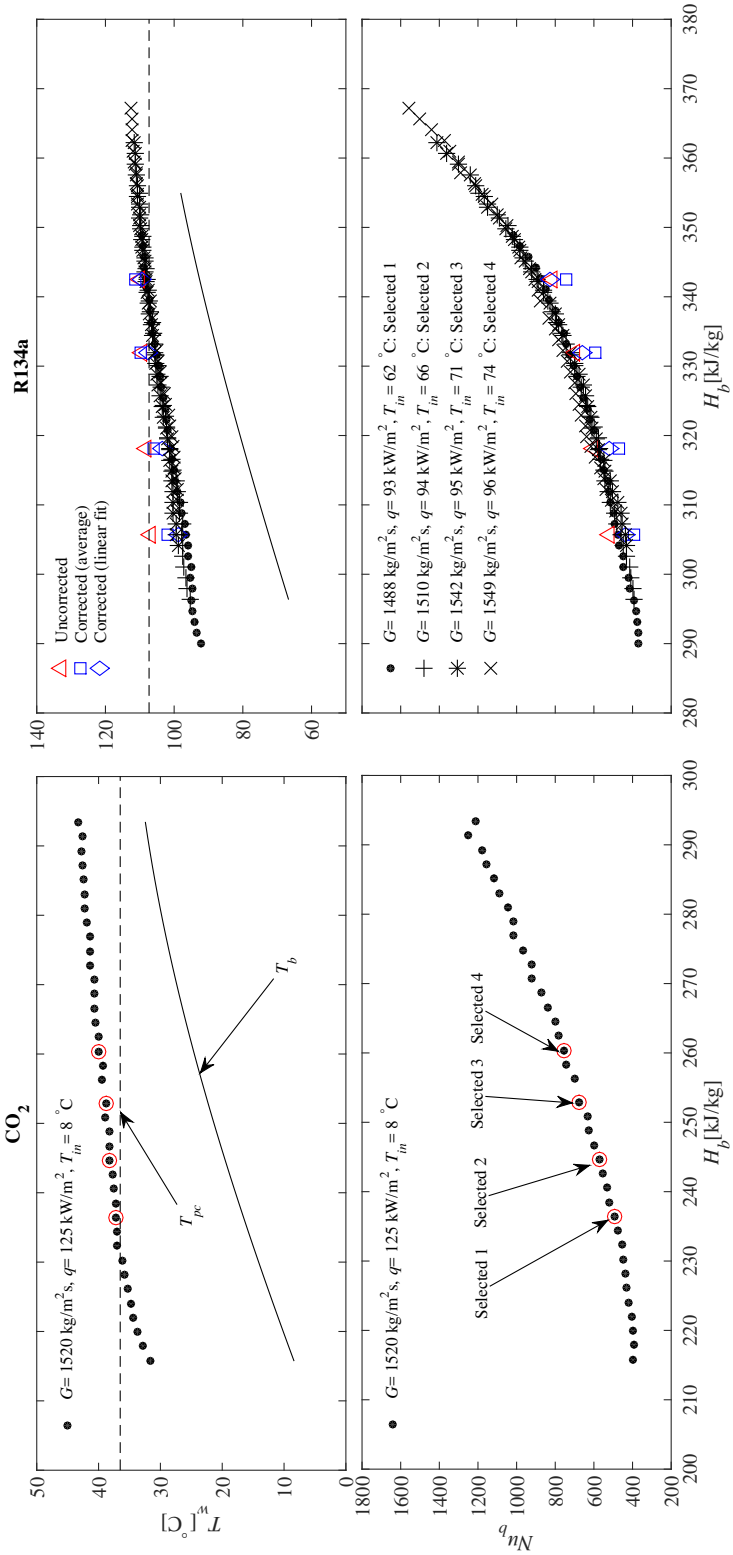

Figure 4.9: Measurements of wall temperature (top) and bulk Nusselt number (bottom) *vs.* bulk enthalpy profiles for NHT at equivalent conditions in CO_2 and R134a.

Figure 4.10 shows the ratio of experimental bulk Nusselt numbers for R134a and CO_2 versus Nu_b in CO_2, for NHT in both fluids. The mean ratio was 1.27, which is a significant bias, as its use reduced the STD of the error from 0.38 to 0.27. A weak downward trend may also be observed, but this may be neglected, as it affected the error only marginally. The previous observations are confirmed by the shapes of the PDF shown in Figure 4.14. To determine whether the Nusselt number ratio depends systematically on the values of the experimental conditions, we have plotted it *vs.* $T_b/T_{pc}, G$ and q in CO_2, respectively, in Figures 4.11 to 4.13. The Nusselt number ratio has a weak upward trend with T_b for $T_b/T_{pc} < 1$ and possibly a downward trend for $T_b/T_{pc} > 1$, but it is essentially independent, on the average, of the values of G and q within the reported ranges of these parameters.

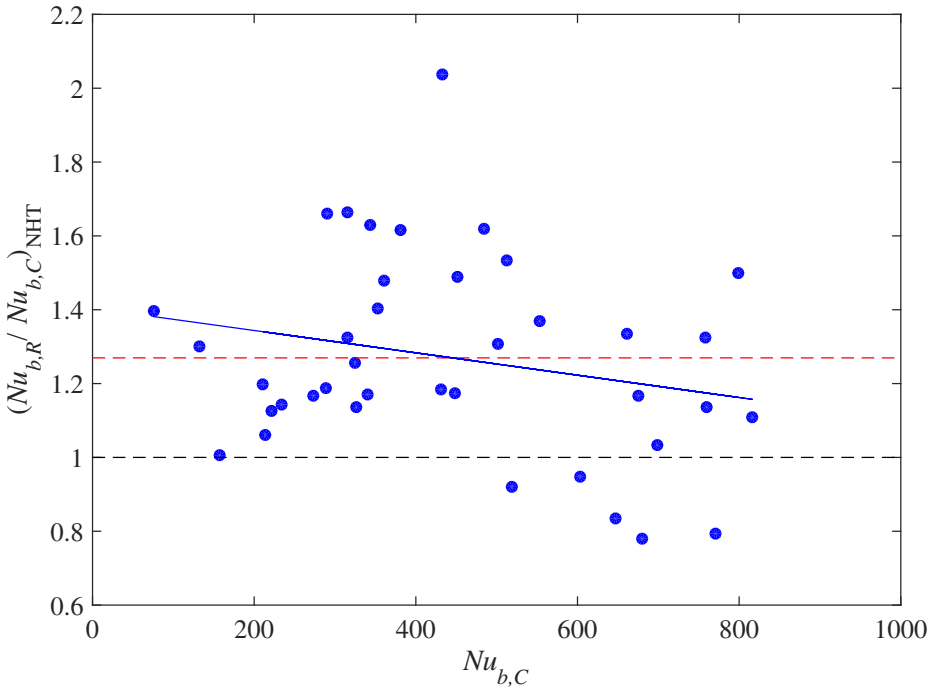

Figure 4.10: Ratio of experimental Nu_b in R134a and CO_2 *vs.* $Nu_{b,C}$ for NHT; black dashed line indicates unit, red dashed line indicates average and solid blue line indicates linear-least-squares fit.

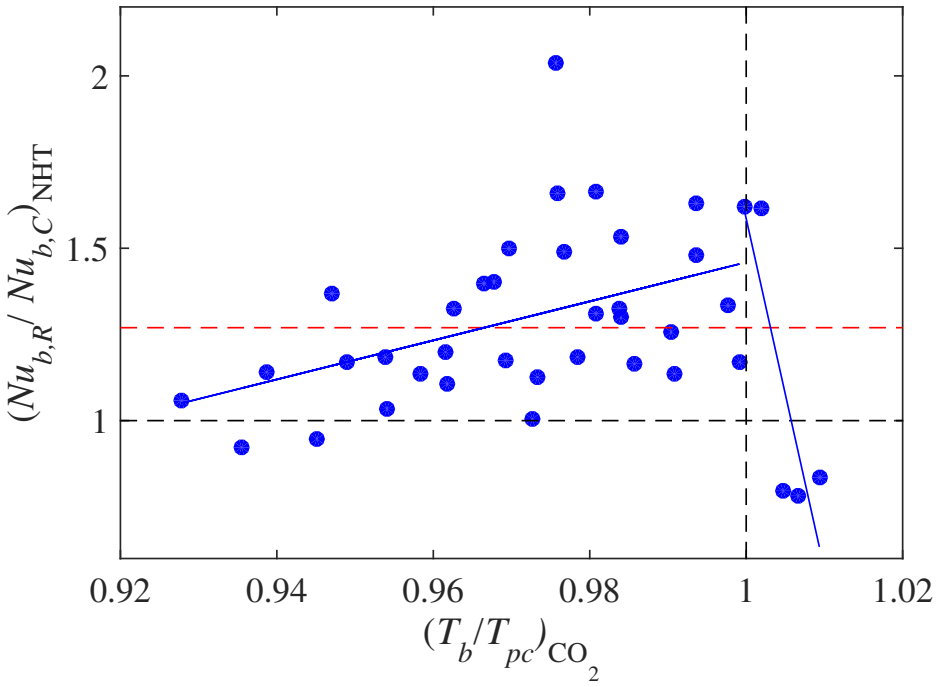

Figure 4.11: Ratios of experimental Nu_b in R134a and CO_2 *vs.* normalised bulk temperature in CO_2 for NHT; horizontal and vertical black dashed lines indicate unit, red dashed line indicates average and solid blue lines indicate, respectively, linear-least-squares fit in liquid- and gas-like region.

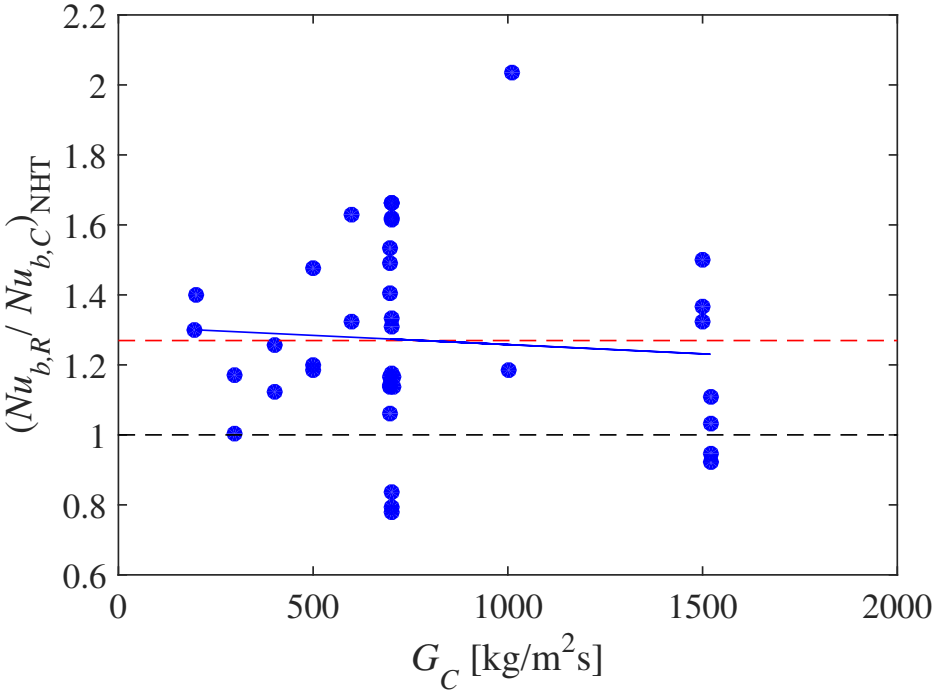

Figure 4.12: Ratios of experimental Nu_b in R134a and CO_2 *vs.* mass flux G in CO_2 for NHT; black dashed line indicates unit, red dashed line indicates average and solid blue line indicates linear-least-squares fit.

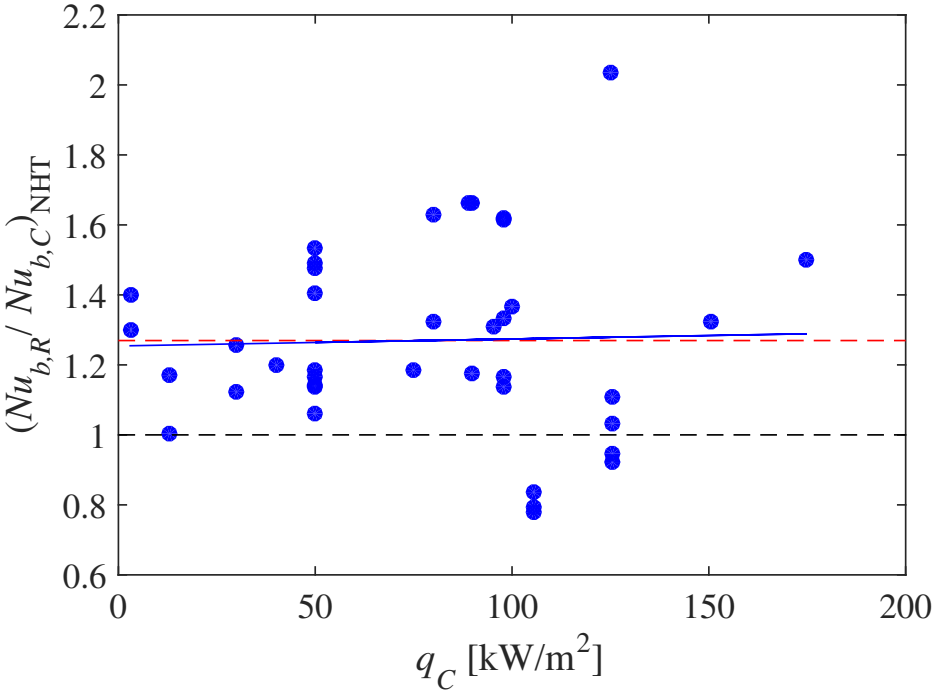

Figure 4.13: Ratios of experimental Nu_b in R134a and CO_2 *vs.* heat flux q in CO_2 for NHT; black dashed line indicates unit, red dashed line indicates average and solid blue line indicates linear-least-squares fit.

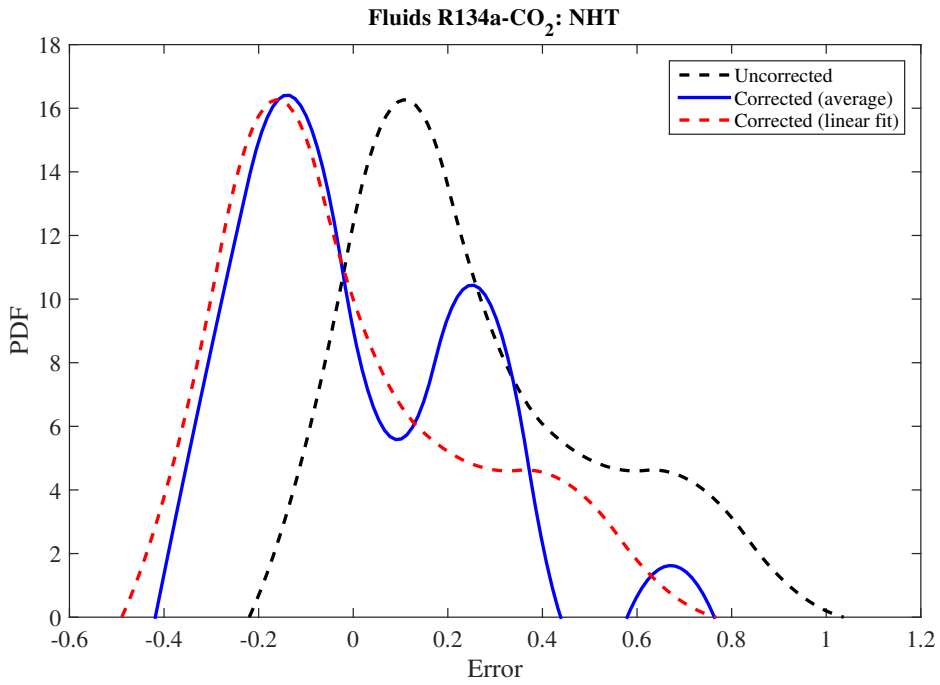

Figure 4.14: Probability density function of scaling errors for R134a and CO_2 *vs.* error for NHT.

Figure 4.15 shows the ratio of experimental bulk Nusselt numbers for CO_2 and R134a versus Nu_b in R134a, for NHT in both fluids. The mean ratio was 0.82, which is a significant bias, as its use reduced the STD of the error from 0.25 to 0.18. The observed weak downward trend may be neglected, as its use did not affect the error within the reported two significant figure precision. The previous observations are confirmed by the shapes of the PDF shown in Figure 4.19. As for the CR case, the Nusselt number ratio had a weak dependence on T_b, which changed direction at T_{pc} (Figure 4.16) and was insensitive to the values of G and q (Figures 4.17 and 4.18).

The previous results demonstrate that the fluid-to-fluid scaling laws for HTC that were developed by Zahlan et al. (2014) for CO_2 and H_2O may also be applied with comparable uncertainty to CO_2 and R134a in NHT, provided that a correction factor is used, whose value depends on the direction of scaling, namely on which fluid is the prototype.

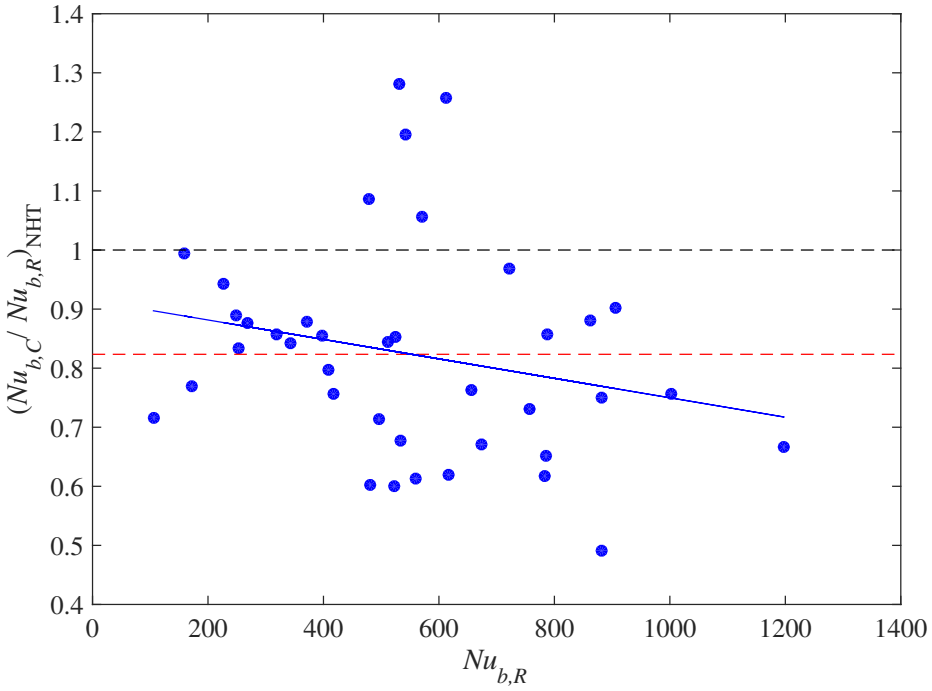

Figure 4.15: Ratios of experimental Nu_b in CO_2 and R134a *vs.* $Nu_{b,R}$ for NHT; black dashed line indicates unit, red dashed line indicates average and solid blue line indicates linear-least-squares fit.

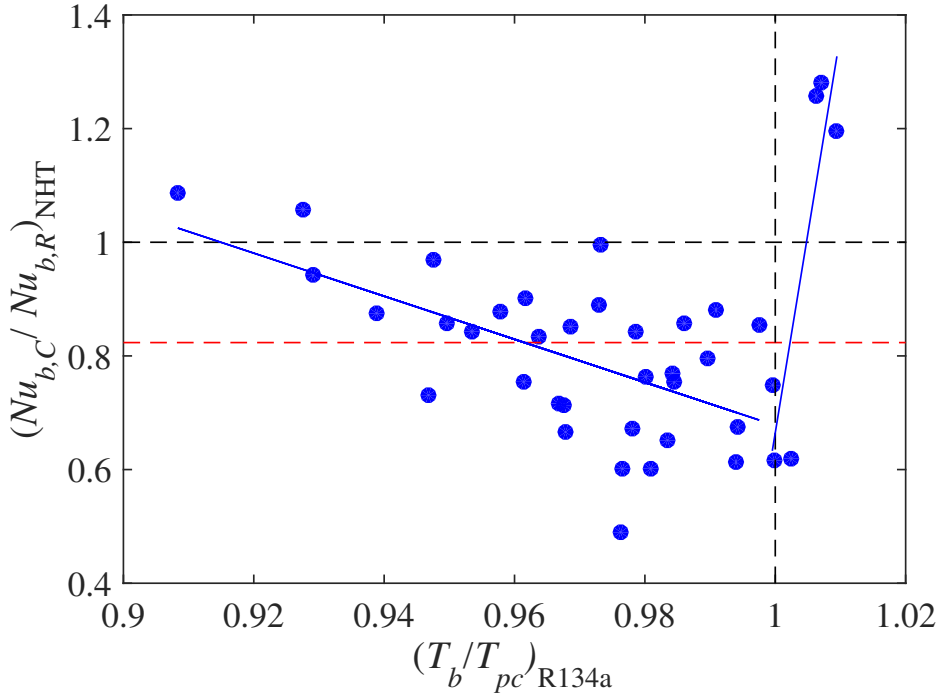

Figure 4.16: Ratio of experimental Nu_b in CO_2 and R134a *vs.* normalised bulk temperature in R134a for NHT; horizontal and vertical black dashed lines indicate unit, red dashed line indicates average and solid blue lines indicate, respectively, linear-least-squares fits in liquid- and gas-like regions.

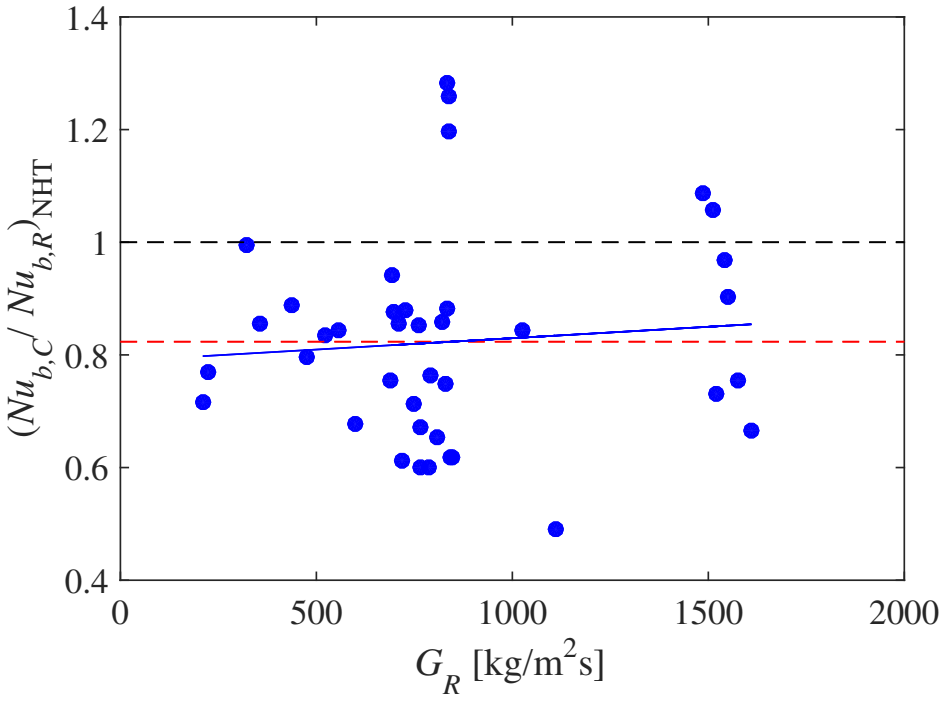

Figure 4.17: Ratios of experimental Nu_b in CO_2 and R134a *vs.* mass flux G in R134a for NHT; black dashed line indicates unit, red dashed line indicates average and solid blue line indicates linear-least-squares fit.

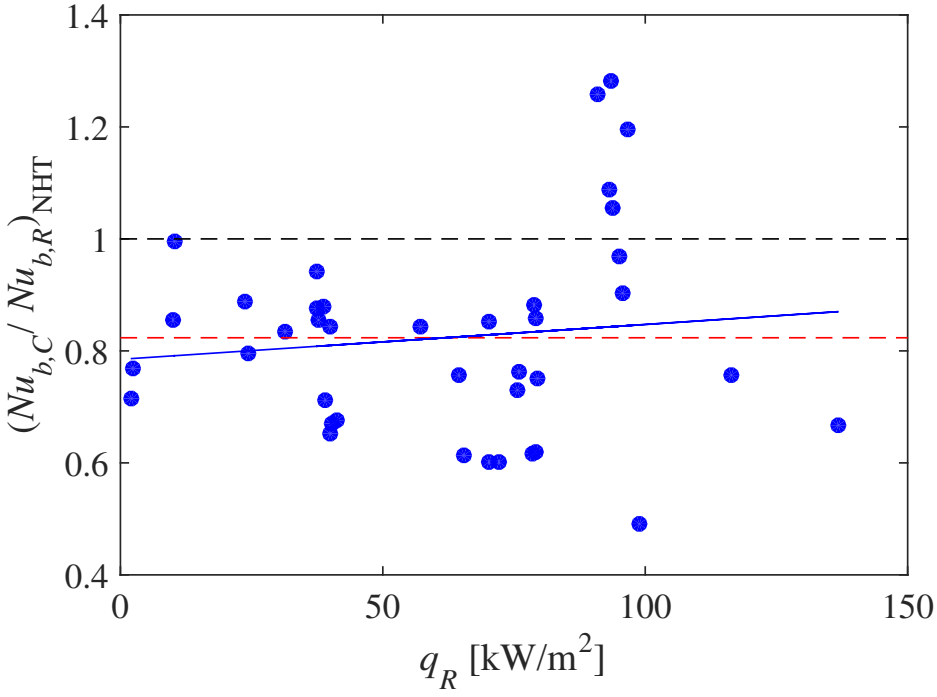

Figure 4.18: Ratios of experimental Nu_b in CO_2 and R134a *vs.* heat flux q in R134a for NHT; black dashed line indicates unit, red dashed line indicates average and solid blue line indicates linear-least-squares fit.

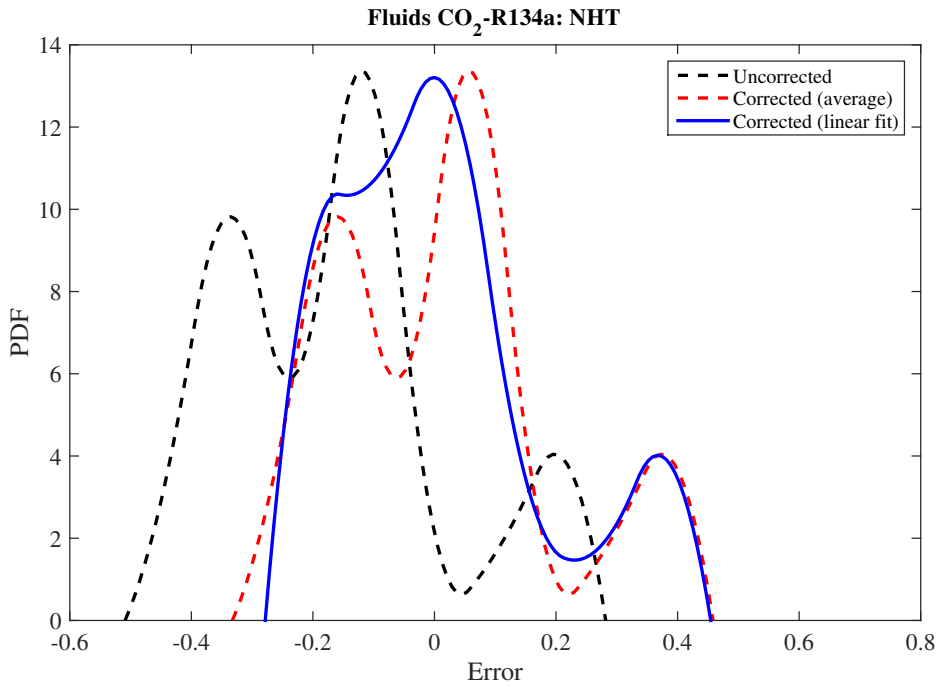

Figure 4.19: Probability density function of the fluids CO_2 and R134a *vs.* error for NHT.

4.5.2 Deteriorated heat transfer

In this section, we consider cases for which DHT occurred in CO_2. Two groups of such cases were observed: a) those with mildly DHT in CO_2, which, when scaled according to the Zahlan et al. (2014) method, resulted in NHT (or possibly EHT) in R134a; and b) those with strongly DHT in CO_2, which, when scaled according to the Zahlan et al. (2014) method, resulted in DHT in R134a. Representative T_w and Nu_b in both fluids for each of these cases are shown, respectively, in Figures 4.20 and 4.21. As expected, the scaled values of T_w and Nu_b in R134a, were significantly different from the measured values for case a. Rather unexpectedly, however, the corresponding values of these parameters in R134a were not very different for case b. Because of the large precision uncertainty observed for both cases, one should avoid generalising these observations. Appendix E contains a full set of experimental profiles of T_w and Nu_b in the two fluids at equivalent conditions for DHT cases.

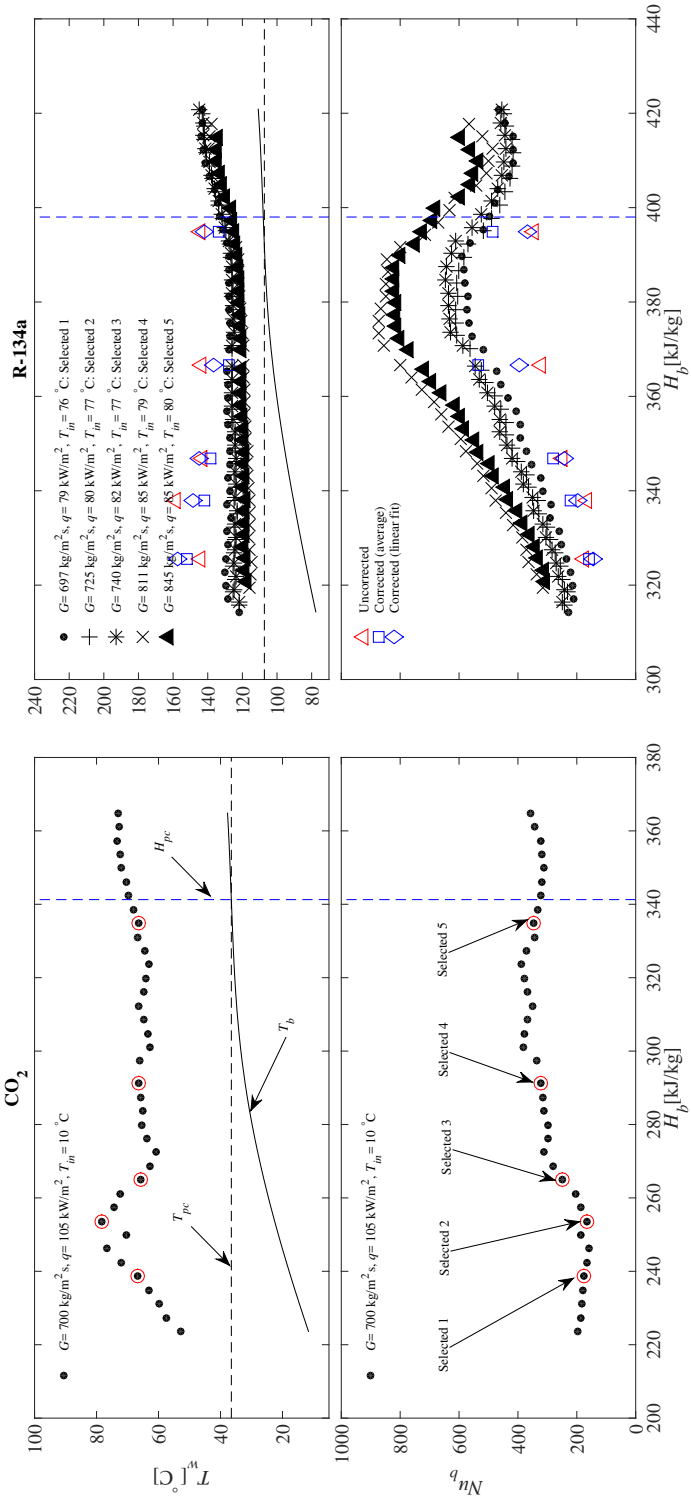

Figure 4.20: Measurements of wall temperature (top) and bulk Nusselt number (bottom) *vs.* bulk enthalpy profiles for mildly DHT in CO_2 at equivalent conditions in CO_2 and R134a.

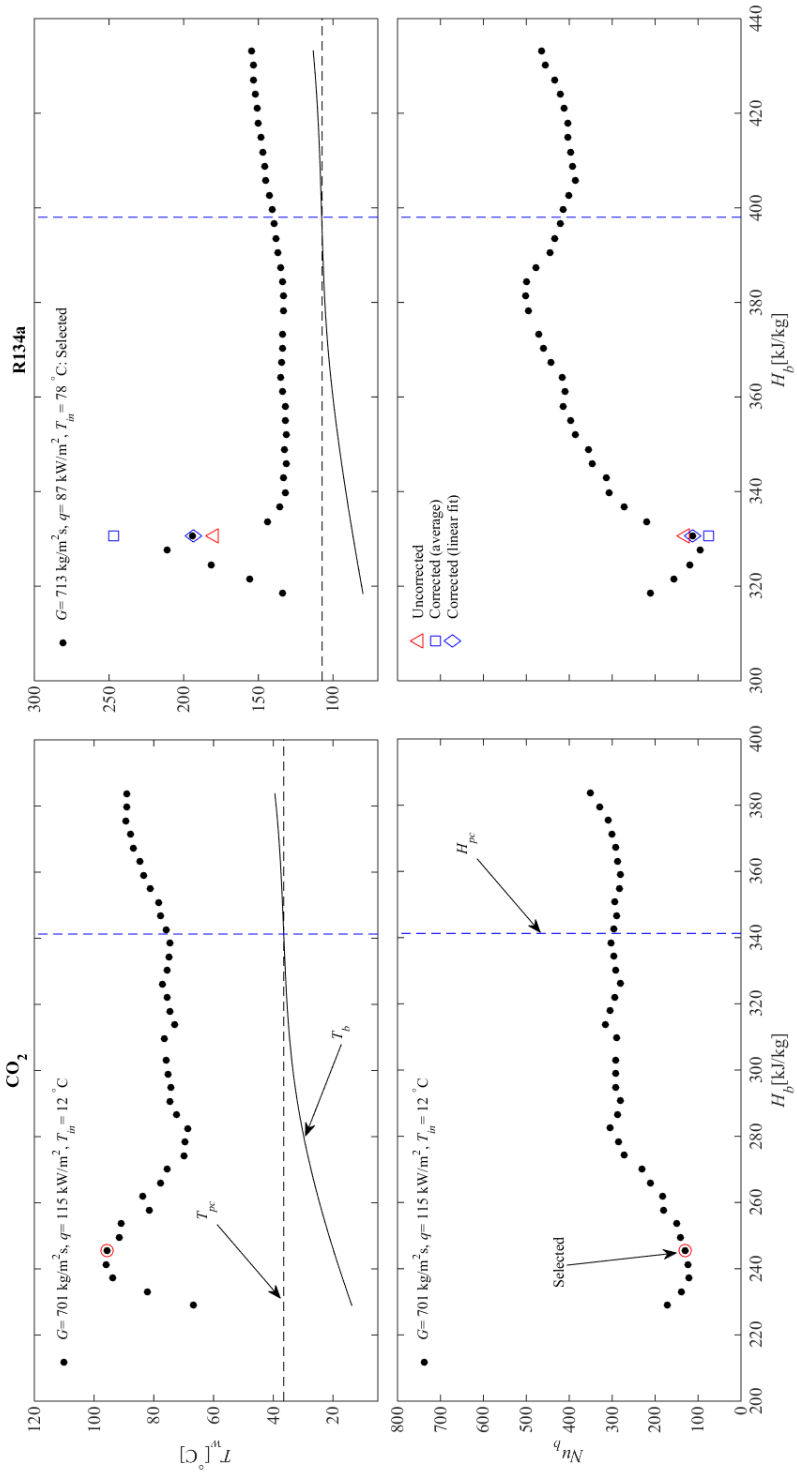

Figure 4.21: Measurements of wall temperature (top) and bulk Nusselt number (bottom) *vs.* bulk enthalpy profiles for strongly DHT in CO_2 at equivalent conditions in CO_2 and R134a.

Hence, the DHT onset in CO_2 would be different to that in R134a therefore scaling for DHT onset relationship in the two fluids would be required.

Figure 4.22 shows the ratio of experimental bulk Nusselt numbers for R134a and CO_2 versus Nu_b in CO_2, for DHT in CO_2 and either NHT (full blue circles) or DHT (full red circles) in R134a. The two sets of results appear compatible, as the NHT cases seem to seggregate at low Nu_b, whereas the DHT cases occupy the relatively large Nu_b range. It is noted, however, that there is some overlap in the ranges and values of the two sets. The mean ratio was 1.72, which is a very significant bias compared to that in the RC pair for NHT in both fluids. Its use reduced the STD of the error from 0.97 to 0.63. A significant upward trend in the data can also be observed. Accounting for this trend further reduced the STD of the error to 0.48. The PDF shown in Figure 4.23 also confirms that the spread of the error was reduced appreciably when the trend was accounted for. As shown in Figure 4.24, there was a significant upward trend of the Nusselt number ratio with T_b, at least for $T_b/T_{pc} < 1$; a possibly downward trend for $T_b/T_{pc} > 1$ cannot be excluded, but additional measurements are required before this can be confirmed. Weak trends of this ratio with G and q may also exist (Figures 4.25 and 4.26) but the large precision uncertainty of the results prevents us from making a definitive statement in this regard.

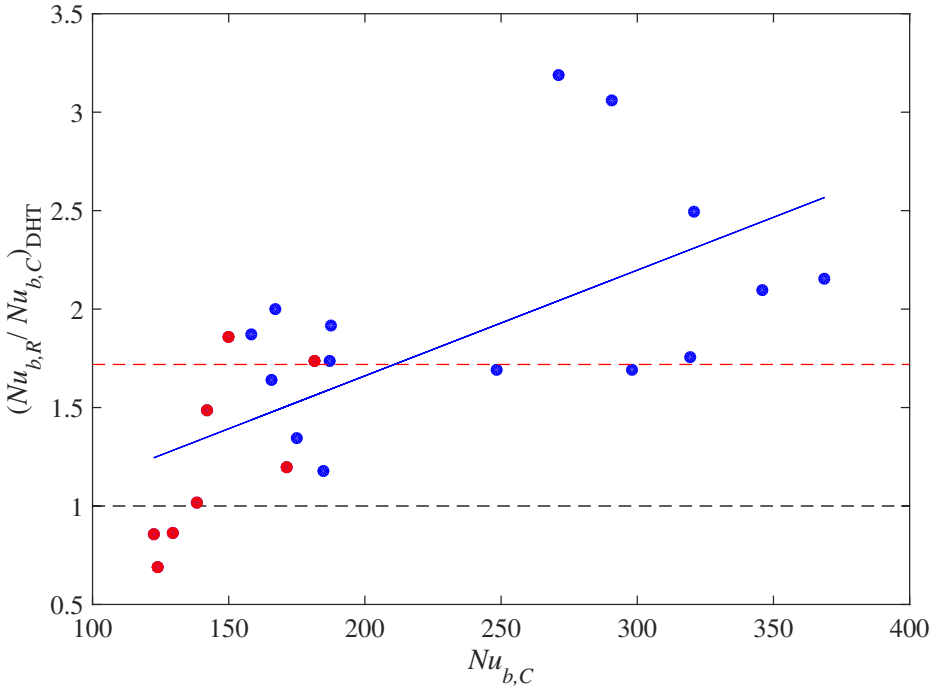

Figure 4.22: Ratios of experimental Nu_b in R134a and CO_2 *vs.* $Nu_{b,C}$ for DHT in CO_2; black dashed line indicates unit, red dashed line indicates average, solid blue line indicates linear-least-squares fit, full red circles indicate DHT in both fluids, and full blue circles indicate DHT in CO_2 but NHT or EHT in R134a.

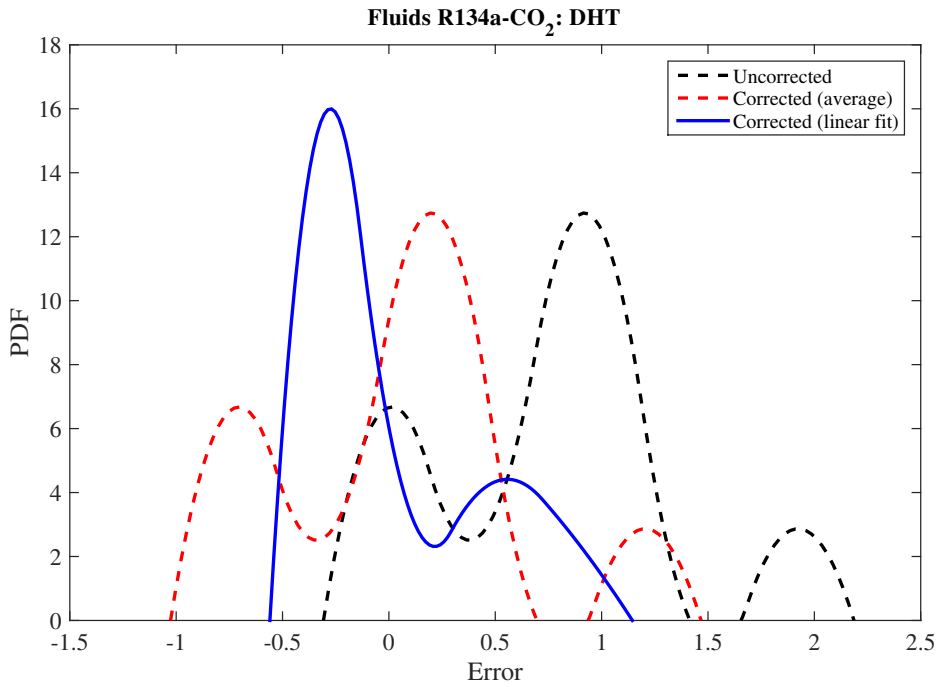

Figure 4.23: Probability density function of the fluids R134a and CO_2 *vs.* error for DHT.

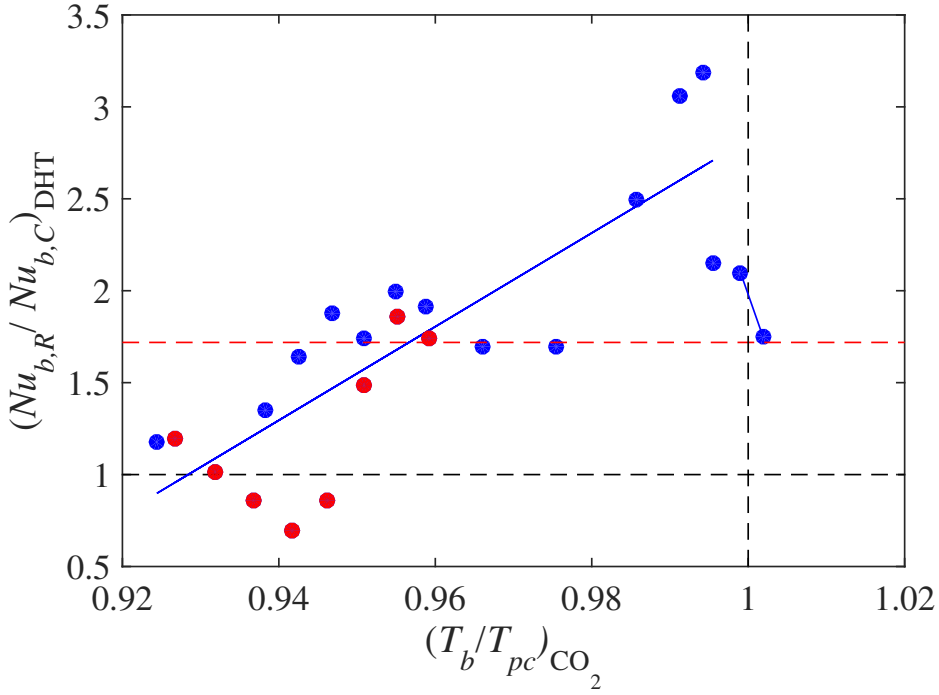

Figure 4.24: Ratios of experimental Nu_b in R134a and CO_2 *vs.* normalised bulk temperature in CO_2 for DHT; horizontal and vertical black dashed lines indicate unit, red dashed line indicates average, solid blue lines indicate, respectively, linear-least-squares fit in liquid- and gas-like region, full red circles indicate DHT in both fluids, and full blue circles indicate DHT in CO_2 but NHT or EHT in R134a.

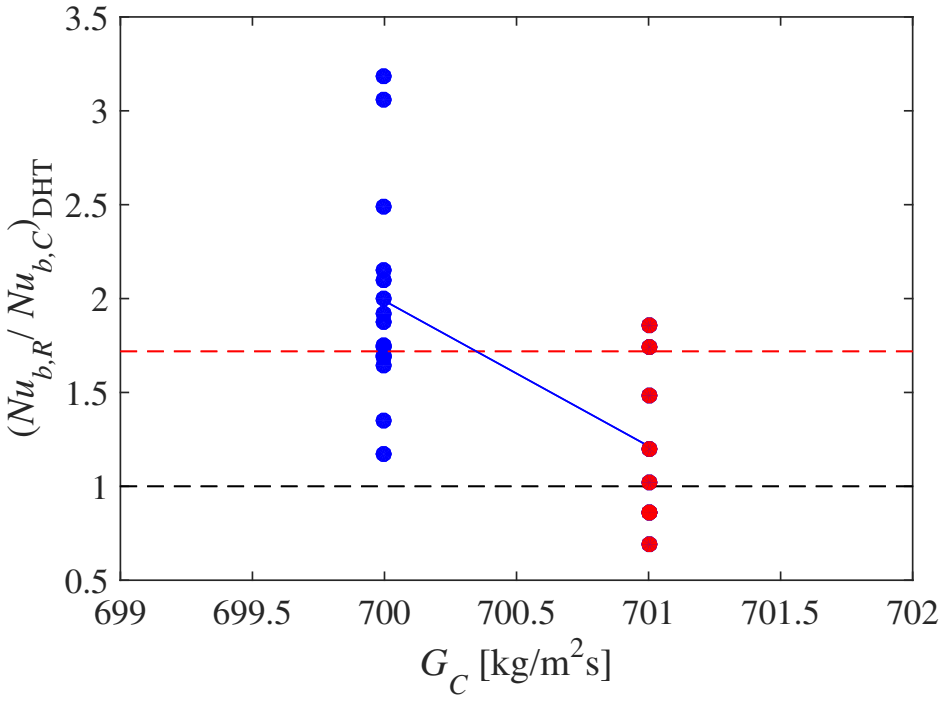

Figure 4.25: Ratios of experimental Nu_b in R134a and CO_2 *vs.* mass flux G in CO_2 for DHT; black dashed line indicates unit, red dashed line indicates average, solid blue line indicates linear-least-squares fit, full red circles indicate DHT in both fluids, and full blue circles indicate DHT in CO_2 but NHT or EHT in R134a.

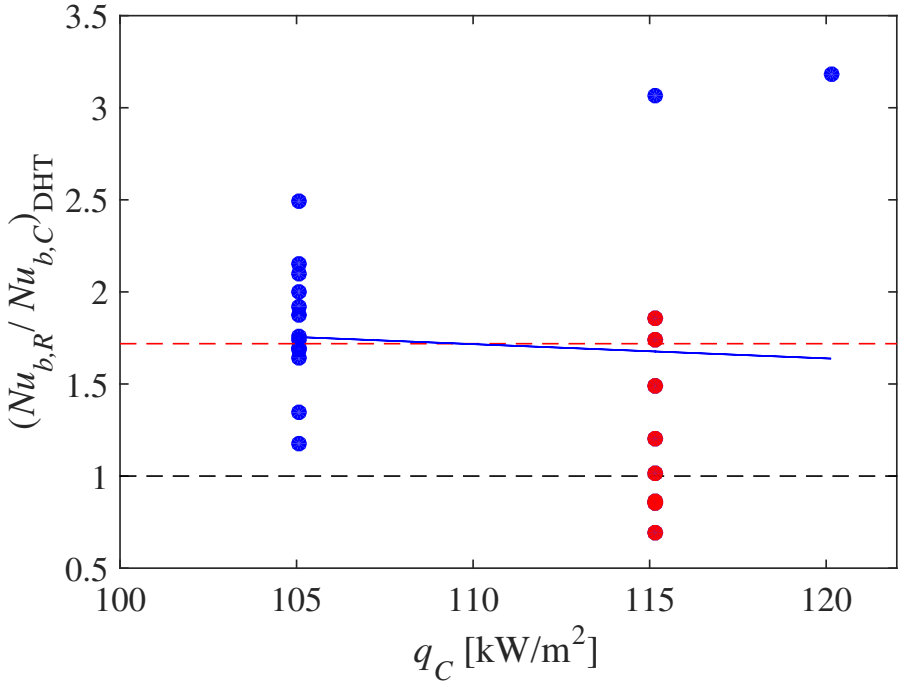

Figure 4.26: Ratios of experimental Nu_b in R134a and CO_2 *vs.* heat flux q in CO_2 for DHT; black dashed line indicates unit, red dashed line indicates average, solid blue line indicates linear-least-squares fit, full red circles indicate DHT in both fluids, and full blue circles indicate DHT in CO_2 but NHT or EHT in R134a.

Figures 4.27 to 4.31 show results of the same type as those in the previous sets of figures for conditions in R134a scaled to values equivalent to those in CO_2 for DHT in CO_2 and either NHT or DHT in R134a. Although the trends are reversed, the general conclusions concerning the CR and RC scalings are the same.

In summary, scaling by Zahlan et al. (2014) laws, may be applied to DHT cases as well, but with the inclusion of a significant correction factor, or preferably a factor that depends linearly on Nu_b. The uncertainty of such predictions would also be much larger than that for NHT cases in both fluids. This scaling approach does not guarantee that mild DHT in one fluid would result in DHT in the other, but it does so for strong DHT cases. The direction of scaling in a pair of fluids is crucial in determining the correction factors and cannot be ignored. Moreover, the corrections depend on the specific pair of fluids considered and are not of universal validity.

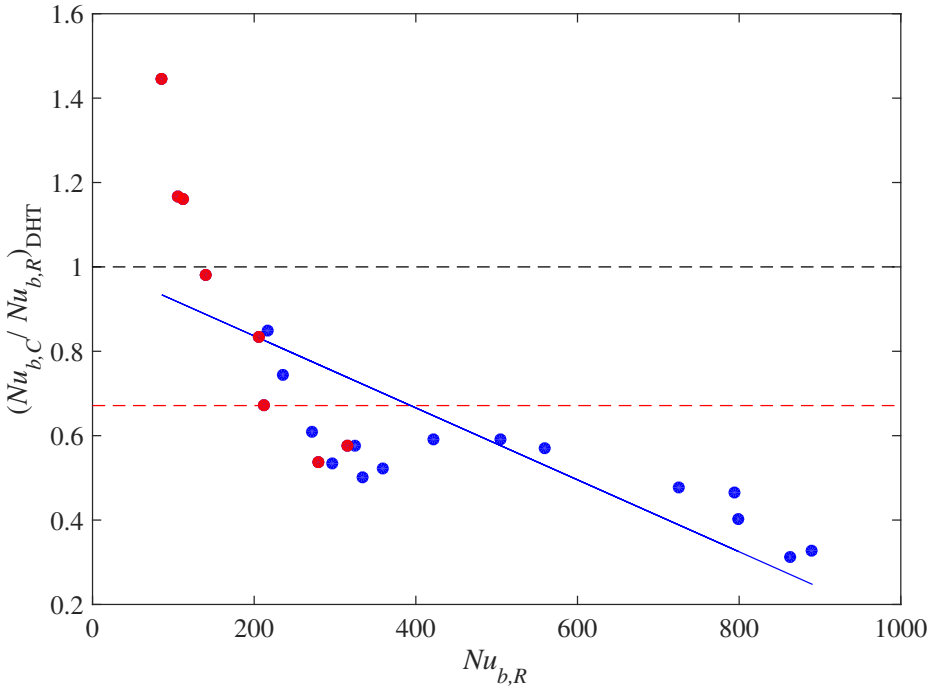

Figure 4.27: Ratios of experimental Nu_b in CO_2 and R134a *vs.* $Nu_{b,R}$ for DHT in CO_2; black dashed line indicates unit, red dashed line indicates average, solid blue line indicates linear-least-squares fit, full red circles indicate DHT in both fluids, and full blue circles indicate DHT in CO_2 but NHT or EHT in R134a.

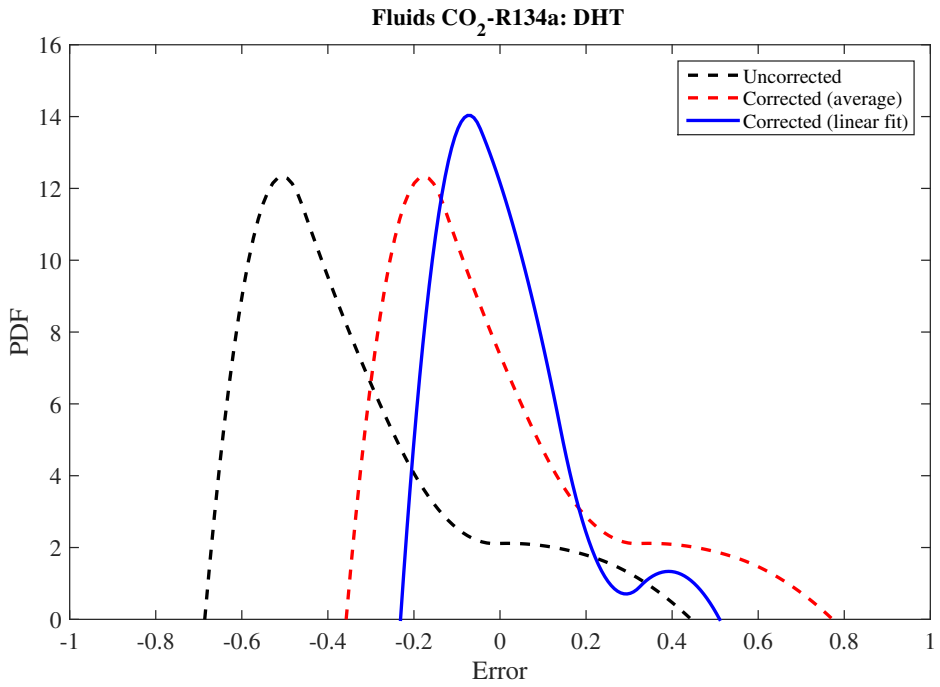

Figure 4.28: Probability density function of the fluids CO_2 and R134a *vs.* error for DHT.

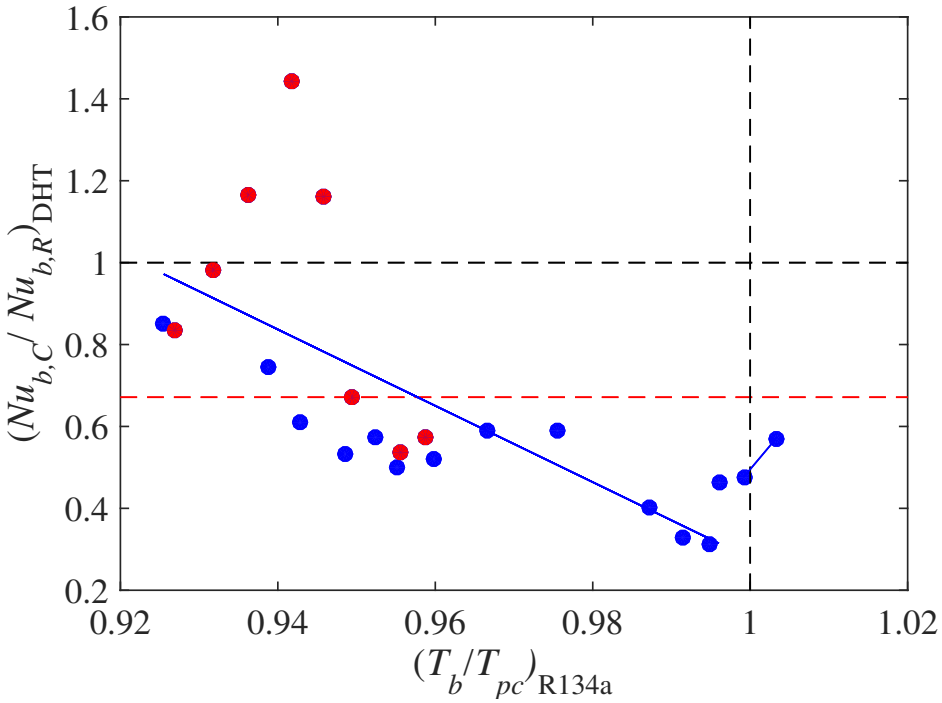

Figure 4.29: Ratios of experimental Nu_b in CO_2 and R134a *vs.* normalised bulk temperature in R134a for DHT; horizontal and vertical black dashed lines indicate unit, red dashed line indicates average, solid blue lines indicate, respectively, linear-least-squares fit in liquid- and gas-like region, full red circles indicate DHT in both fluids, and full blue circles indicate DHT in CO_2 but NHT or EHT in R134a.

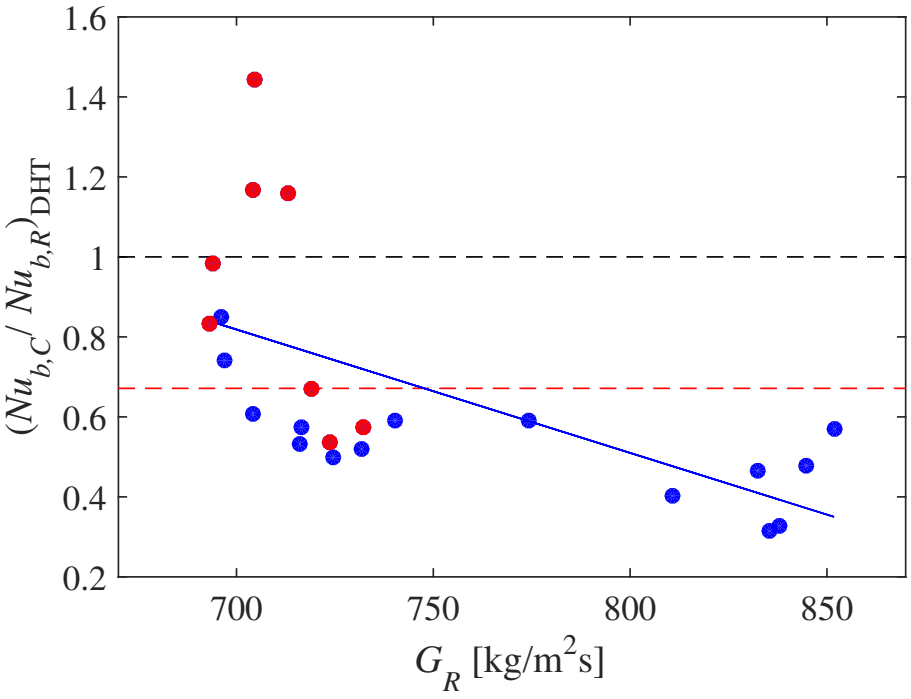

Figure 4.30: Ratios of experimental Nu_b in CO_2 and R134a *vs.* mass flux G in R134a for DHT; black dashed line indicates unit, red dashed line indicates average, solid blue line indicates linear-least-squares fit, full red circles indicate DHT in both fluids, and full blue circles indicate DHT in CO_2 but NHT or EHT in R134a.

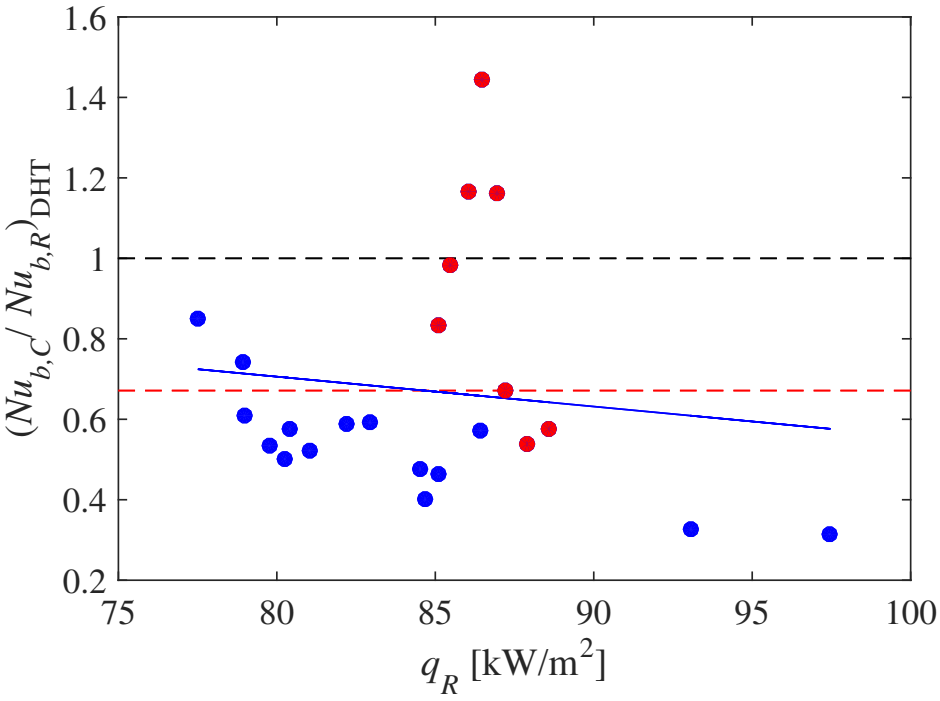

Figure 4.31: Ratios of experimental Nu_b in CO_2 and R134a *vs.* heat flux q in R134a for DHT; black dashed line indicates unit, red dashed line indicates average, solid blue line indicates linear-least-squares fit, full red circles indicate DHT in both fluids, and full blue circles indicate DHT in CO_2 but NHT or EHT in R134a.

4.6 Indirect tests of scaling laws for the R134a−H_2O pair

This section reports the results of tests of the Zahlan et al. (2014) scaling method for R134a and water. These tests are indirect because the HTC values in water were estimated from the TC-LUT tables, whereas the HTC in R134a was measured.

4.6.1 Normal heat transfer

Figure 4.32 shows the ratio of experimental Nusselt numbers for R134a and H_2O versus Nu_b in H_2O, for NHT in R134a. The mean ratio was 1.48, which is a significant bias when compared to that of other pairs of fluids for NHT; its use reduced the STD of the error from 0.65 to 0.44. In fact, the RW correction factor is equal to the product of the correction factors for the RC and CW pairs. It is further noted that this STD was the highest compared to those of other pairs of fluids for NHT. A weak upward trend may also be observed, but this may be neglected, as it affected the error only marginally. The previous observations are confirmed by the shapes of the PDF shown in Figure 4.33. The Nusselt number ratio had a weak but measurable upward trend with T_b for $T_b/T_{pc} < 1$ and possibly a downward trend for $T_b/T_{pc} > 1$, as shown in Figure 4.34. Figures 4.35 and 4.36 show, respectively, a rather negligible trend of the Nusselt number ratio with the mass flux and a weak upward trend with heat flux.

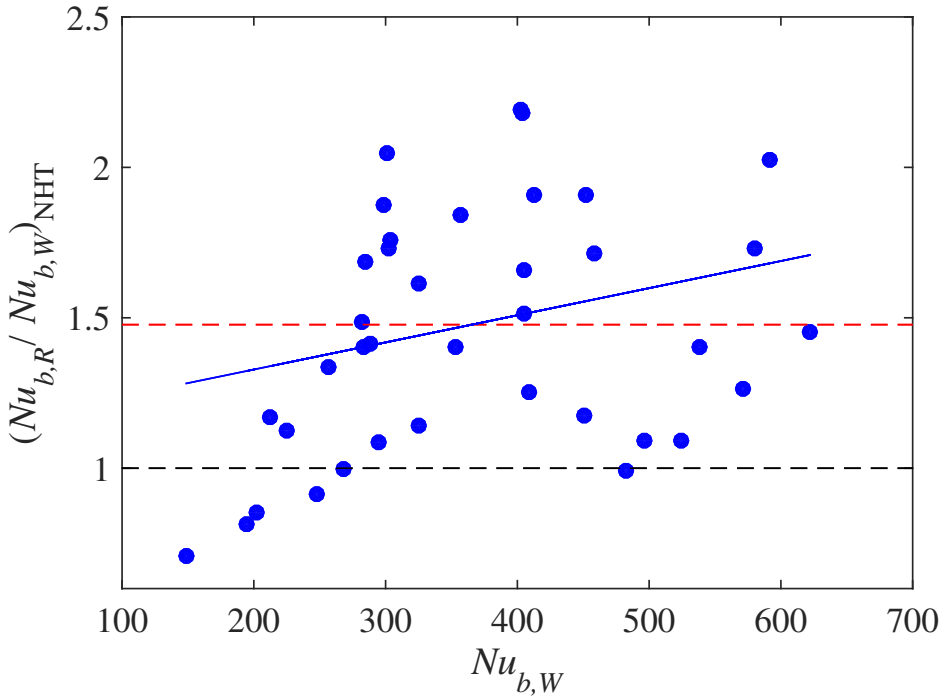

Figure 4.32: Ratios of experimental Nu_b in R134a and H_2O *vs.* $Nu_{b,W}$ for NHT; black dashed line indicates unit, red dashed line indicates average and solid blue line indicates linear-least-squares fit.

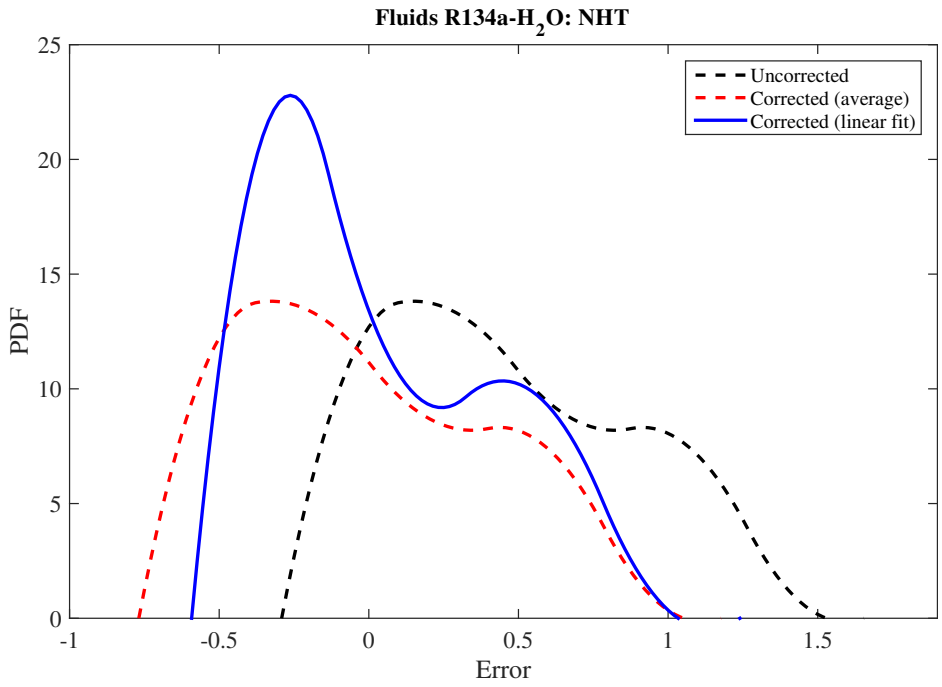

Figure 4.33: Probability density function of the fluids R134a and H_2O *vs.* error for NHT.

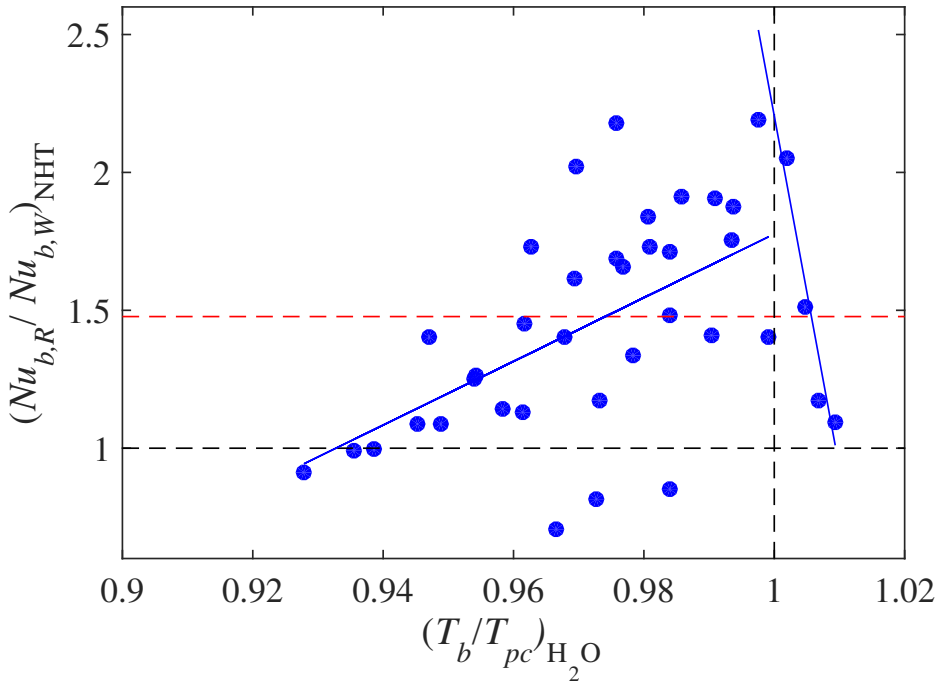

Figure 4.34: Ratio of experimental Nu_b in R134a and H_2O *vs.* normalised bulk temperature in H_2O for NHT; horizontal and vertical black dashed lines indicate unit, red dashed line indicates average and solid blue lines indicate, respectively, linear-least-squares fits in liquid- and gas-like regions.

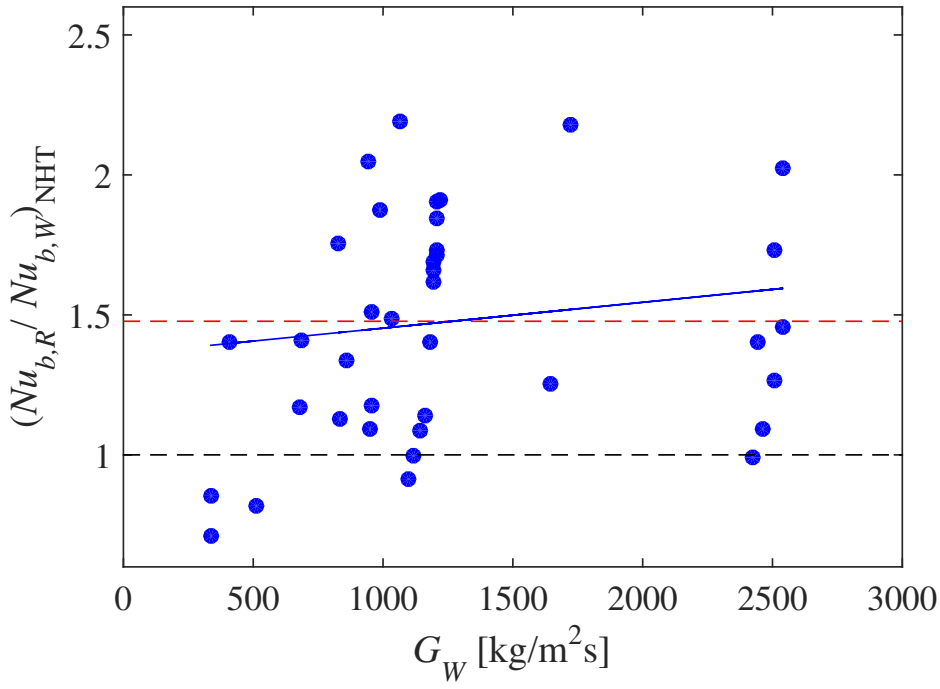

Figure 4.35: Ratios of experimental Nu_b in R134a and H_2O *vs.* mass flux G in H_2O for NHT; black dashed line indicates unit, red dashed line indicates average and solid blue line indicates linear-least-squares fit.

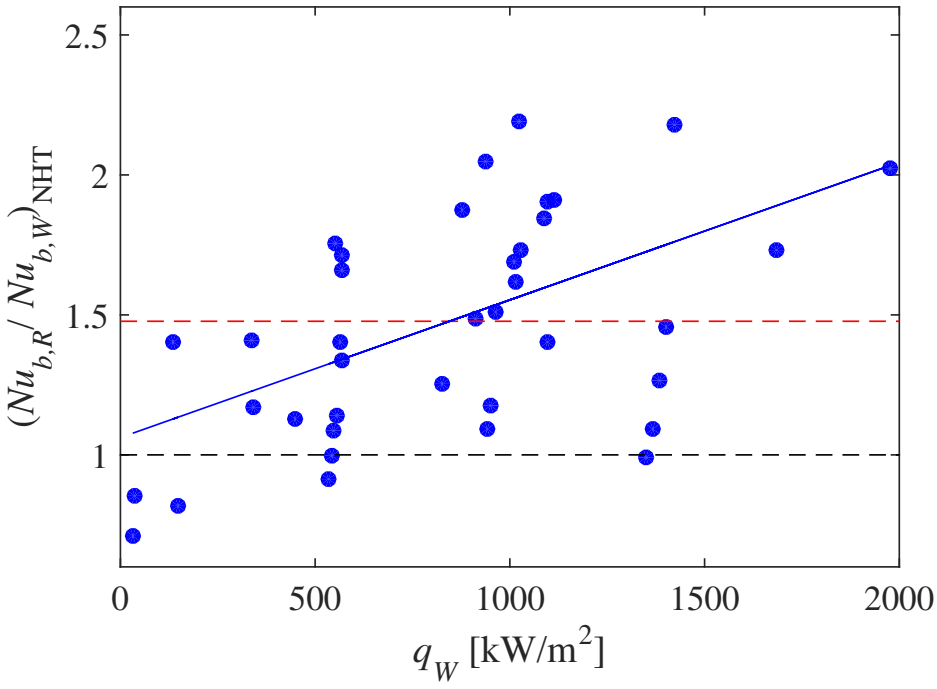

Figure 4.36: Ratios of experimental Nu_b in R134a and H_2O *vs.* heat flux q in H_2O for NHT; black dashed line indicates unit, red dashed line indicates average and solid blue line indicates linear-least-squares fit.

Figure 4.37 shows the ratio of experimental bulk Nusselt numbers for H_2O and R134a versus Nu_b in R134a, for NHT. The mean ratio was 0.74, which is lower than those in the other pairs of fluids for NHT. Its use reduced the STD of the error from 0.35 to 0.23 which is smaller than that for the RW pair. The WR correction factor was the product of the WC and CR correction factors. The data trend was significant and reverse to that for the RW pair. The previous observations are confirmed by the shapes of the PDF shown in Figure 4.38. Measurable downward trends of the Nusselt number ratio were observed with increasing T_b, G and q (Figures 4.39 to 4.41).

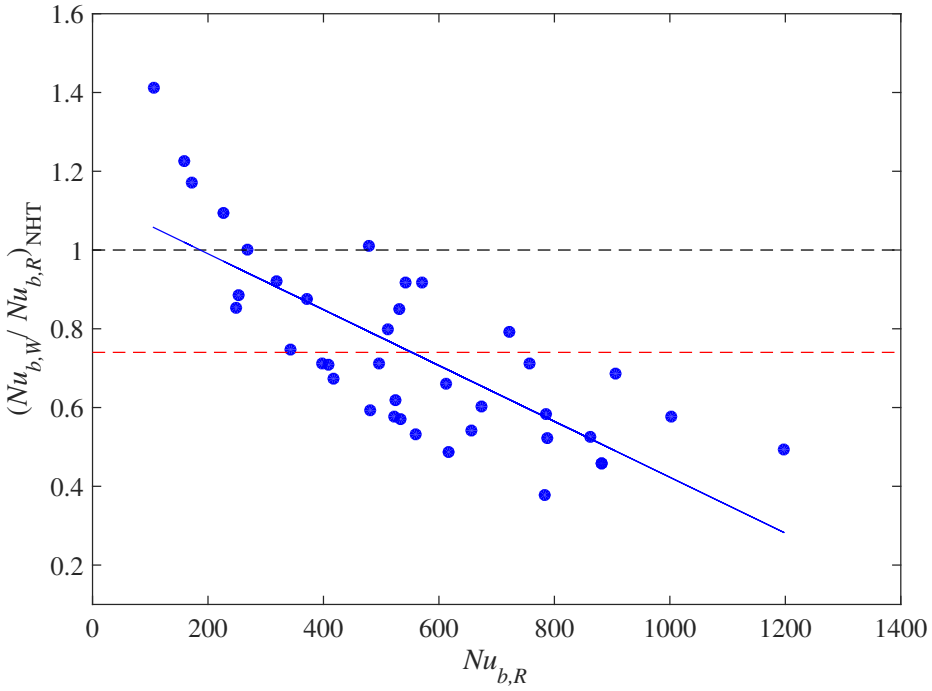

Figure 4.37: Ratios of experimental Nu_b in H_2O and R134a *vs.* $Nu_{b,R}$ for NHT; black dashed line indicates unit, red dashed line indicates average and solid blue line indicates linear-least-squares fit.

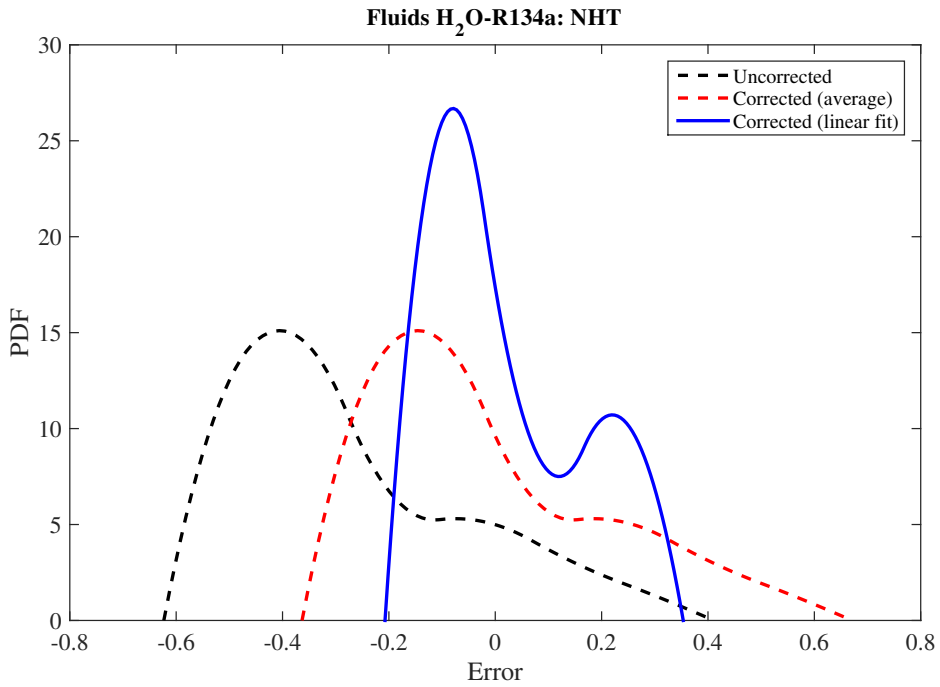

Figure 4.38: Probability density function of the fluids H_2O and R134a *vs.* error for NHT.

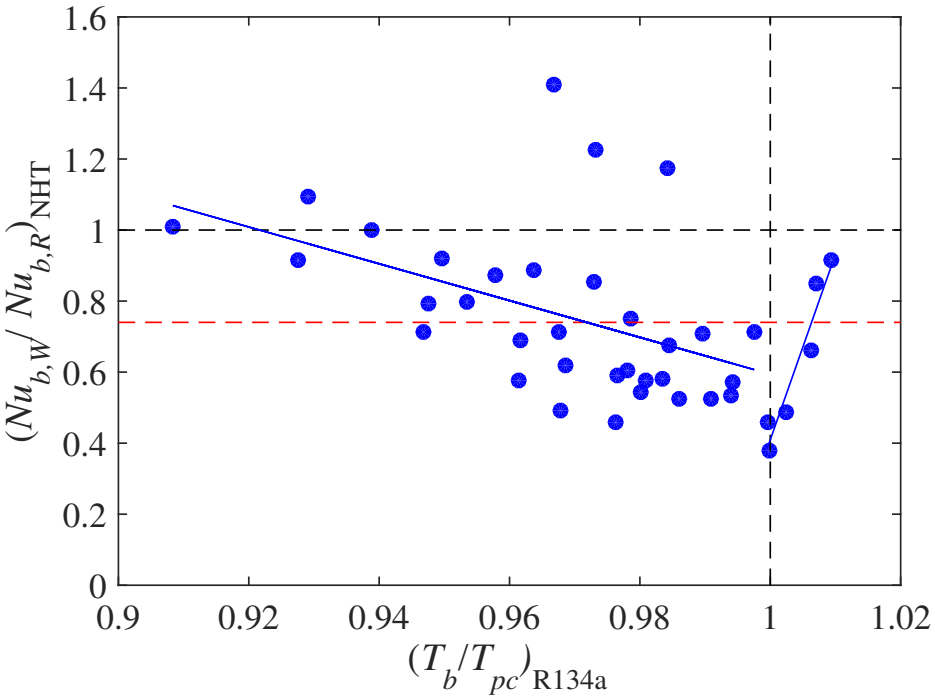

Figure 4.39: Ratio of experimental Nu_b in H_2O and R134a *vs.* normalised bulk temperature in R134a for NHT; horizontal and vertical black dashed lines indicate unit, red dashed line indicates average and solid blue lines indicate, respectively, linear-least-squares fits in liquid- and gas-like regions.

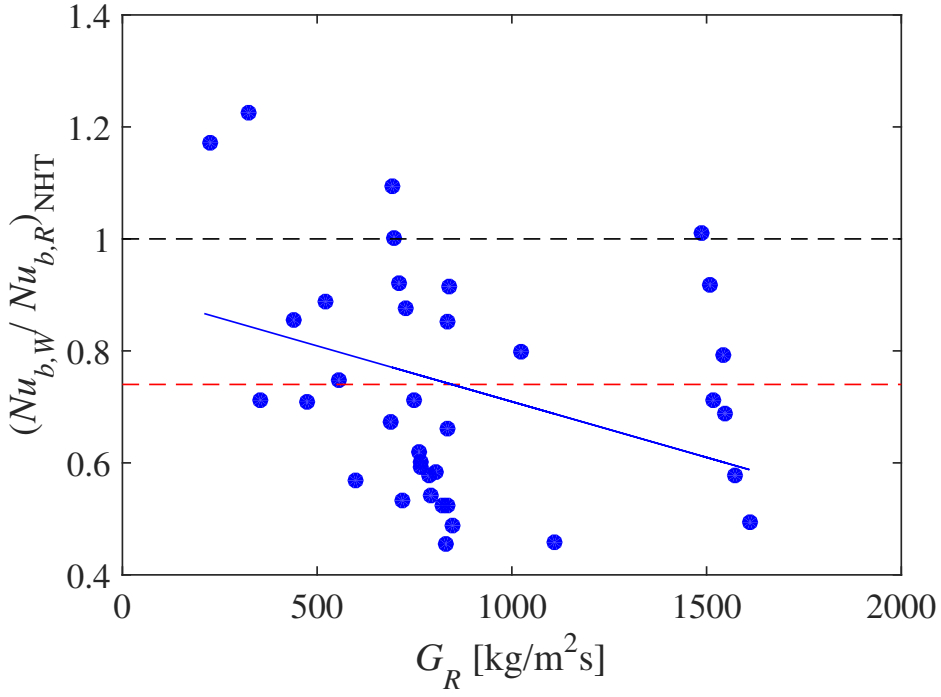

Figure 4.40: Ratios of experimental Nu_b in H_2O and R134a *vs.* mass flux G in R134a for NHT; black dashed line indicates unit, red dashed line indicates average and solid blue line indicates linear-least-squares fit.

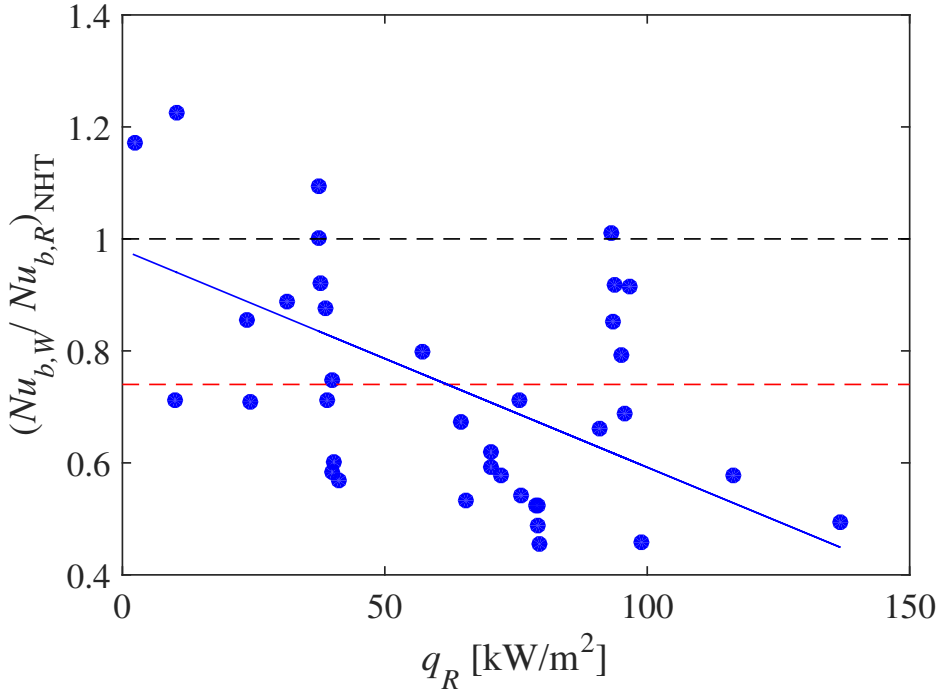

Figure 4.41: Ratios of experimental Nu_b in H_2O and R134a *vs.* heat flux q in R134a for NHT; black dashed line indicates unit, red dashed line indicates average and solid blue line indicates linear-least-squares fit.

4.6.2 Deteriorated heat transfer

Figures 4.42 to 4.46 show results for the RW pair of the same type as those in the previous sets of figures, but for conditions resulting in DHT in R134a. Similar results for the WR pair are shown in Figures 4.47 to 4.51. The mean ratio of experimental Nusselt numbers was 1.86 for RW and 0.65 for WR. These are the most extreme corrections by comparison to other results and show that the Zahlan et al. (2014) fluid-to-fluid scaling laws would apply roughly to R134a and water in DHT, provided that large correction factors are included. In fact, considering the strong dependence of the Nu_b ratio upon Nu_b, it would be preferable to apply corrections that depend linearly on the value of this parameter in the appropriate fluid. The Nu_b ratio also had a fairly strong dependence on T_b.

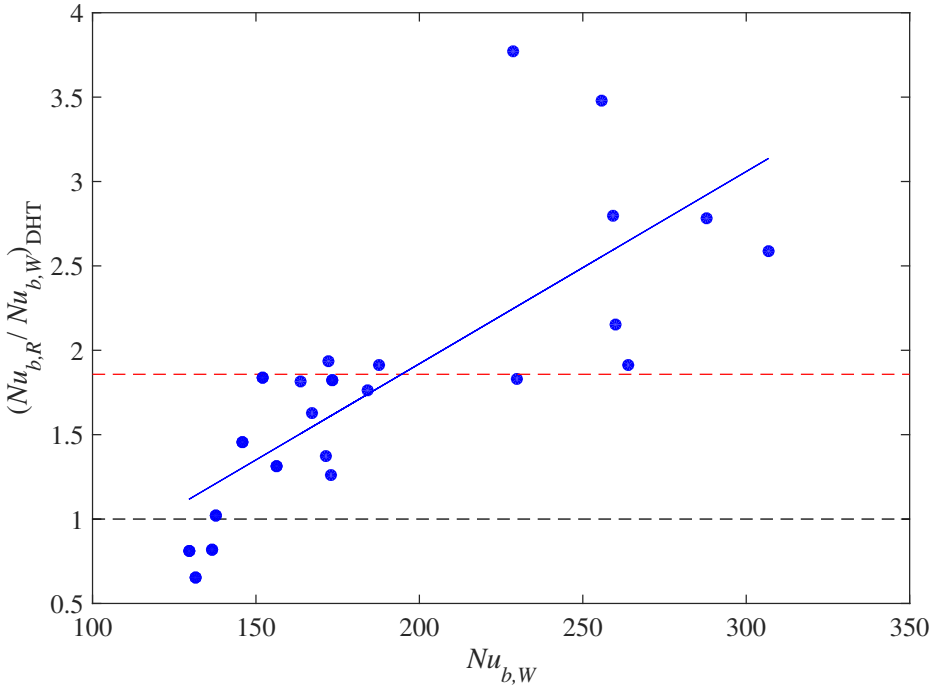

Figure 4.42: Ratios of experimental Nu_b in R134a and H_2O *vs.* $Nu_{b,W}$ for DHT; black dashed line indicates unit, red dashed line indicates average and solid blue line indicates linear-least-squares fit.

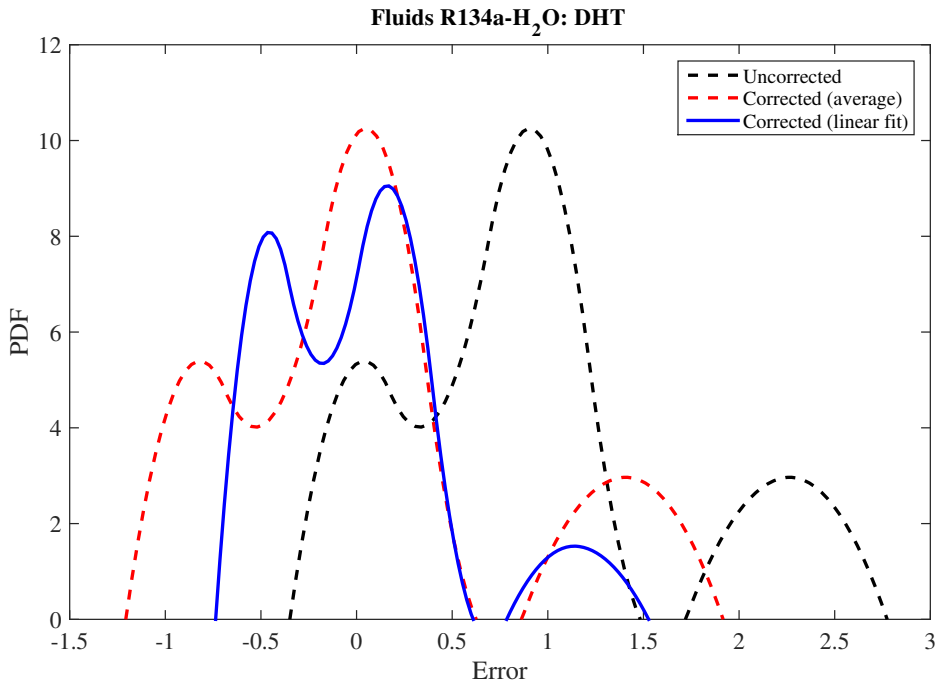

Figure 4.43: Probability density function of the fluids R134a and H_2O *vs.* error for DHT.

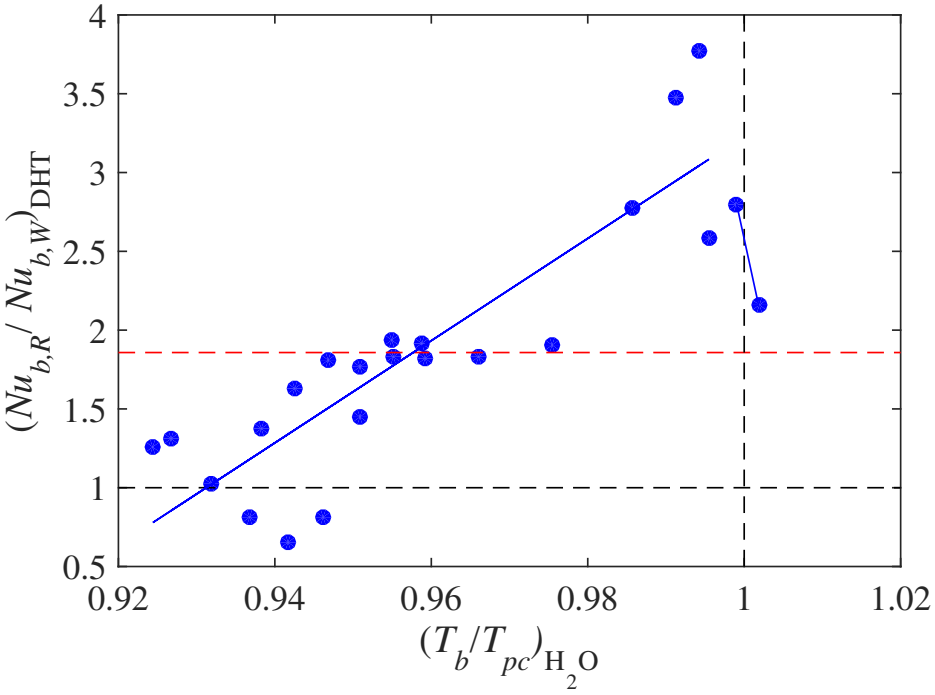

Figure 4.44: Ratio of experimental Nu_b in R134a and H_2O *vs.* normalised bulk temperature in H_2O for DHT; horizontal and vertical black dashed lines indicate unit, red dashed line indicates average and solid blue lines indicate, respectively, linear-least-squares fits in liquid- and gas-like regions.

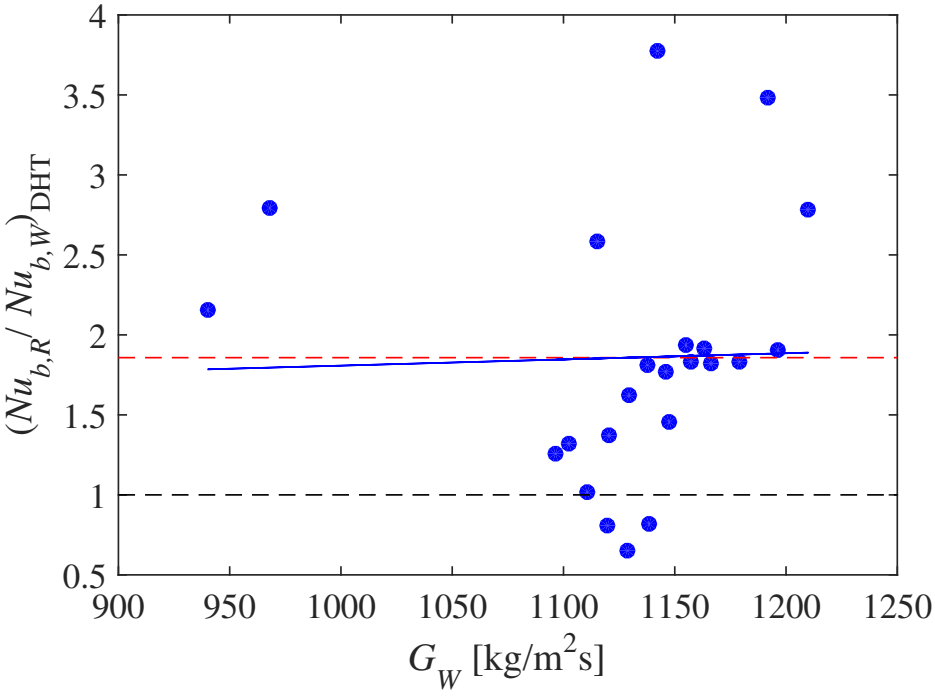

Figure 4.45: Ratios of experimental Nu_b in R134a and H_2O *vs.* mass flux G in H_2O for DHT; black dashed line indicates unit, red dashed line indicates average and solid blue line indicates linear-least-squares fit.

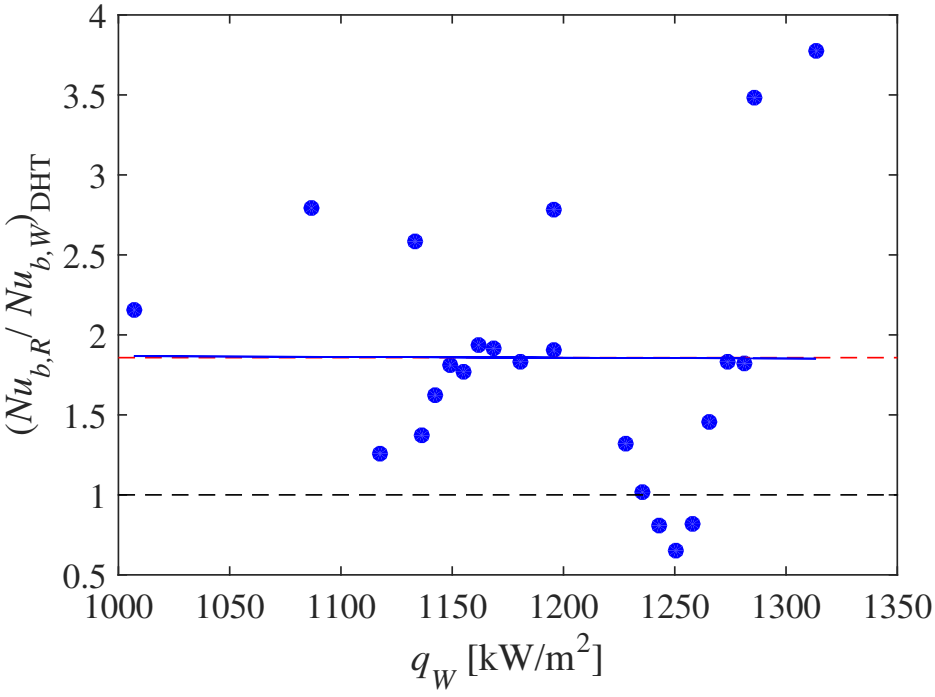

Figure 4.46: Ratios of experimental Nu_b in R134a and H_2O *vs.* heat flux q in H_2O for DHT; black dashed line indicates unit, red dashed line indicates average and solid blue line indicates linear-least-squares fit.

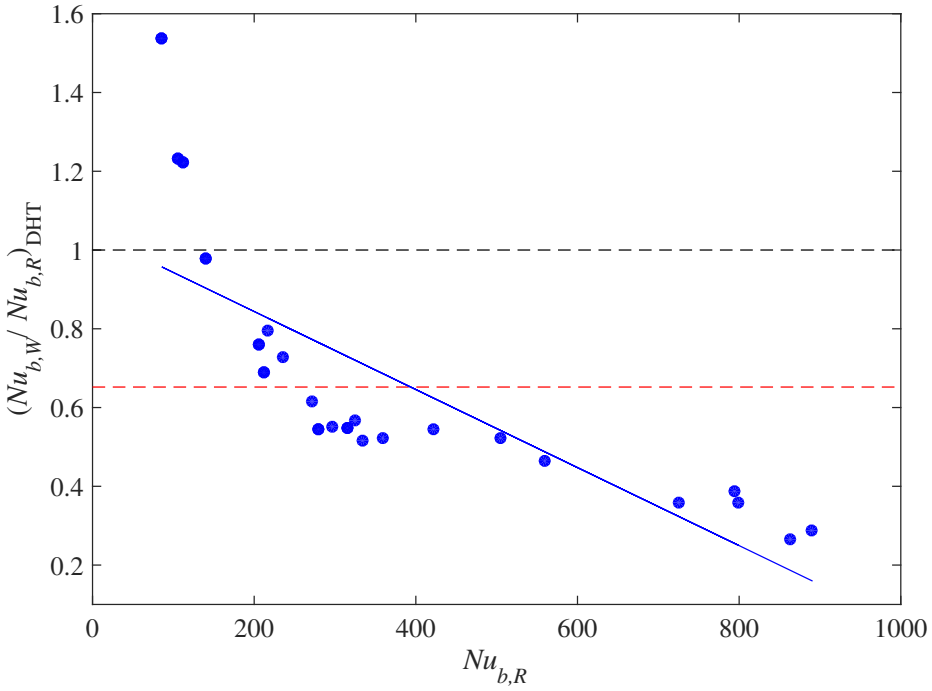

Figure 4.47: Ratios of experimental Nu_b in H_2O and R134a *vs.* $Nu_{b,R}$ for DHT; black dashed line indicates unit, red dashed line indicates average and solid blue line indicates linear-least-squares fit.

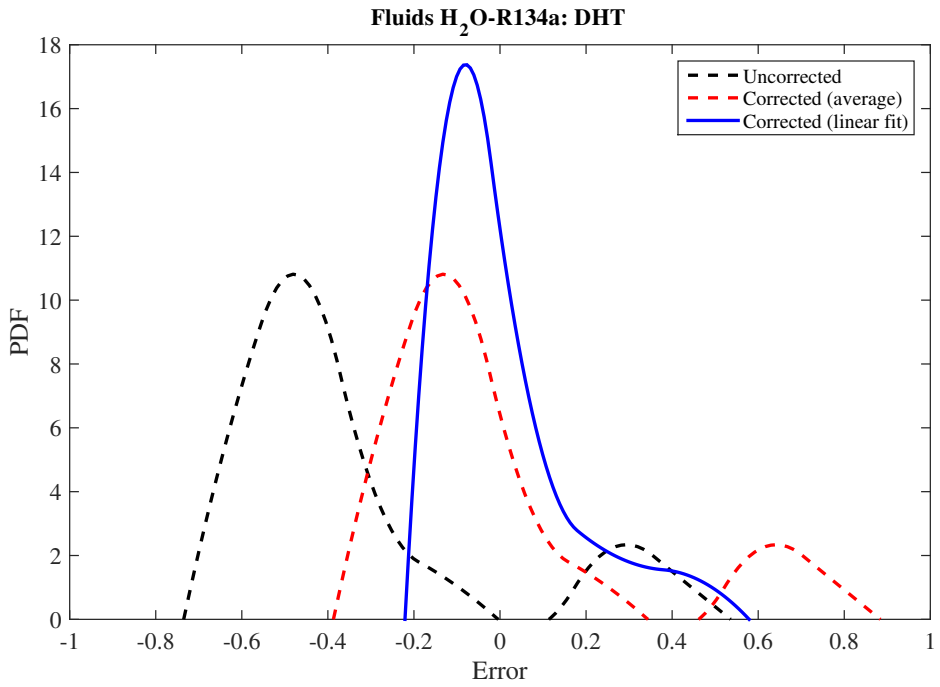

Figure 4.48: Probability density function of the fluids H_2O and R134a *vs.* error for DHT.

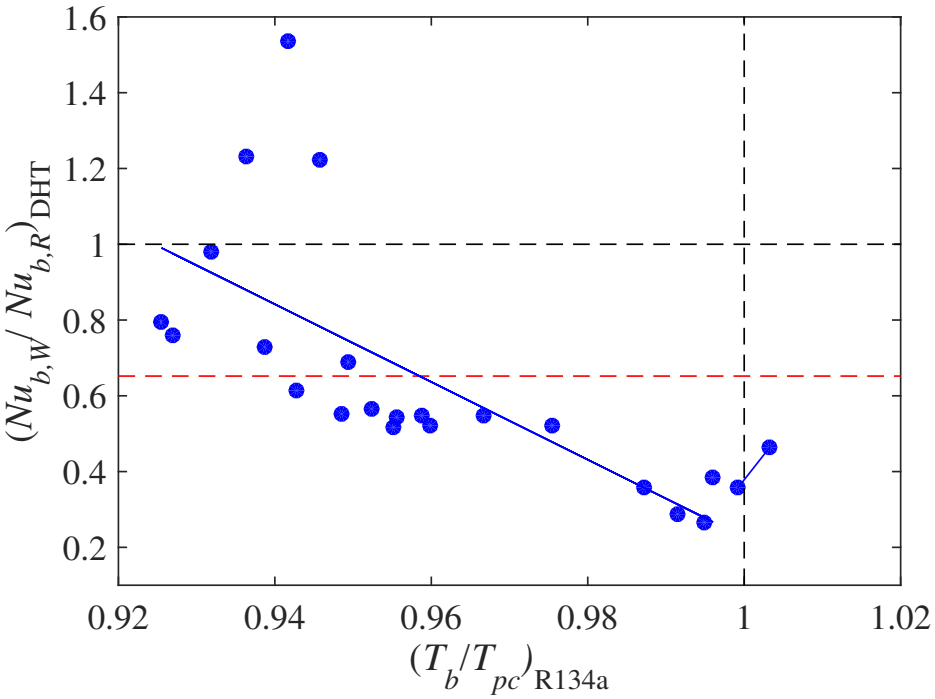

Figure 4.49: Ratio of experimental Nu_b in H_2O and R134a *vs.* normalised bulk temperature in R134a for DHT; horizontal and vertical black dashed lines indicate unit, red dashed line indicates average and solid blue lines indicate, respectively, linear-least-squares fits in liquid- and gas-like regions.

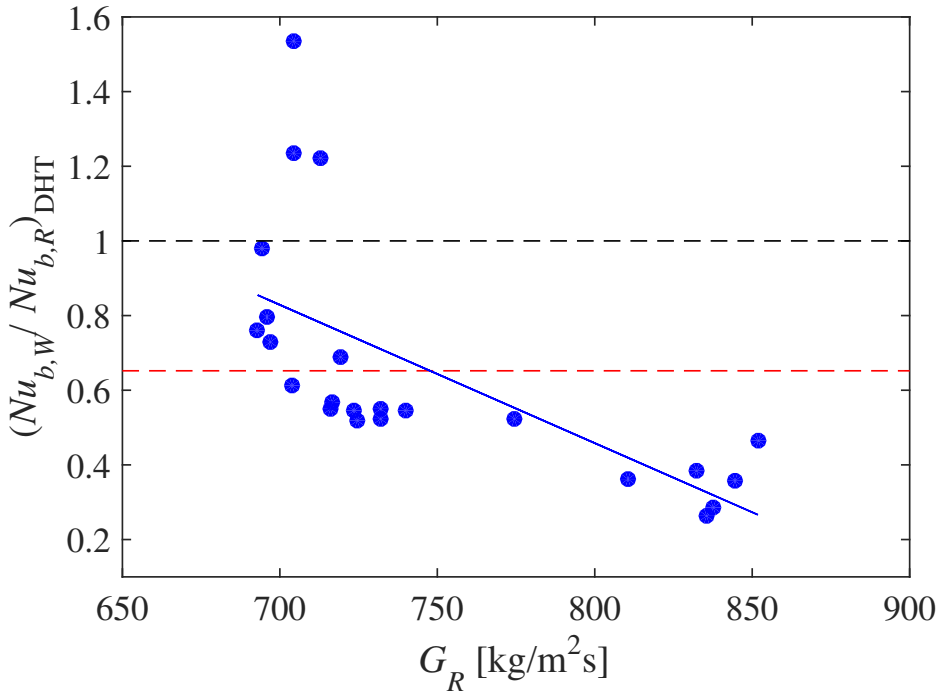

Figure 4.50: Ratios of experimental Nu_b in H_2O and R134a *vs.* mass flux G in R134a for DHT; black dashed line indicates unit, red dashed line indicates average and solid blue line indicates linear-least-squares fit.

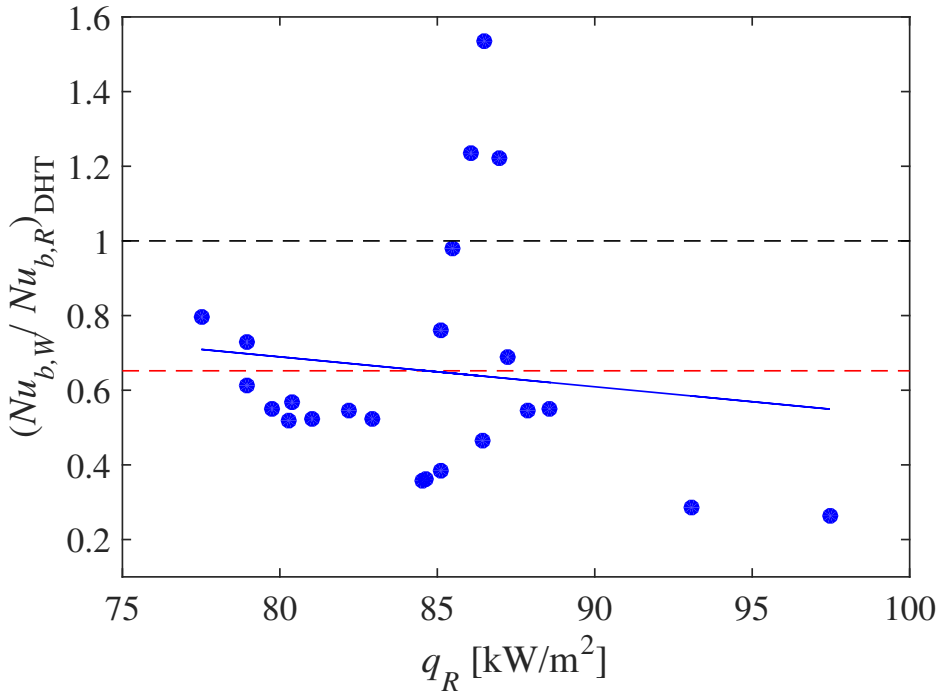

Figure 4.51: Ratios of experimental Nu_b in H_2O and R134a *vs.* heat flux q in R134a for DHT; black dashed line indicates unit, red dashed line indicates average and solid blue line indicates linear-least-squares fit.

4.7 General observations

Previous sections examined the error of the Zahlan et al. (2014) scaling laws applied to each of six pairs of fluids, expressed as the difference between the ratio of the Nusselt numbers $Nu_{b,2}/Nu_{b,1}$ in the two fluids and unit. Statistical analysis resulted in the determination of corrections specific to each pair of fluids, although scaling laws were meant to apply equally to all pairs of suitable fluids. This section contains some general observations that are based on comparisons of all available results.

Dependence on bulk Nusselt number: The Nusselt number ratio for each pair of fluids $2, 1$ under NHT conditions was plotted *vs.* $Nu_{b,1}$. The use of average and linearly varying corrections that were specific to each pair of fluids for NHT or DHT reduced somewhat the corresponding standard deviation of the scaling error. Nevertheless, individual errors remained large, thus compromising one's overall confidence in estimates based on these laws. The complexity of supercritical heat transfer phenomena makes it very difficult to identify the reasons for the presence of large individual errors and to devise appropriate corrections for such cases. When viewed casually, error plots appear to contain large scatter, superimposed on weak fluid–specific trends. A similar analysis to cases with DHT in at least one fluid also produced statistical corrections, but both correction levels and individual errors were larger than the ones corresponding to NHT cases. In conclusion, it is recognised that the fitted corrections make statistical improvement of the Zahlan et al. (2014) scaling laws but cannot account for relatively large errors under certain sets of conditions.

Dependence on mass flux and heat flux: It is self-evident that, if all other conditions were kept constant, the accuracy of fluid-to-fluid scaling laws would depend on the values of mass flux and heat flux. Nevertheless, plots of the Nusselt number ratio *vs.* these properties did not reveal any significant systematic trend and so, for the ranges considered, it does not seem possible to isolate the effects of mass flux and heat flux, if such exist.

Dependence on temperature: Figure 4.52 shows all NHT results plotted *vs.* the reduced temperature T_b/T_{pc}. The results for each pair of fluids show a systematic upward

or downward trend as T_b/T_{pc} increases towards 1 and the reverse trend as T_b/T_{pc} increases further. The important observation that can be made from this figure is that, when the fluids are well in the liquid-like region ($T_b/T_{pc} \leq 0.94$), the scaling errors are relatively small. Although the present results do not extend to sufficiently high temperatures to characterise the fluids as being well in the gas–like region, they show a clear trend that the scaling law errors would likely be relatively small for $T_b/T_{pc} \geq 1.02$. Similar observations can be made when at least one fluid was in DHT, as shown in Figure 4.53. In summary, the present results indicate that the Zahlan et al. (2014) scaling laws (without any fluid–specific correction) would be fairly accurate for the three pairs of fluids considered in the liquid–like region with $T_b/T_{pc} \leq 0.94$ and possibly in the gas–like region with $T_b/T_{pc} \geq 1.02$. Outside this range, scaling errors could be significant and would depend statistically on the pair of fluids and whether the fluids are under NHT or DHT conditions.

Dependence on scaling direction: The coefficients of corrections to the scaling laws for estimating $Nu_{b,2}$ were fitted to data with $Nu_{b,1}$ as the independent variable. Considering the large scatter of these data, it is not evident that the same corrections would also be accurate when the scaling direction is reversed. In other words, how accurately would one estimate $Nu_{b,1}$ from values of $Nu_{b,2}$ by inverting the previous correction expressions? To address this question, Table 4.4 lists the average correction factors for the three examined pairs of fluids and for both scaling directions for each pair, as well as the product of these correction factors, which should ideally be equal to 1. For NHT, the differences of the coefficient products from the ideal value are within 10%, which may be deemed to be within the overall uncertainty of such estimates. For DHT, these differences vary significantly from one pair to another, but remain within 21%, which may also be considered to be within the large uncertainty of DHT results. In conclusion, inversion of scaling corrections should not be expected to introduce dominant additional errors in fluid-to-fluid scaling.

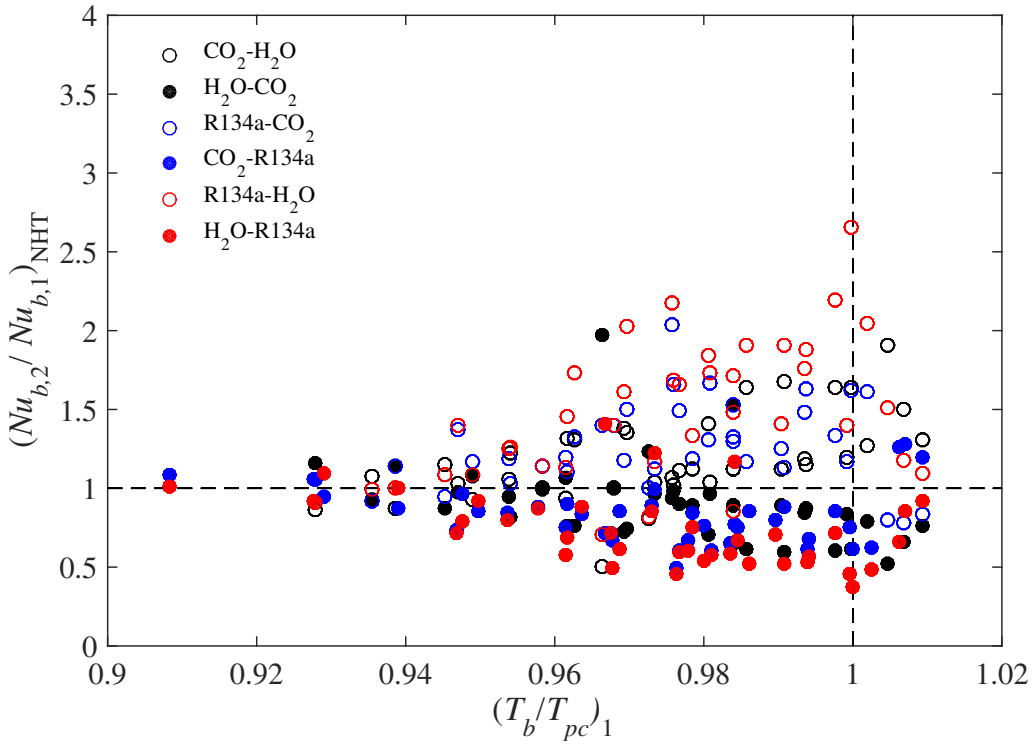

Figure 4.52: Ratios of bulk Nusselt numbers of six pairs of fluids 2 and 1 *vs.* normalised bulk temperature in fluid 1 for NHT in all fluids.

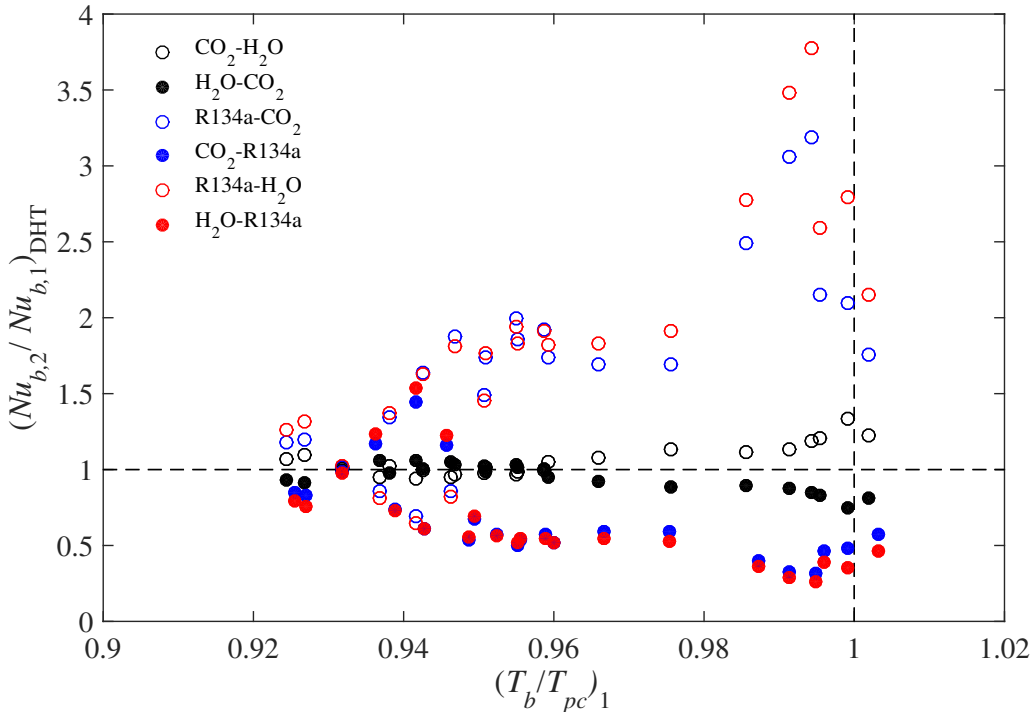

Figure 4.53: Ratios of bulk Nusselt numbers of six pairs of fluids 2 and 1 *vs.* normalised bulk temperature in fluid 1 for DHT in at least one fluid.

Table 4.4: Tests of reversibility of scaling direction

Fluids 2,1	$A_{2,1}$	$A_{1,2}$	$A_{2,1}A_{1,2}$
NHT			
$CO_2 - H_2O$ (CW)	1.17	0.91	1.06
R134a – CO_2 (RC)	1.27	0.82	1.04
R134a – H_2O (RW)	1.48	0.74	1.10
DHT			
$CO_2 - H_2O$ (CW)	1.06	0.95	1.01
R134a – CO_2 (RC)	1.72	0.67	1.15
R134a – H_2O (RW)	1.86	0.65	1.21

Chapter 5

Conclusion

5.1 Conclusions

Direct and indirect tests of fluid-to-fluid scaling laws for convective supercritical heat transfer were conducted for three fluids, H_2O, CO_2 and R134a at $P/P_c = 1.13$. The following main conclusions were based on these tests.

- The scaling laws of Zahlan et al. (2014) were found to have advantages over other suggestions. Differences in equivalent conditions calculated from three sets of laws were mostly relatively small.

- Statistical analysis resulted in the determination of average and linearly varying corrections to the Zahlan et al. (2014) scaling laws that were specific to each pair of fluids and to NHT or DHT conditions. The use of such corrections reduced somewhat the corresponding standard deviation of the scaling error but did not eliminate the presence of large errors under many sets of conditions. As expected, scaling errors were in general larger for DHT than NHT conditions.

- A possible systematic and correctable dependence of the scaling error upon the mass flux or heat flux was not identified in the present data.

- The Zahlan et al. (2014) scaling laws would be fairly accurate for the three pairs of

fluids considered in the liquid–like region with $T_b/T_{pc} \leq 0.94$ and possibly in the gas–like region with $T_b/T_{pc} \geq 1.02$. Outside this range, scaling errors could be significant and would depend statistically on the pair of fluids and whether the fluids are under NHT or DHT conditions.

- Some tests in R134a under conditions equivalent to those in CO_2 under NHT showed NHT in R134a, whereas some others showed DHT. Thus, the Zahlan et al. (2014) scaling laws do not scale accurately the onset of DHT in different fluids.

5.2 Unique features of this work

A comparison of the present study and previous tests of fluid-to-fluid scaling laws for supercritical heat transfer demonstrates that this is the only one in which measurements in two fluids were collected in the same facility and using the same instrumentation and experimental procedures under equivalent conditions of pressure, temperature, mass flux and wall heat flux, which were determined by application of the prevailing scaling laws. By doing so, we avoided the use of heat transfer correlations, which have their own relatively large uncertainty, especially for deteriorated heat transfer. Another unique feature of this work is that it allowed us to investigate by direct tests whether the mode of heat transfer in one fluid, namely whether it was normal or deteriorated, matched the heat transfer mode in the other when conditions were scaled according to the prevailing scaling laws for normal heat transfer.

5.3 Recommendations for future work

The following is a list of recommendations for future work within the capabilities of the SCUOL facility.

- Additional direct tests can be performed, especially under conditions with large discrepancies to ensure repeatability of the findings.

- For normal forced convective heat transfer mode, one could take more data in the

gas-like region to confirm that the trend in the bulk Nusselt number ratio is different from that in the liquid-like region.

- Direct tests of other scaling laws can be performed.
- Experimental determination of the onset of heat transfer deterioration in R134a under different condition can be made for comparison with available results in CO_2.

References

Ambrosini, W. (2011). Discussion of Similarity Principles for Fluid-to-Fluid Scaling of Heat Transfer Behaviour at Supercritical Pressures. *Nucl. Eng. Des.*, 241(12):5149 – 5173. The 18th International Conference on Nuclear Engineering (ICONE-18).

Azih, C. and Yaras, M. I. (2017). Similarity Criteria for Modeling Mixed-Convection Heat Transfer in Ducted Flows of Supercritical Fluids. *J. Heat Transfer*, 139(12):122501.

Cheng, X., Liu, X.J., and Gu, H.Y. (2011). Fluid-to-Fluid Scaling of Heat Transfer in Circular Tubes Cooled with Supercritical Fluids. *Nucl. Eng. Des.*, 241(2):498 – 508.

DuPont™Suva® (2005). Technical Reference Manual. Technical Report H-77939-5, DuPont™ Suva® Refrigerants, Wilmington, DE 19880-0711 (800) 235-SUVA, USA.

Feuerstein, F., Tian, R., Dai, X., and Shi, L. (2017). Fluid-to-Fluid Scaling of the Heat Transfer to Supercritical Fluids Based on Numerical Results. In *Proceedings of the Asian Conference on Thermal Sciences 2017, 1st ACTS*, number ACTS-P00566, Jeju Island, Korea.

Fewster, J. (1976). *Mixed Forced and Free Convective Heat Transferto Supercritical Pressure Fuids Flowing in Vertical Pipes.* PhD thesis, University of Manchester, Manchester, UK.

Fewster, J. and Jackson, J. D. (2004). *Experiments on Supercritical Pressure Convective Heat Transfer Having Relevance to SPWR.* Number 4342 in 1. American Nuclear Society, Pittsburgh, USA.

GIF (2016). GIF Annual Report. Technical report, Generation IV International Forum (GIF).

GIF (2017). Generation IV International Forum. https://www.gen-4.org/gif.

Government of Canada (2017). Regulatory information, Depletion, Impacts, Climate Change and Protection of the Ozone Layer. www.canada.ca/en/environment-climate-change/services/air-pollution/issues/ozone-layer.html.

Jackson, J. D. (2007). Requirements for Similarity in the Case of Heat Transfer to Fluids at Pressures Above the Critical Value and an Approach to Correlation of Experimental Data, Paper G3. in: Proceedings of the 10th UK National Heat Transfer Conference, Edinburgh, September.

Jackson, J. D. (2008). A Semi-Empirical Model of Turbulent Convective Heat Transfer to Fluids at Supercritical Pressure. in: 16th International Conference on Nuclear Engineering, Orlando, Florida, USA, May 11-15.

Jackson, J. D. and Hall, W. B. (1979). Forced Convection Heat Transfer to Fluids at Supercritical Pressure. *Institution of Mechanical Engineers, Conference Publications*, 2:563–611.

Jiang, K. (2015). An Experimental Facility for Studying Heat Transfer in Supercritical Fluids. Master's thesis, University of Ottawa, Ottawa, Canada.

Kline, N. (2017). An experimental study of heat transfer deterioration at supercritical pressures. Master's thesis, University of Ottawa, Ottawa, Canada.

Kline, N., Feuerstein, F., and Tavoularis, S. (2018). Onset of Heat Transfer Deterioration in Vertical Pipe Flows of CO_2 at Supercritical Pressures. *Int. J. Heat Mass Tran.*, 118:1056 – 1068.

Lemmon, E. W., McLinden, M. O., and Friend, D. G. (2002). Thermophysical Properties of Fluid Systems. National Institute of Standards and Technology (NIST) Standard Reference Database Number 69, NIST Reference Fluid Thermodynamics Properties Database (REFPROP): Version 7.0, 2002.

Pioro, I. L. and Duffey, R. B. (2007). *Heat Transfer and Hydraulic Resistance at Supercritical Pressures in Power Engineering Applications*. ASME Press, New York, NY, USA.

Pioro, I. L., Mokry, S., and Draper, S. (2011). Specifics of Thermophysical Properties and Forced-Convective Heat Transfer at Critical and Supercritical Pressures. *Rev. Chem. Eng.*, 27(3-4):191–214.

Poling, B. E., Prausnitz, J. M., and O'Connell, J. P. (2001). *Properties of Gases and Liquids*. McGraw-Hill Global Education Holdings, 5th edition.

Pucciarelli, A. and Ambrosini, W. (2016). Fluid-to-Fluid Scaling of Heat Transfer Phenomena with Supercritical Pressure Fluids: Results from RANS Analyses. *Ann. Nucl. Energy*, 92:21–35.

Tavoularis, S. (2009). *Measurement in Fluid Mechanics*. Cambridge University Press, 1 edition.

Yetisir, M., Gaudet, M., Pencer, J., Michael McDonald, D. R., Hamilton, H., and Leung, L. (2016). Forced Convective Heat Transfer to Supercritical Water Flowing in Tubes. *CNL Nuclear Review*, 5(2):189–202.

Yu, G., Jiang, C., Wang, L., Su, G.H., and Qiu, S.Z. (2018). A New Method on Fluid-to-Fluid Scaling for Heat Transfer in Tubes at Supercritical Pressures. *Int. J. Heat Mass Tran.*, 126:809 – 822.

Zahlan, H., Groeneveld, D.C., and Tavoularis, S. (2014). Fluid-to-Fluid Scaling for Convective Heat Transfer in Tubes at Supercritical and High Pressures. *Int. J. Heat Mass Tran.*, 73(1):274–283.

Zahlan, H., Groeneveld,D.C., and Tavoularis, S. (2015a). Measurements of Convective Heat Transfer to Vertical upwad Flows of CO_2 in Circular Tubes at Near-Critical and Cupercritical Pressures. *Nucl. Eng. Des.*, 289(1):92–107.

Zahlan, H., Tavoularis, S., and Groeneveld, D.C. (2015b). A Look-Up Table for Trans-Critical Heat Transfer in Water-Cooled Tubes. *Nucl. Eng. Des.*, 285:109 – 125.

Zwolinski, S., Anderson, M., Corradini, M., and Lichet, J. (2011). Evaluation of Fluid-to-Fluid Scaling Method for Water and Carbon Dioxide at Supercritical Pressure. in: 15th

International Symposium on Supercritical Water-Cooled Reactors (SCWR5),Vancouver, Canada, March.

Appendices

Appendix A

Thermophysical properties

Supplemental information about thermophysical properties at $P = 1.13P_c$ for H_2O, CO_2 and R134a.

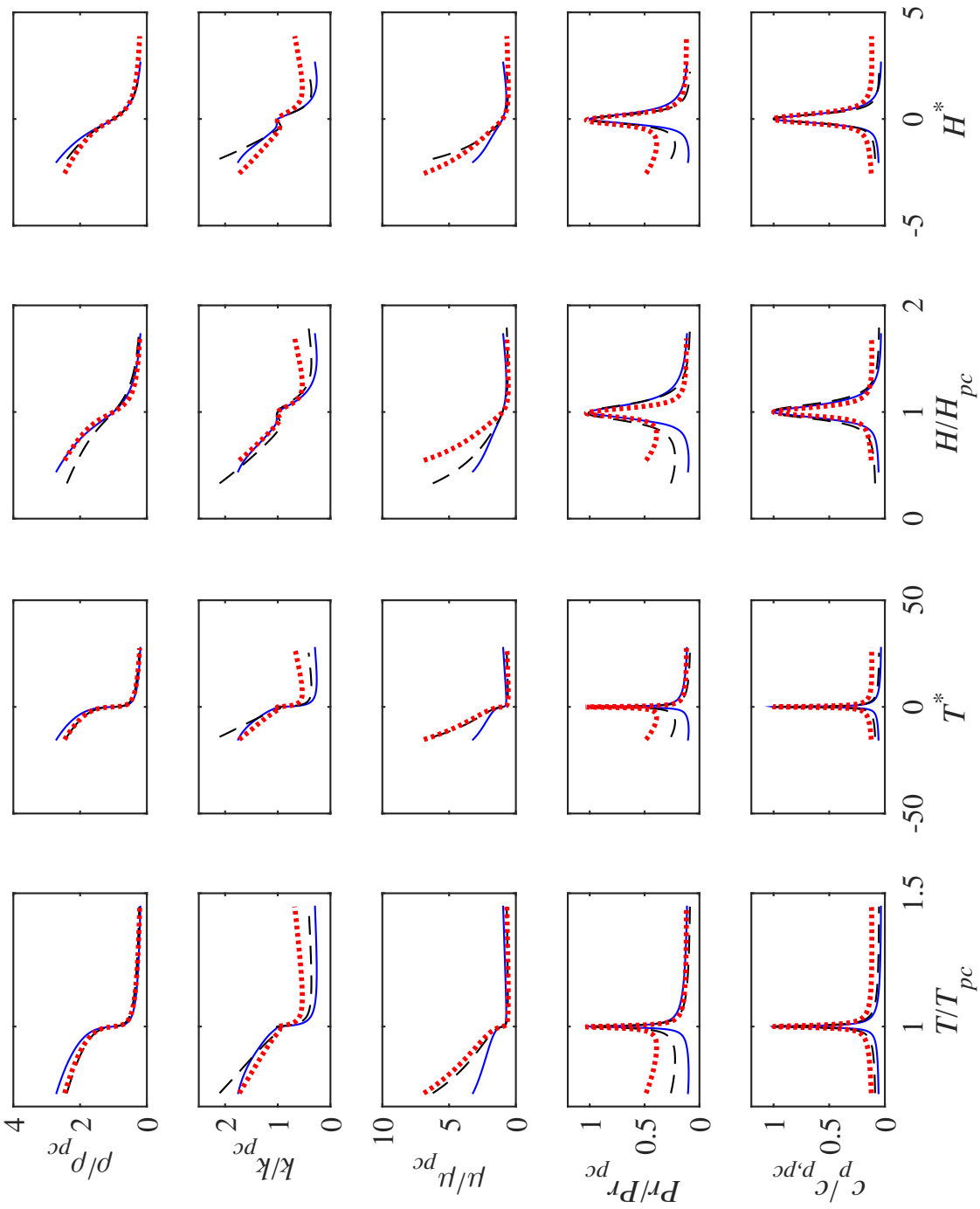

Figure A.1: Summary of the normalised thermophysical properties of the three fluids; blue solid, black dashed, and red dotted lines correspond, respectively, to H_2O, CO_2, and R134a (Lemmon et al., 2002).

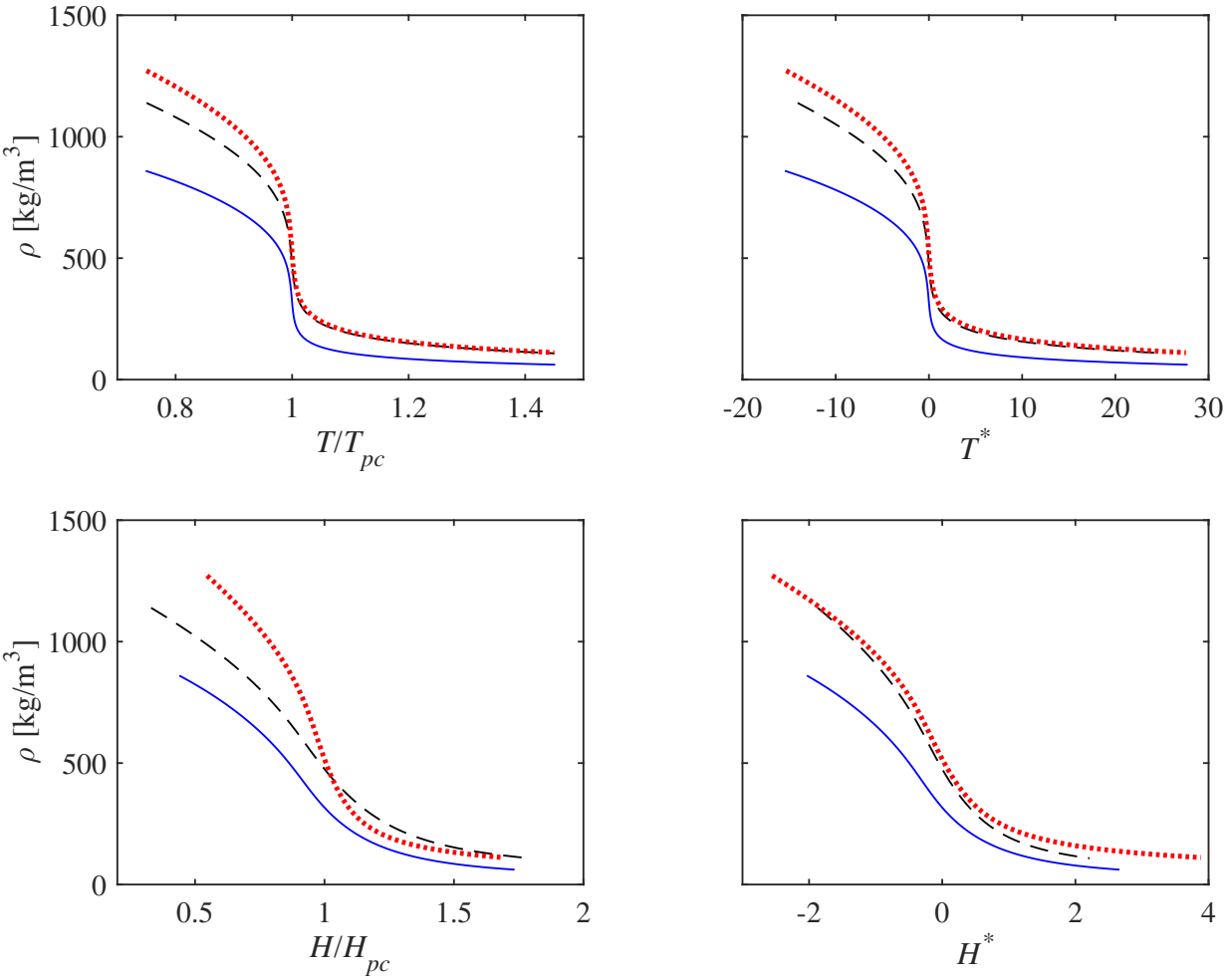

Figure A.2: Density variation of the three fluids; blue solid, black dashed, and red dotted lines correspond, respectively, to H_2O, CO_2, and R134a (Lemmon et al., 2002).

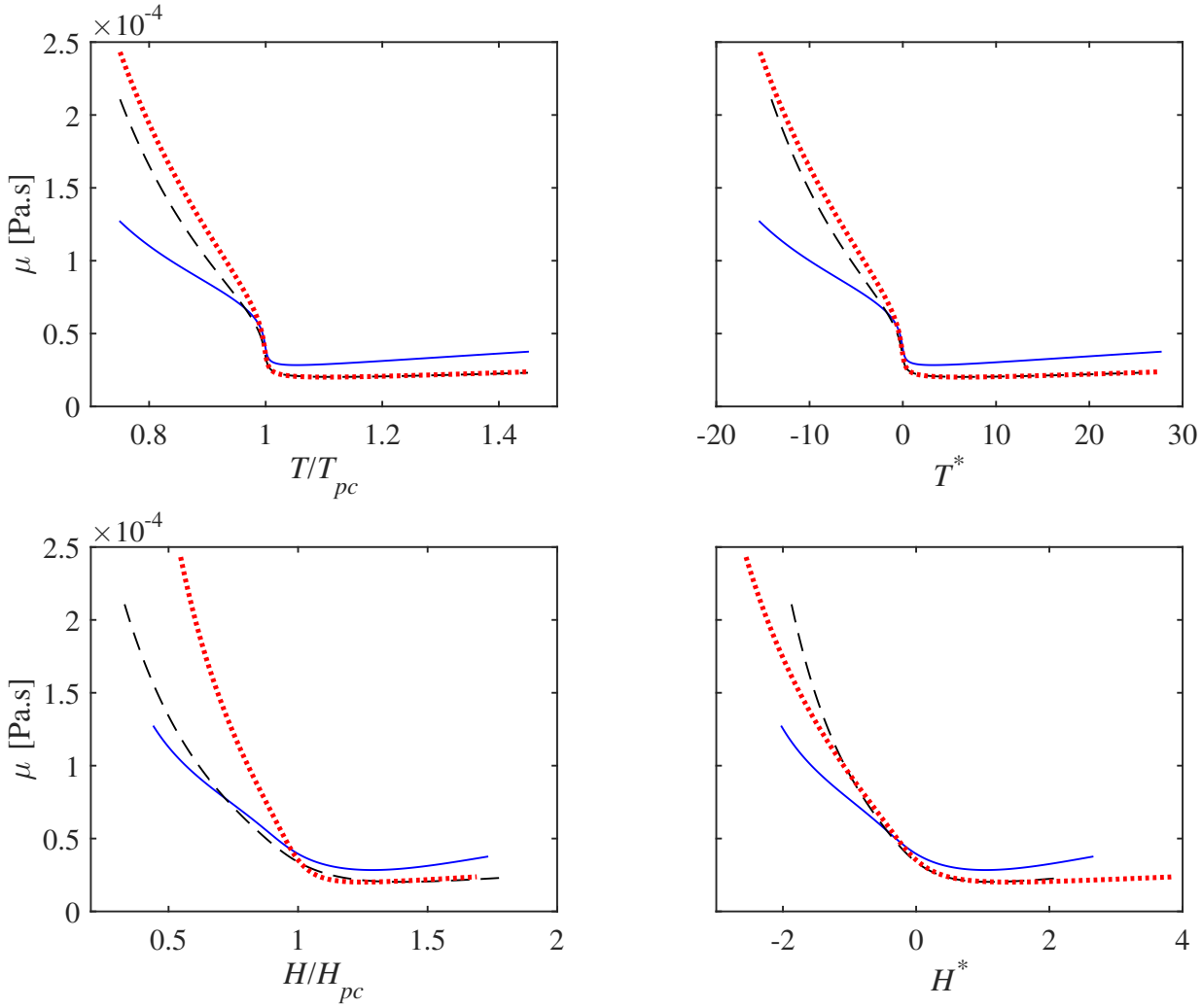

Figure A.3: Dynamic viscosity variation of the three fluids; blue solid, black dashed, and red dotted lines correspond, respectively, to H_2O, CO_2, and R134a (Lemmon et al., 2002).

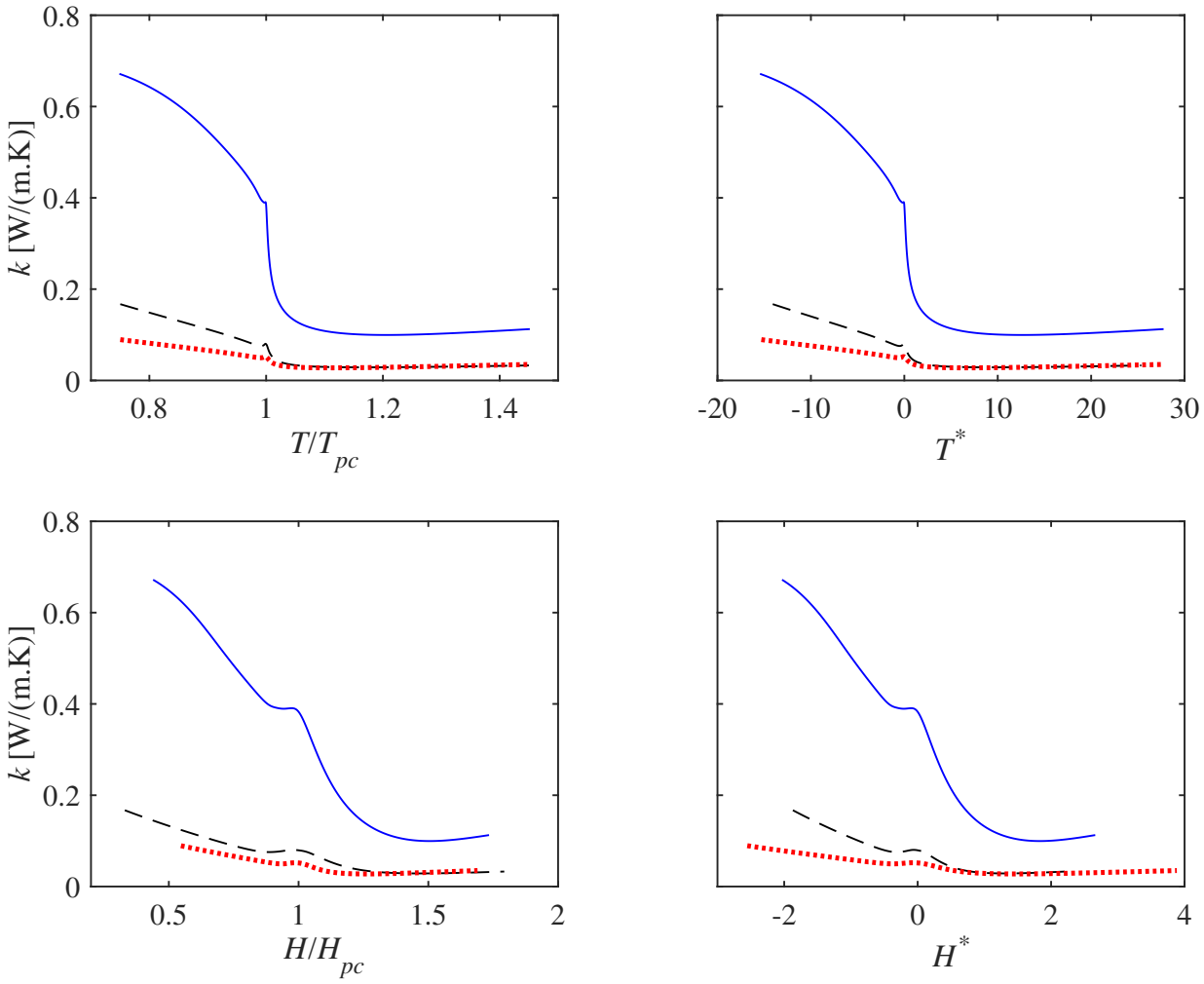

Figure A.4: Thermal conductivity variation of the three fluids; blue solid, black dashed, and red dotted lines correspond, respectively, to H_2O, CO_2, and R134a (Lemmon et al., 2002).

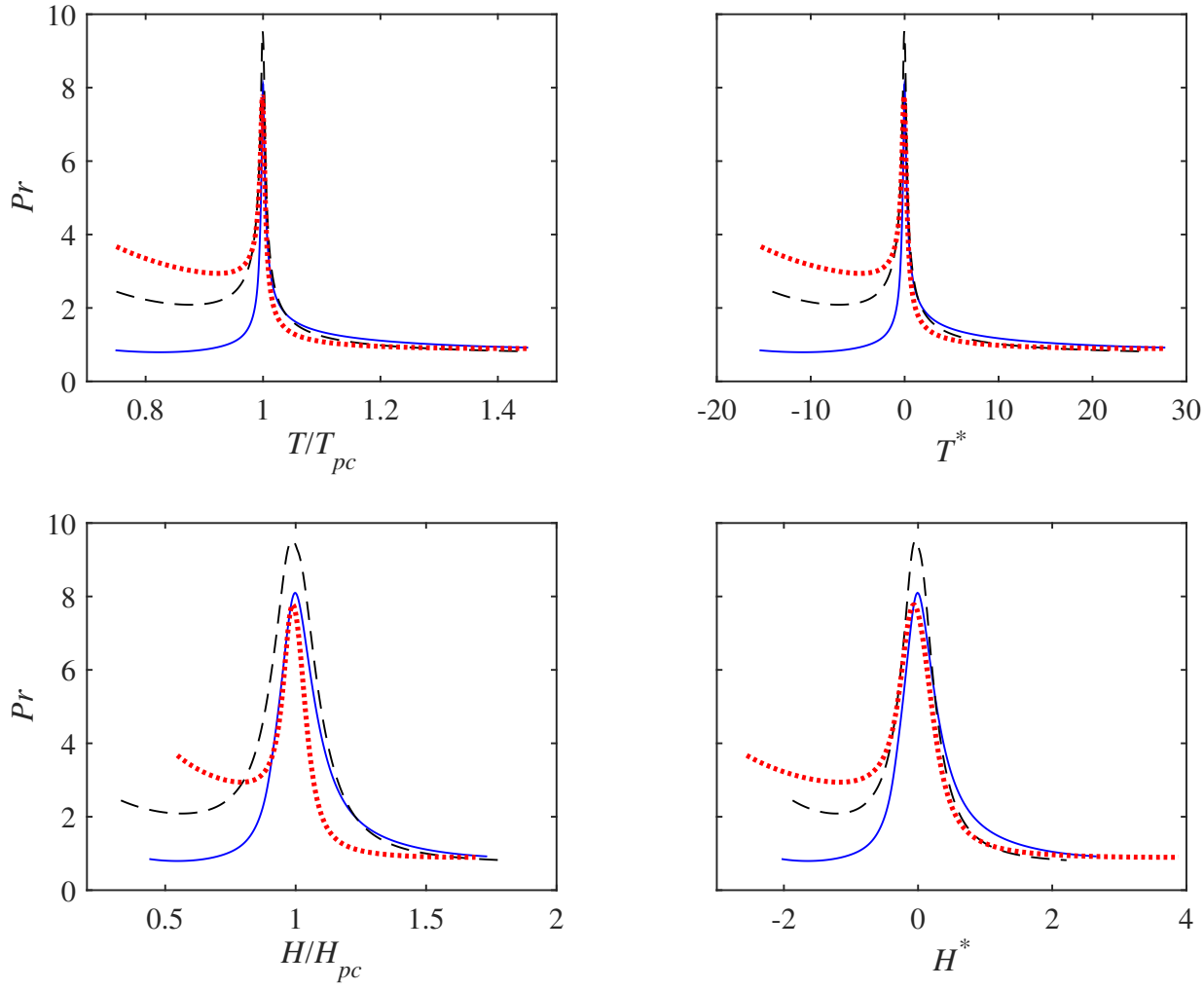

Figure A.5: Prandtl number variation of the three fluids; blue solid, black dashed, and red dotted lines correspond, respectively, to H_2O, CO_2, and R134a (Lemmon et al., 2002).

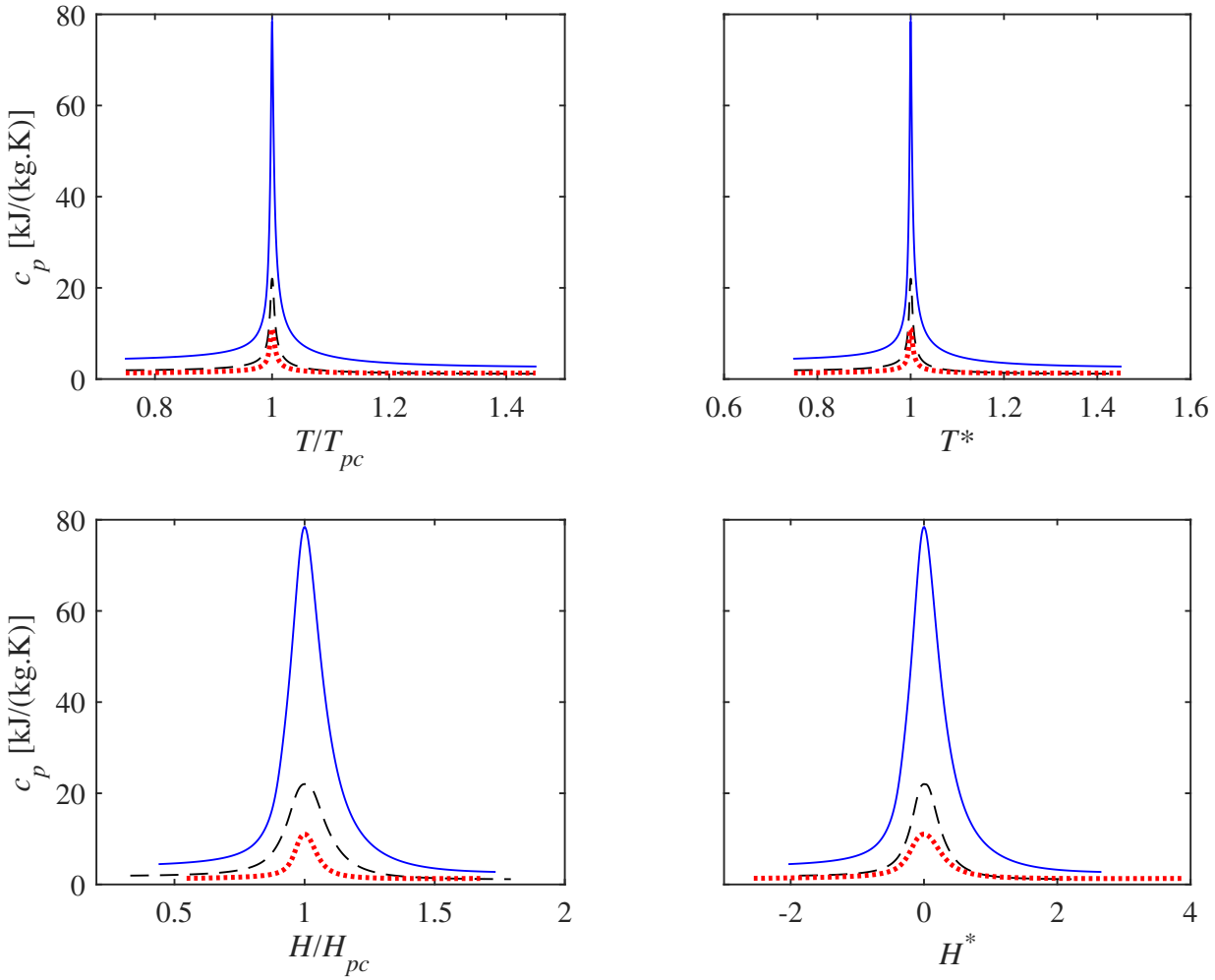

Figure A.6: Specific heat capacity variation of the three fluids; blue solid, black dashed, and red dotted lines correspond, respectively, to H_2O, CO_2, and R134a (Lemmon et al., 2002).

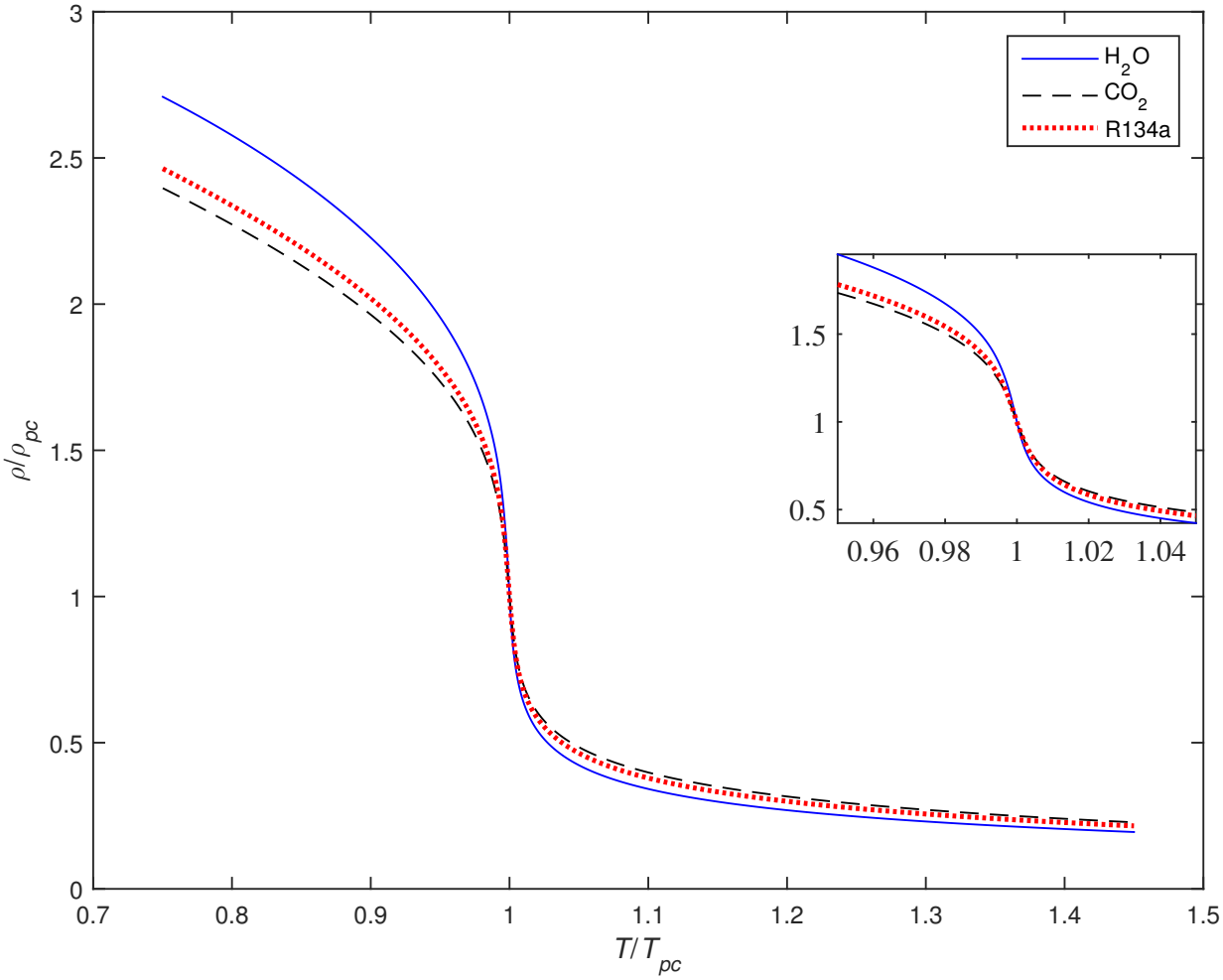

Figure A.7: The Normalised density versus bulk temperature ratio T_b/T_{pc} with its zoom out of the three fluids H_2O, CO_2, and R134a (Lemmon et al., 2002).

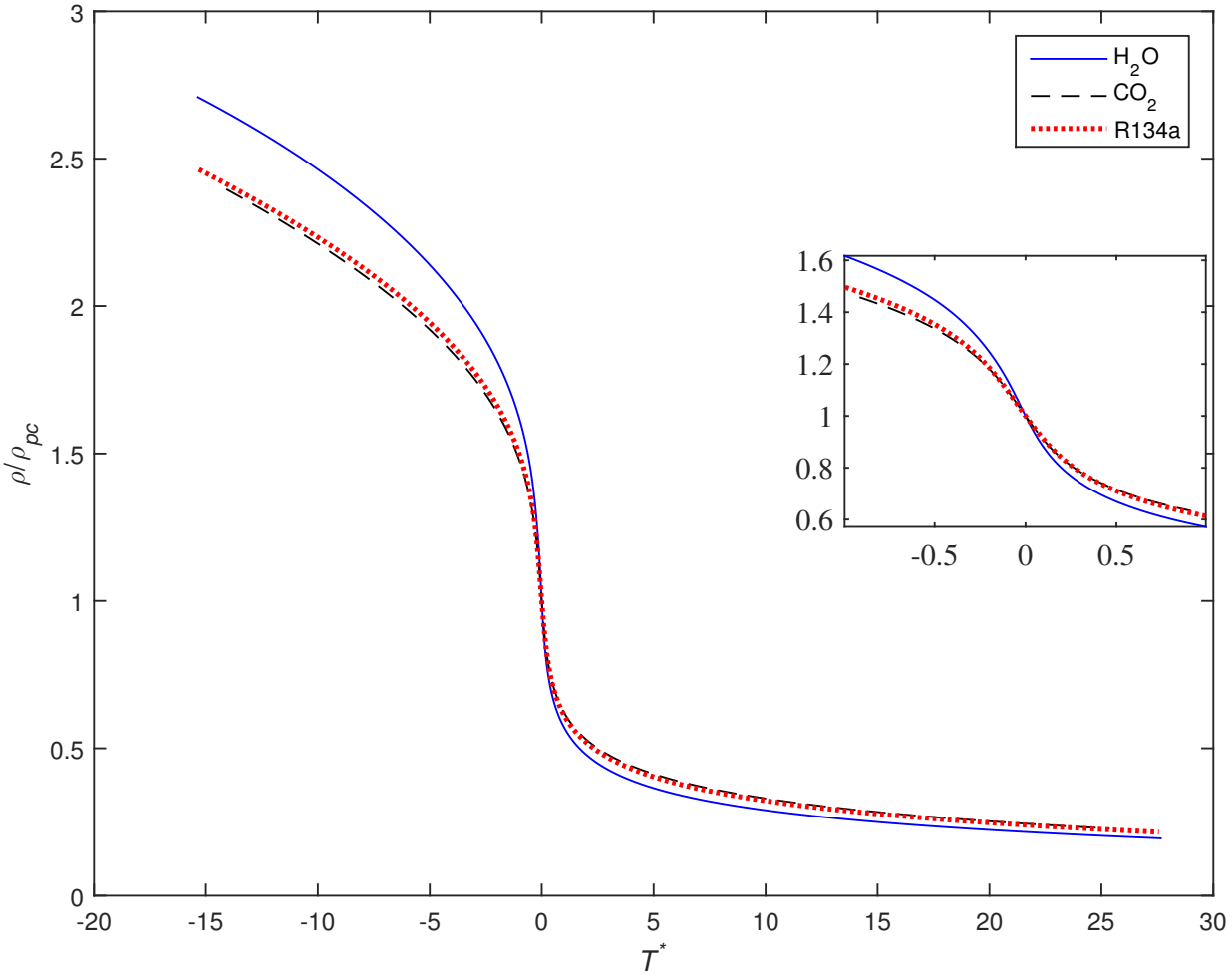

Figure A.8: The Normalised density versus bulk temperature T^* with its zoom out of the three fluids H_2O, CO_2, and R134a (Lemmon et al., 2002).

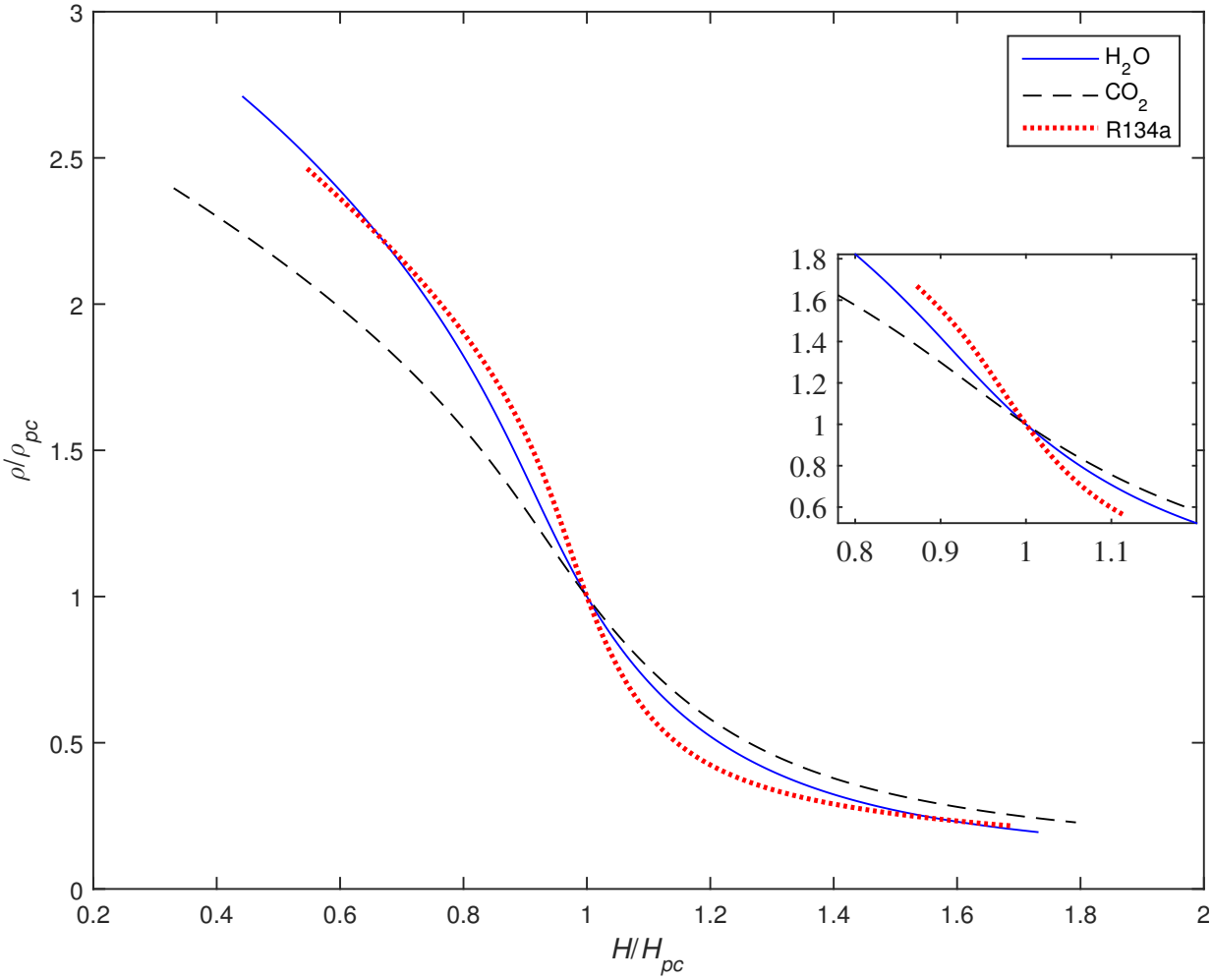

Figure A.9: The Normalised density versus bulk enthalpy ratio H_b/H_{pc} with its zoom out of the three fluids H_2O, CO_2, and R134a (Lemmon et al., 2002).

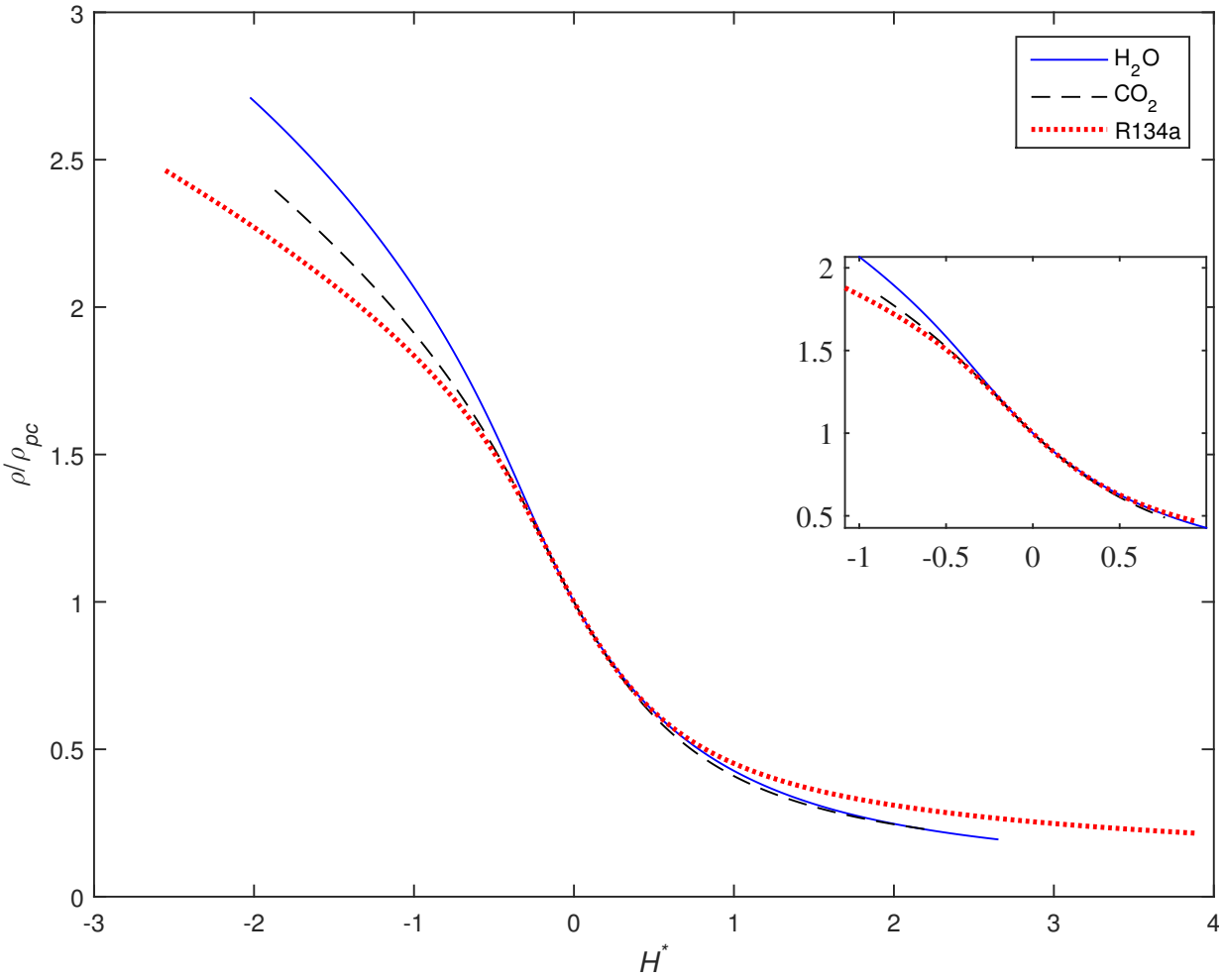

Figure A.10: The Normalised density versus bulk enthalpy H^* with its zoom out of the three fluids H_2O, CO_2, and R134a (Lemmon et al., 2002).

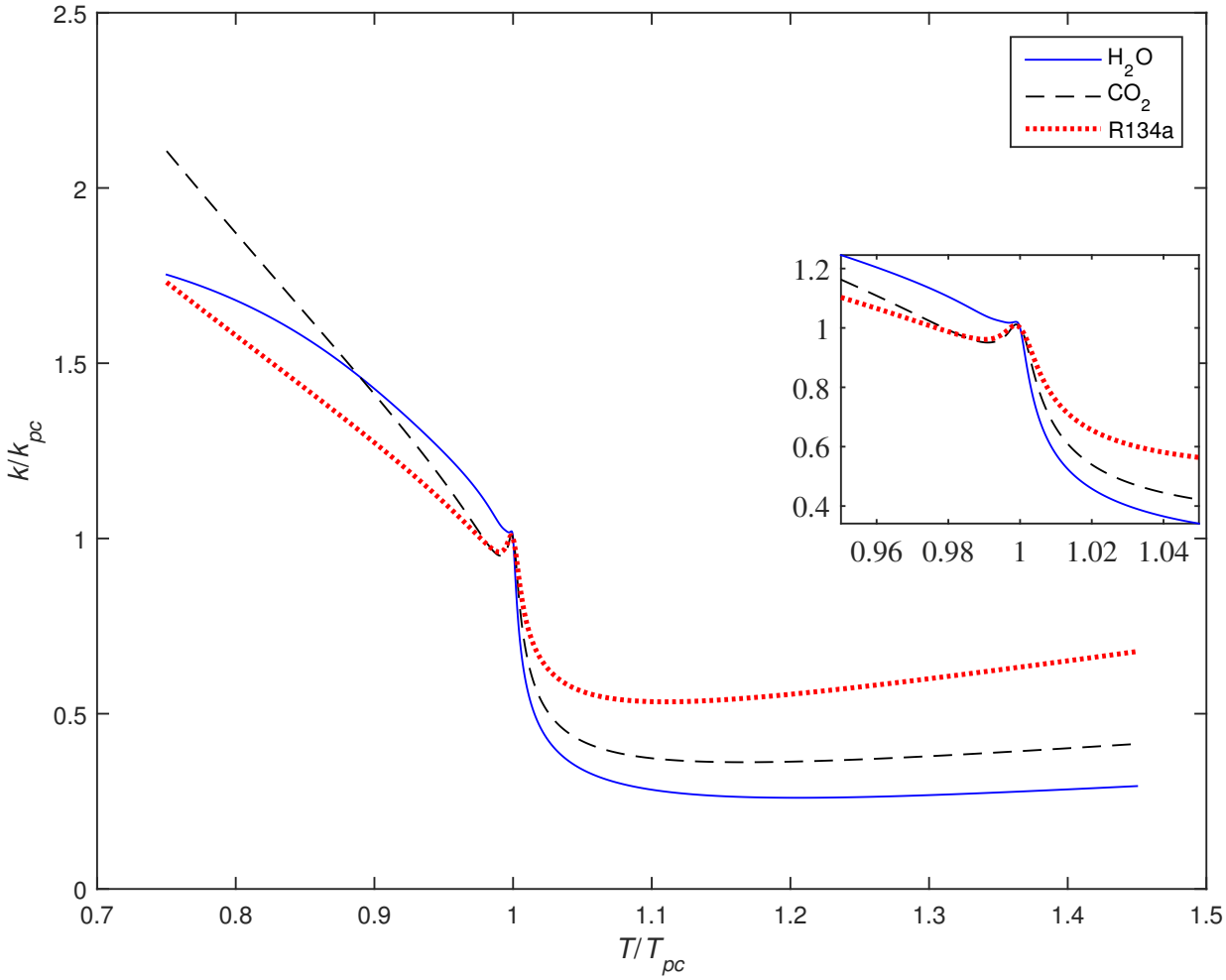

Figure A.11: The Normalised thermal conductivity versus bulk temperature ratio T_b/T_{pc} with its zoom out of the three fluids H_2O, CO_2, and R134a (Lemmon et al., 2002).

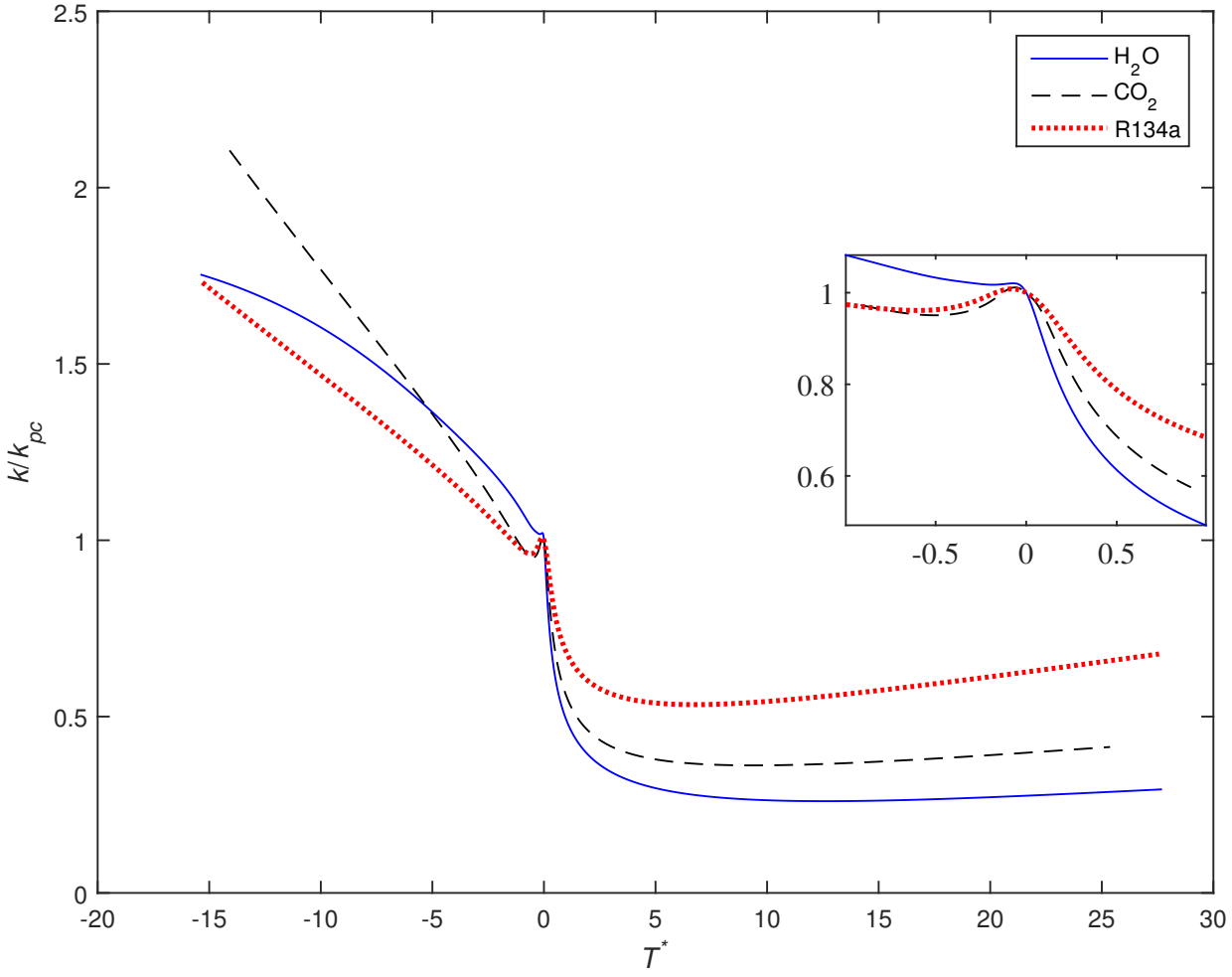

Figure A.12: The Normalised thermal conductivity versus bulk temperature T^* with its zoom out of the three fluids H_2O, CO_2, and R134a (Lemmon et al., 2002).

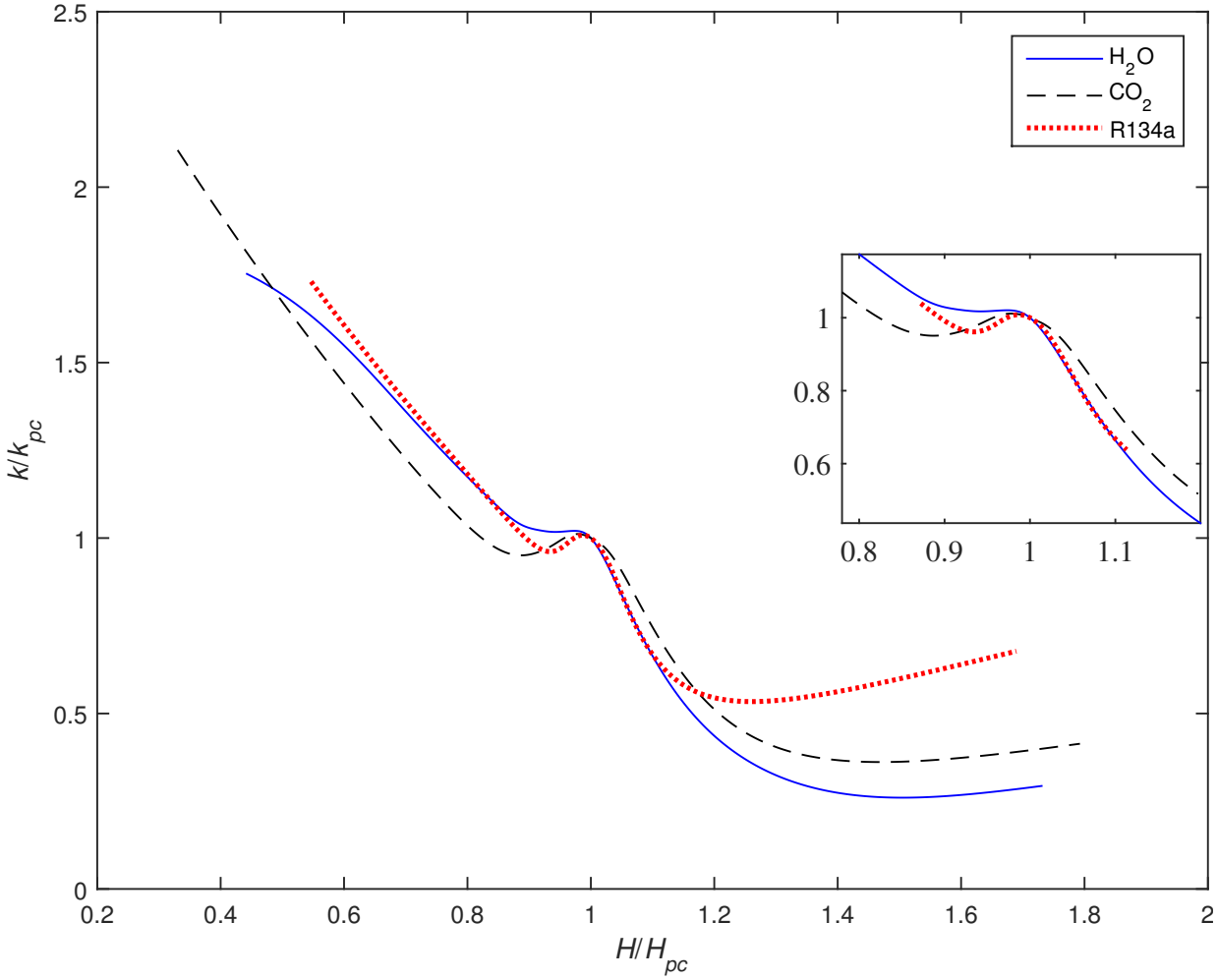

Figure A.13: The Normalised thermal conductivity versus bulk enthalpy ratio H_b/H_{pc} with its zoom out of the three fluids H_2O, CO_2, and R134a (Lemmon et al., 2002).

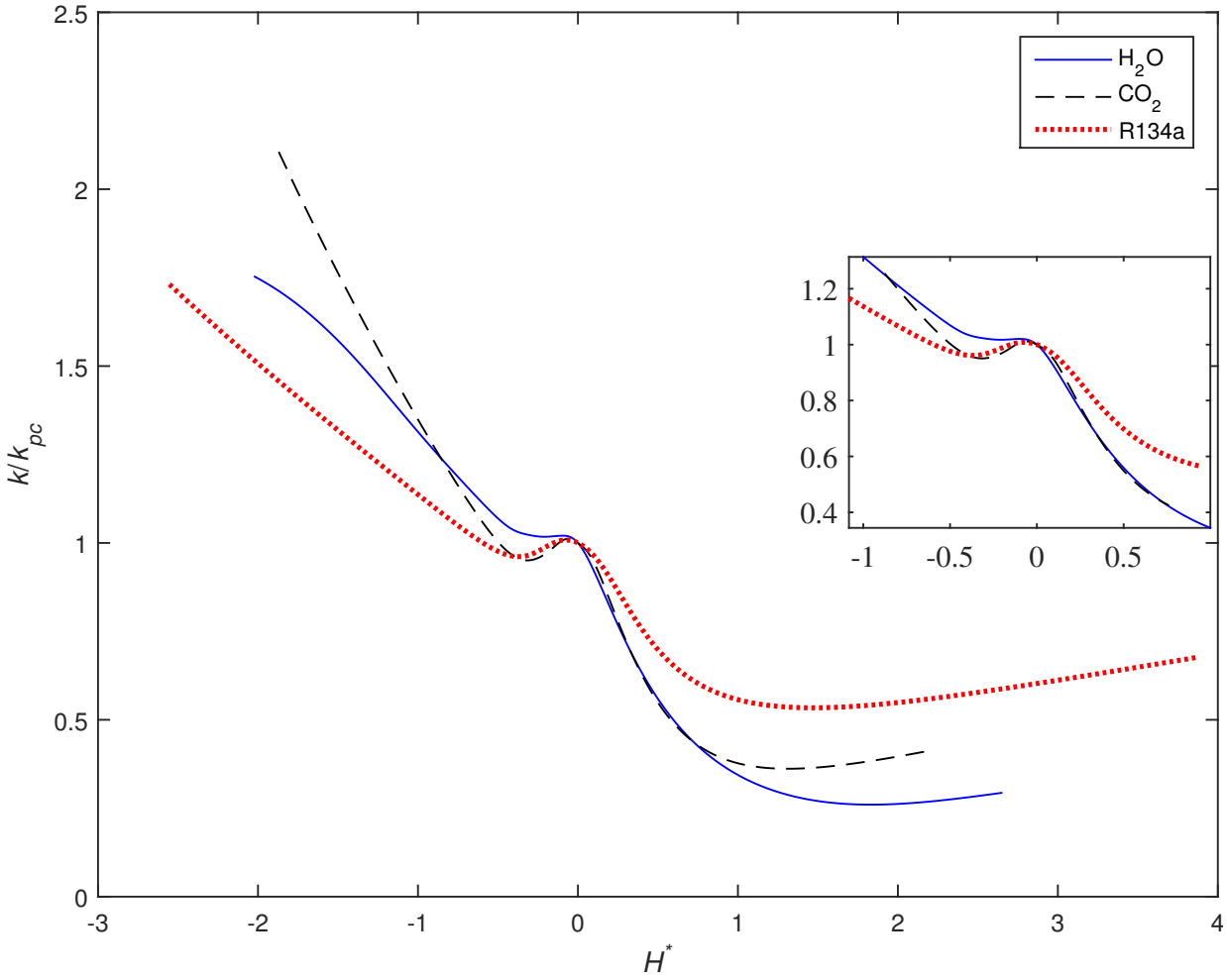

Figure A.14: The Normalised thermal conductivity versus bulk enthalpy H^* with its zoom out of the three fluids H_2O, CO_2, and R134a (Lemmon et al., 2002).

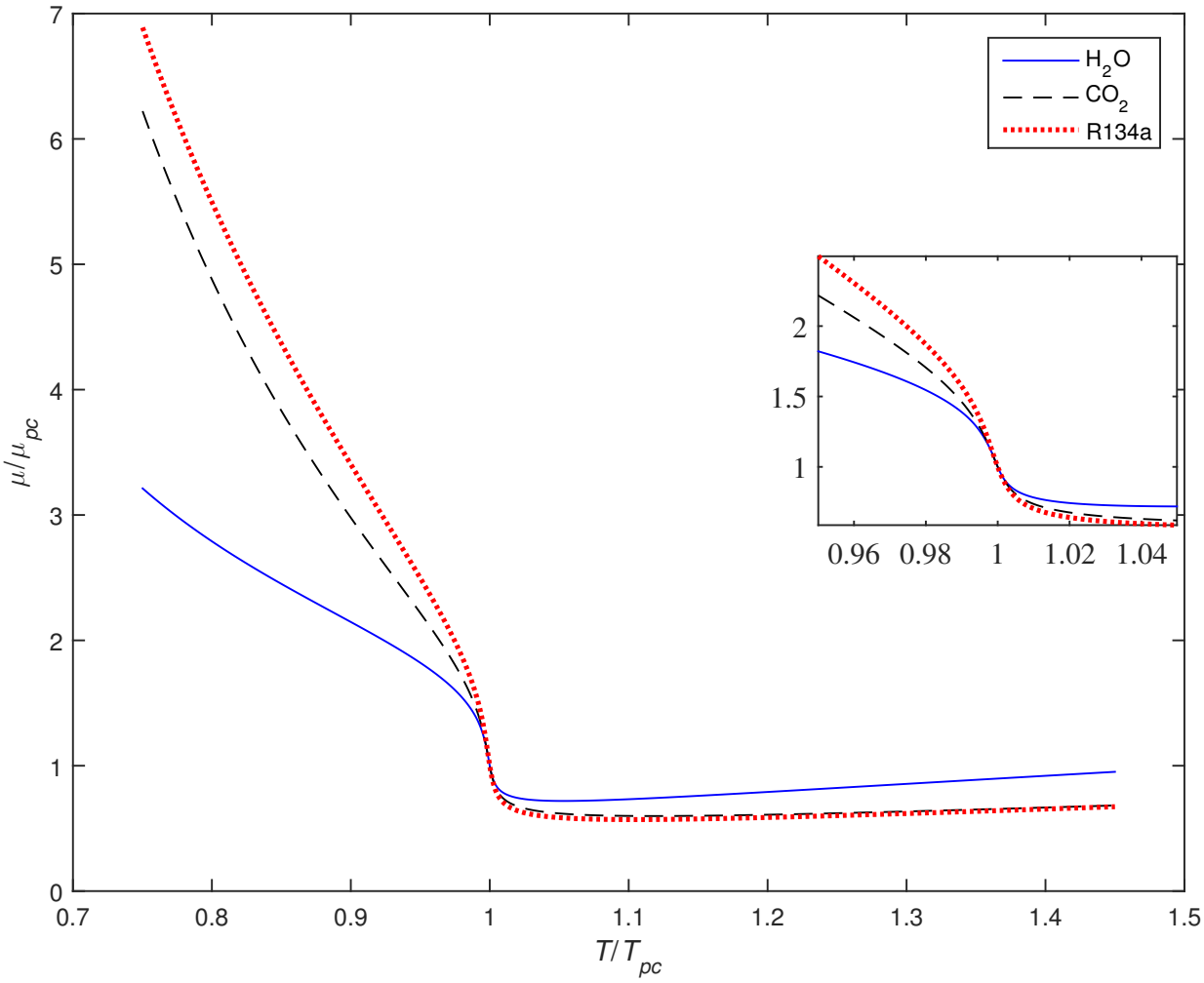

Figure A.15: The Normalised dynamic viscosity versus bulk temperature ratio T_b/T_{pc} with its zoom out of the three fluids H_2O, CO_2, and R134a (Lemmon et al., 2002).

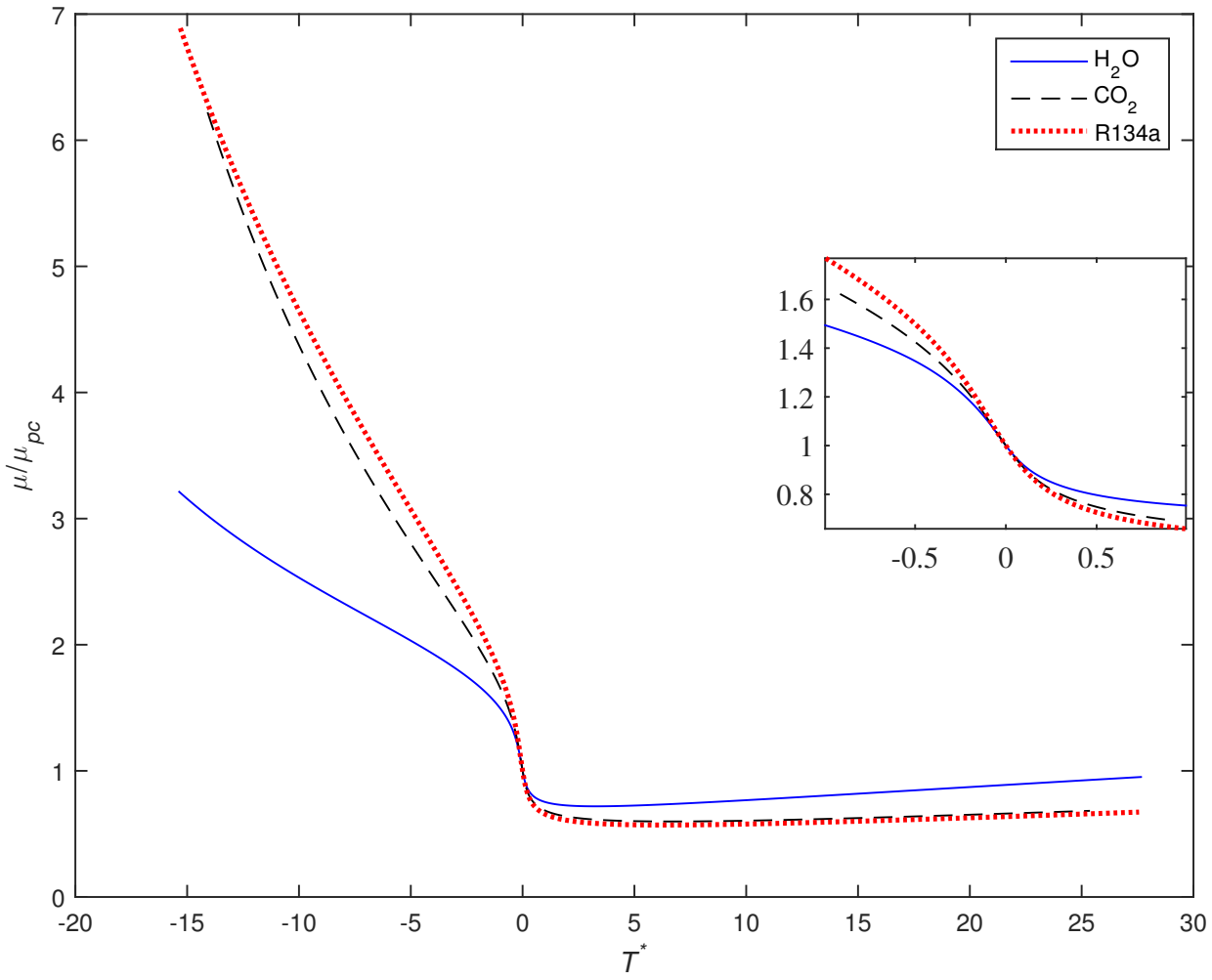

Figure A.16: The Normalised dynamic viscosity versus bulk temperature T^* with its zoom out of the three fluids H_2O, CO_2, and R134a (Lemmon et al., 2002).

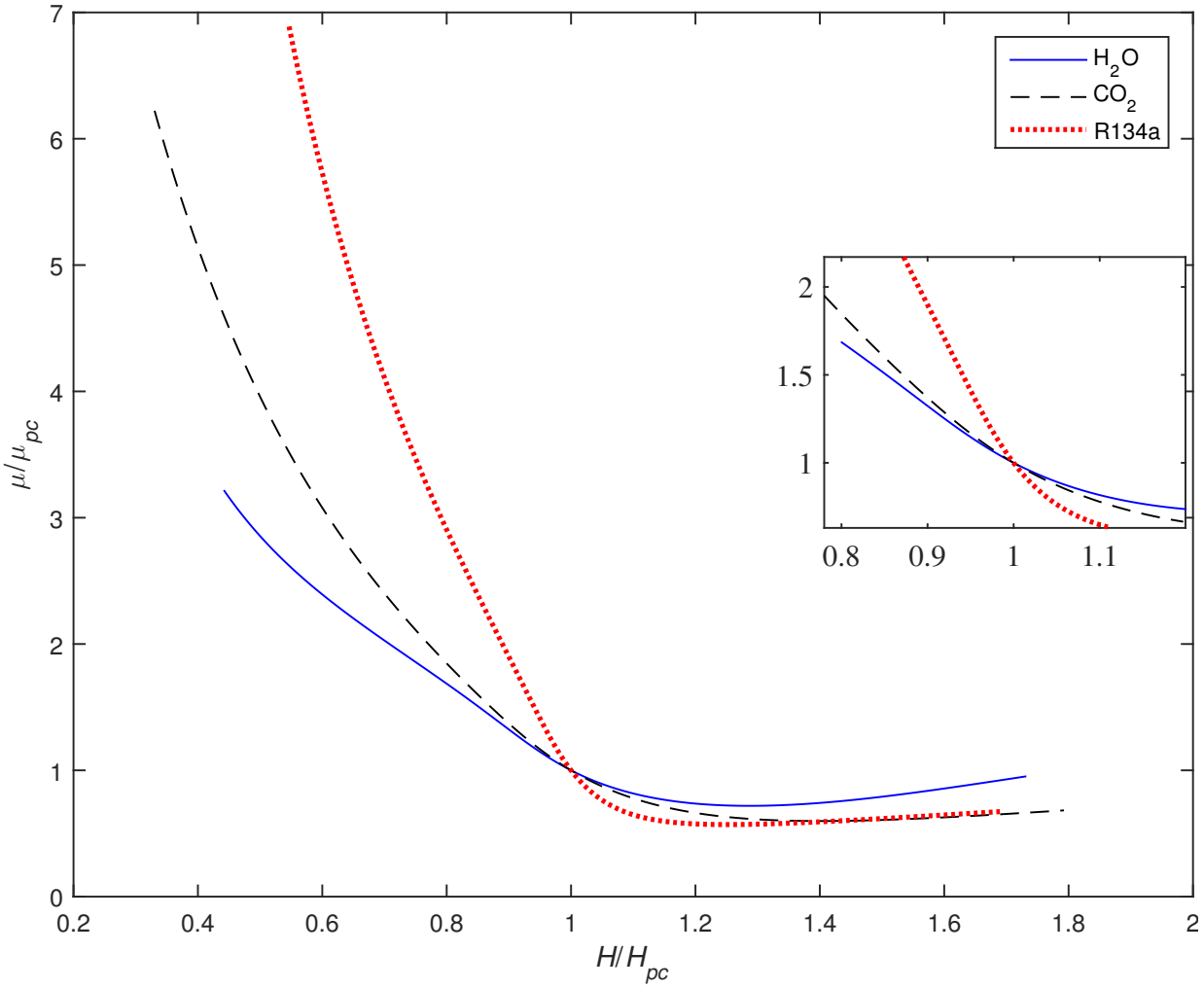

Figure A.17: The Normalised dynamic viscosity versus bulk enthalpy ratio H_b/H_{pc} with its zoom out of the three fluids H_2O, CO_2, and R134a (Lemmon et al., 2002).

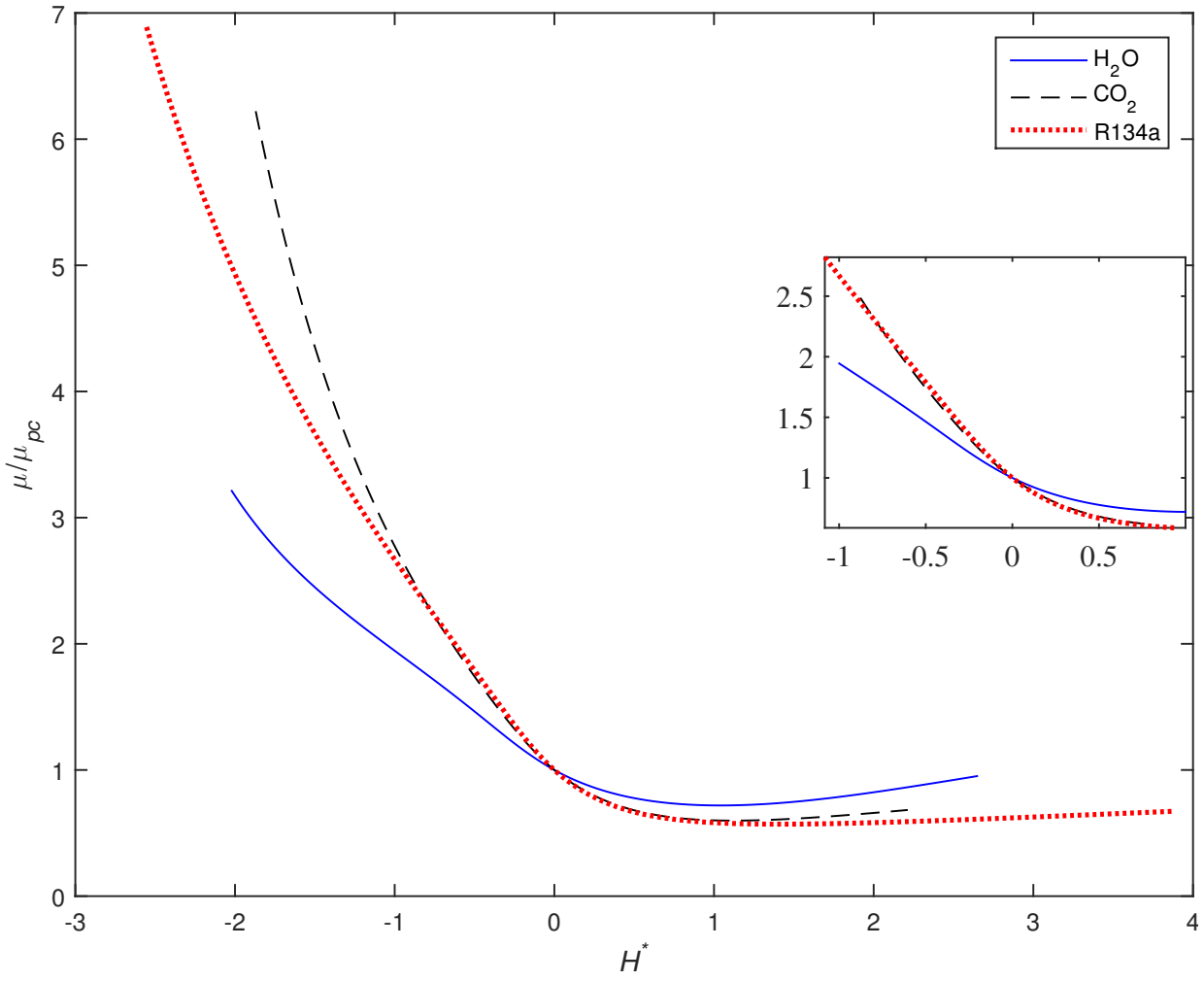

Figure A.18: The Normalised dynamic viscosity versus bulk enthalpy H^* with its zoom out of the three fluids H_2O, CO_2, and R134a (Lemmon et al., 2002).

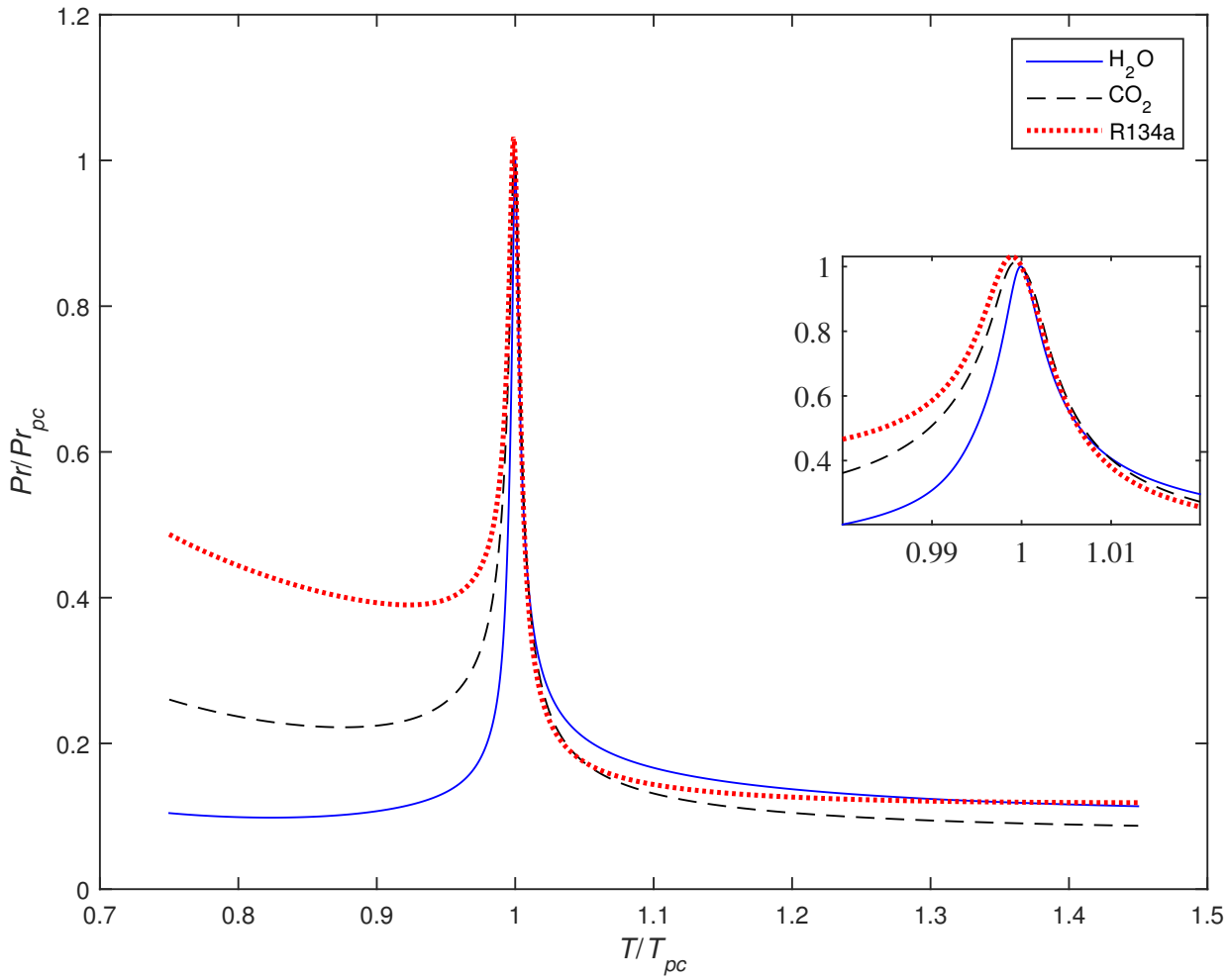

Figure A.19: The Normalised Prandtl number versus bulk temperature ratio T_b/T_{pc} with its zoom out of the three fluids H_2O, CO_2, and R134a (Lemmon et al., 2002).

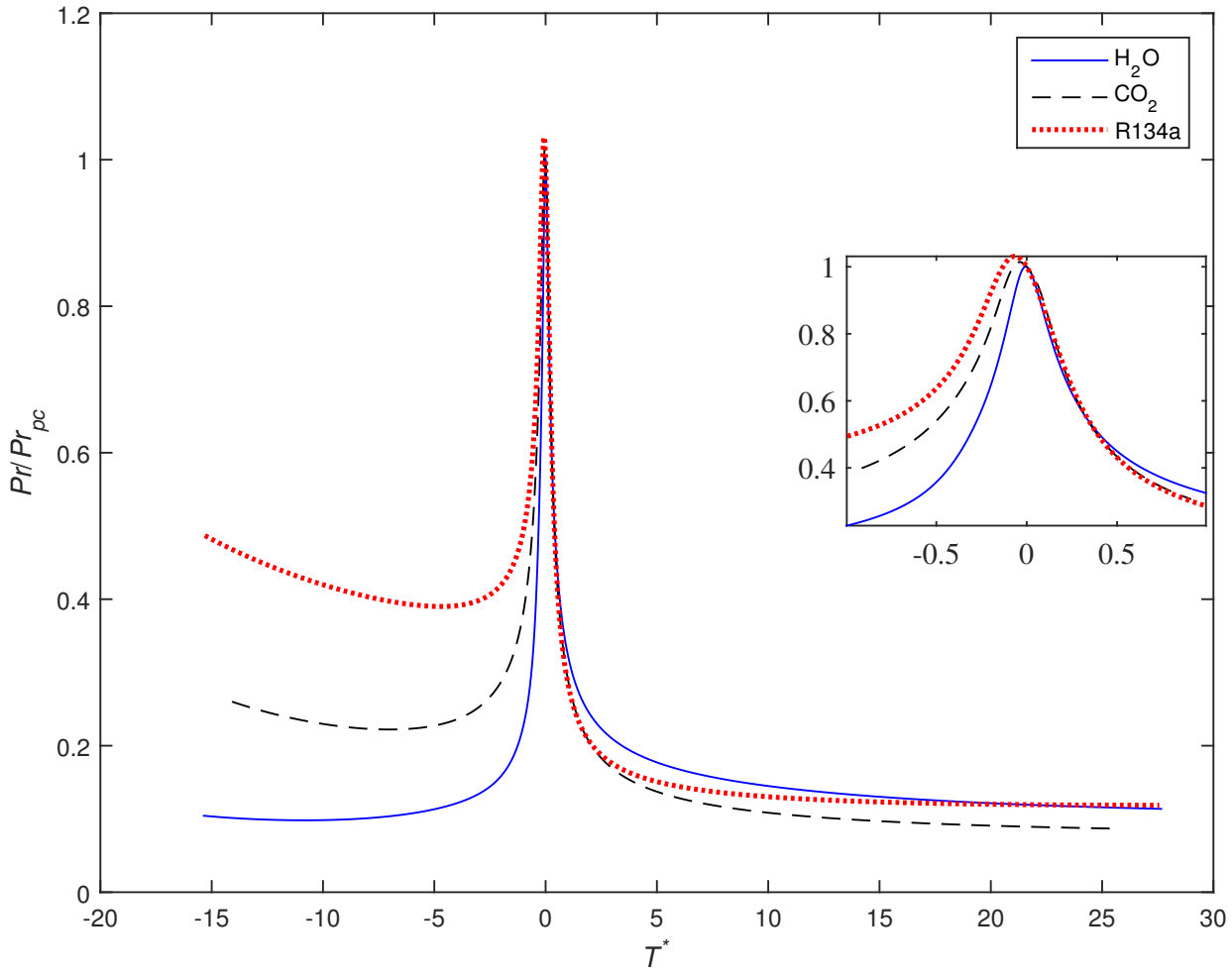

Figure A.20: The Normalised Prandtl number versus bulk temperature T^* with its zoom out of the three fluids H_2O, CO_2, and R134a (Lemmon et al., 2002).

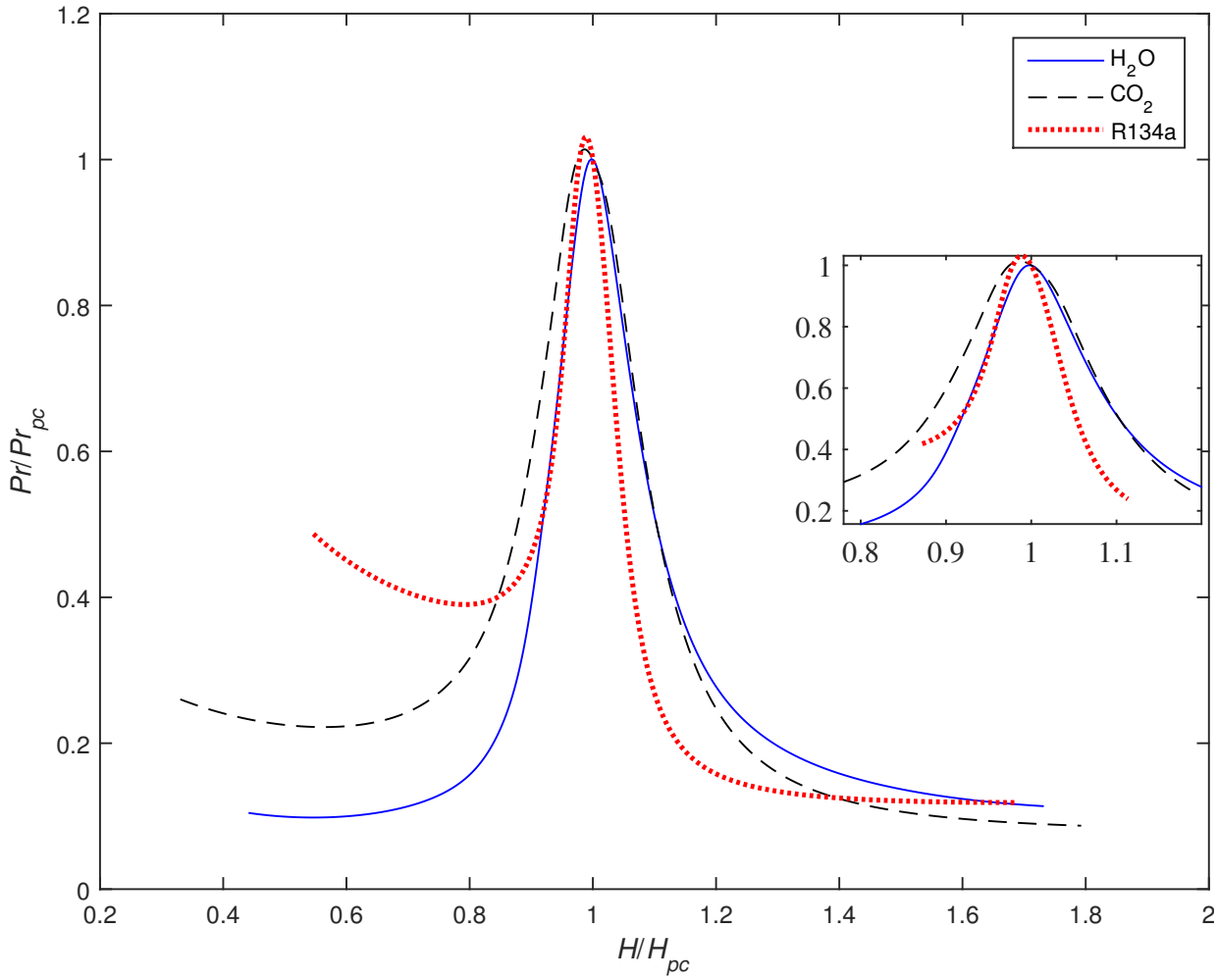

Figure A.21: The Normalised Prandtl number versus bulk enthalpy ratio H_b/H_{pc} with its zoom out of the three fluids H_2O, CO_2, and R134a (Lemmon et al., 2002).

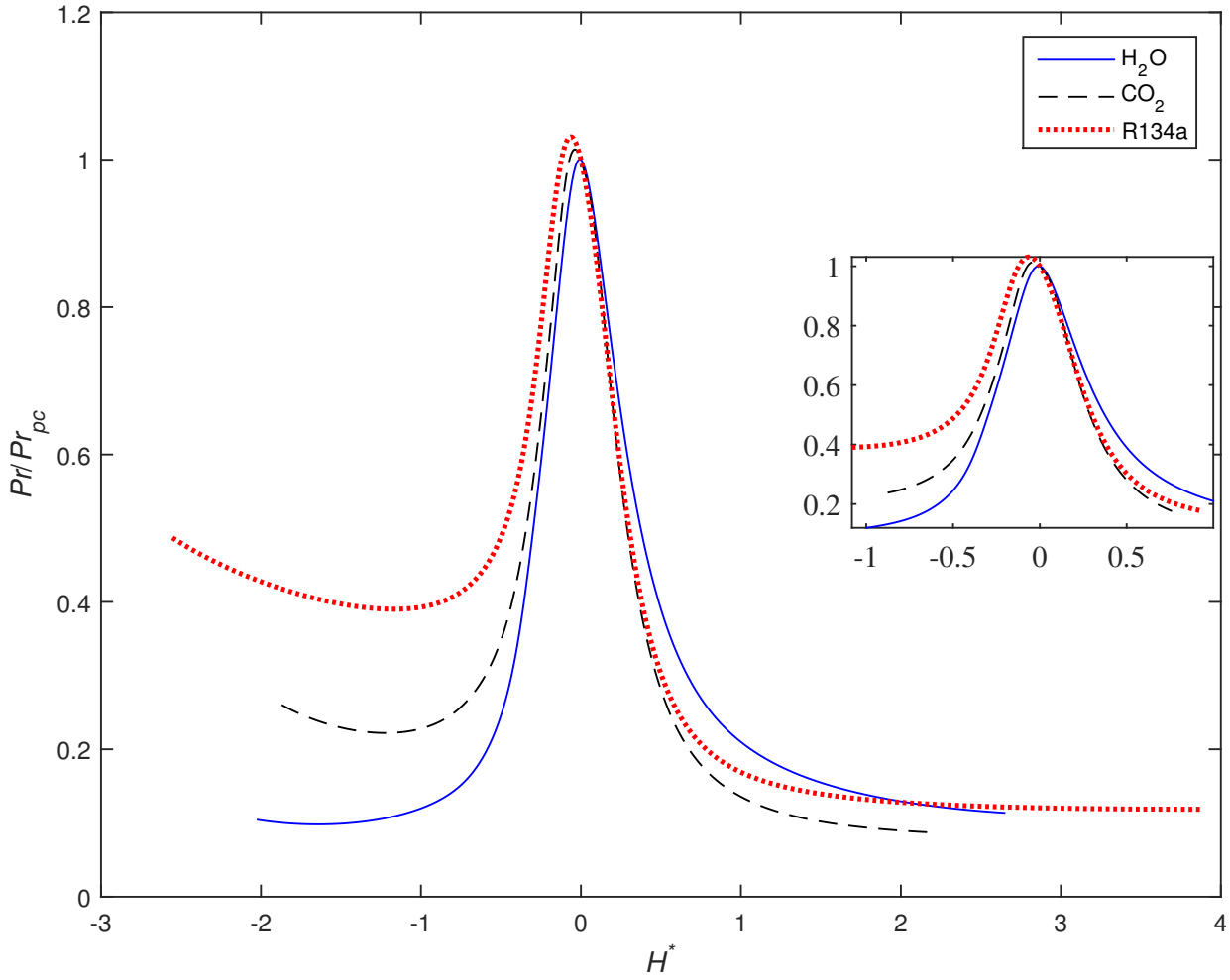

Figure A.22: The Normalised Prandtl number versus bulk enthalpy H^* with its zoom out of the three fluids H_2O, CO_2, and R134a (Lemmon et al., 2002).

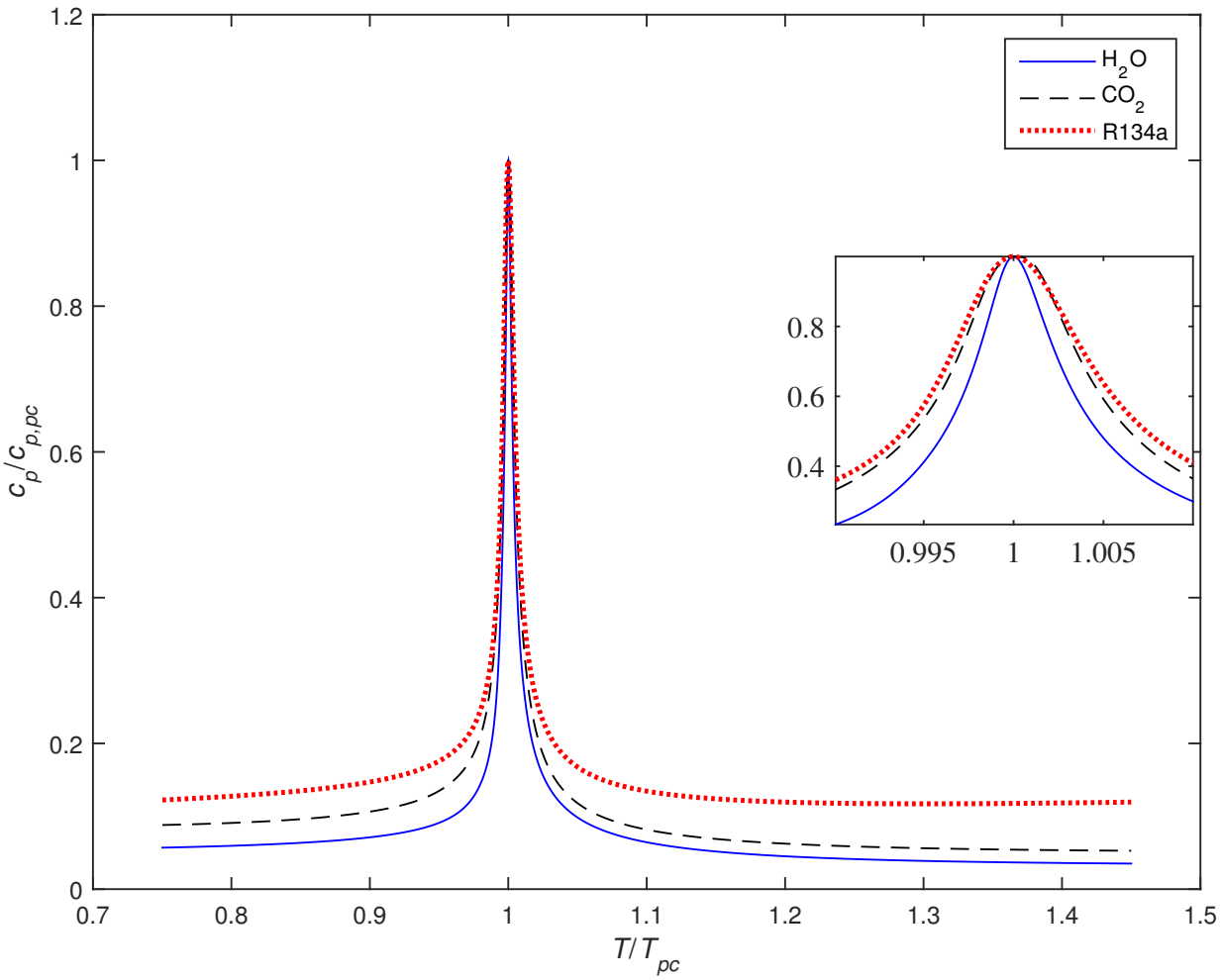

Figure A.23: The Normalised specific heat capacity versus bulk temperature ratio T_b/T_{pc} with its zoom out of the three fluids H_2O, CO_2, and R134a (Lemmon et al., 2002).

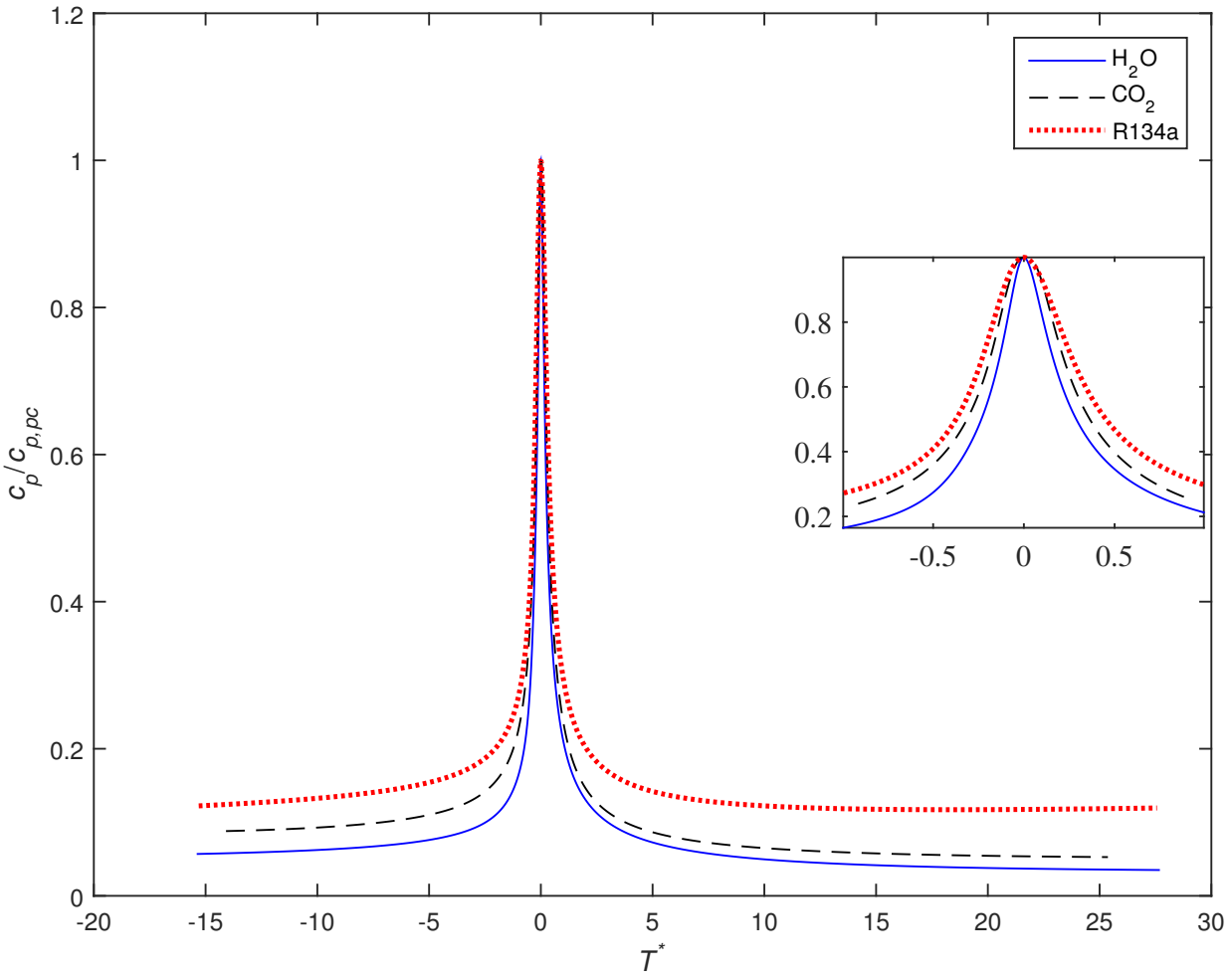

Figure A.24: The Normalised specific heat capacity versus bulk temperature T^* with its zoom out of the three fluids H_2O, CO_2, and R134a (Lemmon et al., 2002).

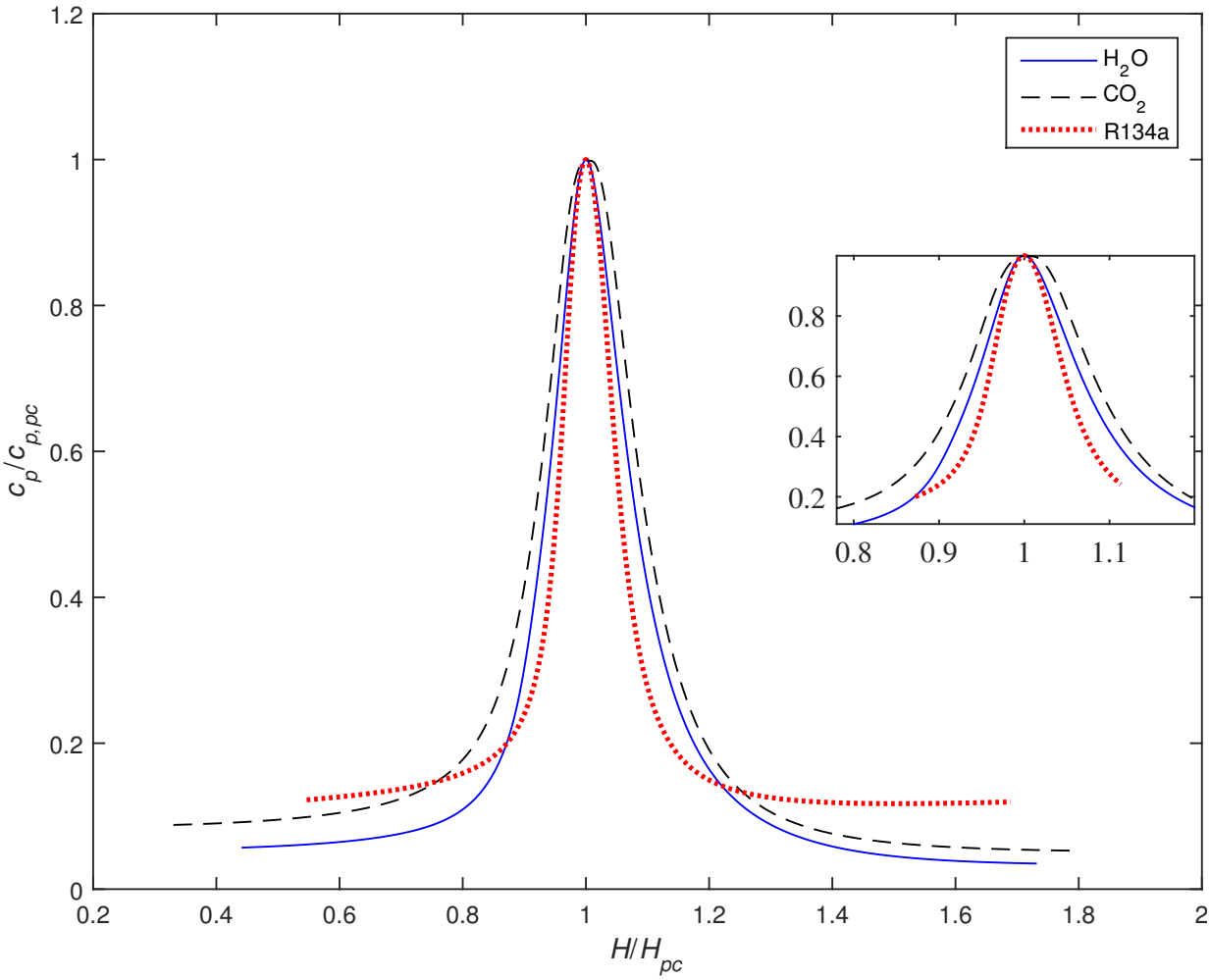

Figure A.25: The Normalised specific heat capacity versus bulk enthalpy ratio H_b/H_{pc} with its zoom out of the three fluids H_2O, CO_2, and R134a (Lemmon et al., 2002).

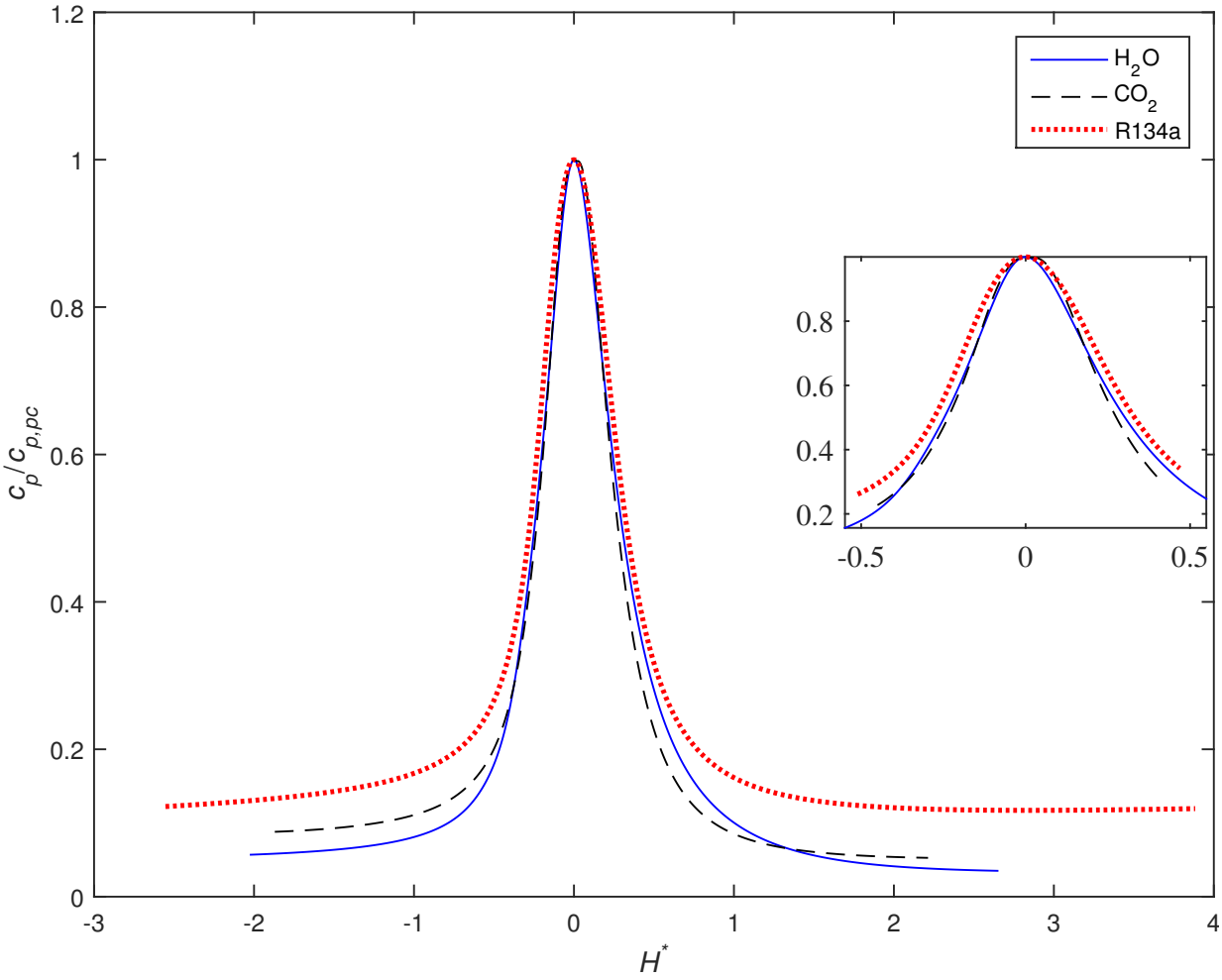

Figure A.26: The Normalised specific heat capacity versus bulk enthalpy H^* with its zoom out of the three fluids H_2O, CO_2, and R134a (Lemmon et al., 2002).

Appendix B

Database for H_2O, CO_2 and R134a for NHT

Table B.1: Test conditions, at $P = 1.13P_c$, of the fluid CO_2 for NHT

Test #	P/P_c [-]	G [kg m^{-2} s^{-1}]	q [kW m^{-2}]	T_{in} [°C]	T_b [°C]	H_b [kJ kg^{-1}]	T_w [°C]	h [kW m^{-2} K^{-1}]	TC#	k_b [W m^{-1} K^{-1}]	μ_b [Pa s]	c_p [kJ kg^{-1} K^{-1}]
1	1.13	200	3	24	26.11	265	29.85	0.80	19	0.0850	6.62×10^{-5}	3.54
2	1.13	197	3	30	31.54	288	33.96	1.28	19	0.0771	5.47×10^{-5}	5.32
3	1.13	300	13	22	28.05	273	36.08	1.62	19	0.0821	6.25×10^{-5}	3.92
4	1.13	300	13	35	36.23	335	40.05	3.40	19	0.0802	3.54×10^{-5}	21.55
5	1.13	400	30	17	28.23	273	41.49	2.26	19	0.0818	6.21×10^{-5}	3.97
6	1.13	400	30	26	33.53	301	43.32	3.06	19	0.0755	4.90×10^{-5}	7.55
7	1.13	500	40	11	24.59	260	41.96	2.30	19	0.0872	6.89×10^{-5}	3.32
8	1.13	500	50	15	29.80	280	47.24	2.87	19	0.0795	5.88×10^{-5}	4.44
9	1.13	500	50	25	34.50	309	49.10	3.43	19	0.0759	4.52×10^{-5}	10.05
10	1.13	600	80	12	31.50	288	57.75	3.05	19	0.0772	5.48×10^{-5}	5.30
11	1.13	600	80	20	34.54	310	59.10	3.26	19	0.0759	4.51×10^{-5}	10.16
12	1.13	700	89	9	29.02	277	59.50	2.92	19	0.0807	6.05×10^{-5}	4.18
13	1.13	700	90	11	30.55	283	59.73	3.08	19	0.0784	5.71×10^{-5}	4.76
14	1.13	1000	75	9	22.23	253	37.59	4.88	19	0.0906	7.30×10^{-5}	3.07
15	1.13	1009	125	9	29.00	276	57.64	4.36	19	0.0807	6.05×10^{-5}	4.17
16	1.13	704	90	5	27.00	269	46.20	4.69	19	0.0837	6.45×10^{-5}	3.70
17	1.13	700	95	10	30.53	283	49.90	4.92	19	0.0785	5.72×10^{-5}	4.75
18	1.13	699	50	11	14.16	230	32.64	2.71	4	0.1013	8.64×10^{-5}	2.59
19	1.13	699	50	11	17.52	239	35.12	2.84	9	0.0970	8.09×10^{-5}	2.74
20	1.13	699	50	11	20.67	248	36.42	3.17	14	0.0928	7.57×10^{-5}	2.94
21	1.13	699	50	11	23.58	257	37.40	3.62	19	0.0887	7.07×10^{-5}	3.21
22	1.13	699	50	11	26.54	267	39.97	3.72	24	0.0844	6.54×10^{-5}	3.61
23	1.13	699	50	11	29.29	278	40.32	4.53	30	0.0803	5.99×10^{-5}	4.26
24	1.13	699	50	11	31.56	288	41.67	4.94	36	0.0771	5.47×10^{-5}	5.34
25	1.13	1502	100	8	20.09	246	35.58	6.46	19	0.0935	7.66×10^{-5}	2.90
26	1.13	1500	175	7	27.09	269	48.05	8.34	19	0.0835	6.43×10^{-5}	3.71
27	1.13	1499	150	7	24.91	261	43.23	8.22	19	0.0868	6.83×10^{-5}	3.37
28	1.13	1520	125	8	16.54	236	36.20	6.38	11	0.0983	8.25×10^{-5}	2.69
29	1.13	1520	125	8	19.52	245	37.16	7.11	15	0.0943	7.76×10^{-5}	2.86
30	1.13	1520	125	8	22.30	253	38.16	7.90	19	0.0905	7.29×10^{-5}	3.08
31	1.13	1520	125	8	24.63	260	38.72	8.90	22	0.0872	6.88×10^{-5}	3.33
32	1.13	705	98	3	32.07	291	47.20	6.46	25	0.0765	5.34×10^{-5}	5.73
33	1.13	705	98	3	33.64	302	47.30	7.16	28	0.0755	4.86×10^{-5}	7.77
34	1.13	701	98	15	35.75	326	50.70	6.56	26	0.0793	3.87×10^{-5}	17.87
35	1.13	701	98	15	36.43	340	56.80	4.81	30	0.0795	3.41×10^{-5}	22.01
36	1.13	701	98	15	37.09	354	64.70	3.55	34	0.0744	3.04×10^{-5}	19.83
37	1.13	700	105	20	37.95	368	78.00	6.18	32	0.0641	2.75×10^{-5}	13.40
38	1.13	700	105	20	38.59	376	80.50	4.98	34	0.0586	2.62×10^{-5}	10.57
39	1.13	700	105	20	39.39	383	82.30	4.34	36	0.0536	2.51×10^{-5}	8.37

Table B.2: Test conditions, at $P = 1.13P_c$, of the fluid CO_2 for NHT (Cont'd)

Test #	ρ_b [kg m^{-3}]	Pr_b [-]	Re_b [-]	Nu_b [-]	T_b/T_{pc} [-]	H_b/H_{pc} [-]	k_b/k_{pc} [-]	μ_b/μ_{pc} [-]	$c_p/c_{p,pc}$ [-]	ρ_b/ρ_{pc} [-]	Pr_b/Pr_{pc} [-]
1	773	2.76	24183	75.46	0.97	0.78	1.07	1.96	0.16	1.63	0.29
2	691	3.78	28776	132.65	0.98	0.84	0.97	1.63	0.24	1.46	0.40
3	748	2.98	38429	157.64	0.97	0.80	1.04	1.85	0.18	1.58	0.32
4	496	9.53	67706	339.66	1.00	0.98	1.01	1.05	0.98	1.05	1.02
5	746	3.01	51548	221.25	0.97	0.80	1.03	1.84	0.18	1.58	0.32
6	641	4.90	65356	324.73	0.99	0.88	0.95	1.45	0.34	1.36	0.52
7	790	2.63	58040	211.19	0.96	0.76	1.10	2.05	0.15	1.67	0.28
8	722	3.29	68027	288.56	0.98	0.82	1.00	1.75	0.20	1.53	0.35
9	606	5.99	88406	361.16	0.99	0.91	0.96	1.34	0.46	1.28	0.64
10	692	3.76	87535	315.93	0.98	0.84	0.97	1.63	0.24	1.46	0.40
11	605	6.04	106418	343.20	0.99	0.91	0.96	1.34	0.46	1.28	0.65
12	734	3.13	92603	289.61	0.98	0.81	1.02	1.80	0.19	1.55	0.33
13	710	3.47	98023	314.56	0.98	0.83	0.99	1.70	0.22	1.50	0.37
14	813	2.48	109550	431.24	0.95	0.74	1.14	2.17	0.14	1.72	0.26
15	735	3.13	133369	432.63	0.98	0.81	1.02	1.80	0.19	1.55	0.33
16	762	2.85	87276	448.08	0.97	0.79	1.06	1.91	0.17	1.61	0.30
17	710	3.46	97968	501.54	0.98	0.83	0.99	1.70	0.22	1.50	0.37
18	878	2.21	64715	213.63	0.93	0.67	1.28	2.57	0.12	1.86	0.24
19	854	2.29	69123	234.32	0.94	0.70	1.22	2.40	0.12	1.81	0.24
20	827	2.40	73897	273.76	0.95	0.73	1.17	2.25	0.13	1.75	0.26
21	800	2.56	79102	326.43	0.96	0.75	1.12	2.10	0.15	1.69	0.27
22	767	2.80	85567	353.11	0.97	0.78	1.07	1.94	0.16	1.62	0.30
23	730	3.18	93346	451.85	0.98	0.81	1.01	1.78	0.19	1.54	0.34
24	691	3.78	102253	513.02	0.98	0.85	0.97	1.62	0.24	1.46	0.40
25	832	2.38	156782	552.75	0.95	0.72	1.18	2.28	0.13	1.76	0.25
26	761	2.86	186578	798.89	0.97	0.79	1.05	1.91	0.17	1.61	0.31
27	786	2.65	175474	757.58	0.96	0.77	1.10	2.03	0.15	1.66	0.28
28	861	2.26	147406	519.39	0.94	0.69	1.24	2.45	0.12	1.82	0.24
29	837	2.36	156724	602.92	0.95	0.72	1.19	2.30	0.13	1.77	0.25
30	813	2.48	166792	698.81	0.95	0.74	1.14	2.16	0.14	1.72	0.27
31	789	2.63	176653	816.81	0.96	0.76	1.10	2.04	0.15	1.67	0.28
32	680	3.99	105662	675.78	0.99	0.85	0.97	1.58	0.26	1.44	0.43
33	638	5.00	116080	759.19	0.99	0.88	0.95	1.44	0.35	1.35	0.53
34	536	8.71	144955	661.08	1.00	0.95	1.00	1.15	0.81	1.13	0.93
35	478	9.44	164444	483.97	1.00	1.00	1.00	1.01	1.00	1.01	1.01
36	426	8.11	184307	381.58	1.00	1.04	0.94	0.90	0.90	0.90	0.87
37	380	5.75	203491	770.59	1.00	1.08	0.81	0.82	0.61	0.80	0.61
38	357	4.73	213315	679.58	1.01	1.10	0.74	0.78	0.48	0.76	0.51
39	336	3.93	222629	647.70	1.01	1.12	0.68	0.75	0.38	0.71	0.42

Table B.3: Scaled test conditions, at $P = 1.13P_c$, of R134a at equivalent condition to that in CO_2 for NHT

Test #	P/P_c [-]	TC#	G [kg m^{-2} s^{-1}]	q [kW m^{-2}]	T_{in} [°C]	T_b [°C]	h [kW m^{-2} K^{-1}]	T_w [°C]	k_b [W m^{-1} K^{-1}]	μ_b [Pa s]	c_p [kJ kg^{-1} K^{-1}]
1	1.13	19	212	2.33	92.00	94.53	0.51	99.13	0.0537	7.67×10^{-5}	2.21
2	1.13	19	225	2.48	99.00	101.20	0.83	104.18	0.0503	6.22×10^{-5}	3.03
3	1.13	19	325	10.20	90.00	96.91	1.03	106.78	0.0524	7.20×10^{-5}	2.38
4	1.13	19	361	10.36	105.00	106.97	2.21	111.66	0.0520	3.73×10^{-5}	10.83
5	1.13	19	435	23.57	85.00	97.14	1.45	113.43	0.0523	7.15×10^{-5}	2.40
6	1.13	19	473	24.25	94.00	103.65	2.02	115.68	0.0497	5.48×10^{-5}	4.08
7	1.13	19	523	30.83	78.00	92.67	1.44	114.01	0.0547	8.03×10^{-5}	2.11
8	1.13	19	555	39.64	83.00	99.07	1.85	120.50	0.0513	6.74×10^{-5}	2.63
9	1.13	19	595	40.52	94.00	104.85	2.26	122.78	0.0500	5.00×10^{-5}	5.36
10	1.13	19	685	64.06	80.00	101.15	1.99	133.41	0.0503	6.23×10^{-5}	3.02
11	1.13	19	714	64.84	89.00	104.89	2.15	135.07	0.0501	4.99×10^{-5}	5.42
12	1.13	19	769	70.23	76.00	98.11	1.88	135.56	0.0518	6.95×10^{-5}	2.50
13	1.13	19	786	71.67	79.00	99.99	2.00	135.84	0.0508	6.52×10^{-5}	2.77
14	1.13	19	1027	57.19	75.00	89.77	3.03	108.64	0.0562	8.55×10^{-5}	1.99
15	1.13	19	1107	98.63	77.00	98.08	2.80	133.27	0.0518	6.96×10^{-5}	2.50
16	1.13	19	754	70.22	72.00	95.63	2.98	119.22	0.0531	7.46×10^{-5}	2.28
17	1.13	19	786	75.88	77.00	99.96	3.19	123.76	0.0508	6.53×10^{-5}	2.77
18	1.13	4	685	37.00	77.00	79.85	1.63	102.56	0.0610	1.02×10^{-4}	1.75
19	1.13	9	696	37.42	77.10	83.98	1.73	105.60	0.0591	9.54×10^{-5}	1.83
20	1.13	14	710	37.88	77.50	87.85	1.96	107.20	0.0572	8.88×10^{-5}	1.93
21	1.13	19	725	38.35	78.00	91.43	2.26	108.41	0.0554	8.25×10^{-5}	2.05
22	1.13	24	746	38.92	78.30	95.07	2.36	111.56	0.0534	7.57×10^{-5}	2.24
23	1.13	30	770	39.52	78.80	98.44	2.92	111.99	0.0516	6.88×10^{-5}	2.54
24	1.13	36	799	40.05	79.00	101.23	3.22	113.65	0.0503	6.21×10^{-5}	3.03
25	1.13	19	1519	75.70	74.00	87.14	3.98	106.18	0.0575	9.01×10^{-5}	1.91
26	1.13	19	1609	136.51	74.00	95.74	5.30	121.49	0.0531	7.44×10^{-5}	2.29
27	1.13	19	1574	116.16	74.00	93.06	5.16	115.57	0.0545	7.95×10^{-5}	2.12
28	1.13	11	1507	93.54	62.00	82.78	3.87	106.93	0.0596	9.74×10^{-5}	1.81
29	1.13	15	1532	94.56	66.00	86.43	4.36	108.11	0.0579	9.13×10^{-5}	1.89
30	1.13	19	1561	95.64	70.50	89.85	4.91	109.34	0.0562	8.53×10^{-5}	1.99
31	1.13	22	1592	96.66	74.00	92.72	5.58	110.03	0.0547	8.02×10^{-5}	2.11
32	1.13	25	813	78.55	71.00	101.85	4.22	120.45	0.0500	6.04×10^{-5}	3.21
33	1.13	28	835	79.09	72.00	103.79	4.71	120.57	0.0497	5.43×10^{-5}	4.19
34	1.13	26	830	78.68	84.00	106.38	4.28	124.75	0.0518	4.13×10^{-5}	9.35
35	1.13	30	845	78.32	84.00	107.22	3.13	132.24	0.0517	3.56×10^{-5}	11.03
36	1.13	34	851	79.98	83.00	108.02	2.36	141.95	0.0494	3.13×10^{-5}	9.95
37	1.13	32	835	90.77	84.00	109.08	1.84	130.05	0.0449	2.78×10^{-5}	7.23
38	1.13	34	836	93.21	82.60	109.86	1.81	135.87	0.0422	2.63×10^{-5}	5.82
39	1.13	36	839	95.63	81.00	110.85	1.81	140.72	0.0395	2.51×10^{-5}	4.69

Table B.4: Scaled test conditions, at $P = 1.13P_c$, of R134a at equivalent condition to that in CO_2 for NHT (Cont'd)

Test #	ρ_b [kg m^{-3}]	Pr_b [-]	Re_b [-]	Nu_b [-]	T_b/T_{pc} [-]	k_b/k_{pc} [-]	μ_b/μ_{pc} [-]	$c_p/c_{p,pc}$ [-]	ρ_b/ρ_{pc} [-]	Pr_b/Pr_{pc} [-]
1	862	3.15	22137	75.46	0.97	1.04	2.19	0.20	1.68	0.42
2	771	3.75	28934	132.65	0.98	0.97	1.77	0.27	1.50	0.50
3	835	3.27	36141	157.64	0.97	1.02	2.05	0.22	1.62	0.44
4	541	7.76	77537	339.66	1.00	1.01	1.06	0.98	1.05	1.03
5	832	3.29	48622	221.25	0.97	1.01	2.04	0.22	1.62	0.44
6	715	4.50	69079	324.73	0.99	0.96	1.56	0.37	1.39	0.60
7	881	3.09	52169	211.19	0.96	1.06	2.29	0.19	1.71	0.41
8	806	3.45	65923	288.56	0.98	0.99	1.92	0.24	1.57	0.46
9	674	5.36	95175	361.16	0.99	0.97	1.43	0.49	1.31	0.71
10	771	3.74	87941	315.93	0.98	0.97	1.77	0.27	1.50	0.50
11	672	5.40	114606	343.20	0.99	0.97	1.42	0.49	1.31	0.72
12	819	3.36	88477	289.61	0.98	1.00	1.98	0.23	1.59	0.45
13	792	3.55	96412	314.56	0.98	0.99	1.86	0.25	1.54	0.47
14	908	3.02	96085	431.24	0.95	1.09	2.43	0.18	1.77	0.40
15	820	3.36	127375	432.63	0.98	1.00	1.98	0.23	1.60	0.45
16	850	3.20	80841	448.08	0.97	1.03	2.13	0.21	1.65	0.43
17	792	3.55	96315	501.54	0.98	0.99	1.86	0.25	1.54	0.47
18	981	2.94	53562	213.63	0.93	1.18	2.92	0.16	1.91	0.39
19	953	2.96	58372	234.32	0.94	1.14	2.72	0.17	1.85	0.39
20	924	2.99	63909	273.76	0.95	1.11	2.53	0.17	1.80	0.40
21	893	3.06	70323	326.43	0.96	1.07	2.35	0.19	1.74	0.41
22	856	3.17	78770	353.11	0.97	1.04	2.16	0.20	1.67	0.42
23	815	3.39	89609	451.85	0.98	1.00	1.96	0.23	1.59	0.45
24	770	3.75	102868	513.02	0.98	0.97	1.77	0.28	1.50	0.50
25	929	2.98	134941	552.75	0.95	1.12	2.57	0.17	1.81	0.40
26	849	3.21	173038	798.89	0.97	1.03	2.12	0.21	1.65	0.43
27	877	3.10	158307	757.58	0.96	1.06	2.26	0.19	1.71	0.41
28	961	2.95	123693	519.39	0.94	1.16	2.78	0.16	1.87	0.39
29	935	2.98	134279	602.92	0.95	1.12	2.60	0.17	1.82	0.40
30	907	3.02	146385	698.81	0.95	1.09	2.43	0.18	1.76	0.40
31	881	3.09	158859	816.81	0.96	1.06	2.28	0.19	1.71	0.41
32	758	3.88	107626	675.78	0.99	0.97	1.72	0.29	1.47	0.52
33	710	4.58	123027	759.19	0.99	0.96	1.55	0.38	1.38	0.61
34	588	7.46	160652	661.08	1.00	1.00	1.18	0.85	1.14	0.99
35	520	7.59	189796	483.97	1.00	1.00	1.01	1.00	1.01	1.01
36	461	6.30	217768	381.58	1.00	0.96	0.89	0.90	0.90	0.84
37	407	4.48	240059	770.59	1.00	0.87	0.79	0.66	0.79	0.60
38	380	3.63	254039	679.58	1.01	0.82	0.75	0.53	0.74	0.48
39	356	2.97	267611	647.70	1.01	0.77	0.71	0.43	0.69	0.40

Table B.5: Experimental conditions, at $P = 1.13P_c$, of the fluid R134a for NHT

Experimental database in R134a for NHT cases															
Test #	P/P_c [-]	TC#	G [kg m^{-2} s^{-1}]	q [kW m^{-2}]	T_{in} [°C]	T_w [°C]	T_b [°C]	h [kW m^{-2} K^{-1}]	H_b [kJ kg^{-1}]	k_b [W m^{-1} K^{-1}]	μ_b [Pa s]	c_p [kJ kg^{-1} K^{-1}]	Nu_b [-]	Re_b [-]	T_b/T_{pc} [-]
1	1.13	19	212	2.13	92.42	97.63	94.62	0.71	347	0.0535	7.61×10^{-5}	2.24	105.47	22319	0.97
2	1.13	19	225	2.51	99.40	103.57	101.26	1.08	364	0.0502	6.19×10^{-5}	3.05	172.59	29107	0.98
3	1.13	19	323	10.40	90.02	107.15	97.14	1.04	352	0.0524	7.19×10^{-5}	2.38	158.54	35973	0.97
4	1.13	19	356	10.15	104.70	110.25	106.36	2.61	392	0.0526	3.88×10^{-5}	11.08	397.14	73449	1.00
5	1.13	19	439	23.66	84.54	111.55	97.01	1.63	352	0.0523	7.16×10^{-5}	2.41	248.90	49053	0.97
6	1.13	19	475	24.42	94.21	112.97	103.32	2.53	370	0.0496	5.63×10^{-5}	3.78	407.76	67518	0.99
7	1.13	19	523	31.43	78.31	111.74	93.46	1.72	344	0.0544	7.90×10^{-5}	2.14	253.08	52983	0.96
8	1.13	19	557	39.82	83.00	117.32	99.12	2.19	358	0.0511	6.65×10^{-5}	2.70	342.39	67047	0.98
9	1.13	19	599	41.10	94.06	117.38	105.08	3.34	378	0.0501	4.95×10^{-5}	5.47	534.00	96756	0.99
10	1.13	19	688	64.38	80.27	125.90	101.39	2.63	364	0.0503	6.24×10^{-5}	2.99	417.99	88236	0.98
11	1.13	19	719	65.39	88.67	123.68	104.99	3.50	378	0.0500	4.99×10^{-5}	5.37	559.59	115399	0.99
12	1.13	19	765	70.08	76.22	120.95	98.40	3.11	356	0.0517	6.89×10^{-5}	2.53	481.26	88716	0.98
13	1.13	19	789	72.16	79.04	121.84	100.08	3.32	361	0.0507	6.45×10^{-5}	2.84	523.31	97846	0.98
14	1.13	19	1024	57.25	75.00	105.61	89.63	3.58	337	0.0561	8.51×10^{-5}	2.00	511.17	96356	0.95
15	1.13	19	1109	98.93	76.59	115.61	98.30	5.71	355	0.0519	6.98×10^{-5}	2.47	881.23	127107	0.98
16	1.13	19	761	70.38	71.59	115.41	95.36	3.51	348	0.0534	7.56×10^{-5}	2.24	525.70	80605	0.97
17	1.13	19	792	76.03	76.56	117.75	99.69	4.21	358	0.0513	6.75×10^{-5}	2.58	656.45	93874	0.98
18	1.13	4	692	37.28	77.13	101.90	80.28	1.72	319	0.0609	1.02×10^{-4}	1.76	226.57	54379	0.93
19	1.13	9	697	37.46	77.17	103.03	84.06	1.97	326	0.0591	9.54×10^{-5}	1.83	267.49	58434	0.94
20	1.13	14	709	37.79	77.76	104.67	88.14	2.29	333	0.0572	8.89×10^{-5}	1.92	319.70	63741	0.95
21	1.13	19	729	38.73	77.61	106.30	91.25	2.57	340	0.0554	8.28×10^{-5}	2.04	371.35	70468	0.96
22	1.13	24	748	39.00	78.20	106.72	94.95	3.31	348	0.0535	7.59×10^{-5}	2.24	495.44	78861	0.97
23	1.13	30	767	40.27	78.87	108.22	98.92	4.33	357	0.0515	6.82×10^{-5}	2.56	673.17	89964	0.98
24	1.13	36	806	40.10	79.42	109.13	101.02	4.94	363	0.0503	6.22×10^{-5}	3.04	786.33	103614	0.98
25	1.13	19	1519	75.79	73.61	100.97	87.05	5.44	331	0.0576	9.03×10^{-5}	1.90	756.01	134581	0.95
26	1.13	19	1610	136.80	73.50	112.15	95.01	7.98	348	0.0533	7.52×10^{-5}	2.27	1198.26	171207	0.97
27	1.13	19	1575	116.27	73.52	109.58	92.64	6.86	343	0.0548	8.04×10^{-5}	2.10	1002.35	156669	0.96
28	1.13	11	1488	93.08	61.65	96.63	72.43	3.85	306	0.0644	1.15×10^{-4}	1.65	478.00	103696	0.91
29	1.13	15	1510	93.88	65.70	101.33	79.77	4.36	318	0.0611	1.02×10^{-4}	1.75	570.72	117891	0.93
30	1.13	19	1542	95.17	70.51	105.69	87.34	5.18	332	0.0575	9.00×10^{-5}	1.91	721.14	137126	0.95
31	1.13	22	1549	95.69	73.53	108.12	92.70	6.21	342	0.0549	8.07×10^{-5}	2.09	905.29	153455	0.96
32	1.13	25	820	79.04	71.53	118.06	102.01	4.92	366	0.0499	5.99×10^{-5}	3.28	788.44	109573	0.99
33	1.13	28	833	78.79	71.80	118.52	103.79	5.35	372	0.0497	5.44×10^{-5}	4.17	861.67	122497	0.99
34	1.13	26	830	79.40	83.63	121.29	107.13	5.61	389	0.0509	4.20×10^{-5}	8.12	881.98	158306	1.00
35	1.13	30	842	78.44	83.70	122.73	107.25	5.07	397	0.0517	3.60×10^{-5}	10.86	784.09	187271	1.00
36	1.13	34	848	79.30	83.24	129.13	108.26	3.80	405	0.0493	3.16×10^{-5}	9.72	616.31	214702	1.00
37	1.13	32	837	91.01	83.45	135.84	109.69	3.48	414	0.0455	2.87×10^{-5}	7.31	612.25	233123	1.01
38	1.13	34	835	93.31	83.23	144.00	109.99	2.74	421	0.0414	2.59×10^{-5}	5.48	530.21	258067	1.01
39	1.13	36	839	96.57	81.51	147.97	110.89	2.60	427	0.0385	2.45×10^{-5}	4.34	541.32	274116	1.01

Table B.6: Experimental conditions, at $P = 1.13P_c$, of the fluid R134a for NHT (Cont'd)

R134a database for NHT-Experimental							Comparison	
Test #	H_b/H_{pc} [-]	k_b/k_{pc} [-]	μ_b/μ_{pc} [-]	$c_p/c_{p,pc}$ [-]	ρ_b/ρ_{pc} [-]	Pr_b/Pr_{pc} [-]	h_{sca}/h_{exp} [-]	$Nu_{R/C}/Nu_{exp}$ [-]
1	0.87	1.04	2.17	0.20	1.67	0.42	0.72	0.72
2	0.91	0.97	1.76	0.28	1.50	0.50	0.77	0.77
3	0.89	1.02	2.05	0.22	1.62	0.44	1.00	0.99
4	0.98	1.02	1.10	1.00	1.09	1.09	0.85	0.86
5	0.89	1.01	2.04	0.22	1.62	0.44	0.89	0.89
6	0.93	0.96	1.60	0.34	1.41	0.57	0.80	0.80
7	0.86	1.05	2.25	0.19	1.70	0.41	0.84	0.83
8	0.90	0.99	1.89	0.24	1.56	0.47	0.85	0.84
9	0.95	0.97	1.41	0.50	1.30	0.72	0.68	0.68
10	0.91	0.97	1.78	0.27	1.50	0.00	0.76	0.76
11	0.95	0.97	1.42	0.49	1.31	0.71	0.61	0.61
12	0.89	1.00	1.96	0.23	1.59	0.45	0.60	0.60
13	0.91	0.98	1.84	0.26	1.53	0.48	0.60	0.60
14	0.85	1.09	2.42	0.18	1.76	0.40	0.85	0.84
15	0.89	1.01	1.99	0.22	1.60	0.44	0.49	0.49
16	0.88	1.04	2.15	0.20	1.66	0.42	0.85	0.85
17	0.90	0.99	1.92	0.23	1.57	0.45	0.76	0.76
18	0.80	1.18	2.90	0.16	1.90	0.39	0.95	0.94
19	0.82	1.14	2.72	0.17	1.85	0.39	0.88	0.88
20	0.84	1.11	2.53	0.17	1.80	0.40	0.86	0.86
21	0.85	1.07	2.36	0.19	1.74	0.41	0.88	0.88
22	0.87	1.04	2.16	0.20	1.67	0.42	0.71	0.71
23	0.90	1.00	1.94	0.23	1.58	0.45	0.67	0.67
24	0.91	0.97	1.77	0.28	1.50	0.50	0.65	0.65
25	0.83	1.12	2.57	0.17	1.81	0.40	0.73	0.73
26	0.87	1.03	2.14	0.21	1.66	0.43	0.66	0.67
27	0.86	1.06	2.29	0.19	1.72	0.41	0.75	0.76
28	0.77	1.25	3.27	0.15	2.00	0.39	1.01	1.09
29	0.80	1.18	2.92	0.16	1.91	0.39	1.00	1.06
30	0.83	1.11	2.56	0.17	1.81	0.40	0.95	0.97
31	0.86	1.06	2.30	0.19	1.72	0.41	0.90	0.90
32	0.92	0.97	1.71	0.30	1.47	0.52	0.86	0.86
33	0.94	0.96	1.55	0.38	1.38	0.61	0.88	0.88
34	0.98	0.99	1.19	0.74	1.16	0.89	0.76	0.75
35	1.00	1.00	1.03	0.98	1.02	1.01	0.62	0.62
36	1.02	0.96	0.90	0.88	0.91	0.83	0.62	0.62
37	1.04	0.88	0.82	0.66	0.82	0.61	0.53	1.26
38	1.06	0.80	0.74	0.50	0.72	0.46	0.66	1.28
39	1.07	0.75	0.70	0.39	0.67	0.37	0.70	1.20

Table B.7: Scaled test conditions, at $P = 1.13P_c$, of H_2O at equivalent condition to that in CO_2 for NHT

Test #	P/P_c [-]	TC#	G [kg m^{-2} s^{-1}]	q [kW m^{-2}]	T_{in} [°C]	T_b [°C]	h [kW m^{-2} K^{-1}]	T_w [°C]	k_b [W m^{-1} K^{-1}]	μ_b [Pa s]	c_p [kJ kg^{-1} K^{-1}]	ρ_b [kg m^{-3}]	Pr_b [-]
1	1.13	19	337	33.73	358.05	362.53	4.24	370.47	0.4500	6.67×10^{-5}	8.53	578	1.26
2	1.13	19	340	35.35	370.79	374.06	6.86	379.20	0.4140	5.90×10^{-5}	12.98	512	1.85
3	1.13	19	511	147.42	353.80	366.64	8.64	383.71	0.4384	6.43×10^{-5}	9.49	558	1.39
4	1.13	19	412	134.48	381.41	384.03	16.58	392.14	0.3905	4.18×10^{-5}	70.79	343	7.59
5	1.13	19	681	340.44	343.18	367.04	12.09	395.20	0.4372	6.41×10^{-5}	9.60	556	1.41
6	1.13	19	686	336.43	362.30	378.28	16.17	399.09	0.3984	5.46×10^{-5}	18.63	472	2.55
7	1.13	19	835	446.52	330.43	359.30	12.10	396.20	0.4584	6.84×10^{-5}	8.00	592	1.19
8	1.13	19	858	570.15	338.93	370.38	15.39	407.41	0.4268	6.19×10^{-5}	10.81	537	1.57
9	1.13	19	826	549.94	360.17	380.36	17.74	411.36	0.3929	5.15×10^{-5}	25.98	442	3.41
10	1.13	19	1036	912.27	332.56	373.98	16.36	429.74	0.4143	5.90×10^{-5}	12.91	513	1.84
11	1.13	19	990	879.15	349.55	380.43	16.85	432.61	0.3928	5.14×10^{-5}	26.34	441	3.45
12	1.13	19	1197	1012.78	325.12	368.71	15.64	433.46	0.4321	6.30×10^{-5}	10.15	547	1.48
13	1.13	19	1204	1027.26	330.43	371.96	16.57	433.94	0.4215	6.07×10^{-5}	11.59	527	1.67
14	1.13	19	1647	827.99	325.97	354.29	25.38	386.92	0.4708	7.08×10^{-5}	7.38	611	1.11
15	1.13	19	1725	1422.33	326.40	368.66	23.38	429.51	0.4323	6.30×10^{-5}	10.13	548	1.48
16	1.13	19	1191	1016.05	317.69	364.42	24.91	405.20	0.4448	6.56×10^{-5}	8.93	569	1.32
17	1.13	19	1204	1087.75	327.25	371.91	26.43	413.06	0.4216	6.07×10^{-5}	11.57	528	1.67
18	1.13	4	1101	533.84	331.07	337.15	13.60	376.40	0.5093	7.80×10^{-5}	6.21	663	0.95
19	1.13	9	1120	540.82	331.07	344.28	14.46	381.67	0.4938	7.51×10^{-5}	6.59	643	1.00
20	1.13	14	1140	548.10	331.07	350.97	16.38	384.43	0.4786	7.23×10^{-5}	7.07	622	1.07
21	1.13	19	1161	555.49	331.07	357.16	18.93	386.51	0.4638	6.94×10^{-5}	7.71	600	1.15
22	1.13	24	1181	563.31	331.07	363.45	19.75	391.97	0.4475	6.62×10^{-5}	8.72	574	1.29
23	1.13	30	1196	569.43	331.07	369.28	24.30	392.71	0.4303	6.26×10^{-5}	10.36	544	1.51
24	1.13	36	1207	570.07	331.07	374.10	26.54	395.58	0.4138	5.89×10^{-5}	13.01	512	1.85
25	1.13	19	2442	1095.12	323.83	349.74	33.27	382.66	0.4815	7.28×10^{-5}	6.97	626	1.05
26	1.13	19	2541	1975.10	322.86	364.61	44.36	409.13	0.4442	6.55×10^{-5}	8.97	569	1.32
27	1.13	19	2509	1682.52	322.89	359.99	43.25	398.89	0.4567	6.80×10^{-5}	8.10	589	1.21
28	1.13	11	2423	1351.08	323.00	342.21	32.36	383.97	0.4984	7.60×10^{-5}	6.46	649	0.99
29	1.13	15	2463	1367.70	323.00	348.52	36.50	386.00	0.4843	7.34×10^{-5}	6.87	630	1.04
30	1.13	19	2504	1384.80	323.00	354.43	41.10	388.13	0.4705	7.07×10^{-5}	7.40	610	1.11
31	1.13	22	2540	1400.12	323.00	359.39	46.78	389.32	0.4582	6.83×10^{-5}	8.01	591	1.19
32	1.13	25	1218	1112.75	312.59	375.18	34.61	407.33	0.4098	5.79×10^{-5}	13.96	503	1.97
33	1.13	28	1205	1094.80	312.59	378.53	37.74	407.54	0.3976	5.43×10^{-5}	19.23	469	2.62
34	1.13	26	1064	1022.29	339.14	383.01	32.20	414.76	0.3896	4.53×10^{-5}	50.58	380	5.89
35	1.13	30	917	1012.73	339.14	384.46	23.41	427.72	0.3870	4.02×10^{-5}	77.60	325	8.06
36	1.13	34	942	937.97	339.14	385.84	15.99	444.50	0.3353	3.60×10^{-5}	62.25	275	6.68
37	1.13	32	955	964.35	348.70	387.68	11.34	472.75	0.2762	3.32×10^{-5}	39.69	238	4.77
38	1.13	34	953	952.08	348.70	389.03	10.69	478.06	0.2492	3.21×10^{-5}	31.19	221	4.01
39	1.13	36	950	942.69	348.70	390.74	10.34	481.89	0.2255	3.11×10^{-5}	24.78	206	3.42

Table B.8: Scaled test conditions, at $P = 1.13P_c$, of H_2O at equivalent condition to that in CO_2 for NHT (Cont'd)

Scaled H_2O database for NHT									TC-LUT (Zahlan et al., 2015b)		Comparison	
Test #	Re_b [-]	Nu_b [-]	T_b/T_{pc} [-]	k_b/k_{pc} [-]	μ_b/μ_{pc} [-]	$c_p/c_{p,pc}$ [-]	ρ_b/ρ_{pc} [-]	Pr_b/Pr_{pc} [-]	h [kW m^{-2} K^{-1}]	Nu [-]	$hsca/h_{TC-LUT}$ [-]	$Nu_{exp,R}/Nu_{TC-LUT}$ [-]
1	40438	0.08	0.97	1.17	1.68	0.11	1.81	0.16	8.37	148.81	0.51	0.71
2	46118	0.13	0.98	1.08	1.49	0.17	1.61	0.23	10.47	202.26	0.66	0.85
3	63521	0.16	0.97	1.14	1.62	0.12	1.75	0.17	10.65	194.32	0.81	0.82
4	78692	0.34	1.00	1.02	1.05	0.90	1.08	0.94	13.81	282.90	1.20	1.40
5	85095	0.22	0.97	1.14	1.61	0.12	1.74	0.17	11.62	212.61	1.04	1.17
6	100494	0.32	0.99	1.04	1.38	0.24	1.48	0.32	14.39	288.93	1.12	1.41
7	97733	0.21	0.96	1.19	1.72	0.10	1.86	0.15	12.86	224.40	0.94	1.13
8	110921	0.29	0.98	1.11	1.56	0.14	1.68	0.19	13.68	256.36	1.13	1.34
9	128358	0.36	0.99	1.02	1.30	0.33	1.39	0.42	14.93	304.08	1.19	1.76
10	140353	0.32	0.98	1.08	1.49	0.16	1.61	0.23	14.58	281.64	1.12	1.48
11	154112	0.34	0.99	1.02	1.29	0.34	1.38	0.43	14.65	298.30	1.15	1.88
12	151975	0.29	0.98	1.13	1.59	0.13	1.72	0.18	15.39	284.97	1.02	1.69
13	158748	0.31	0.98	1.10	1.53	0.15	1.65	0.21	15.94	302.53	1.04	1.73
14	186095	0.43	0.95	1.23	1.78	0.09	1.91	0.14	24.03	408.37	1.06	1.25
15	218921	0.43	0.98	1.13	1.59	0.13	1.72	0.18	21.85	404.35	1.07	2.18
16	145227	0.45	0.97	1.16	1.65	0.11	1.79	0.16	18.09	325.31	1.38	1.62
17	158691	0.50	0.98	1.10	1.53	0.15	1.65	0.21	18.78	356.40	1.41	1.84
18	112927	0.21	0.93	1.33	1.96	0.08	2.08	0.12	15.78	247.84	0.86	0.91
19	119247	0.23	0.94	1.29	1.89	0.08	2.02	0.12	16.55	268.04	0.87	1.00
20	126182	0.27	0.95	1.25	1.82	0.09	1.95	0.13	17.61	294.28	0.93	1.09
21	133728	0.33	0.96	1.21	1.75	0.10	1.88	0.14	18.84	324.87	1.00	1.14
22	142751	0.35	0.97	1.17	1.67	0.11	1.80	0.16	19.75	353.16	1.00	1.40
23	152864	0.45	0.98	1.12	1.58	0.13	1.71	0.19	21.82	405.62	1.11	1.66
24	163839	0.51	0.98	1.08	1.48	0.17	1.60	0.23	23.72	458.65	1.12	1.71
25	268212	0.55	0.95	1.25	1.84	0.09	1.96	0.13	32.42	538.63	1.03	1.40
26	310298	0.80	0.97	1.16	1.65	0.11	1.78	0.16	32.87	592.01	1.35	2.02
27	295074	0.76	0.96	1.19	1.71	0.10	1.85	0.15	33.09	579.68	1.31	1.73
28	255122	0.52	0.94	1.30	1.91	0.08	2.03	0.12	30.06	482.50	1.08	0.99
29	268609	0.60	0.95	1.26	1.85	0.09	1.97	0.13	31.70	523.72	1.15	1.09
30	283267	0.70	0.95	1.22	1.78	0.09	1.91	0.14	33.56	570.70	1.22	1.26
31	297409	0.82	0.96	1.19	1.72	0.10	1.85	0.15	35.66	622.60	1.31	1.45
32	168183	0.68	0.99	1.07	1.46	0.18	1.58	0.24	21.15	412.91	1.64	1.91
33	177641	0.76	0.99	1.04	1.37	0.25	1.47	0.32	22.46	451.87	1.68	1.91
34	187799	0.66	1.00	1.01	1.14	0.65	1.19	0.73	19.61	402.66	1.64	2.19
35	182401	0.48	1.00	1.01	1.01	0.99	1.02	1.00	14.29	295.43	1.64	2.65
36	209413	0.38	1.00	0.87	0.91	0.79	0.86	0.83	12.60	300.67	1.27	2.05
37	230172	0.33	1.00	0.72	0.84	0.51	0.75	0.59	13.97	404.64	0.81	1.51
38	237856	0.34	1.01	0.65	0.81	0.40	0.69	0.50	14.06	451.33	0.76	1.17
39	244029	0.37	1.01	0.59	0.78	0.32	0.65	0.42	13.98	495.98	0.74	1.09

Appendix C

Database for H_2O, CO_2 and R134a for DHT

Table C.1: Test conditions, at $P = 1.13P_c$, of the fluid CO_2 for DHT

Test #	P/P_c [-]	G [kg m^{-2} s^{-1}]	q [kW m^{-2}]	T_{in} [°C]	T_b [°C]	H_b [kJ kg^{-1}]	T_w [°C]	h [kW m^{-2} K^{-1}]	TC#	k_b [W m^{-1} K^{-1}]	μ_b [Pa s]	c_p [kJ kg^{-1} K^{-1}]
1	1.13	700	115	12.00	33.81	303	75.80	2.74	19	0.0755	4.80×10^{-5}	8.11
2	1.13	700	120	14.00	34.72	311	81.29	2.58	19	0.0762	4.43×10^{-5}	10.87
3	1.13	700	105	10.00	13.09	227	57.36	2.37	2	0.1027	8.82×10^{-5}	2.55
4	1.13	700	105	10.00	17.36	239	66.86	2.12	5	0.0972	8.12×10^{-5}	2.74
5	1.13	700	105	10.00	18.72	242	71.88	1.98	6	0.0954	7.89×10^{-5}	2.81
6	1.13	700	105	10.00	20.03	246	76.73	1.85	7	0.0936	7.67×10^{-5}	2.90
7	1.13	700	105	10.00	21.31	250	70.22	2.15	8	0.0919	7.46×10^{-5}	2.99
8	1.13	700	105	10.00	22.54	254	78.38	1.88	9	0.0902	7.25×10^{-5}	3.10
9	1.13	700	105	10.00	23.73	257	74.37	2.08	10	0.0885	7.04×10^{-5}	3.22
10	1.13	700	105	10.00	25.96	265	65.64	2.65	12	0.0852	6.64×10^{-5}	3.52
11	1.13	700	105	10.00	28.92	276	63.83	3.01	15	0.0808	6.07×10^{-5}	4.15
12	1.13	700	105	10.00	32.05	291	66.29	3.07	19	0.0765	5.34×10^{-5}	5.71
13	1.13	700	105	10.00	35.10	316	64.73	3.55	25	0.0770	4.24×10^{-5}	12.77
14	1.13	700	105	10.00	36.20	335	66.49	3.47	30	0.0802	3.56×10^{-5}	21.43
15	1.13	700	105	10.00	37.07	354	72.39	2.98	35	0.0745	3.05×10^{-5}	19.92
16	1.13	701	115	12.10	13.81	229	66.63	2.18	1	0.1018	8.70×10^{-5}	2.58
17	1.13	701	115	12.10	15.38	233	82.26	1.72	2	0.0998	8.44×10^{-5}	2.64
18	1.13	701	115	12.10	16.92	237	93.87	1.50	3	0.0978	8.19×10^{-5}	2.71
19	1.13	701	115	12.10	18.41	242	96.10	1.48	4	0.0958	7.94×10^{-5}	2.79
20	1.13	701	115	12.10	19.86	246	95.59	1.52	5	0.0939	7.70×10^{-5}	2.89
21	1.13	701	115	12.10	21.26	250	91.72	1.63	6	0.0919	7.47×10^{-5}	2.99
22	1.13	701	115	12.10	22.60	254	90.82	1.69	7	0.0901	7.24×10^{-5}	3.11
23	1.13	701	115	12.10	23.90	258	81.40	2.00	8	0.0882	7.01×10^{-5}	3.24

Table C.2: Test conditions, at $P = 1.13P_c$, of the fluid CO_2 for DHT (Cont'd)

Test #	ρ_b [kg m^{-3}]	Pr_b [-]	Re_b [-]	Nu_b [-]	T_b/T_{pc} [-]	H_b/H_{pc} [-]	k_b/k_{pc} [-]	μ_b/μ_{pc} [-]	$c_p/c_{p,pc}$ [-]	ρ_b/ρ_{pc} [-]	Pr_b/Pr_{pc} [-]
1	632	5.16	116728	290.75	0.99	0.89	0.95	1.42	0.37	1.34	0.55
2	597	6.32	126403	270.94	0.99	0.91	0.96	1.32	0.49	1.26	0.68
3	886	2.19	63519	184.98	0.92	0.67	1.30	2.62	0.12	1.87	0.23
4	855	2.28	69006	174.80	0.94	0.70	1.23	2.41	0.12	1.81	0.24
5	844	2.33	70957	165.78	0.94	0.71	1.20	2.34	0.13	1.79	0.25
6	833	2.38	72977	158.39	0.95	0.72	1.18	2.28	0.13	1.76	0.25
7	822	2.43	75069	187.09	0.95	0.73	1.16	2.22	0.14	1.74	0.26
8	810	2.49	77241	167.00	0.95	0.74	1.14	2.15	0.14	1.71	0.27
9	799	2.57	79497	187.63	0.96	0.75	1.12	2.09	0.15	1.69	0.27
10	774	2.74	84287	248.59	0.97	0.78	1.08	1.97	0.16	1.64	0.29
11	736	3.12	92288	298.06	0.98	0.81	1.02	1.80	0.19	1.56	0.33
12	680	3.99	104879	320.90	0.99	0.85	0.97	1.59	0.26	1.44	0.43
13	577	7.04	131968	368.74	1.00	0.93	0.97	1.26	0.58	1.22	0.75
14	498	9.52	157145	346.00	1.00	0.98	1.01	1.06	0.97	1.05	1.02
15	427	8.14	183736	319.39	1.00	1.04	0.94	0.91	0.90	0.90	0.87
16	881	2.20	64472	171.39	0.93	0.67	1.28	2.58	0.12	1.86	0.24
17	870	2.23	66445	138.10	0.93	0.68	1.26	2.51	0.12	1.84	0.24
18	858	2.27	68489	122.47	0.94	0.70	1.23	2.43	0.12	1.82	0.24
19	846	2.32	70608	123.80	0.94	0.71	1.21	2.36	0.13	1.79	0.25
20	834	2.37	72807	129.62	0.95	0.72	1.18	2.29	0.13	1.77	0.25
21	822	2.43	75093	142.21	0.95	0.73	1.16	2.22	0.14	1.74	0.26
22	810	2.50	77473	149.95	0.96	0.74	1.14	2.15	0.14	1.71	0.27
23	797	2.58	79955	181.60	0.96	0.76	1.11	2.08	0.15	1.69	0.28

Table C.3: Scaled test conditions, at $P = 1.13P_c$, of R134a at equivalent condition to that in CO_2 for DHT

Test #	P/P_c [-]	TC#	G [kg m^{-2} s^{-1}]	q [kW m^{-2}]	T_{in} [°C]	T_b [°C]	h [kW m^{-2} K^{-1}]	T_w [°C]	k_b [W m^{-1} K^{-1}]	μ_b [Pa s]	c_p [kJ kg^{-1} K^{-1}]
1	1.13	19	831	93.17	81.00	103.99	1.81	155.59	0.0497	5.36×10^{-5}	4.36
2	1.13	19	832	97.40	83.00	105.11	1.70	162.33	0.0503	4.88×10^{-5}	5.80
3	1.13	2	683	77.50	78.80	78.54	1.42	132.93	0.0616	1.05×10^{-4}	1.73
4	1.13	5	697	78.62	75.60	83.79	1.29	144.60	0.0592	9.58×10^{-5}	1.83
5	1.13	6	702	79.01	76.13	85.45	1.21	150.77	0.0584	9.29×10^{-5}	1.86
6	1.13	7	708	79.41	76.00	87.07	1.14	156.73	0.0576	9.02×10^{-5}	1.90
7	1.13	8	714	79.82	76.50	88.63	1.33	148.73	0.0568	8.75×10^{-5}	1.95
8	1.13	9	720	80.24	76.60	90.15	1.17	158.75	0.0560	8.48×10^{-5}	2.00
9	1.13	10	727	80.66	76.80	91.60	1.30	153.83	0.0553	8.22×10^{-5}	2.06
10	1.13	12	742	81.55	77.00	94.35	1.67	143.10	0.0538	7.71×10^{-5}	2.19
11	1.13	15	768	82.88	77.00	97.99	1.93	140.87	0.0519	6.98×10^{-5}	2.49
12	1.13	19	807	84.40	78.00	101.83	2.01	143.90	0.0500	6.05×10^{-5}	3.21
13	1.13	25	826	85.19	79.00	105.58	2.34	141.98	0.0508	4.63×10^{-5}	6.86
14	1.13	30	842	83.74	80.00	106.94	2.25	144.15	0.0520	3.75×10^{-5}	10.78
15	1.13	35	850	85.70	79.00	108.01	1.98	151.40	0.0495	3.13×10^{-5}	9.98
16	1.13	1	686	85.12	77.50	79.42	1.31	144.32	0.0612	1.03×10^{-4}	1.75
17	1.13	2	691	85.56	77.70	81.36	1.04	163.52	0.0603	9.98×10^{-5}	1.78
18	1.13	3	696	86.01	77.90	83.24	0.91	177.79	0.0594	9.67×10^{-5}	1.82
19	1.13	4	702	86.48	78.00	85.07	0.91	180.53	0.0585	9.36×10^{-5}	1.86
20	1.13	5	708	86.96	78.20	86.85	0.93	179.90	0.0577	9.05×10^{-5}	1.90
21	1.13	6	715	87.45	78.40	88.57	1.01	175.15	0.0568	8.76×10^{-5}	1.95
22	1.13	7	722	87.95	78.60	90.23	1.05	174.04	0.0560	8.47×10^{-5}	2.00
23	1.13	8	729	88.47	78.70	91.82	1.25	162.47	0.0552	8.18×10^{-5}	2.07

Table C.4: Scaled test conditions, at $P = 1.13P_c$, of R134a at equivalent condition to that in CO_2 for DHT (Cont'd)

Test #	ρ_b [kg m^{-3}]	Pr_b [-]	Re_b [-]	Nu_b [-]	T_b/T_{pc} [-]	k_b/k_{pc} [-]	μ_b/μ_{pc} [-]	$c_p/c_{p,pc}$ [-]	ρ_b/ρ_{pc} [-]	Pr_b/Pr_{pc} [-]
1	704	4.70	124181	290.75	0.99	0.96	1.53	0.39	1.37	0.63
2	662	5.64	136340	270.94	0.99	0.97	1.39	0.53	1.29	0.75
3	989	2.94	52286	184.98	0.92	1.19	2.98	0.16	1.93	0.39
4	954	2.96	58213	174.80	0.94	1.15	2.73	0.17	1.86	0.39
5	942	2.97	60428	165.78	0.94	1.13	2.65	0.17	1.83	0.40
6	930	2.98	62781	158.39	0.95	1.12	2.57	0.17	1.81	0.40
7	917	3.00	65284	187.09	0.95	1.10	2.49	0.18	1.79	0.40
8	904	3.03	67947	167.00	0.95	1.09	2.42	0.18	1.76	0.40
9	891	3.06	70781	187.63	0.96	1.07	2.34	0.19	1.73	0.41
10	864	3.14	77009	248.59	0.97	1.04	2.20	0.20	1.68	0.42
11	821	3.35	88028	298.06	0.98	1.01	1.99	0.23	1.60	0.45
12	758	3.88	106790	320.90	0.99	0.97	1.72	0.29	1.48	0.52
13	639	6.26	142683	368.74	1.00	0.98	1.32	0.62	1.24	0.83
14	544	7.77	179725	346.00	1.00	1.01	1.07	0.98	1.06	1.03
15	462	6.32	217105	319.39	1.00	0.96	0.89	0.91	0.90	0.84
16	984	2.94	53263	171.39	0.93	1.19	2.94	0.16	1.91	0.39
17	971	2.95	55369	138.10	0.93	1.17	2.84	0.16	1.89	0.39
18	958	2.95	57609	122.47	0.94	1.15	2.75	0.16	1.86	0.39
19	945	2.97	59997	123.80	0.94	1.13	2.67	0.17	1.84	0.39
20	931	2.98	62548	129.62	0.95	1.12	2.58	0.17	1.81	0.40
21	918	3.00	65276	142.21	0.95	1.10	2.49	0.18	1.79	0.40
22	904	3.03	68196	149.95	0.96	1.09	2.41	0.18	1.76	0.40
23	889	3.06	71321	181.60	0.96	1.07	2.33	0.19	1.73	0.41

Table C.5: Experimental conditions, at $P = 1.13P_c$, of the fluid R134a for DHT

Experimental database in R134a for DHT cases in CO_2															
Test #	P/P_c [-]	TC#	G [kg m^{-2} s^{-1}]	q [kW m^{-2}]	T_{in} [°C]	T_w [°C]	T_b [°C]	h [kW m^{-2} K^{-1}]	H_b [kJ kg^{-1}]	k_b [W m^{-1} K^{-1}]	μ_b [Pa s]	c_p [kJ kg^{-1} K^{-1}]	Nu_b [-]	Re_b [-]	T_b/T_{pc} [-]
1	1.13	19	838	93.07	80.55	120.92	104.03	5.51	372	0.0495	5.49×10^{-5}	3.98	890.14	122091	0.99
2	1.13	19	835	97.47	82.51	123.47	105.37	5.38	379	0.0499	4.96×10^{-5}	5.31	863.33	134614	0.99
3	1.13	2	696	77.51	75.63	125.45	78.96	1.67	317	0.0613	1.03×10^{-4}	1.75	217.52	53816	0.93
4	1.13	5	697	78.95	75.83	129.37	84.01	1.74	326	0.0592	9.57×10^{-5}	1.82	235.28	58241	0.94
5	1.13	6	704	78.96	75.90	125.22	85.51	1.99	328	0.0585	9.32×10^{-5}	1.86	272.13	60420	0.94
6	1.13	7	716	79.77	76.86	125.37	87.74	2.12	333	0.0572	8.88×10^{-5}	1.93	296.68	64509	0.95
7	1.13	8	717	80.40	76.78	124.18	89.17	2.30	336	0.0564	8.63×10^{-5}	1.98	325.47	66462	0.95
8	1.13	9	725	80.27	76.63	124.76	90.27	2.33	338	0.0558	8.41×10^{-5}	2.02	333.59	68930	0.96
9	1.13	10	732	81.01	77.16	124.86	92.05	2.47	342	0.0549	8.09×10^{-5}	2.10	359.87	72385	0.96
10	1.13	12	740	82.21	77.00	123.71	94.62	2.83	347	0.0537	7.66×10^{-5}	2.21	421.28	77337	0.97
11	1.13	15	774	82.93	77.83	123.45	97.97	3.25	355	0.0517	6.88×10^{-5}	2.56	504.03	90010	0.98
12	1.13	19	811	84.66	79.03	119.40	102.42	4.99	367	0.0499	6.00×10^{-5}	3.22	799.58	108134	0.99
13	1.13	25	832	85.11	78.97	122.71	105.79	5.03	382	0.0507	4.62×10^{-5}	6.80	793.92	144246	1.00
14	1.13	30	845	84.51	79.71	124.93	107.00	4.71	395	0.0520	3.70×10^{-5}	10.90	725.08	182687	1.00
15	1.13	35	852	86.44	78.60	133.88	108.54	3.41	407	0.0487	3.12×10^{-5}	9.29	560.22	218560	1.00
16	1.13	1	693	85.11	77.62	133.55	79.50	1.57	318	0.0613	1.03×10^{-4}	1.75	205.63	53743	0.93
17	1.13	2	694	85.48	77.76	162.05	81.38	1.06	321	0.0603	9.98×10^{-5}	1.78	140.59	55662	0.93
18	1.13	3	704	86.06	77.79	193.42	83.08	0.78	324	0.0594	9.67×10^{-5}	1.82	105.00	58267	0.94
19	1.13	4	705	86.48	78.13	222.91	85.11	0.63	328	0.0586	9.37×10^{-5}	1.85	85.71	60179	0.94
20	1.13	5	713	86.97	78.09	194.40	86.66	0.81	331	0.0578	9.10×10^{-5}	1.89	111.68	62653	0.95
21	1.13	6	719	87.23	77.97	145.87	88.08	1.51	333	0.0571	8.84×10^{-5}	1.93	211.62	65064	0.95
22	1.13	7	724	87.88	78.79	135.47	90.37	1.95	338	0.0560	8.45×10^{-5}	2.00	278.63	68474	0.96
23	1.13	8	732	88.58	78.60	132.28	91.64	2.18	341	0.0553	8.22×10^{-5}	2.06	315.58	71283	0.96

Table C.6: Experimental conditions, at $P = 1.13P_c$, of the fluid R134a for DHT (Cont'd)

R134a database for DHT cases in CO_2-Experimental							Comparison	
Test #	H_b/H_{pc} [-]	k_b/k_{pc} [-]	μ_b/μ_{pc} [-]	$c_p/c_{p,pc}$ [-]	ρ_b/ρ_{pc} [-]	Pr_b/Pr_{pc} [-]	h_{sca}/h_{exp} [-]	$Nu_{R/C}/Nu_{exp}$ [-]
1	0.94	0.96	1.56	0.36	1.39	0.59	0.33	0.33
2	0.95	0.97	1.41	0.48	1.30	0.70	0.32	0.31
3	0.80	1.19	2.95	0.16	1.92	0.39	0.85	0.85
4	0.82	1.15	2.73	0.17	1.86	0.39	0.74	0.74
5	0.83	1.13	2.66	0.17	1.84	0.39	0.61	0.61
6	0.84	1.11	2.53	0.17	1.80	0.40	0.54	0.53
7	0.84	1.09	2.46	0.18	1.77	0.40	0.58	0.57
8	0.85	1.08	2.40	0.18	1.75	0.41	0.50	0.50
9	0.86	1.06	2.30	0.19	1.72	0.41	0.53	0.52
10	0.87	1.04	2.18	0.20	1.68	0.42	0.59	0.59
11	0.89	1.00	1.96	0.23	1.59	0.46	0.59	0.59
12	0.92	0.97	1.71	0.29	1.47	0.52	0.40	0.40
13	0.96	0.98	1.31	0.62	1.24	0.83	0.47	0.46
14	0.99	1.01	1.05	0.99	1.05	1.03	0.48	0.48
15	1.02	0.94	0.89	0.84	0.89	0.79	0.58	0.57
16	0.80	1.19	2.94	0.16	1.92	0.39	0.83	0.83
17	0.81	1.17	2.84	0.16	1.89	0.39	0.98	0.98
18	0.81	1.15	2.75	0.16	1.86	0.39	1.17	1.17
19	0.82	1.14	2.67	0.17	1.84	0.39	1.44	1.44
20	0.83	1.12	2.59	0.17	1.82	0.40	1.16	1.16
21	0.84	1.11	2.52	0.18	1.79	0.40	0.67	0.67
22	0.85	1.08	2.41	0.18	1.76	0.40	0.54	0.54
23	0.86	1.07	2.34	0.19	1.73	0.41	0.57	0.58

Table C.7: Scaled test conditions, at $P = 1.13P_c$, of H_2O at equivalent condition to that in CO_2 for DHT

Test #	P/P_c [-]	TC#	G [kg m^{-2} s^{-1}]	q [kW m^{-2}]	T_{in} [°C]	T_b [°C]	h [kW m^{-2} K^{-1}]	T_w [°C]	k_b [W m^{-1} K^{-1}]	μ_b [Pa s]	c_p [kJ kg^{-1} K^{-1}]	ρ_b [kg m^{-3}]	Pr_b [-]
1	1.13	19	1192	1286	333	378.88	14.41	468.08	0.3965	5.38×10^{-5}	20.19	464.28	2.74
2	1.13	19	1142	1313	337	380.81	13.28	479.74	0.3920	5.07×10^{-5}	28.54	434.17	3.69
3	1.13	2	1097	1118	328	334.88	11.89	428.91	0.5141	7.89×10^{-5}	6.11	668.46	0.94
4	1.13	5	1121	1136	328	343.95	10.81	449.08	0.4945	7.53×10^{-5}	6.57	643.75	1.00
5	1.13	6	1129	1142	328	346.82	10.12	459.75	0.4881	7.41×10^{-5}	6.75	635.17	1.02
6	1.13	7	1138	1149	328	349.62	9.54	470.06	0.4818	7.29×10^{-5}	6.96	626.41	1.05
7	1.13	8	1146	1155	328	352.32	11.12	456.22	0.4755	7.17×10^{-5}	7.19	617.46	1.08
8	1.13	9	1155	1162	328	354.94	9.80	473.55	0.4692	7.05×10^{-5}	7.45	608.30	1.12
9	1.13	10	1163	1168	328	357.46	10.86	465.04	0.4631	6.93×10^{-5}	7.75	598.94	1.16
10	1.13	12	1179	1181	328	362.21	14.01	446.49	0.4508	6.69×10^{-5}	8.47	579.54	1.26
11	1.13	15	1196	1195	328	368.50	16.12	442.65	0.4328	6.31×10^{-5}	10.07	548.48	1.47
12	1.13	19	1210	1196	328	375.15	16.44	447.88	0.4099	5.80×10^{-5}	13.93	503.07	1.97
13	1.13	25	1116	1133	328	381.63	18.00	444.57	0.3906	4.90×10^{-5}	34.44	417.26	4.32
14	1.13	30	968	1087	328	383.97	16.89	448.30	0.3906	4.21×10^{-5}	69.56	345.45	7.49
15	1.13	35	940	1007	328	385.82	13.42	460.84	0.3362	3.60×10^{-5}	62.65	275.49	6.72
16	1.13	1	1102	1228	333	336.40	10.94	448.60	0.5109	7.83×10^{-5}	6.17	664.53	0.95
17	1.13	2	1111	1235	333	339.75	8.70	481.80	0.5037	7.70×10^{-5}	6.33	655.61	0.97
18	1.13	3	1120	1243	333	343.01	7.60	506.46	0.4966	7.57×10^{-5}	6.51	646.48	0.99
19	1.13	4	1129	1250	333	346.18	7.58	511.20	0.4896	7.44×10^{-5}	6.71	637.14	1.02
20	1.13	5	1138	1258	333	349.25	7.82	510.12	0.4826	7.30×10^{-5}	6.93	627.59	1.05
21	1.13	6	1148	1266	333	352.22	8.46	501.90	0.4757	7.17×10^{-5}	7.18	617.81	1.08
22	1.13	7	1157	1274	333	355.08	8.79	499.99	0.4689	7.04×10^{-5}	7.47	607.79	1.12
23	1.13	8	1166	1281	333	357.83	10.49	479.98	0.4621	6.91×10^{-5}	7.79	597.53	1.17

Table C.8: Scaled test conditions, at $P = 1.13P_c$, of H_2O at equivalent condition to that in CO_2 for DHT (Cont'd)

Scaled H_2O database for DHT									TC-LUT (Zahlan et al., 2015b)		Comparison	
Test #	Re_b [-]	Nu_b [-]	T_b/T_{pc} [-]	k_b/k_{pc} [-]	μ_b/μ_{pc} [-]	$c_p/c_{p,pc}$ [-]	ρ_b/ρ_{pc} [-]	Pr_b/Pr_{pc} [-]	h [kW m^{-2} K^{-1}]	Nu [-]	$hsca/h_{TC-LUT}$ [-]	$Nu_{exp,C}/Nu_{TC-LUT}$ [-]
1	177251	290.75	0.99	1.03	1.36	0.26	1.46	0.34	12.68	255.85	1.14	3.48
2	180374	270.94	0.99	1.02	1.28	0.36	1.36	0.46	11.21	228.73	1.18	3.77
3	111257	184.98	0.92	1.34	1.99	0.08	2.10	0.12	11.10	172.80	1.07	1.26
4	119105	174.80	0.94	1.29	1.90	0.08	2.02	0.12	10.61	171.56	1.02	1.37
5	121929	165.78	0.94	1.27	1.87	0.09	1.99	0.13	10.20	167.18	0.99	1.63
6	124867	158.39	0.95	1.25	1.84	0.09	1.96	0.13	9.85	163.63	0.97	1.81
7	127917	187.09	0.95	1.24	1.81	0.09	1.94	0.13	10.96	184.36	1.01	1.77
8	131073	167.00	0.95	1.22	1.78	0.10	1.91	0.14	10.11	172.31	0.97	1.94
9	134323	187.63	0.96	1.21	1.75	0.10	1.88	0.14	10.87	187.83	1.00	1.92
10	141047	248.59	0.97	1.17	1.68	0.11	1.82	0.16	12.96	230.01	1.08	1.83
11	151576	298.06	0.98	1.13	1.59	0.13	1.72	0.18	14.27	263.84	1.13	1.91
12	166972	320.90	0.99	1.07	1.46	0.18	1.58	0.24	14.74	287.74	1.12	2.78
13	182285	368.74	1.00	1.02	1.23	0.44	1.31	0.53	14.98	306.81	1.20	2.59
14	184057	346.00	1.00	1.02	1.06	0.89	1.08	0.92	12.66	259.20	1.33	2.80
15	208671	319.39	1.00	0.88	0.91	0.80	0.86	0.83	10.93	260.02	1.23	2.15
16	112640	171.39	0.93	1.33	1.97	0.08	2.08	0.12	9.98	156.23	1.10	1.32
17	115455	138.10	0.93	1.31	1.94	0.08	2.06	0.12	8.66	137.61	1.00	1.02
18	118388	122.47	0.94	1.29	1.91	0.08	2.03	0.12	8.04	129.49	0.95	0.81
19	121449	123.80	0.94	1.27	1.87	0.09	2.00	0.13	8.06	131.66	0.94	0.65
20	124646	129.62	0.95	1.26	1.84	0.09	1.97	0.13	8.24	136.59	0.95	0.82
21	127978	142.21	0.95	1.24	1.81	0.09	1.94	0.13	8.66	145.69	0.98	1.45
22	131437	149.95	0.96	1.22	1.77	0.10	1.91	0.14	8.90	151.89	0.99	1.83
23	135008	181.60	0.96	1.20	1.74	0.10	1.87	0.14	10.00	173.19	1.05	1.82

Appendix D

Measurements of T_w and Nu_b profiles for NHT

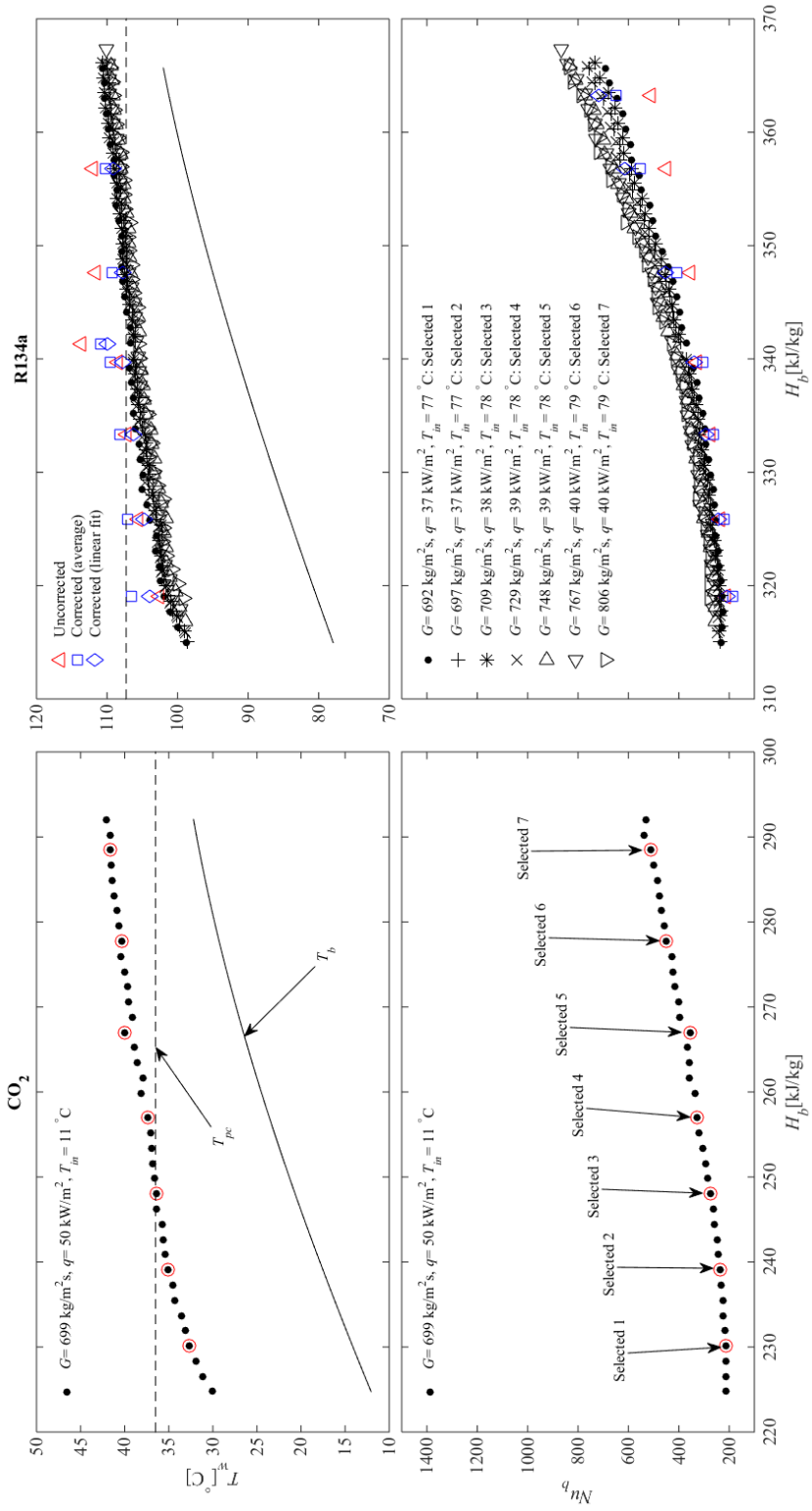

Figure D.1: Measurements of wall temperature (top) and bulk Nusselt number (bottom) *vs.* bulk enthalpy profiles in the fluids CO_2 and R134a at equivalent conditions for NHT; CO_2 test condition: $G = 699$ kg m^{-2} s^{-1}, $q = 50$ kW m^{-2}, $T_{in} = 11$ °C.

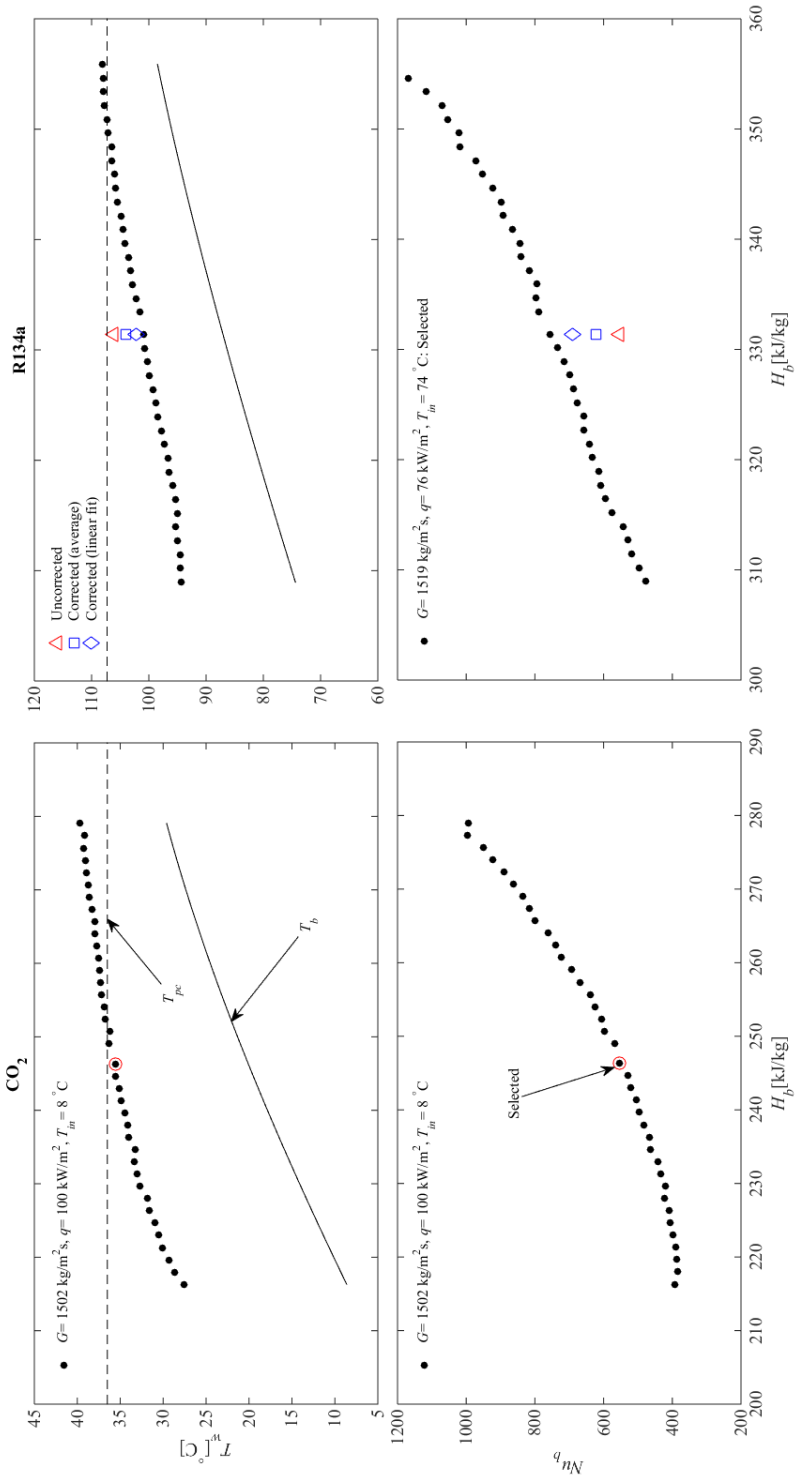

Figure D.2: Measurements of wall temperature (top) and bulk Nusselt number (bottom) *vs.* bulk enthalpy profiles in the fluids CO_2 and R134a at equivalent conditions for NHT; CO_2 test condition: $G = 1502\ \mathrm{kg\,m^{-2}\,s^{-1}}$, $q = 100$ $\mathrm{kW\,m^{-2}}$, $T_{in} = 8$ °C.

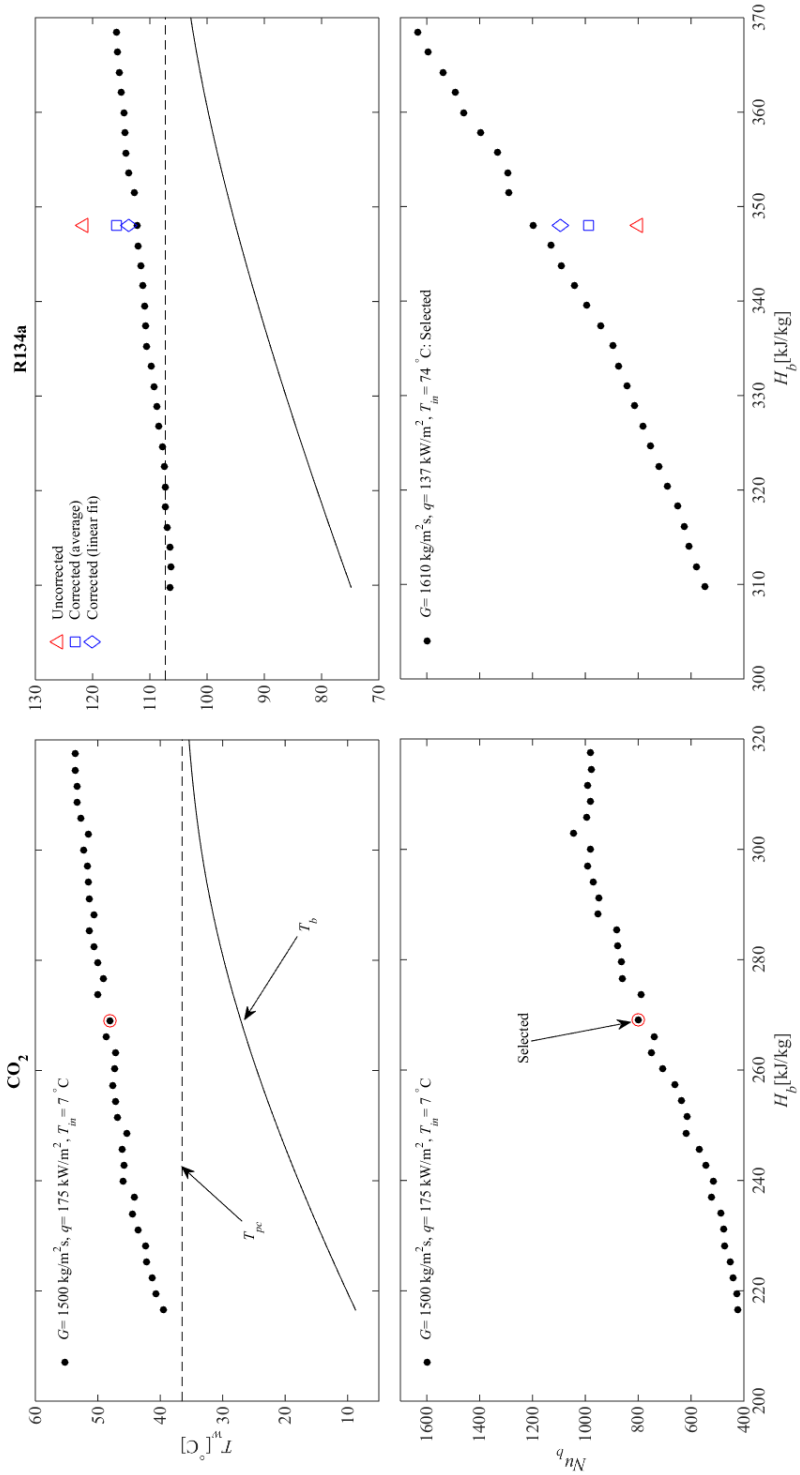

Figure D.3: Measurements of wall temperature (top) and bulk Nusselt number (bottom) *vs.* bulk enthalpy profiles in the fluids CO_2 and R134a at equivalent conditions for NHT; CO_2 test condition: $G = 1500\ \mathrm{kg\,m^{-2}\,s^{-1}}$, $q = 175$ $\mathrm{kW\,m^{-2}}$, $T_{in} = 7$ °C.

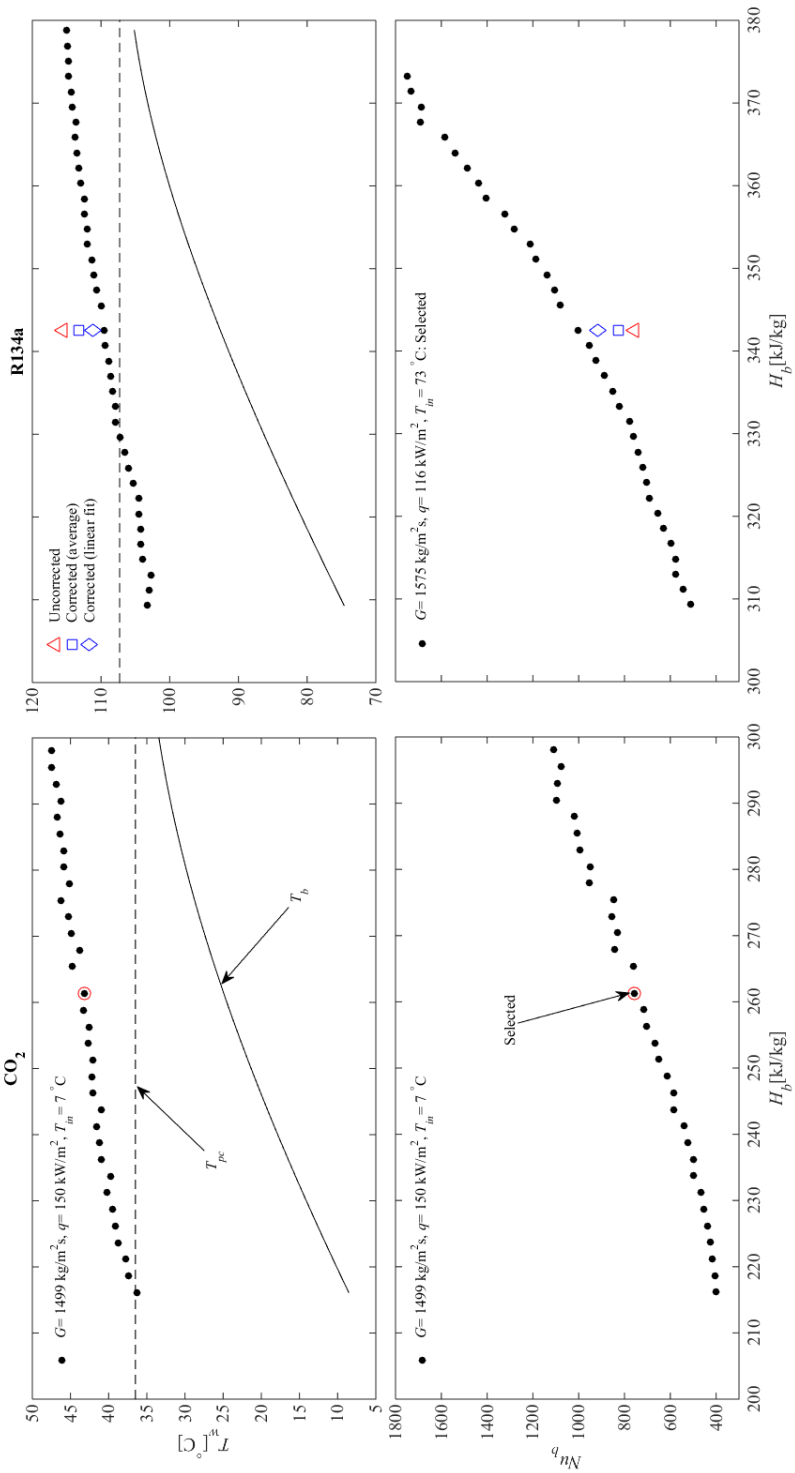

Figure D.4: Measurements of wall temperature (top) and bulk Nusselt number (bottom) *vs.* bulk enthalpy profiles in the fluids CO_2 and R134a at equivalent conditions for NHT; CO_2 test condition: $G = 1499\ \mathrm{kg\,m^{-2}\,s^{-1}}$, $q = 150\ \mathrm{kW\,m^{-2}}$, $T_{in} = 7\ ^{\circ}\mathrm{C}$.

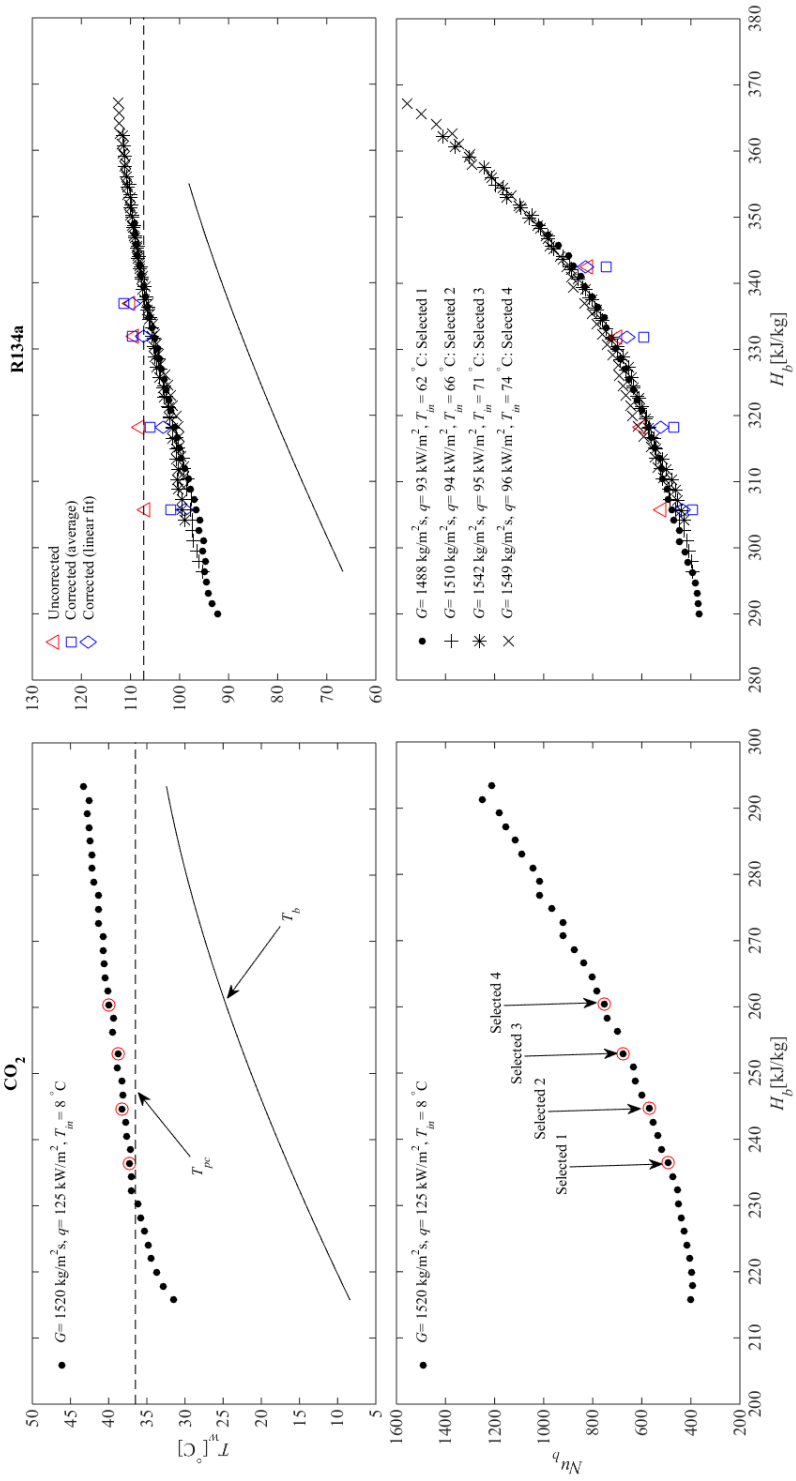

Figure D.5: Measurements of wall temperature (top) and bulk Nusselt number (bottom) *vs.* bulk enthalpy profiles in the fluids CO_2 and R134a at equivalent conditions for NHT; CO_2 test condition: $G = 1520$ kg m^{-2} s^{-1}, $q = 125$ kW m^{-2}, $T_{in} = 8$ °C.

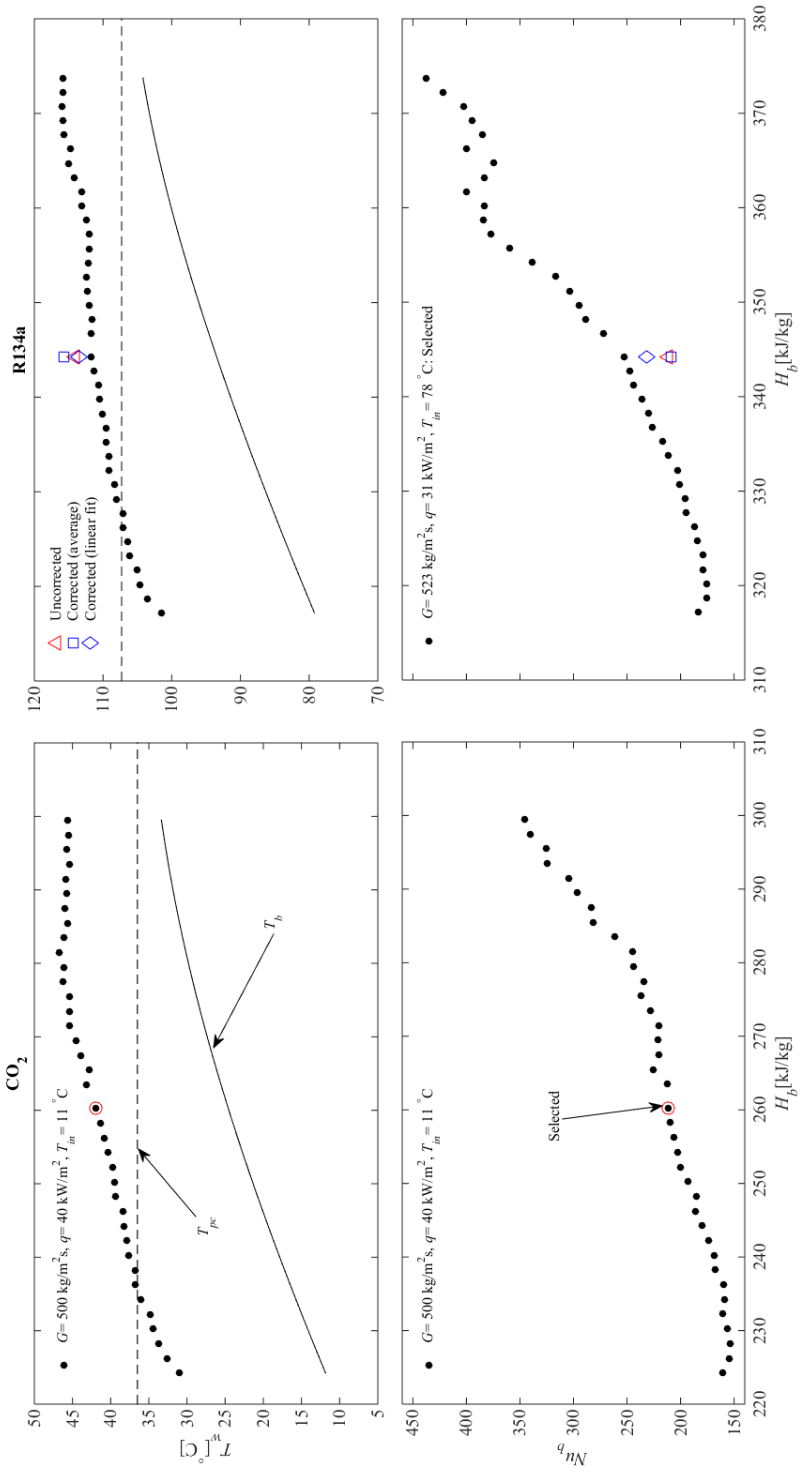

Figure D.6: Measurements of wall temperature (top) and bulk Nusselt number (bottom) *vs.* bulk enthalpy profiles in the fluids CO_2 and R134a at equivalent conditions for NHT; CO_2 test condition: $G = 500\ \mathrm{kg\,m^{-2}\,s^{-1}}$, $q = 40$ $\mathrm{kW\,m^{-2}}$, $T_{in} = 11$ °C.

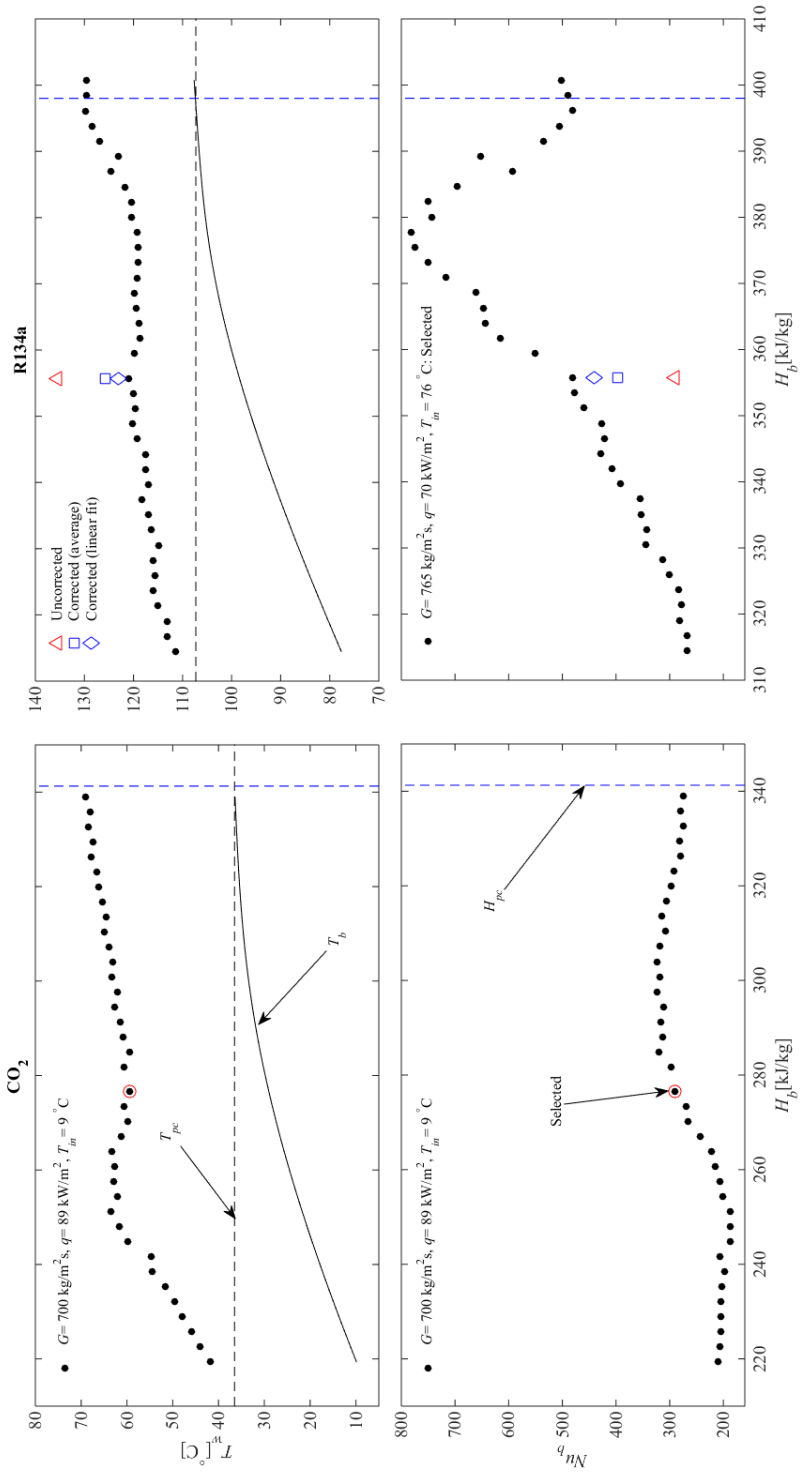

Figure D.7: Measurements of wall temperature (top) and bulk Nusselt number (bottom) *vs.* bulk enthalpy profiles in the fluids CO_2 and R134a at equivalent conditions for NHT; CO_2 test condition: $G = 700\ \mathrm{kg\,m^{-2}\,s^{-1}}$, $q = 89$ $\mathrm{kW\,m^{-2}}$, $T_{in} = 9$ °C.

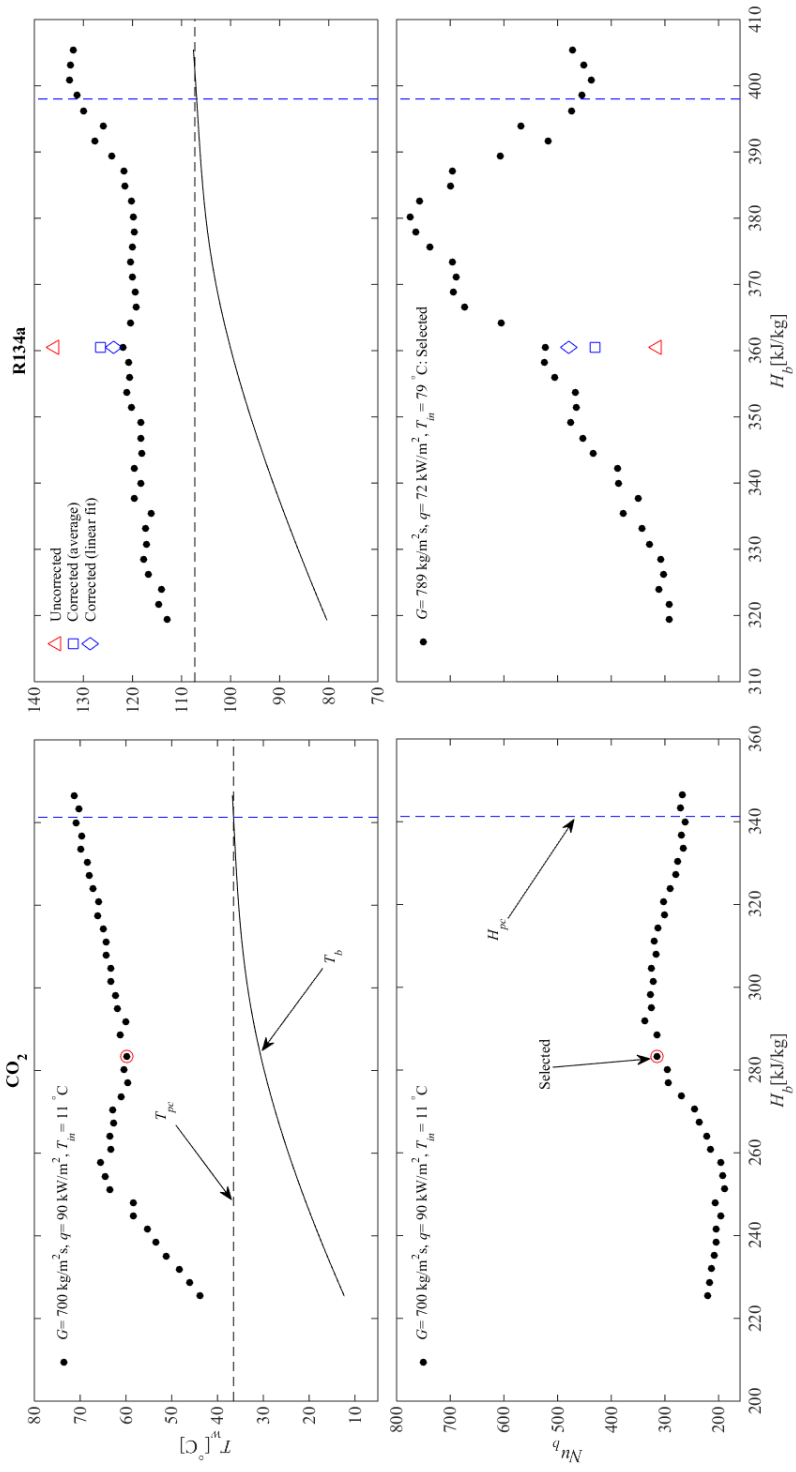

Figure D.8: Measurements of wall temperature (top) and bulk Nusselt number (bottom) *vs.* bulk enthalpy profiles in the fluids CO_2 and R134a at equivalent conditions for NHT; CO_2 test condition: $G = 700\ \mathrm{kg\,m^{-2}\,s^{-1}}$, $q = 90$ $\mathrm{kW\,m^{-2}}$, $T_{in} = 11$ °C.

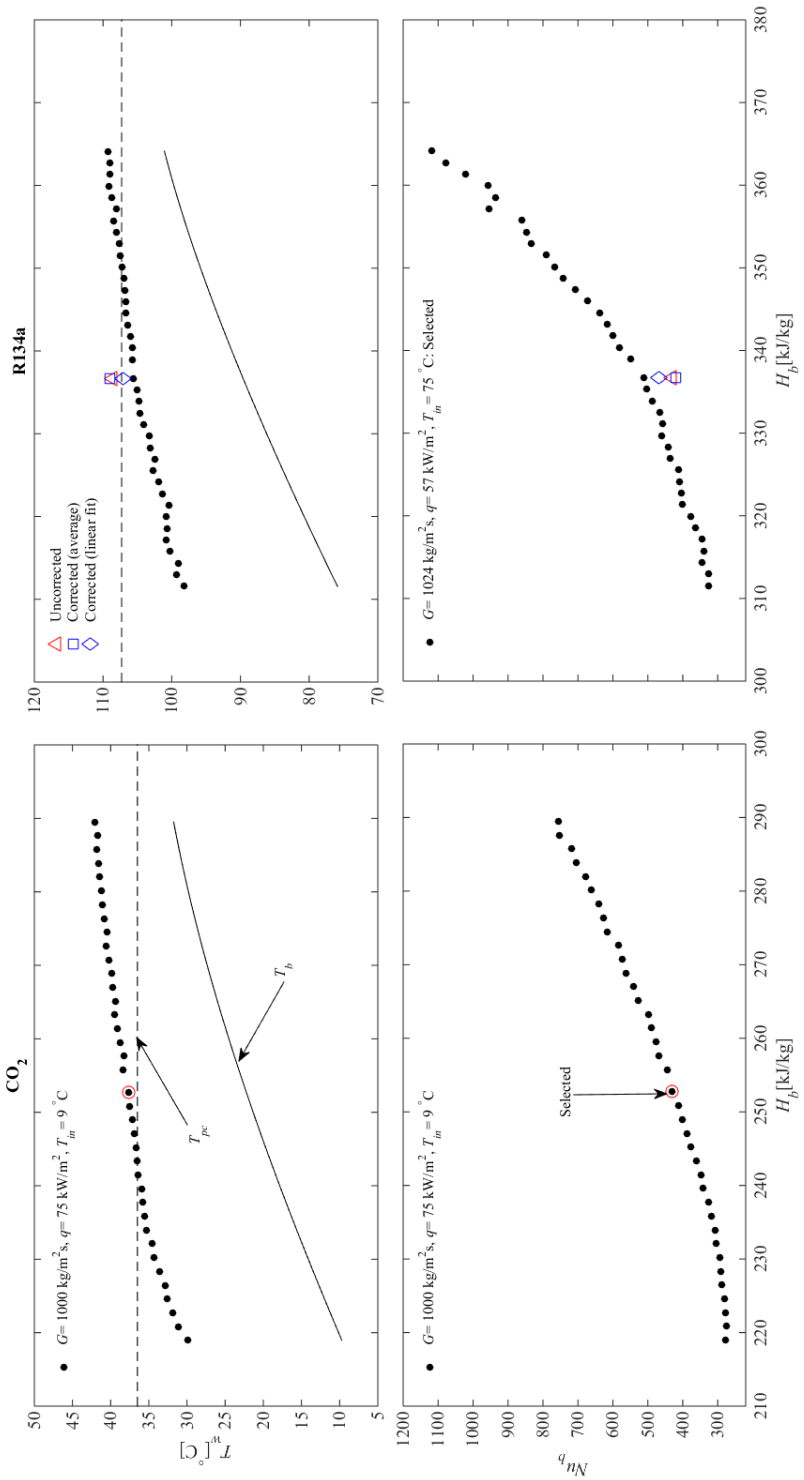

Figure D.9: Measurements of wall temperature (top) and bulk Nusselt number (bottom) *vs.* bulk enthalpy profiles in the fluids CO_2 and R134a at equivalent conditions for NHT; CO_2 test condition: $G = 1000$ kg m^{-2} s^{-1}, $q = 75$ kW m^{-2}, $T_{in} = 9$ °C.

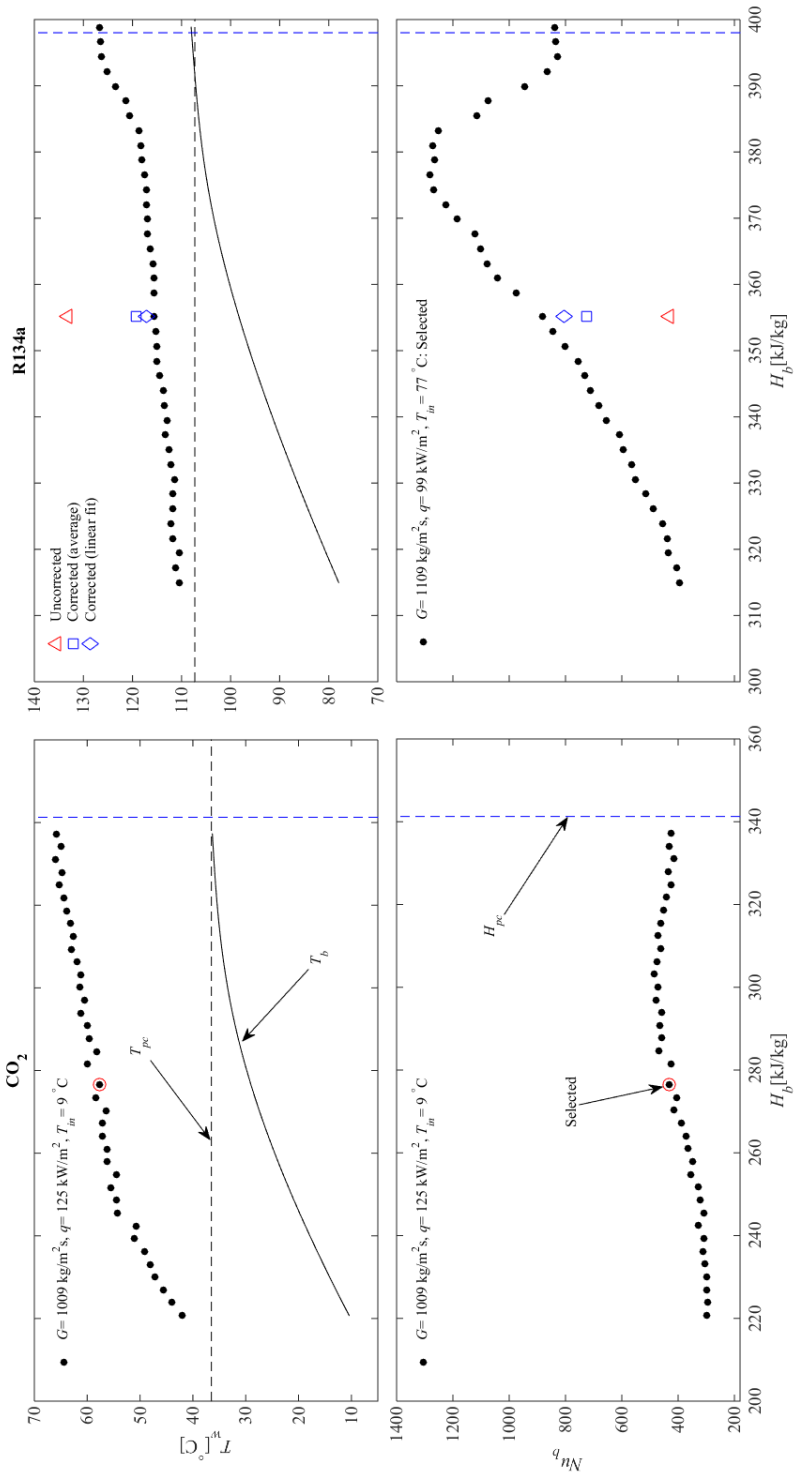

Figure D.10: Measurements of wall temperature (top) and bulk Nusselt number (bottom) *vs.* bulk enthalpy profiles in the fluids CO_2 and R134a at equivalent conditions for NHT; CO_2 test condition: $G = 1009$ kg m^{-2} s^{-1}, $q = 125$ kW m^{-2}, $T_{in} = 9$ °C.

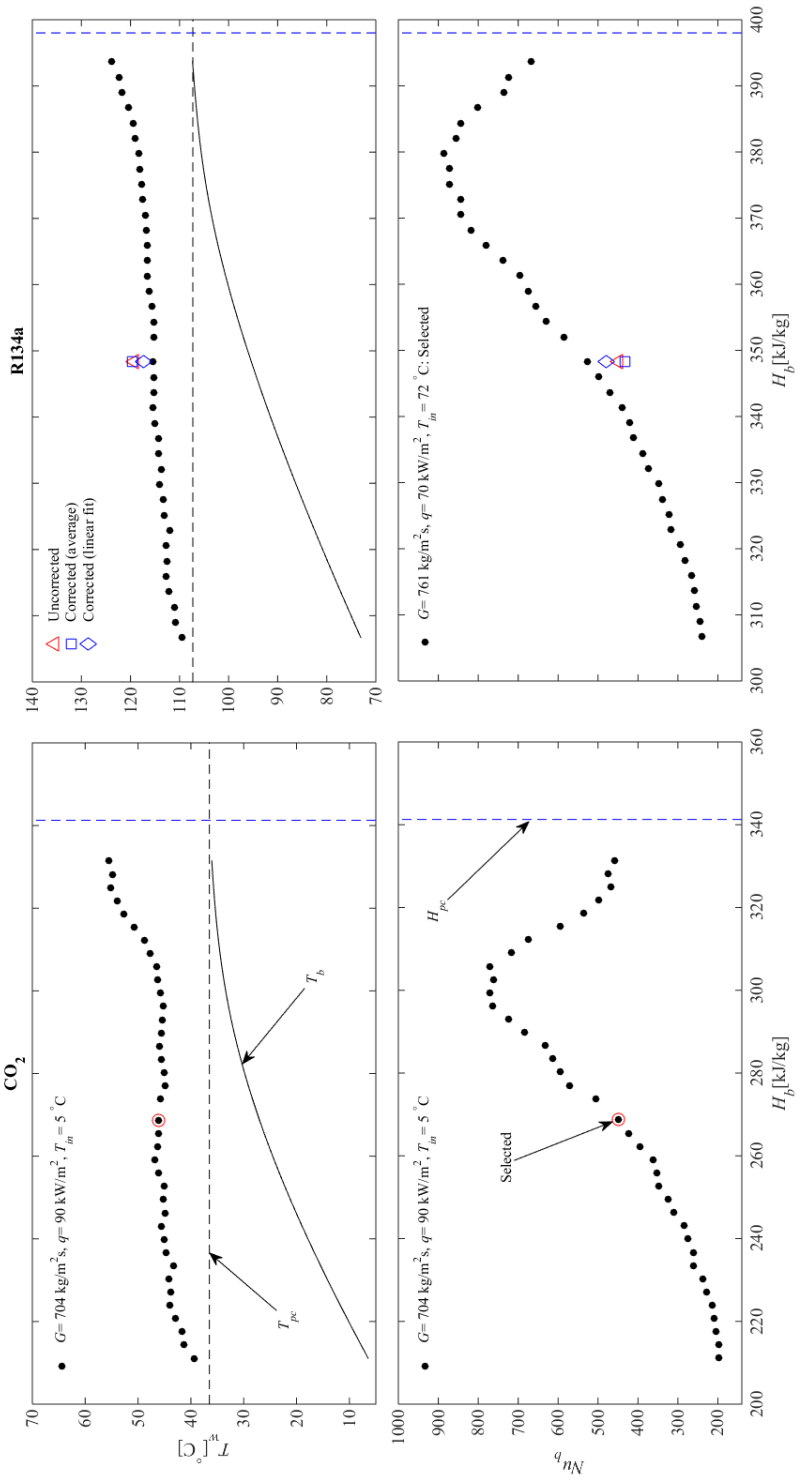

Figure D.11: Measurements of wall temperature (top) and bulk Nusselt number (bottom) *vs.* bulk enthalpy profiles in the fluids CO_2 and R134a at equivalent conditions for NHT; CO_2 test condition: $G = 704\ \mathrm{kg\,m^{-2}\,s^{-1}}$, $q = 90$ $\mathrm{kW\,m^{-2}}$, $T_{in} = 5$ °C.

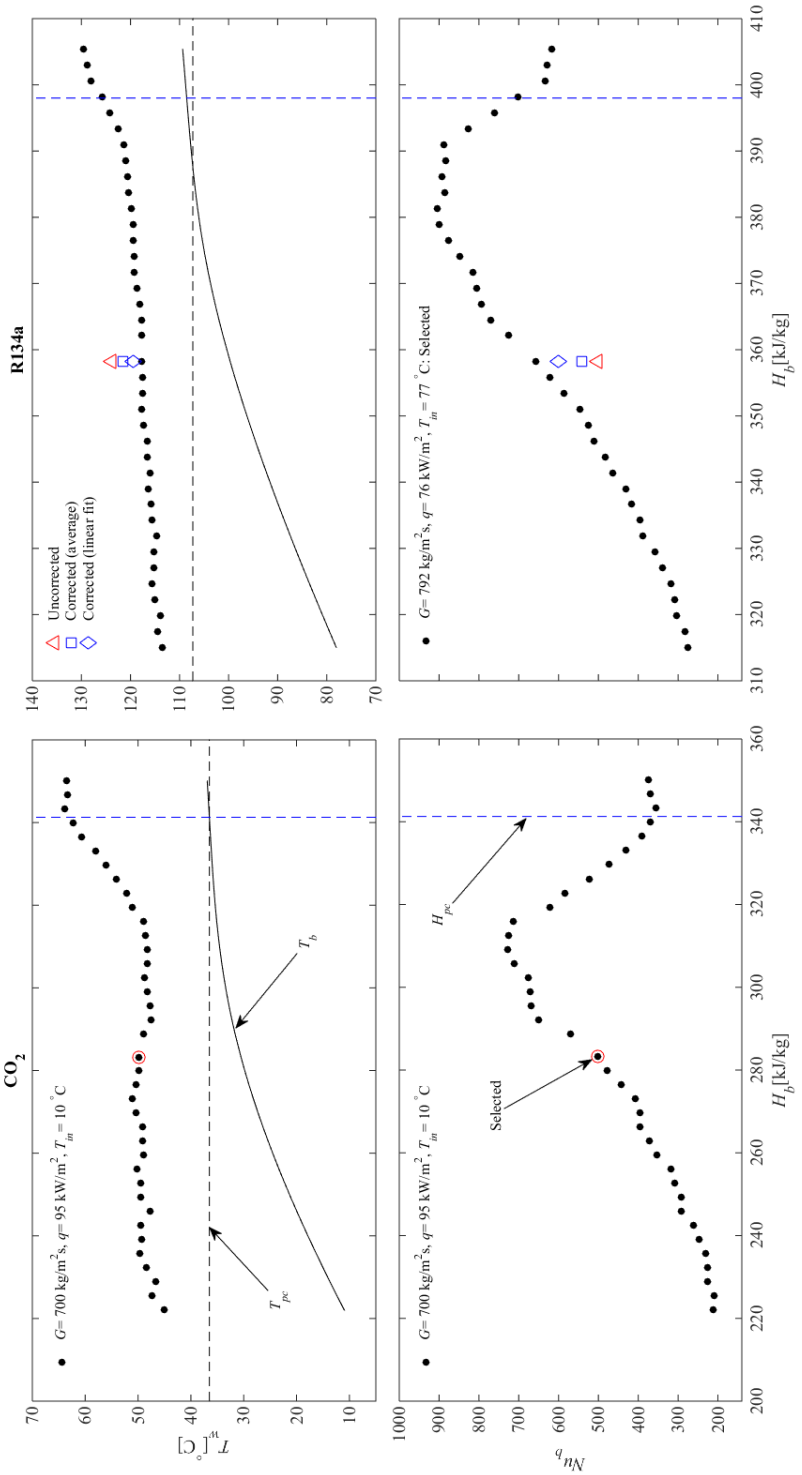

Figure D.12: Measurements of wall temperature (top) and bulk Nusselt number (bottom) *vs.* bulk enthalpy profiles in the fluids CO_2 and R134a at equivalent conditions for NHT; CO_2 test condition: $G = 700\ \mathrm{kg\,m^{-2}\,s^{-1}}$, $q = 95$ $\mathrm{kW\,m^{-2}}$, $T_{in} = 10$ °C.

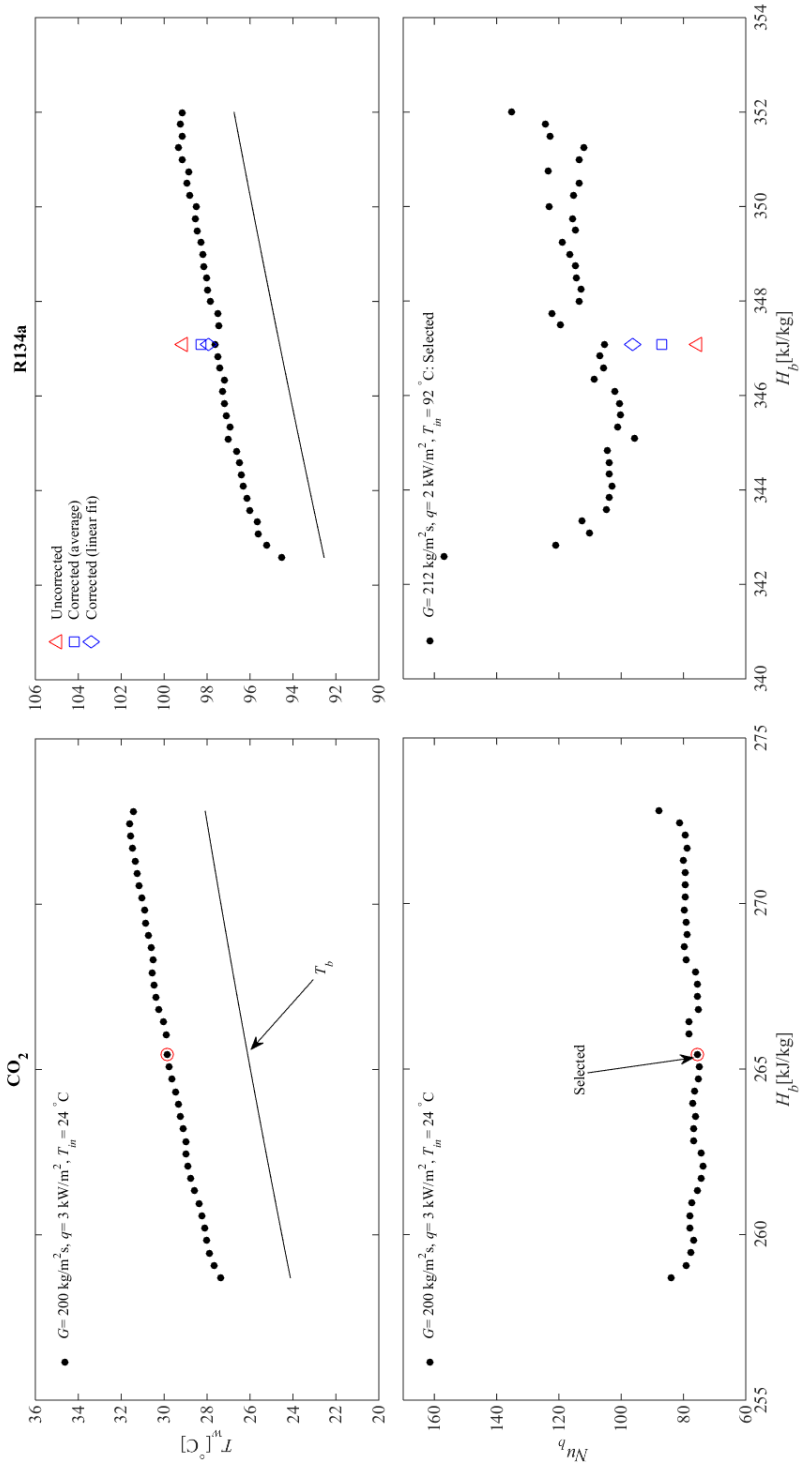

Figure D.13: Measurements of wall temperature (top) and bulk Nusselt number (bottom) *vs.* bulk enthalpy profiles in the fluids CO_2 and R134a at equivalent conditions for NHT; CO_2 test condition: $G = 200$ kg m^{-2} s^{-1}, $q = 3$ kW m^{-2}, $T_{in} = 24$ °C.

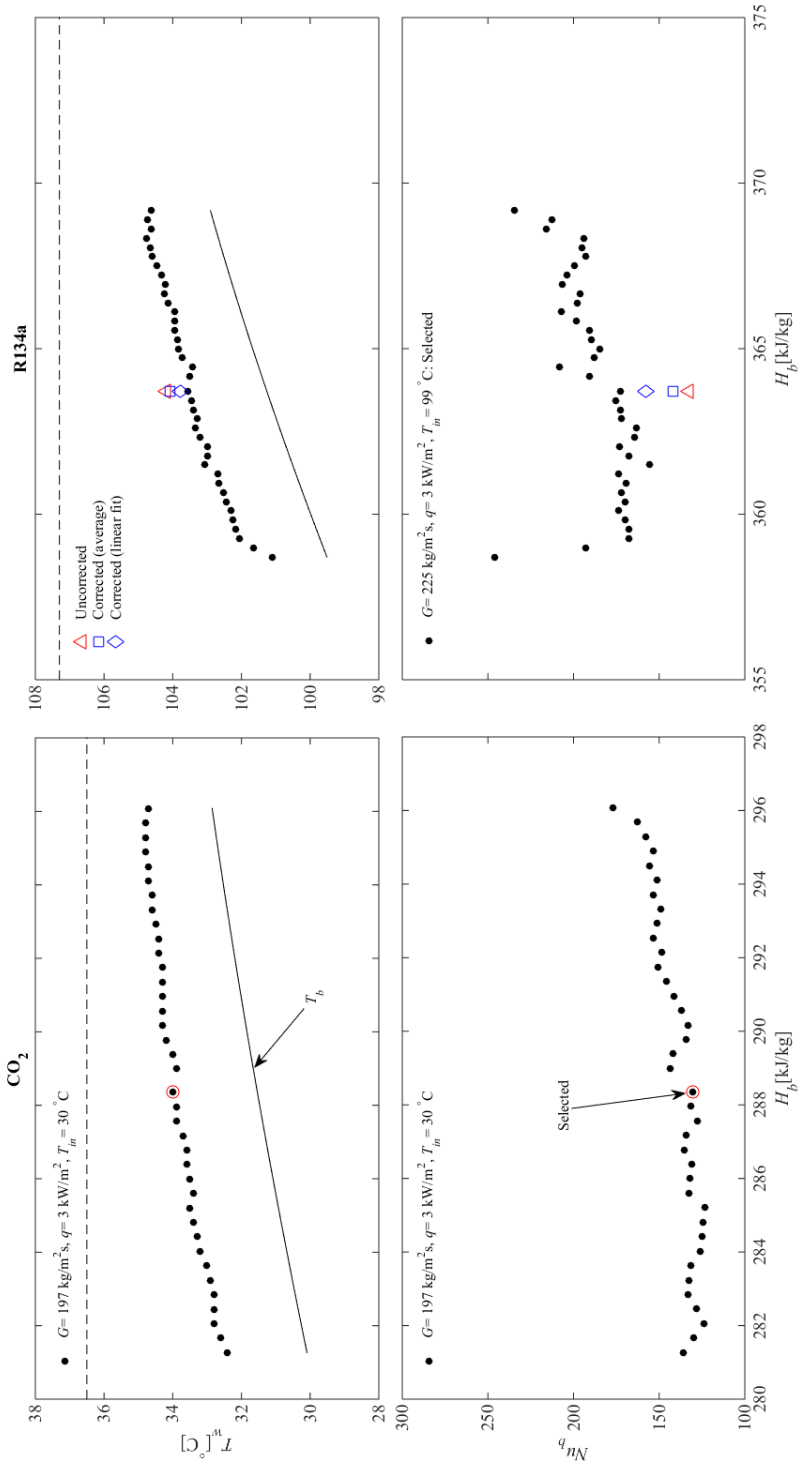

Figure D.14: Measurements of wall temperature (top) and bulk Nusselt number (bottom) *vs.* bulk enthalpy profiles in the fluids CO_2 and R134a at equivalent conditions for NHT; CO_2 test condition: $G = 197\ \mathrm{kg\,m^{-2}\,s^{-1}}$, $q = 3\ \mathrm{kW\,m^{-2}}$, $T_{in} = 30\ ^{\circ}\mathrm{C}$.

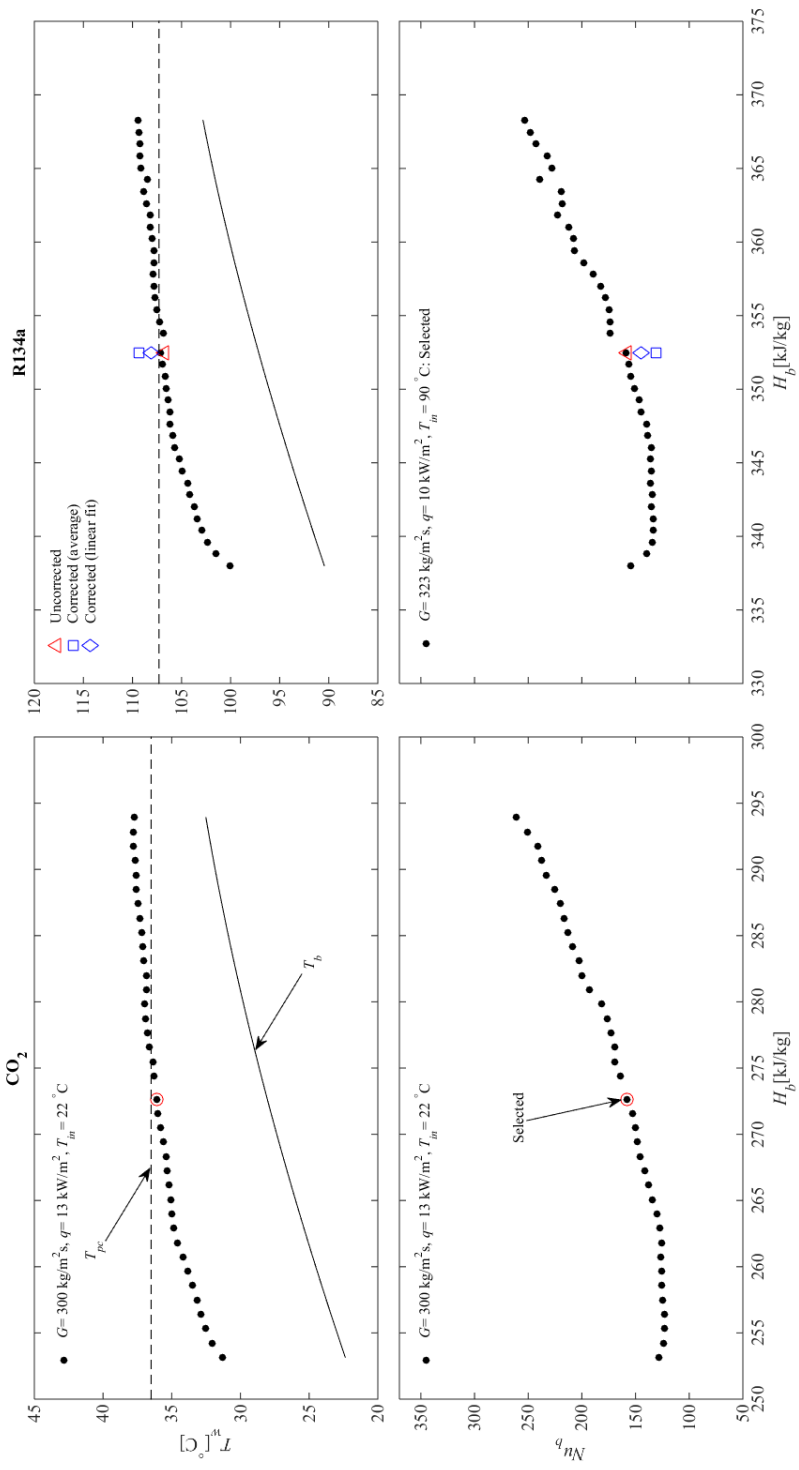

Figure D.15: Measurements of wall temperature (top) and bulk Nusselt number (bottom) *vs.* bulk enthalpy profiles in the fluids CO_2 and R134a at equivalent conditions for NHT; CO_2 test condition: $G = 300\ \mathrm{kg\,m^{-2}\,s^{-1}}$, $q = 13\ \mathrm{kW\,m^{-2}}$, $T_{in} = 22\ ^{\circ}\mathrm{C}$.

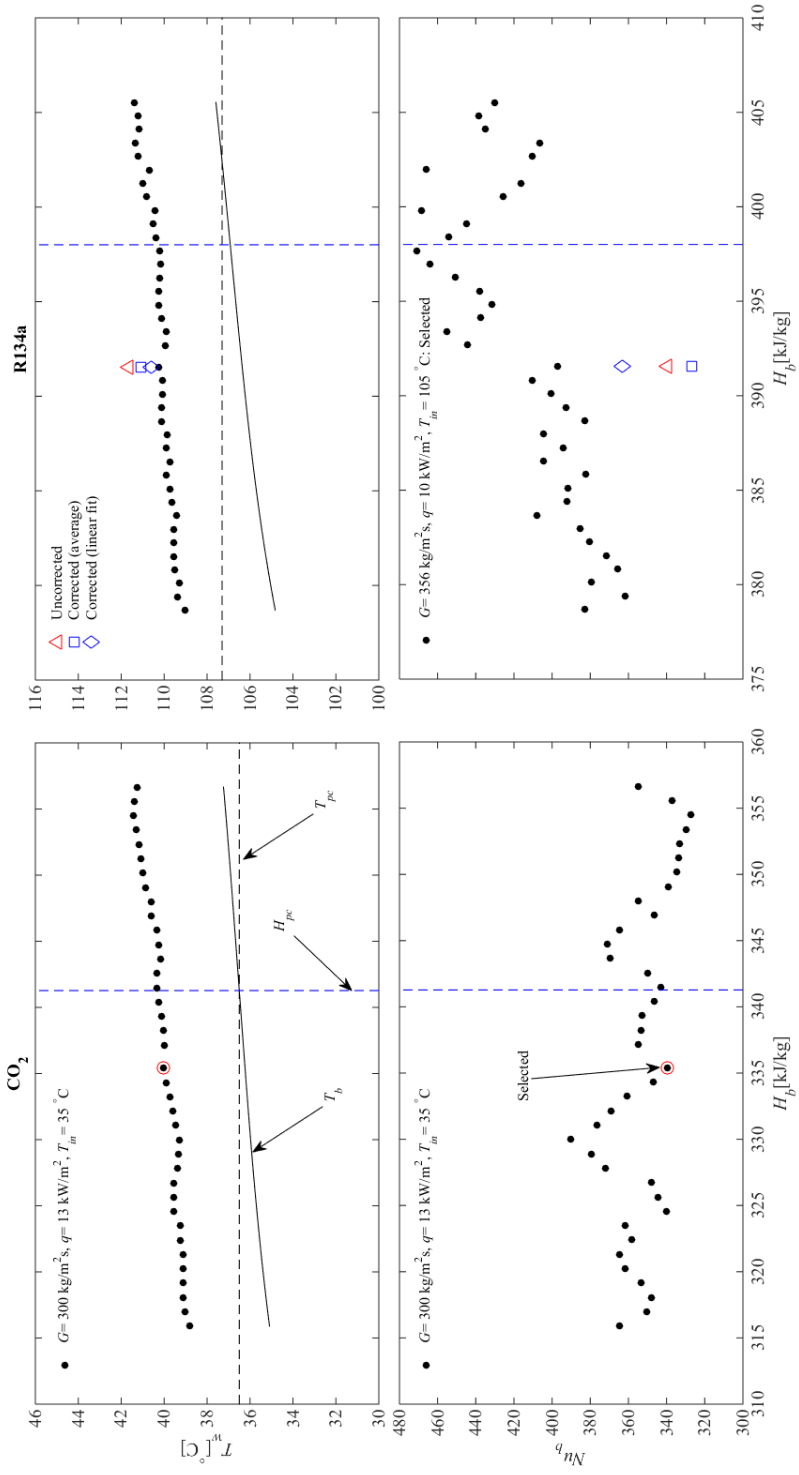

Figure D.16: Measurements of wall temperature (top) and bulk Nusselt number (bottom) *vs.* bulk enthalpy profiles in the fluids CO_2 and R134a at equivalent conditions for NHT; CO_2 test condition: $G = 300\ \mathrm{kg\,m^{-2}\,s^{-1}}$, $q = 13\ \mathrm{kW\,m^{-2}}$, $T_{in} = 35\ ^{\circ}\mathrm{C}$.

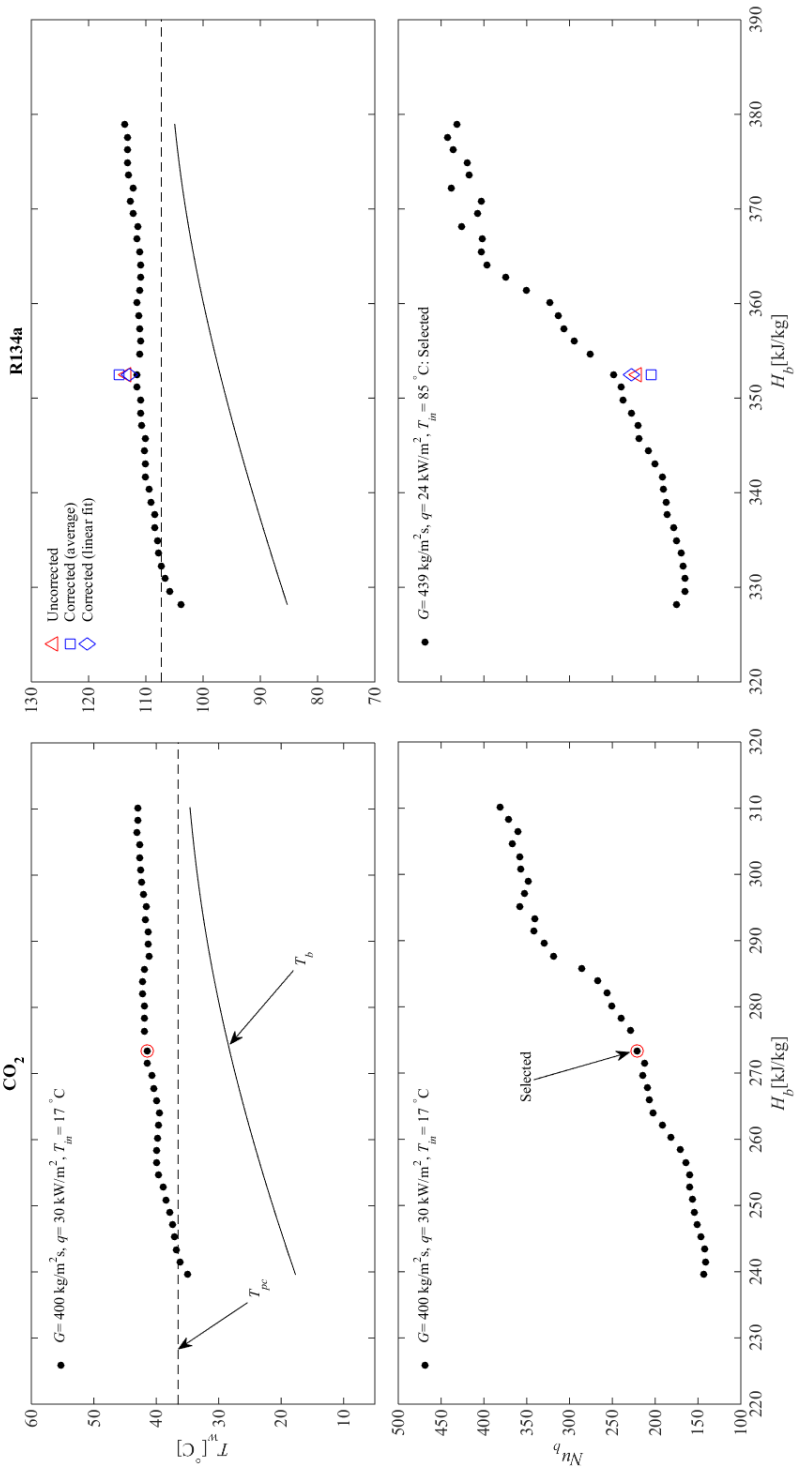

Figure D.17: Measurements of wall temperature (top) and bulk Nusselt number (bottom) *vs.* bulk enthalpy profiles in the fluids CO_2 and R134a at equivalent conditions for NHT; CO_2 test condition: $G = 400\ \mathrm{kg\,m^{-2}\,s^{-1}}$, $q = 30$ $\mathrm{kW\,m^{-2}}$, $T_{in} = 17$ °C.

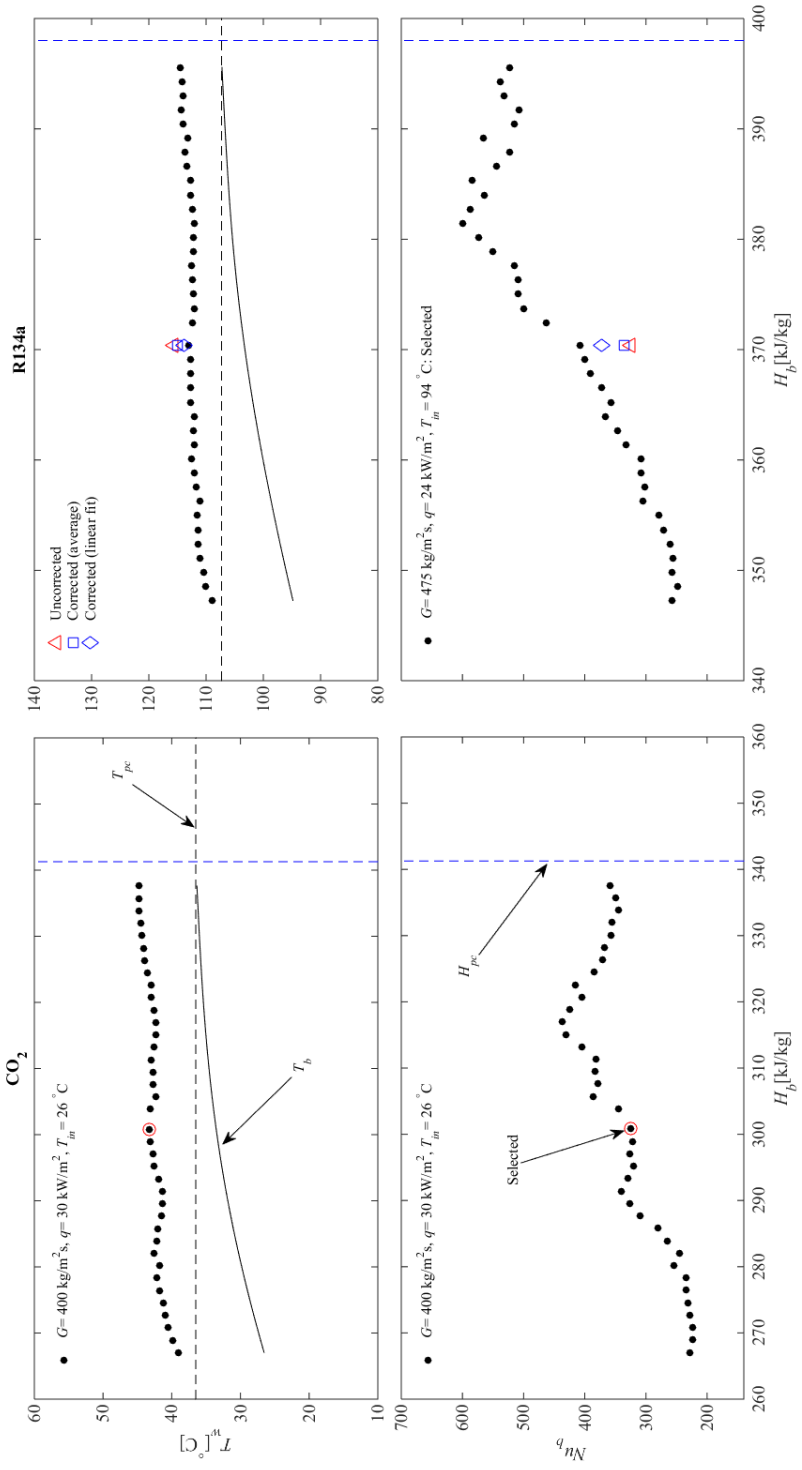

Figure D.18: Measurements of wall temperature (top) and bulk Nusselt number (bottom) *vs.* bulk enthalpy profiles in the fluids CO_2 and R134a at equivalent conditions for NHT; CO_2 test condition: $G = 400\ \mathrm{kg\,m^{-2}\,s^{-1}}$, $q = 30$ $\mathrm{kW\,m^{-2}}$, $T_{in} = 26$ °C.

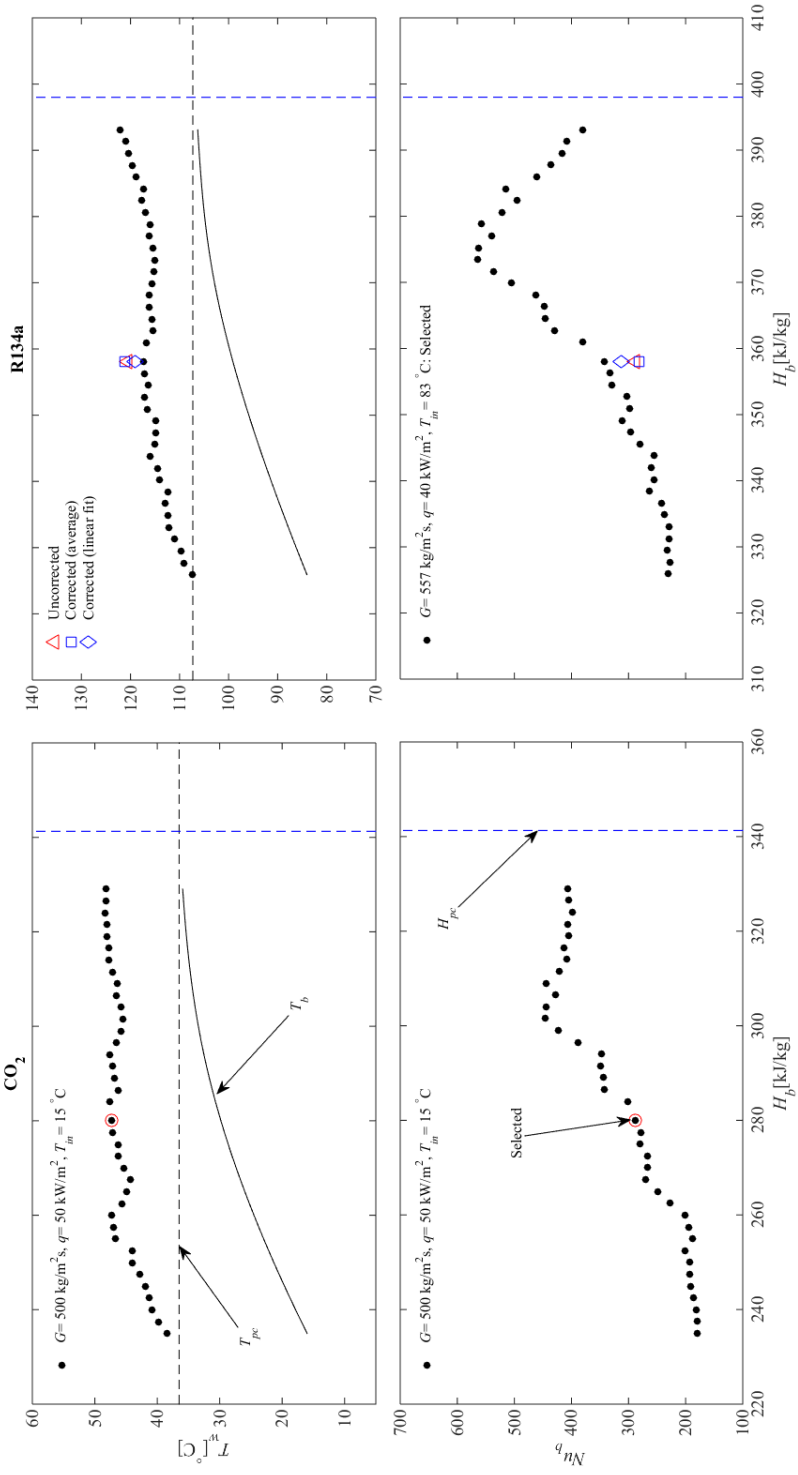

Figure D.19: Measurements of wall temperature (top) and bulk Nusselt number (bottom) *vs.* bulk enthalpy profiles in the fluids CO_2 and R134a at equivalent conditions for NHT; CO_2 test condition: $G = 500\ \mathrm{kg\,m^{-2}\,s^{-1}}$, $q = 50\ \mathrm{kW\,m^{-2}}$, $T_{in} = 15\ ^{\circ}\mathrm{C}$.

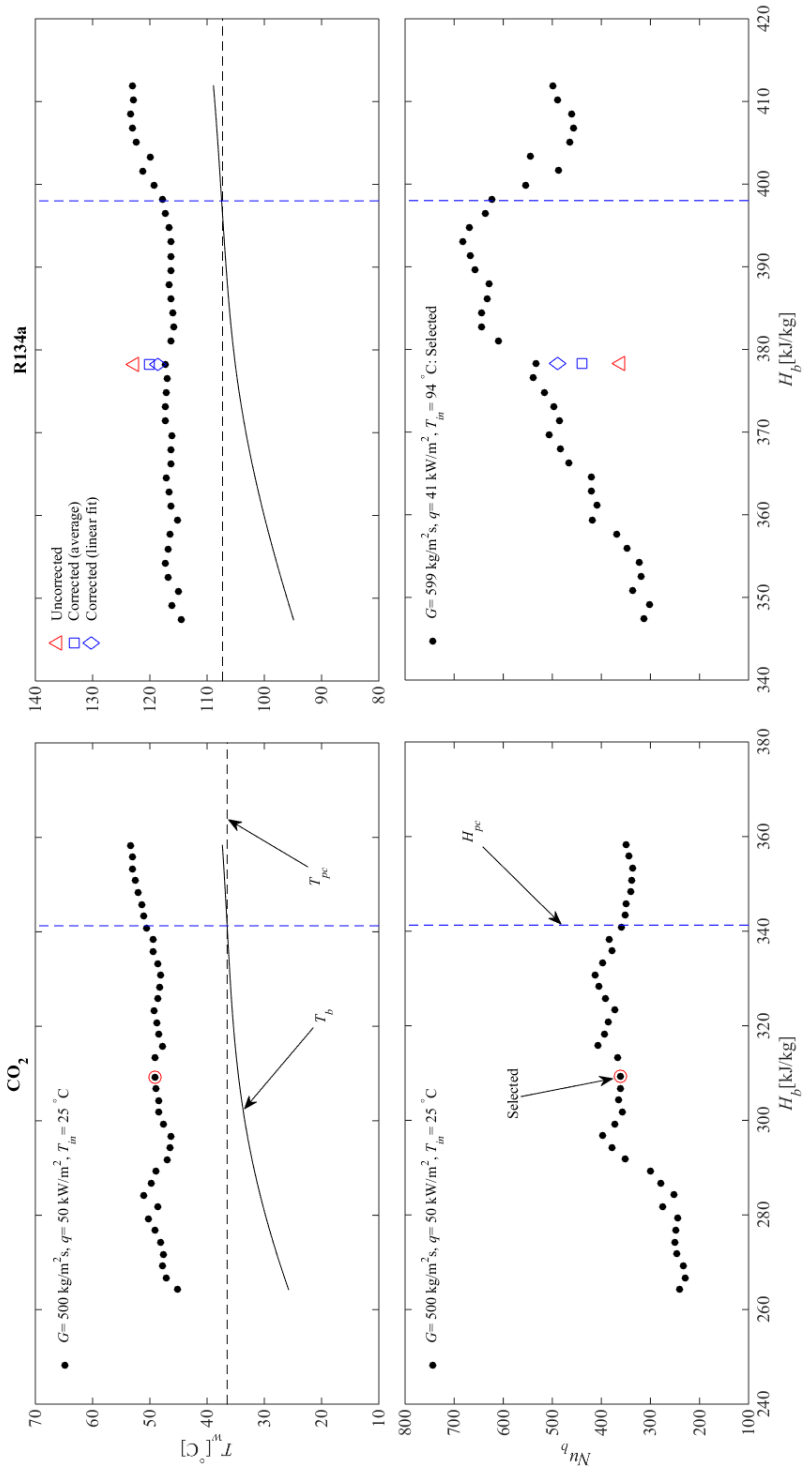

Figure D.20: Measurements of wall temperature (top) and bulk Nusselt number (bottom) *vs.* bulk enthalpy profiles in the fluids CO_2 and R134a at equivalent conditions for NHT; CO_2 test condition: $G = 500\ \mathrm{kg\,m^{-2}\,s^{-1}}$, $q = 50$ $\mathrm{kW\,m^{-2}}$, $T_{in} = 25$ °C.

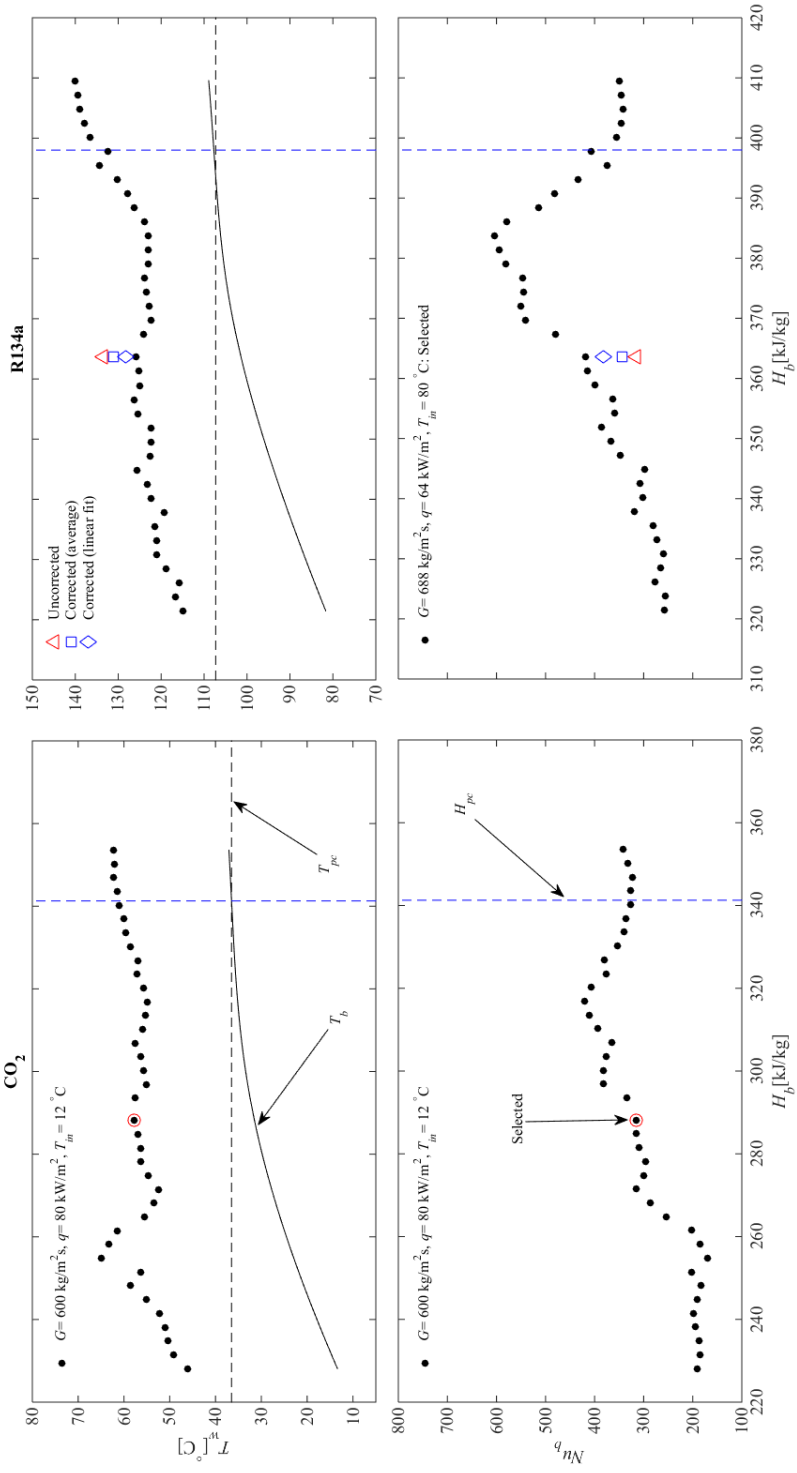

Figure D.21: Measurements of wall temperature (top) and bulk Nusselt number (bottom) *vs.* bulk enthalpy profiles in the fluids CO_2 and R134a at equivalent conditions for NHT; CO_2 test condition: $G = 600\ \mathrm{kg\,m^{-2}\,s^{-1}}$, $q = 80$ $\mathrm{kW\,m^{-2}}$, $T_{in} = 12$ °C.

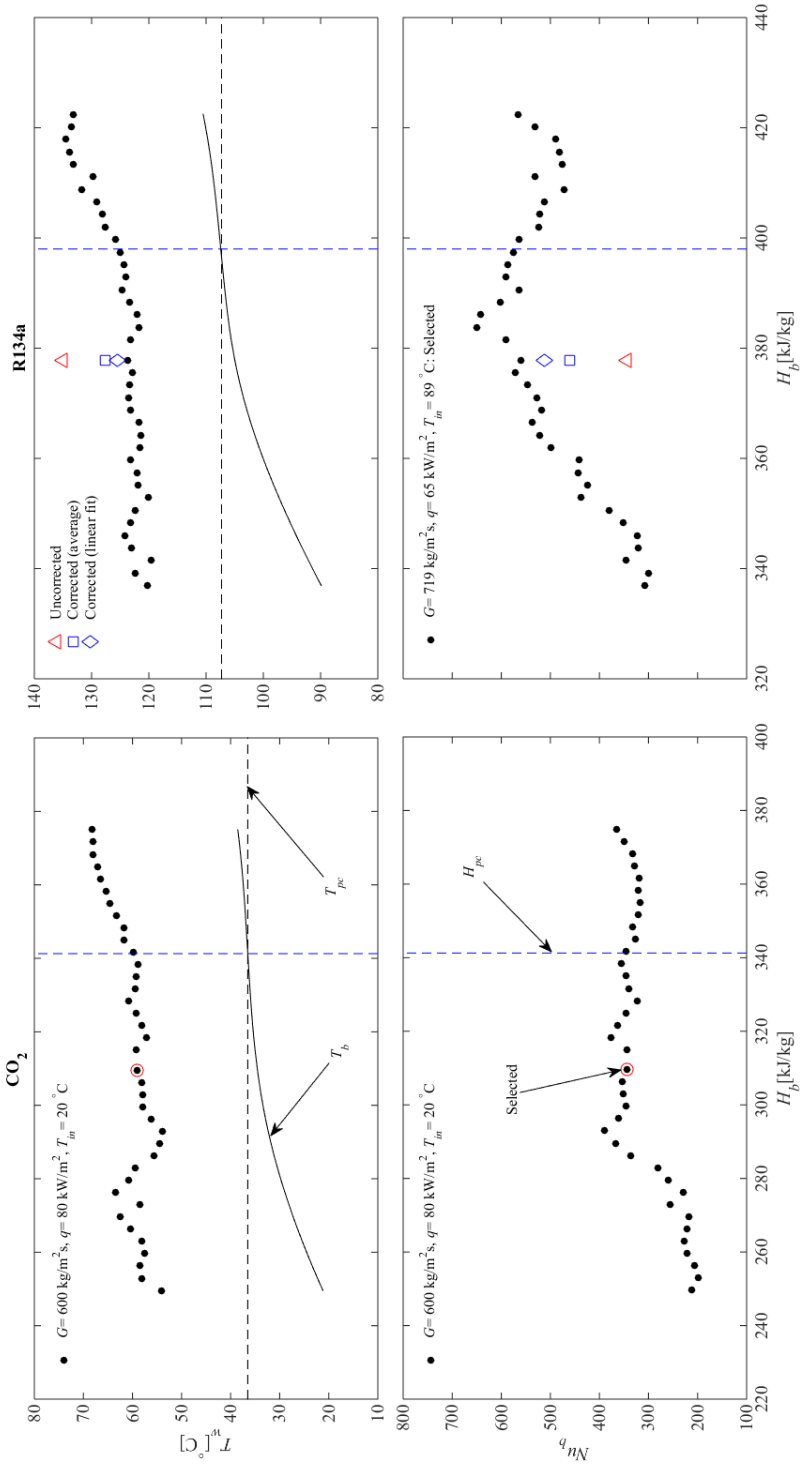

Figure D.22: Measurements of wall temperature (top) and bulk Nusselt number (bottom) *vs.* bulk enthalpy profiles in the fluids CO_2 and R134a at equivalent conditions for NHT; CO_2 test condition: $G = 600\ \mathrm{kg\,m^{-2}\,s^{-1}}$, $q = 80$ $\mathrm{kW\,m^{-2}}$, $T_{in} = 20$ °C.

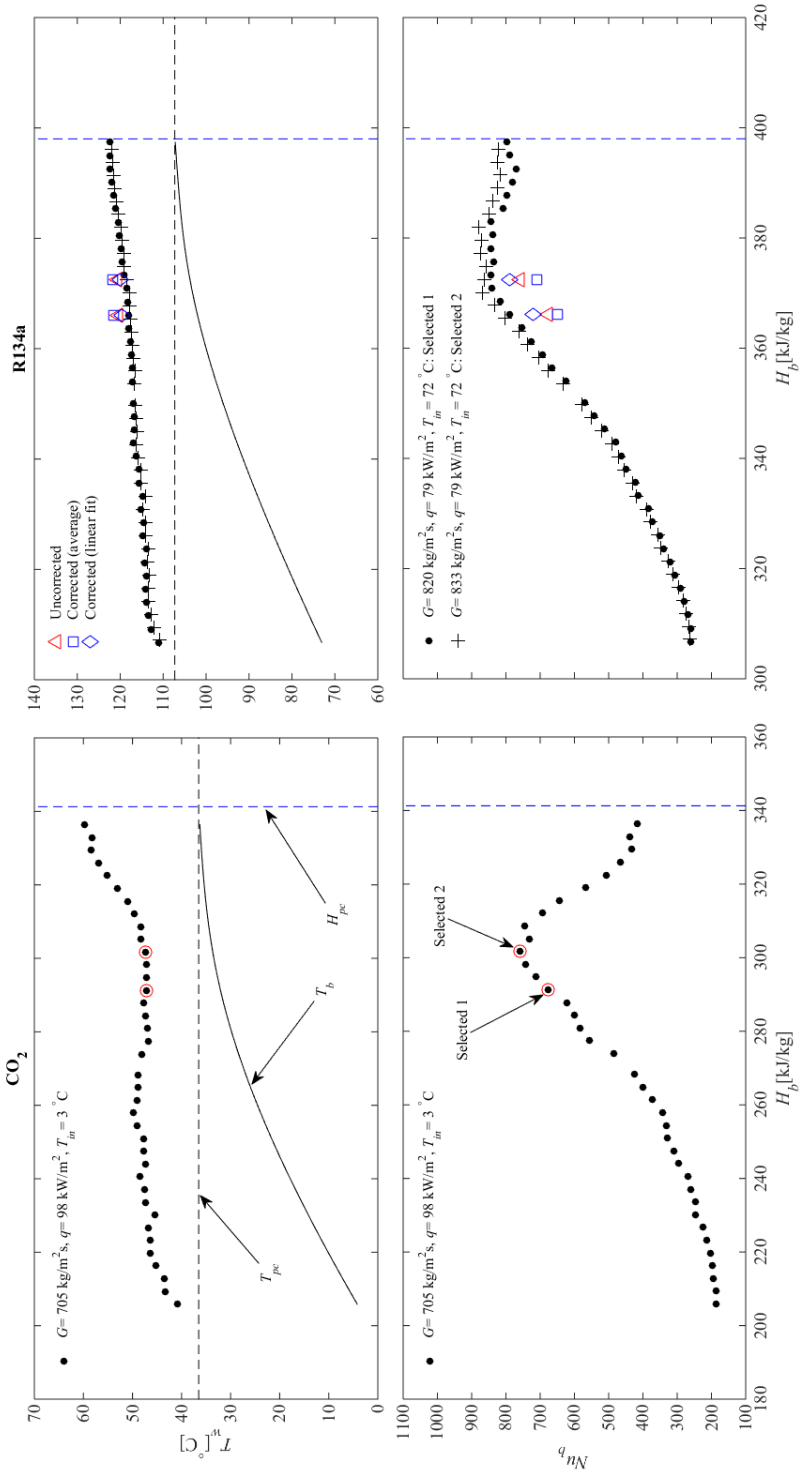

Figure D.23: Measurements of wall temperature (top) and bulk Nusselt number (bottom) *vs.* bulk enthalpy profiles in the fluids CO_2 and R134a at equivalent conditions for NHT; CO_2 test condition: $G = 705\ \mathrm{kg\,m^{-2}\,s^{-1}}$, $q = 98$ $\mathrm{kW\,m^{-2}}$, $T_{in} = 3$ °C.

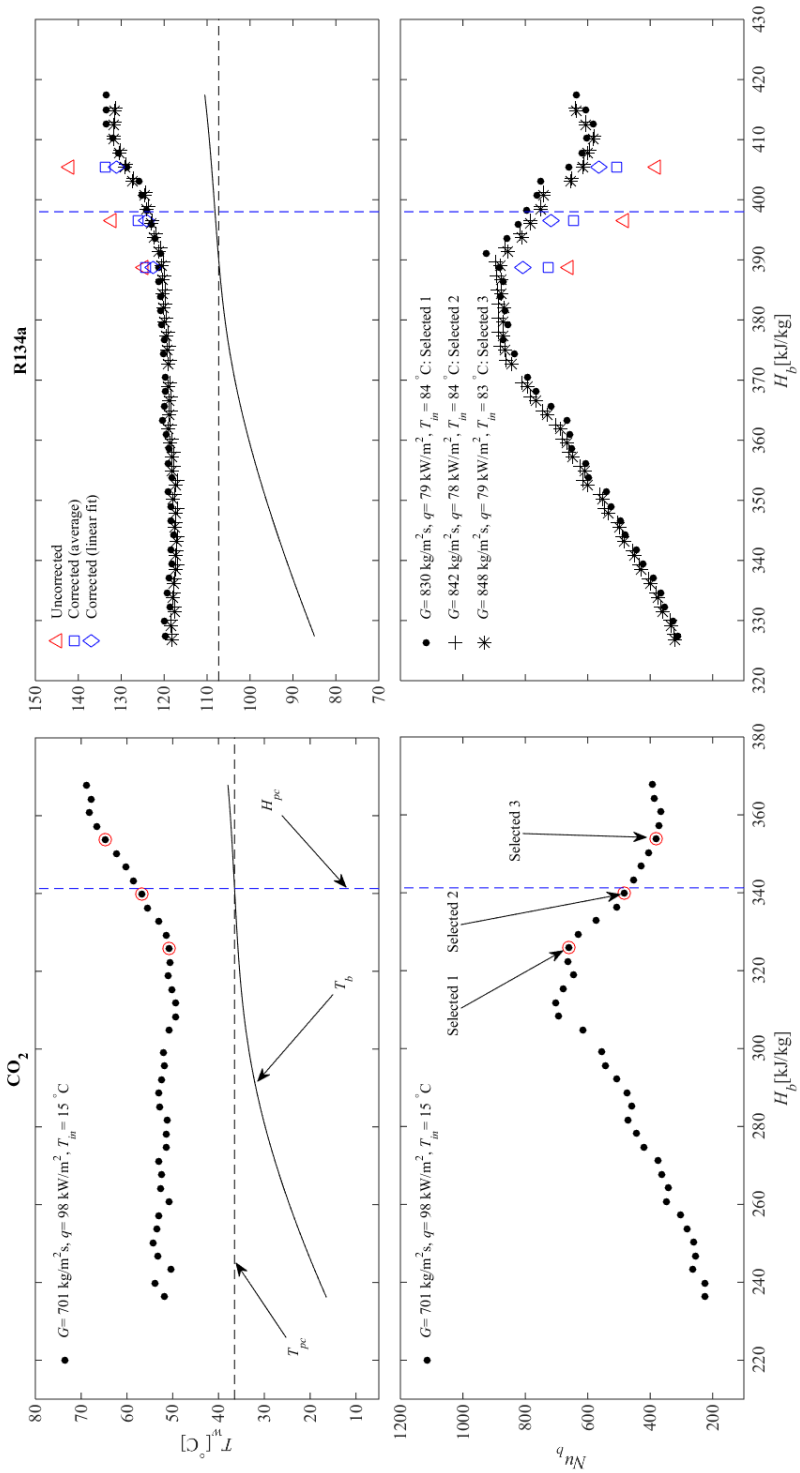

Figure D.24: Measurements of wall temperature (top) and bulk Nusselt number (bottom) *vs.* bulk enthalpy profiles in the fluids CO_2 and R134a at equivalent conditions for NHT; CO_2 test condition: $G = 701\ \mathrm{kg\,m^{-2}\,s^{-1}}$, $q = 98$ $\mathrm{kW\,m^{-2}}$, $T_{in} = 15$ °C.

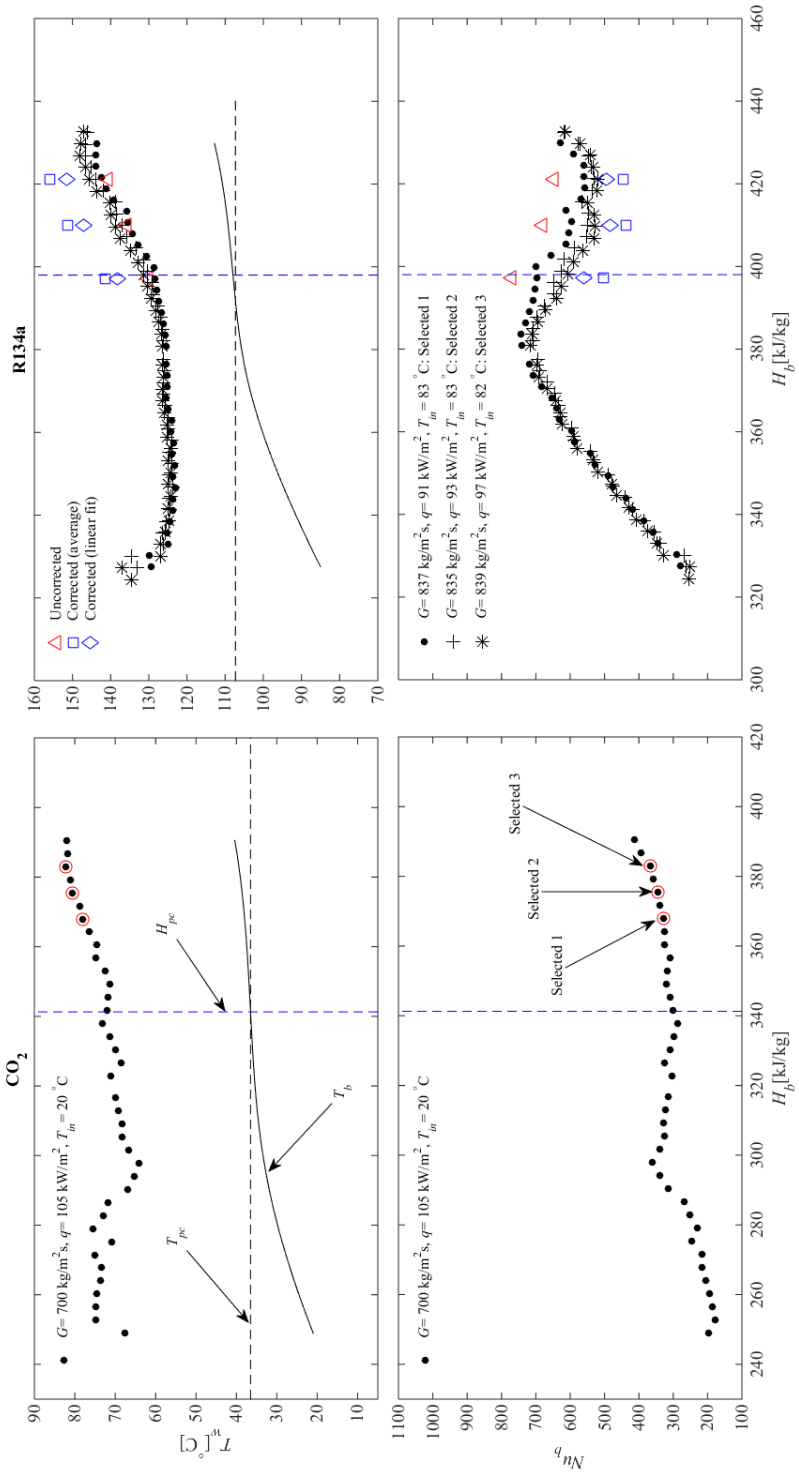

Figure D.25: Measurements of wall temperature (top) and bulk Nusselt number (bottom) *vs.* bulk enthalpy profiles in the fluids CO_2 and R134a at equivalent conditions for NHT; CO_2 test condition: $G = 700$ kg m^{-2} s^{-1}, $q = 105$ kW m^{-2}, $T_{in} = 20$ °C.

Appendix E

Measurements of T_w and Nu_b profiles for DHT

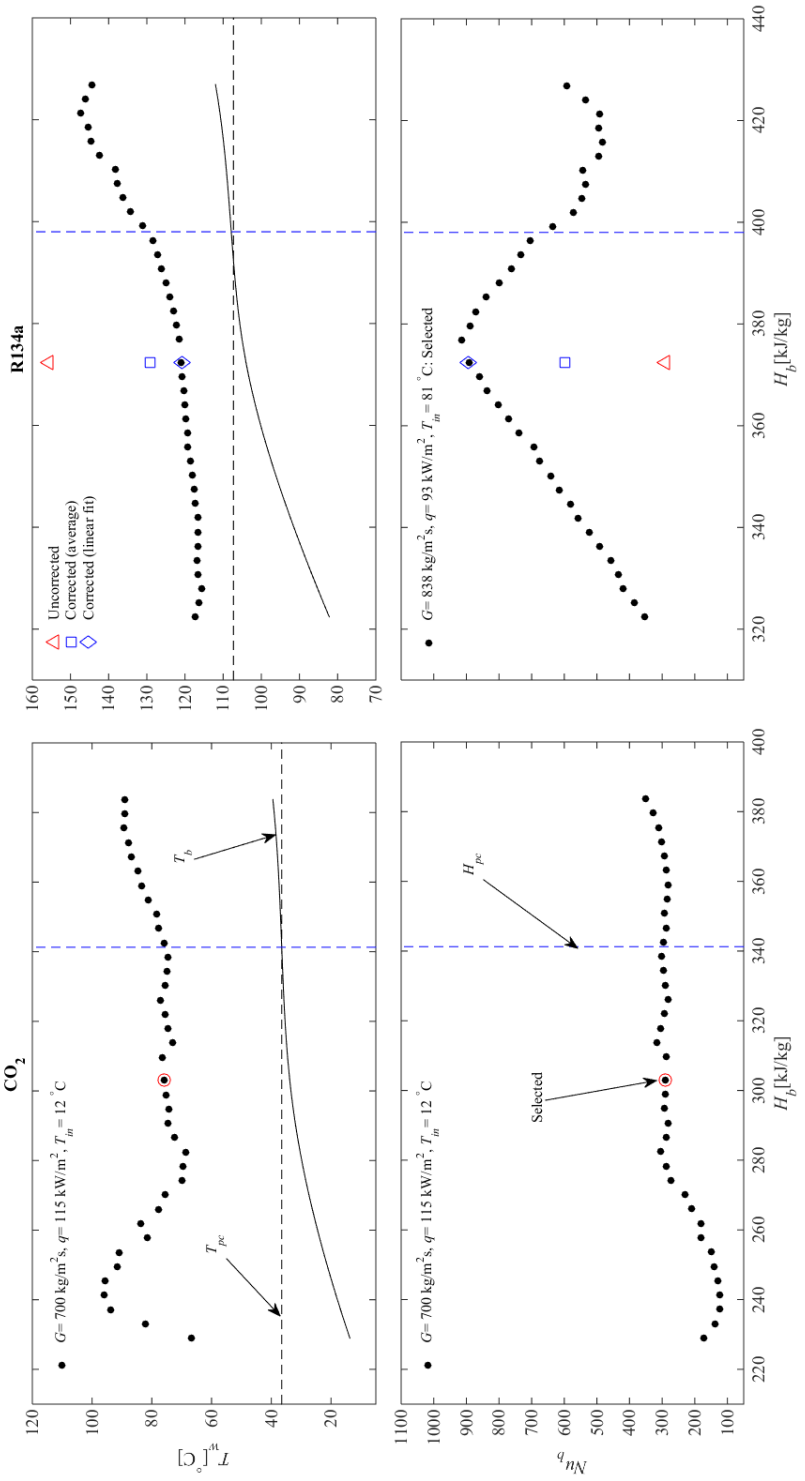

Figure E.1: Measurements of wall temperature (top) and bulk Nusselt number (bottom) *vs.* bulk enthalpy profiles in the fluids CO_2 and R134a at equivalent conditions for DHT; CO_2 test condition: $G = 700\ \mathrm{kg\,m^{-2}\,s^{-1}}$, $q = 115$ $\mathrm{kW\,m^{-2}}$, $T_{in} = 12$ °C.

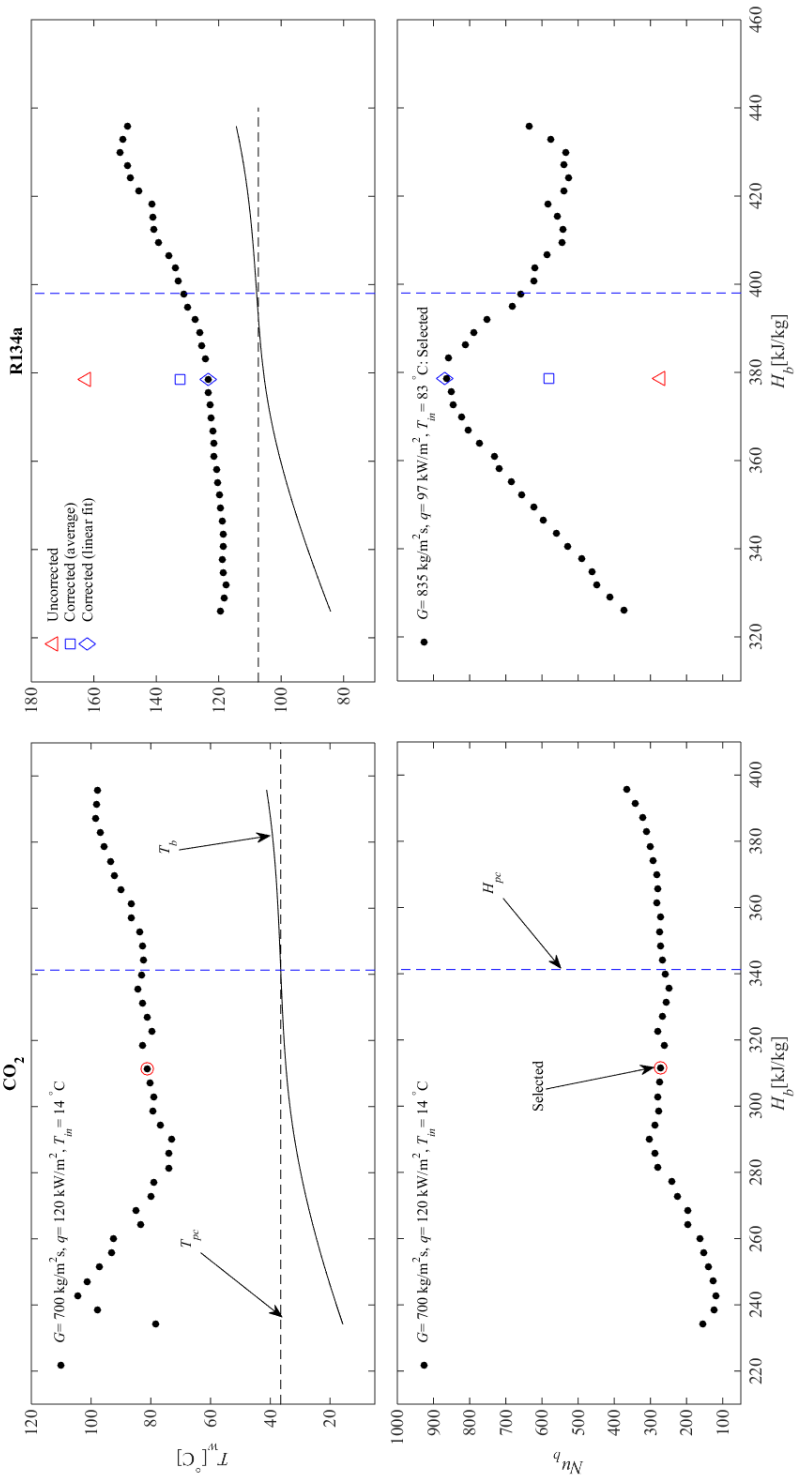

Figure E.2: Measurements of wall temperature (top) and bulk Nusselt number (bottom) *vs.* bulk enthalpy profiles in the fluids CO_2 and R134a at equivalent conditions for DHT; CO_2 test condition: $G = 700\ \mathrm{kg\,m^{-2}\,s^{-1}}$, $q = 120$ $\mathrm{kW\,m^{-2}}$, $T_{in} = 14$ °C.

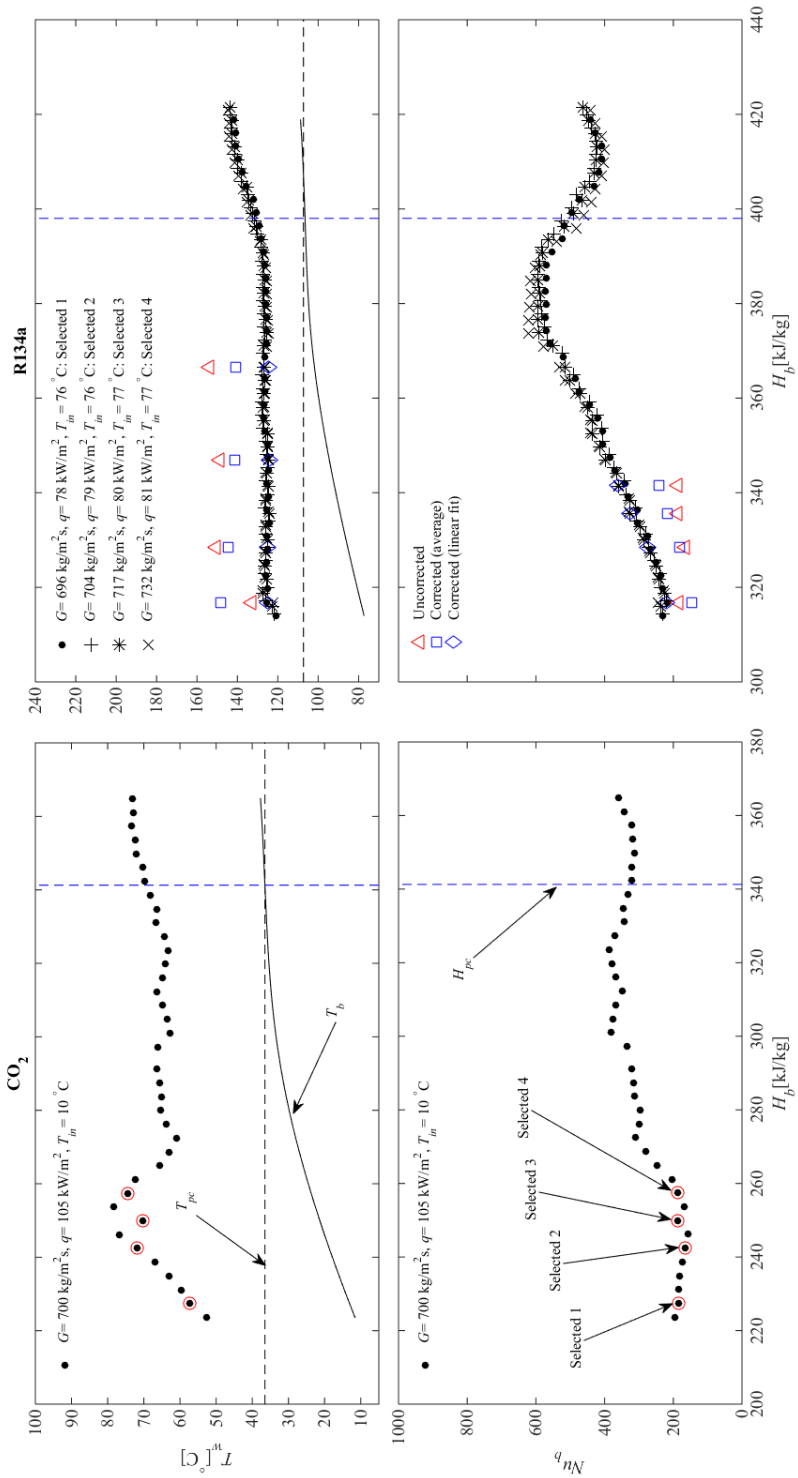

Figure E.3: Measurements of wall temperature (top) and bulk Nusselt number (bottom) *vs.* bulk enthalpy profiles in the fluids CO_2 and R134a at equivalent conditions for DHT; CO_2 test condition: $G = 700\ \mathrm{kg\,m^{-2}\,s^{-1}}$, $q = 105$ $\mathrm{kW\,m^{-2}}$, $T_{in} = 10\ ^{\circ}\mathrm{C}$.

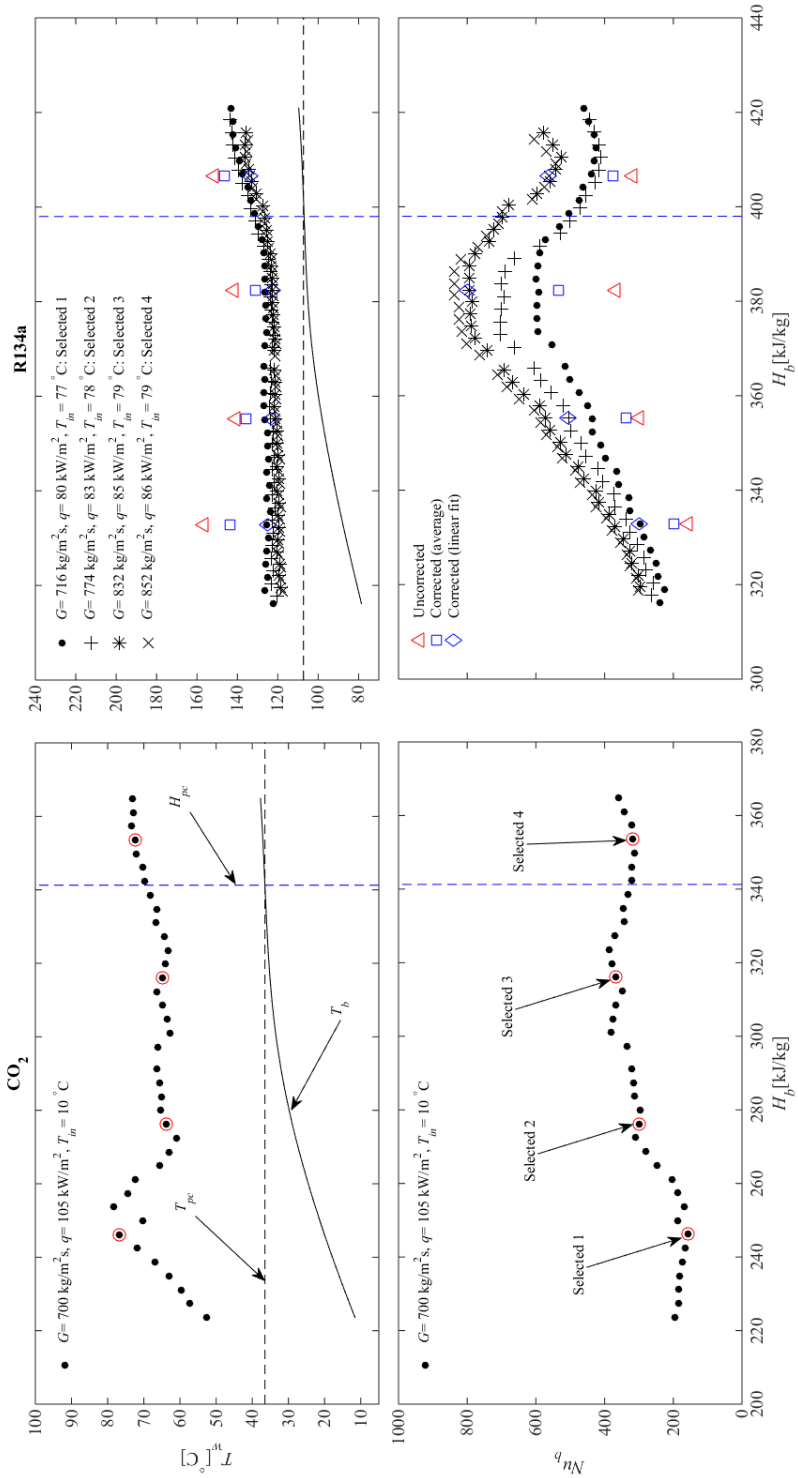

Figure E.4: Measurements of wall temperature (top) and bulk Nusselt number (bottom) *vs.* bulk enthalpy profiles in the fluids CO_2 and R134a at equivalent conditions for DHT; CO_2 test condition: $G = 700\ \mathrm{kg\,m^{-2}\,s^{-1}}$, $q = 105\ \mathrm{kW\,m^{-2}}$, $T_{in} = 10\ ^{\circ}\mathrm{C}$.

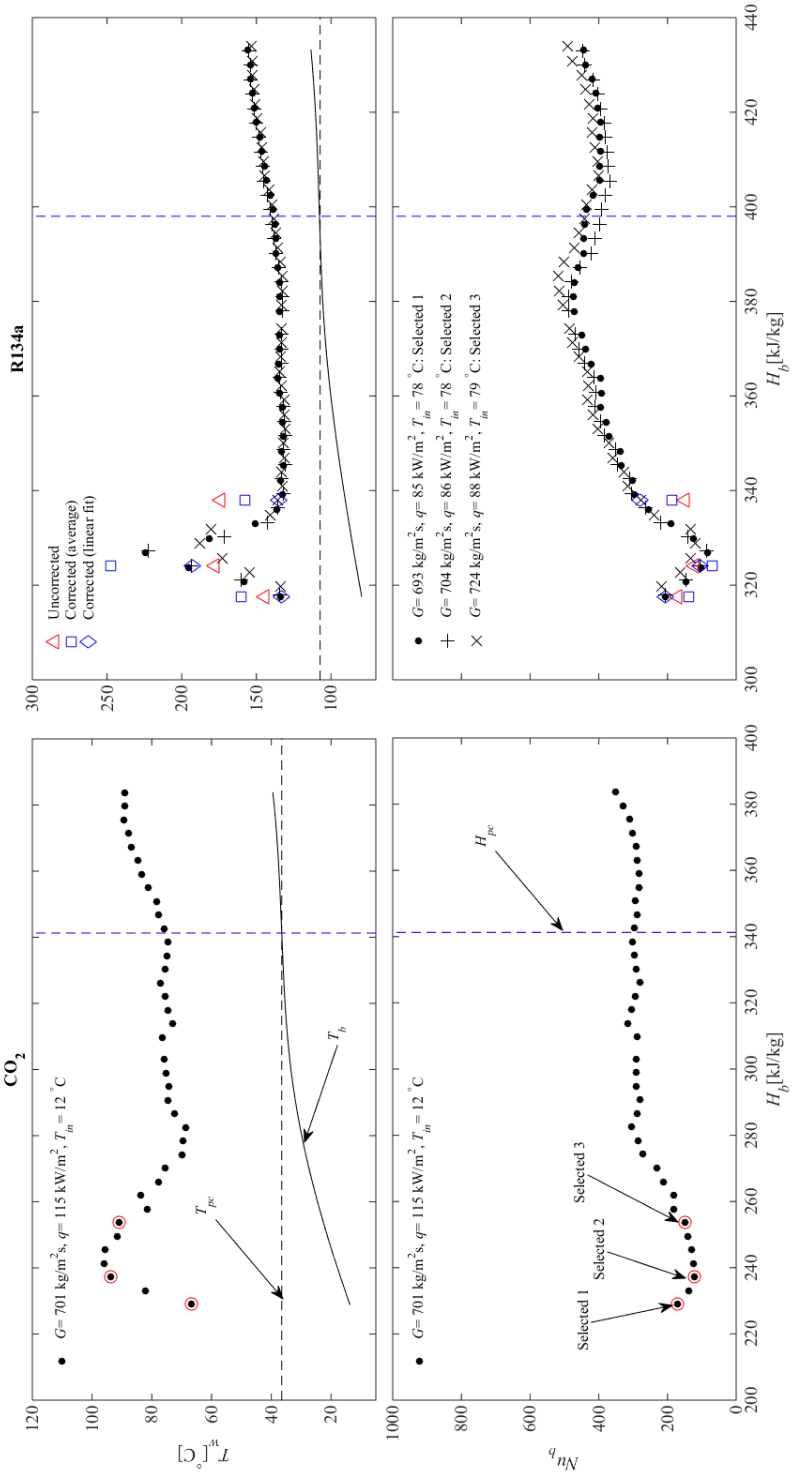

Figure E.5: Measurements of wall temperature (top) and bulk Nusselt number (bottom) *vs.* bulk enthalpy profiles in the fluids CO_2 and R134a at equivalent conditions for DHT; CO_2 test condition: $G = 701\ \mathrm{kg\,m^{-2}\,s^{-1}}$, $q = 115$ $\mathrm{kW\,m^{-2}}$, $T_{in} = 12$ °C.

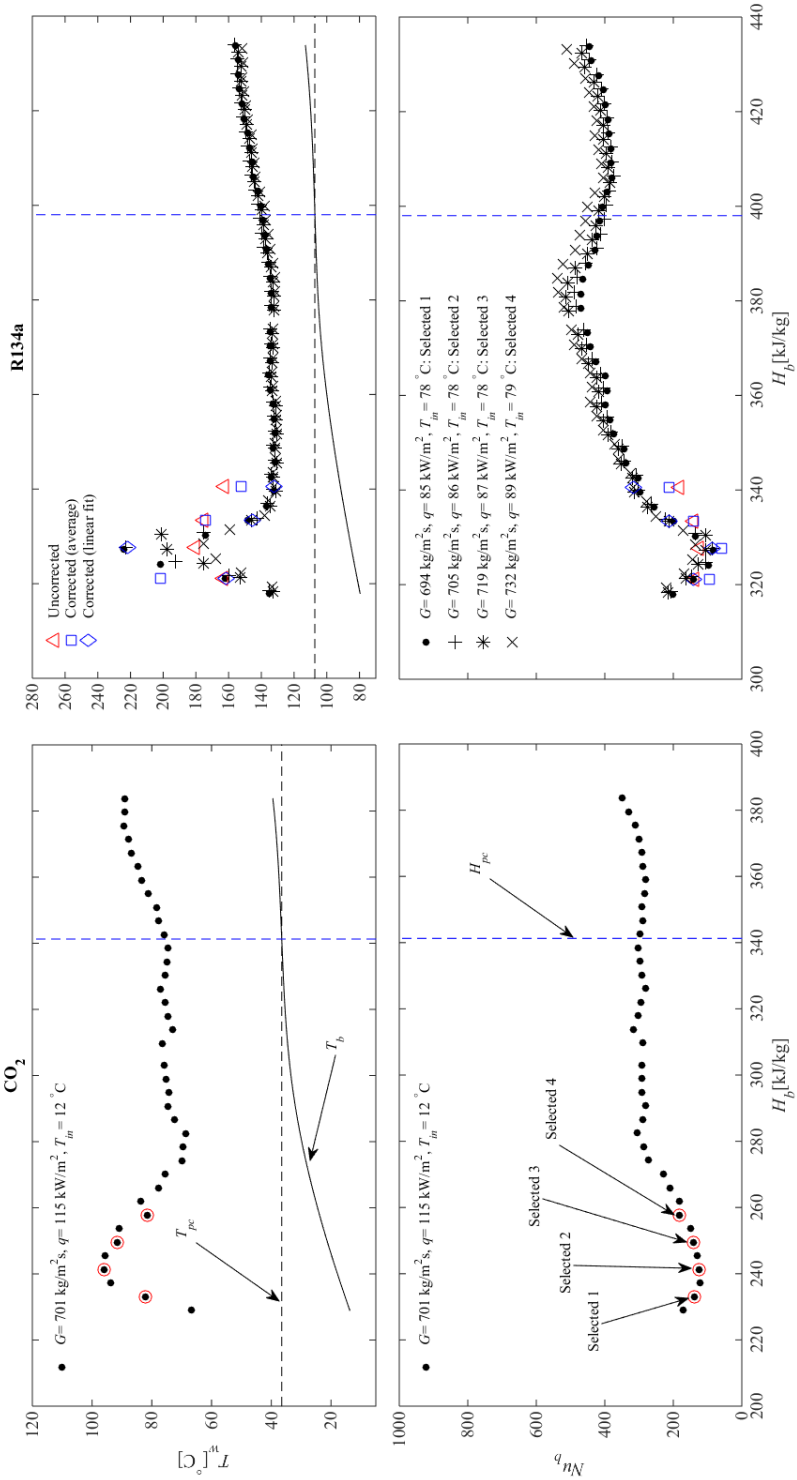

Figure E.6: Measurements of wall temperature (top) and bulk Nusselt number (bottom) *vs.* bulk enthalpy profiles in the fluids CO_2 and R134a at equivalent conditions for DHT; CO_2 test condition: $G = 701\ \mathrm{kg\,m^{-2}\,s^{-1}}$, $q = 155\ \mathrm{kW\,m^{-2}}$, $T_{in} = 12\ ^{\circ}\mathrm{C}$.

Appendix F

Supercritical fluid-to-fluid scaling laws summary

Table F.1: Summary of fluid-to-fluid scaling laws for supercritical heat transfer of a fluids 1 and 2

Authors	Tube geometry	Pressure	Bulk temperature
Jackson and Hall (1979)	$\left(\frac{z_h}{d}\right)_1 = \left(\frac{z_h}{d}\right)_2$	$\left(\frac{P}{P_c}\right)_1 = \left(\frac{P}{P_c}\right)_2$	$\left(\frac{T_b}{T_c}\right)_1 = \left(\frac{T_b}{T_c}\right)_2$
Pioro and Duffey (2007)	Not provided	$\left(\frac{P}{P_c}\right)_1 = \left(\frac{P}{P_c}\right)_2$	$\left(\frac{T_b}{T_c}\right)_1 = \left(\frac{T_b}{T_c}\right)_2$
Jackson (2007, 2008)	$\left(\frac{z_h}{d}\right)_1 = \left(\frac{z_h}{d}\right)_2$	$\left(\frac{P_{in}}{P_c}\right)_1 = \left(\frac{P_{in}}{P_c}\right)_2$	$\left(\frac{T_{in}}{T_c}\right)_1 = \left(\frac{T_{in}}{T_c}\right)_2$
Zwolinski et al. (2011)	$\left(\frac{z_h}{d}\right)_1 = \left(\frac{z_h}{d}\right)_2$	$\left(\frac{P_{in}}{P_c}\right)_1 = \left(\frac{P_{in}}{P_c}\right)_2$	$\left(\frac{T_{in}}{T_{pc}}\right)_1 = \left(\frac{T_{in}}{T_{pc}}\right)_2$
Cheng et al. (2011)	$d_1 = d_2$	$\left(\frac{P}{P_c}\right)_1 = \left(\frac{P}{P_c}\right)_2$	$\left(\frac{T_b - T_{pc}}{T_{pc} - T_c}\right)_1 = \left(\frac{T_b - T_{pc}}{T_{pc} - T_c}\right)_2$
Ambrosini (2011)	$z_{h,1} = m^{-3/2} z_{h,2}$;$m$ values refer to Section 2.4	Refer to Section 2.4	$\left(\frac{(H_b - H_{pc})\beta_{pc}}{c_{p,pc}}\right)_1 = \left(\frac{(H_b - H_{pc})\beta_{pc}}{c_{p,pc}}\right)_2$
Zahlan et al. (2014)	$d_1 = d_2$	$\left(\frac{P}{P_c}\right)_1 = \left(\frac{P}{P_c}\right)_2$	$\left(\frac{T_b}{T_{pc}}\right)_1 = \left(\frac{T_b}{T_{pc}}\right)_2$
Feuerstein et al. (2017)	Not provided	$\left(\frac{P}{P_c}\right)_1 = \left(\frac{P}{P_c}\right)_2$	$\left(\frac{(H_b - H_{pc})\beta_{pc}}{c_{p,pc}}\right)_1 = \left(\frac{(H_b - H_{pc})\beta_{pc}}{c_{p,pc}}\right)_2$
Azih and Yaras (2017)	Not provided	$\left(\frac{P}{P_c}\right)_1 = \left(\frac{P}{P_c}\right)_2$	$\left(\frac{(H_{in} - H_{pc})\beta_{pc}}{c_{p,pc}}\right)_1 = \left(\frac{(H_{in} - H_{pc})\beta_{pc}}{c_{p,pc}}\right)_2$
Yu et al. (2018)	Not provided	$\left(\frac{P}{P_c}\right)_1 = \left(\frac{P}{P_c}\right)_2$ and $\left(\frac{\Delta P}{\rho^* v^2}\right)_1 = \left(\frac{\Delta P}{\rho^* v^2}\right)_2$	$\left(\frac{T_b}{T_{pc}}\right)_1 = \left(\frac{T_b}{T_{pc}}\right)_2$

Table F.2: Summary of fluid-to-fluid scaling laws for supercritical heat transfer of a fluids 1 and 2 (Cont'd)

Authors	Heat flux	Mass flux	HTC
Jackson and Hall (1979)	$\left(\frac{qd}{k_b T_b}\right)_1 = \left(\frac{qd}{k_b T_b}\right)_2$	$\left(\frac{Gd}{\mu_b}\right)_1 = \left(\frac{Gd}{\mu_b}\right)_2$	$\left(\frac{hd}{k_b}\right)_1 = \left(\frac{hd}{k_b}\right)_2$
Pioro and Duffey (2007)	Not provided	$\left(\frac{Gd}{\mu_b}\right)_1 = \left(\frac{Gd}{\mu_b}\right)_2$	Not provided
Jackson (2007, 2008)	$\left(\frac{qd}{k_{in,b} T_{in}}\right)_1 = \left(\frac{qd}{k_{in,b} T_{in}}\right)_2$	$\left(\frac{Gd}{\mu_{in,b}}\right)_1 = \left(\frac{Gd}{\mu_{in,b}}\right)_2$	Not provided
Zwolinski et al. (2011)	$\left(\frac{qd}{k_{in,b} T_{in}}\right)_1 = \left(\frac{qd}{k_{in,b} T_{in}}\right)_2$	$\left(\frac{Gd}{\mu_{in,b}}\right)_1 = \left(\frac{Gd}{\mu_{in,b}}\right)_2$	$\left(\frac{hd}{k_{in,b}}\right)_1 = \left(\frac{hd}{k_{in,b}}\right)_2$
Cheng et al. (2011)	$\left(\frac{qd}{k_b(T_{pc}-T_c)}\right)_1 = \left(\frac{qd}{k_b(T_{pc}-T_c)}\right)_2$	$\left(\frac{GdPr_b^{\frac{5}{12}}}{\mu_b}\right)_1 = \left(\frac{GdPr_b^{\frac{5}{12}}}{\mu_b}\right)_2$	$\left(\frac{hd}{k_b}\right)_1 = \left(\frac{hd}{k_b}\right)_2$
Ambrosini (2011)	$\left(\frac{q\beta_{pc}}{AGc_{p,pc}}\right)_1 = \left(\frac{q\beta_{pc}}{AGc_{p,pc}}\right)_2$	$v_{in,1} = m^{-3/2} v_{in,2}$; $G = \rho v_{in}$	Not provided
Zahlan et al. (2014)	$\left(\frac{qd}{k_b T_{pc}}\right)_1 = \left(\frac{qd}{k_b T_{pc}}\right)_2$	$\left(\frac{GdPr_b^{0.66}}{\mu_b}\right)_1 = \left(\frac{GdPr_b^{0.66}}{\mu_b}\right)_2$	$\left(\frac{hd}{k_b}\right)_1 = \left(\frac{hd}{k_b}\right)_2$
Feuerstein et al. (2017)	$\left(\frac{qd}{k_b(T_{pc}-T_c)}\right)_1 = \left(\frac{qd}{k_b(T_{pc}-T_c)}\right)_2$	$\left(\frac{q\beta Re^{-0.9}}{Gc_p}\right)_1 = \left(\frac{q\beta Re^{-0.9}}{Gc_p}\right)_2$	$\left(\frac{hd}{k_b}\right)_1 = \left(\frac{hd}{k_b}\right)_2$
Azih and Yaras (2017)	$\left(\frac{q\beta_{pc}}{Gc_{p,pc}}\right)_1 = \left(\frac{q\beta_{pc}}{Gc_{p,pc}}\right)_2$	$\left(\frac{Gd}{\mu_{in}}\right)_1 = \left(\frac{Gd}{\mu_{in}}\right)_2$	Refer to Section 2.4
Yu et al. (2018)	$\left(\frac{q}{Gd(H_{pc}-H_c)}\right)_1 = \left(\frac{q}{Gd(H_{pc}-H_c)}\right)_2$	$\left(\frac{Gd}{\mu_b^*}\right)_1 = \left(\frac{Gd}{\mu_b^*}\right)_2$	$\left(\frac{hd}{k_b^*}\right)_1 = \left(\frac{hd}{k_b^*}\right)_2$ or $h_2 = \left(\frac{q}{\Delta T}\right)_2$

Appendix G

Example verification from literature

Table G.1: Verification of an example provided by Yu et al. (2018)

	Yu et al. (2018)		Verification	
	R134a	H_2O	H_2O	H_2O (T_b scaled by T_c)
P [MPa]	4.2	22.83	22.83	22.83
T_b [K]	375.76	649.7	641.9	649.8
d [mm]	10	8	8	8
G [$\mathrm{kg\,m^{-2}\,s^{-1}}$]	800	1391	2646	1318
q [$\mathrm{kW\,m^{-2}}$]	33.1	445.5	895.7	446.3